Investigating energy metabolism pathways for therapeutic development and prognostication in chronic lymphocytic leukaemia

Lara Marie Escane

BMedSc, BSc (Hons)

Department of Molecular Medicine & Genetics

College of Medicine and Public Health

Flinders University

February 2021

Thesis is submitted to fulfil the requirements for the degree of

Doctor of Philosophy

Contents

Abstract

Chronic lymphocytic leukaemia (CLL) is the most common leukaemia of the western world and remains incurable. Uncontrolled proliferation of mature B-lymphocytes results in a compromised immune system and patients often succumb to infection. Despite there being multiple molecular prognostic indicators, one or a combination of these is unable to accurately predict the disease course which varies greatly. Lipoprotein lipase (LPL) expression can be used to predict disease course and implicates the ability of CLL B-lymphocytes to metabolise lipids in disease progression. Additionally, CLL B-lymphocytes have higher intracellular reactive oxygen species (ROS) levels due to highly active mitochondria. We hypothesised that ROS and lipid metabolism are fundamental pathways of CLL pathophysiology and abnormalities in these pathways result in intrinsic resistance of CLL B-lymphocytes to therapy.

In order to test our hypothesis, several objectives were formed.

Firstly, the antioxidant capacity of CLL and healthy B-lymphocytes was assessed with respect to intracellular ROS and cell death to determine if CLL B-lymphocytes from patients with bulky lymphadenopathy (BLA) were better able to handle ROS, preventing ROS-mediated cell death. Individuals with BLA exhibited faster disease progression compared to those without. BLA CLL B-lymphocytes had lower basal intracellular ROS levels, however there was no difference in ROS levels in response to cross-linked RTX therapy. Rotenone caused cell death in CLL B-lymphocytes but not healthy controls implicating an intolerance to the blocking of oxidative phosphorylation and/or increasing intracellular ROS beyond the CLL cell's capacity to detoxify them.

Secondly, the promoter of the tumour suppressor and antioxidant superoxide dismutase 2 (SOD2) was sequenced to determine if the presence of mutations in transcription factor binding sites that promote *SOD2* expression or the introduction of inhibitory transcription factor binding sites are responsible for low SOD2 expression in a pilot cohort of individuals with CLL. The *SOD2* promoter was found to be identical to that of the healthy controls. The SOD2 promoter was also assessed for possible suppression by cytosine methylation, however no consistent methylation was detected.

Thirdly, and lastly, lipid metabolic pathways in healthy and CLL B-lymphocytes were assessed in hopes of identifying novel therapeutic targets. CD36/fatty acid translocase was identified as being absent from CLL B-lymphocytes which was unexpected due to the fatty acid-metabolising nature of CLL. RNA expression of fatty acid import genes was assessed, and the tumour suppressor *CAV2* and fatty acid transport protein *FATP6* were expressed at lower and higher levels in CLL cells compared to healthy controls, respectively. Our fatty acid import inhibition data showed that pinocytosis is the primary mechanism of fatty acid uptake in the CLL B-lymphocyte cell line HG-3. This work was expanded by measuring the fatty acid uptake rate in CLL B-lymphocytes based on their circulatory stage with respect

to surface expression of the CXCR4 homing molecule. CLL B-lymphocytes that had recently exited the secondary lymphoid organs had a higher fatty acid uptake rate compared to those homing back to these tissues. Our data suggests that lipids are scavenged in the periphery for storage and use in the proliferative compartment where perfusion is low and hence there is limited nutrient availability.

Our work identified the importance of oxidative phosphorylation and intracellular ROS handling in the survival of CLL B-lymphocytes, particularly those from individuals with BLA which may have a higher antioxidant capacity.

List of Figures

List of Tables

Abbreviations

°C	degrees Celsius
$^{\bullet}O_2^-$	superoxide
$^{\bullet}OH$	hydroxyl radical
2D-DIGE	two-dimensional differential in-gel electrophoresis
2ME	2-mercaptoethanol
ACSL	long-chain fatty acid-CoA ligase
ADCC	antibody-dependent cellular cytotoxicity
ADP	adenosine diphosphate
AP-1	activating protein-1
AP-2	activating protein-2
APC	allophycocyanin
ARE	antioxidant response element
ASK1	apoptosis signal-regulating kinase 1
ATM	Ataxia-telangiectasia mutated
ATP	adenosine triphosphate
B2M	beta 2-microglobulin
BCL	B-cell lymphoma
BCR	B-cell receptor
BLA	bulky lymphadenopathy
bp	base pairs
BSA	bovine serum albumin
BTK	Bruton's tyrosine kinase
C7-dGTP	7-deaza-deoxyguanine triphosphate
Ca^{2+}	calcium
CAC	citric acid cycle
CAT	catalase
CD	cluster of differentiation
CDC	complement-dependent cytotoxicity
CDDO	2-cyano-3,12-dioxooleana-1,9-dien-28-oic acid
cDNA	complementary DNA
CEBP	CCAAT/enhancer-binding protein
CLL	chronic lymphocytic leukaemia
C^m	methylated cytosine
CM-H_2DCFDA	chloromethyl derivative of 2',7'-dichlorodihydrofluorescein diacetate
CO_2	carbon dioxide
CoA	coenzyme A
CoQ	coenzyme Q
C_t	cycle threshold
CXCR4	chemokine C-X-C motif receptor 4
Cy	cyanine
del11q	deletion at the q arm of chromosome 11
del13q	deletion at the q arm of chromosome 13
del17p	deletion at the p arm of chromosome 17
DEPC	diethyl pyrocarbonate
dGTP	deoxyguanine triphosphate
DMSO	dimethyl sulphoxide
DNA	deoxyribonucleic acid
dNTP	deoxynucleoside triphosphate
DTT	dithiothreitol
EBV	Epstein-Barr virus
EDTA	ethylenediaminetetraacetic acid
EIPA	ethylisopropyl amiloride

FABPpm	plasma membrane-associated fatty acid binding protein
FACS	fluorescence-activated cell sorting
FADH2	reduced flavin adenine dinucleotide
FATP	fatty acid transport protein
FCR	fludarabine cyclophosphamide rituximab
FCS	foetal calf serum
FDG	fluorine-18 fluoro-deoxyglucose
Fe^{3+}/Fe^{2+}	iron
FISH	fluorescence in situ hybridisation
FITC	fluorescein isothiocyanate
g	gravity
GA101	obinutuzumab
GC	guanine cytosine
GEO	Gene Expression Omnibus
GPX	glutathione peroxidase
GSH	glutathione
H^+	proton
H_2O	water
H_2O_2	hydrogen peroxide
HBSS	Hank's balanced salt solution
HEPES	4-(2-hydroxyethyl)-1-piperazineethanesulfonic acid
HIF	hypoxia-inducible factor
HREC	human research ethics committee
IDT	Integrated DNA Technologies
Ig	immunoglobulin
IGHV	immunoglobulin heavy chain variable gene
IL	interleukin
ins	insertion
IκB	NF-κB inhibitor proteins
JNK1	c-Jun N-terminal kinase 1
kDa	kilodaltons
Keap1	Kelch-like ECH-associated protein 1
L	litre
LPL	lipoprotein lipase
M	molar
mAb	monoclonal antibody
MDR	minimum deleted region
mETC	mitochondrial electron transport chain
Mg^{2+}	magnesium
MGL	monoglyceride lipase
miR	micro RNA
mL	millilitres
mM	millimolar
mm^2	millimetres squared
MnSOD/SOD2	manganese superoxide dismutase/superoxide dismutase 2
mRNA	messenger RNA
NAD^+	nicotinamide adenine dinucleotide
NADH	reduced nicotinamide adenine dinucleotide
$NADP^+$	nicotinamide adenine dinucleotide phosphate
NADPH	reduced nicotinamide adenine dinucleotide phosphate
NEB	New England Biolabs
NF-κB	kappa-light-chain-enhancer of activated B-cells
ng	nanograms
NK	natural killer
nm	nanometre

nM	nanomolar
NO	nitric oxide
NOTCH1	Notch receptor 1
Nrf-2	nuclear factor erythroid 2-related factor 2
O_2	oxygen
OFA	ofatumumab
PBMC	peripheral blood mononuclear cells
PBS	phosphate buffered saline
PCR	polymerase chain reaction
PE	phycoerythrin
PEITC	phenethyl isothiocyanate
PET	positron emission topography
PFS	progression-free survival
PI	propidium iodide
PI3K	phosphoinositol 3-kinase
PPARα	peroxisome proliferator-activated receptor-alpha
PRDX	peroxiredoxin
PVDF	polyvinylidene difluoride
qPCR	quantitative polymerase chain reaction
RIPA	radioimmunoprecipitation assay buffer
RNA	ribonucleic acid
ROS	reactive oxygen species
RPMI	Roswell Park Memorial Institute
RTX	rituximab
s	seconds
SAP	shrimp alkaline phosphatase
SDS-PAGE	sodium dodecyl sulphate polyacrylamide gel electrophoresis
SNP	single nucleotide polymorphism
SOD	superoxide dismutase
SOD1	copper/zinc superoxide dismutase/superoxide dismutase 1
Sp1	specificity protein 1
STAT3	signal transducer and activator of transcription
SUV	Standardised Uptake Values
TAE	trisaminomethane-acetic acid-ethylenediaminetetraacetic acid
Taq	*Thermus aquaticus*
TK1	thymidine kinase 1
TNFα	tumour necrosis factor alpha
TSS	transcription start site
TTFT	time to first treatment
U	units
V	volts
w/v	weight per volume
ZAP-70	zeta-chain-associated protein kinase 70
µg	microgram
µL	microlitre
µM	micromolar

Acknowledgements

The work described in this thesis was funded by the Cancer Council Beat Cancer Project, Flinders Foundation Seeding Grant, and the Australian Postgraduate Award.

Many thanks go to the CLL patients and healthy donors who consented to the use of their tissue in this study. Without their generous donation, this work would not have been possible.

***

Special thanks go to my supervisors Associate Professor Karen Lower, Dr. Lauren Thurgood, and Associate Professor Bryone Kuss, for their constant encouragement and support throughout my postgraduate studies. I cannot stress enough how much you have helped me to believe in and complete my project. Your insight and expert opinion throughout this time are greatly appreciated. I would also like to thank my supervisors for finding me teaching and research work throughout my PhD, I really do appreciate it, the experience has been invaluable.

I would like to thank the Department of Molecular Medicine and Genetics who were always available to help me with any troubles that I had. I would particularly like to thank Dr. Lauren Thurgood for her constant devotion to helping me with my project, and for always providing words of encouragement when I needed them. It's been a blast working on the lipid project together – and sharing an office! To the other members of the Department, Dr. Giles (LW) Best, Dr. Binoy Appukuttan, Di Luke, Dr. Anya Hotinski, and Dr. Stephen Gregory, who have always been there to cheer me on whether my experiments were working or not, I appreciate your support.

Special thanks go to now Dr. Chloé Thompson-Peach, my BFF and fellow PhD student, whom without I would not have been able to complete my PhD. Thank you for being there for me during the times when it was only us (and Di) in the department and we were trying to help each other plan our experiments. Thank you for always listening to me complain about my sore hand from pipetting so many 384-well plates and being there for me when I was so close to walking away. These past 5+ years have been a roller coaster, and I'm so grateful that you went through the highs, lows, and loop-the-loops with me!

I would also like to thank Angela Binns for finding a place for me in the Technical Services family. I have really enjoyed working in the various roles that you have entrusted to me, and I look forward to developing my future professional life with you. On that note, I would like to thank everyone I have worked with in those roles who have always encouraged me with my studies: Lauren Mortimer, Pat Vilimas, Dr. Voula Gaganis, Dr. Helen Harrison, Dr. Sara Tommasi, Lauren Jones, and Negara Tajbakhsh.

Last but not least, I would like to thank my family. Thank you Kaspr for emotionally and financially supporting me while I was trying to live off a part-time scholarship (and no scholarship). Thank you to my parents for letting us live in your house rent-free while I have been studying and you've been working and living interstate. To Katie, thank you for the balance of emotionally supporting me whilst constantly reminding me that it's taking me a long time to complete my PhD. Weirdly, I thank myself for making it all the way to the finish line!

Declaration

'I certify that this thesis:

1. does not incorporate without acknowledgement any material previously submitted for a degree or diploma in any university; and
2. to the best of my knowledge and belief, does not contain any material previously published or written by another person except where due reference is made in the text.'

Lara Escane
19th November 2020

Chapter 1:
Introduction

Cells are the basic structural, functional, and biological unit of all known living organisms. Many important cellular processes, such as cellular respiration, are essential to life and integral to cellular homeostasis. In cancer, cellular metabolism is frequently altered which causes an increase in energy demands, sources, and by-products (Hanahan & Weinberg, 2011). Chronic lymphocytic leukaemia (CLL) is a cancer of the blood that causes an uncontrolled proliferation of mature B-lymphocytes. Altered cellular metabolism in CLL and how this affects disease pathogenesis and response to therapy are the focus of this thesis.

1.1 Cellular metabolism

Adenosine triphosphate (ATP) is the 'molecular currency' of the cell where it stores and transfers energy by the hydrolysis of the terminal phosphate group. There are three main pathways that regenerate ATP from its hydrolysed form: glycolysis, the citric acid cycle (CAC), and oxidative phosphorylation (Nelson & Cox, 2016).

As Figure 1.1 shows, in the cytoplasm, glycolytic enzymes convert glucose to pyruvate producing two ATP molecules from one glucose molecule – this process is anaerobic. Pyruvate is then shuttled into the mitochondrial matrix and converted to acetyl-Coenzyme A (CoA) which enters the CAC. Acetyl-CoA can also be generated through β-oxidation of lipids and will be discussed in section 1.1.1. Sequential oxidation of substrates allows the CAC to produce two molecules of ATP from one molecule of acetyl-CoA – this process is aerobic. The final product of the CAC is oxaloacetate which reacts with acetyl-CoA to form citrate, and thus another cycle of the CAC begins. In addition to the production of ATP, the high energy molecules nicotinamide adenine dinucleotide (NADH) and flavin adenine dinucleotide ($FADH_2$) are regenerated. NADH and $FADH_2$ work as electron donors for the mitochondrial electron transport chain (mETC) which will be discussed in section 1.1.2. The production of acetyl-CoA from fatty acids will be discussed in the next section.

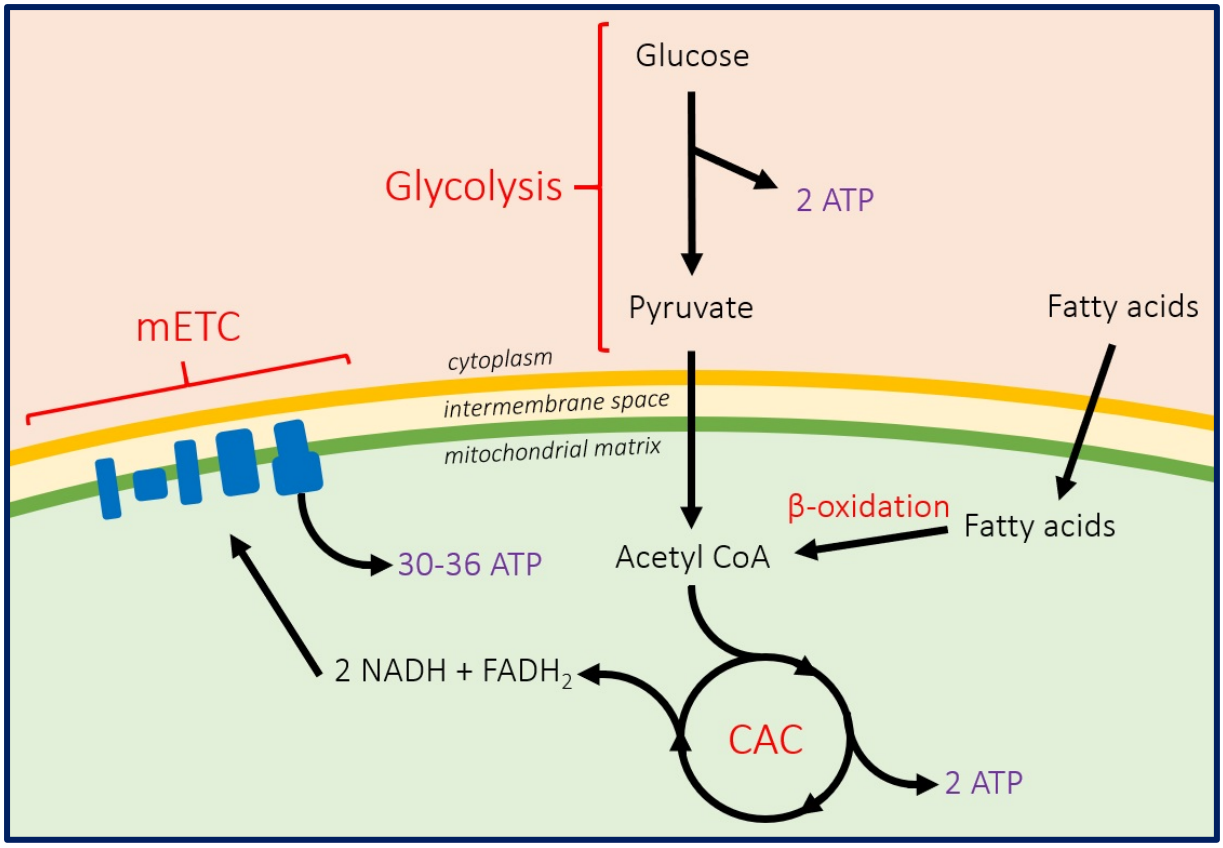

Figure 1.1: ATP production through cellular metabolism.
Glycolysis produces pyruvate through catabolism of glucose. Pyruvate enters the mitochondrial matrix where it is converted to acetyl-CoA. Acetyl-CoA is also produced through β-oxidation of fatty acids. Acetyl-CoA enters the citric acid cycle which regenerates electron donors. Electrons are donated to the complexes of the mETC which produces the greatest amount of ATP.

1.1.1 β-oxidation

Lipids are hydrophobic organic molecules that have multiple roles within the cell, including signal mediation, cell membrane composition, and energy production and are often synthesised from fatty acids (Cullis & de Kruijff, 1979; Murakami, 2011). Fatty acids are comprised of a hydrocarbon chain and terminal carboxylic acid group, and can be classed as either long, medium, or short chain depending on the carbon chain length. Fatty acids can also be either saturated or unsaturated based on the presence of double bonds in the carbon chain (Deng et al., 2017). Fatty acids can either be acquired exogenously or generated endogenously through *de novo* synthesis (Glatz, Luiken, & Bonen, 2010; Weiss et al., 1986). Investigating the processes behind fatty acid uptake and synthesis in chronic lymphocytic leukaemia is a major focus of this thesis.

In terms of their use as an energy source, fatty acids are ultimately broken down by β-oxidation into acetyl-CoA which can enter the CAC. However, fatty acids cannot cross the mitochondrial membranes due to their hydrophobic nature, therefore enzymatic modification of fatty acids are required for them to be transported into the mitochondria (Schulz, 2008). Fatty acids are converted to fatty acyl-CoA and

then to fatty acyl carnitine for transfer across the outer and inner mitochondrial membranes into the mitochondrial matrix. Fatty acyl carnitine is then transformed back into fatty acyl-CoA, which enters the β-oxidation cycle. Subsequent dehydrogenation and modification of the carbon chain results in a chain that is two carbons shorter after each cycle of β-oxidation (Schulz, 2008). One cycle produces an acetyl-CoA molecule which enters the CAC. The amount of ATP produced from a fatty acid molecule depends on the length of the carbon chain, for example, an 18-carbon long fatty acid produces 138 ATP molecules. Additionally, $FADH_2$ and NADH are by-products of this process and are used as electron donors in the mETC. **Figure 1.2** depicts the process of fatty acid metabolism for energy production.

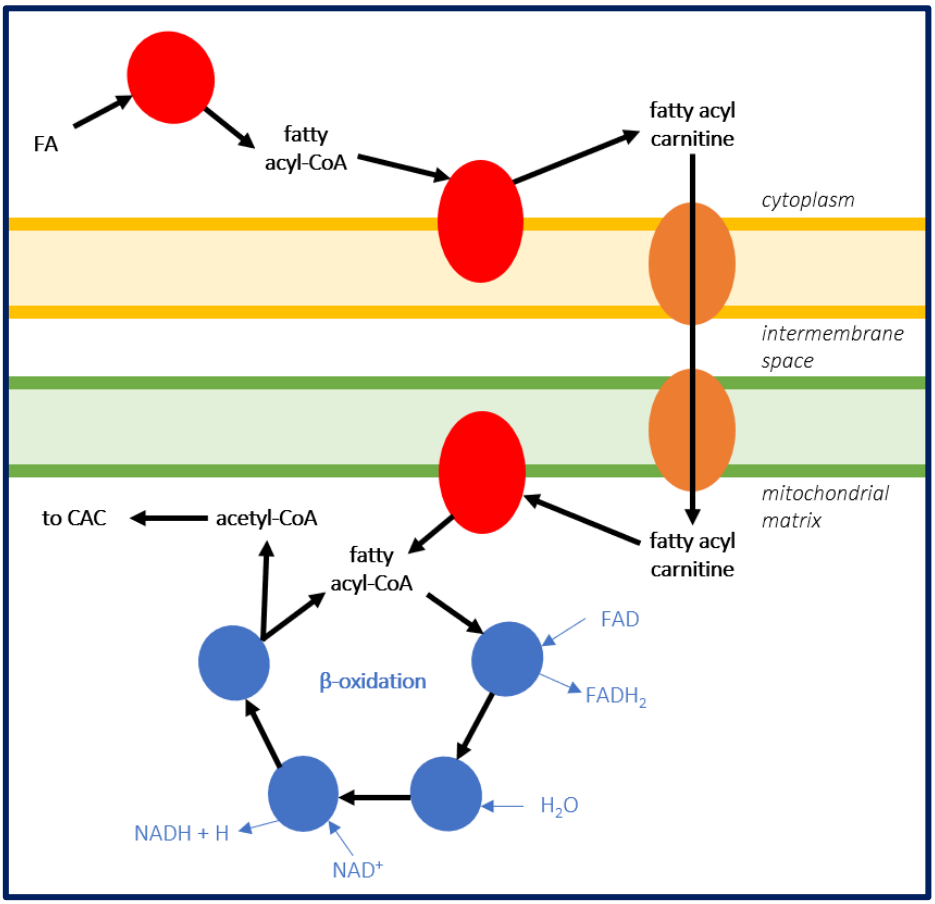

Figure 1.2: β-oxidation of fatty acids results in acetyl-CoA which is fed into the citric acid cycle.
Fatty acids are modified (red) and shuttled (orange) into the mitochondria through the outer (yellow) and inner (green) mitochondrial membranes to the mitochondrial matrix where carbons are removed by β-oxidation enzymes (blue) to form acetyl-CoA which enters the CAC. NADH, $FADH_2$ and water are required for β-oxidation. β-oxidation of the fatty acyl-CoA chain continues until only one acetyl-CoA is remaining.

Altered fatty acid metabolism is associated with many cancers including prostate, ovarian, and breast cancer (DeFilippis et al., 2012; Nieman et al., 2011; Ros et al., 2012). Lipid metabolism is increased in order to meet the high energy demands associated with uncontrolled proliferation, and this is usually achieved through *de novo* fatty acid synthesis (Kuhajda et al., 1994; Ookhtens, Kannan, Lyon, & Baker, 1984). Altered lipid metabolism has also been identified in CLL (Rozovski et al., 2015), and this forms a main area of research within this thesis.

1.1.2 Oxidative phosphorylation

The mETC fuels chemiosmosis which is the main site of ATP production in the cell and can produce between 30 and 36 ATP molecules. A group of enzymes that exist in the inner mitochondrial membrane are used to drive the transfer of protons from the mitochondrial matrix to the intermembrane space. This transfer produces a proton gradient that allows for chemiosmotic ATP regeneration (Nelson & Cox, 2016).

Complexes of the mETC that transfer protons to the inner mitochondrial membrane do this by utilising energy from electrons that are transferred between iron and copper groups within these complexes (Papa et al., 2012). The NADH which is regenerated during both glycolysis and the CAC is an electron donor for complex I of the mETC (NADH-ubiquinone oxidoreductase) which pumps protons across the inner mitochondrial membrane and transfers an electron to the electron carrier coenzyme Q (CoQ; ubiquinone) (Berrisford & Sazanov, 2009; Hunte, Zickermann, & Brandt, 2010). An electron is also donated to CoQ by complex II (succinate dehydrogenase) an enzyme which is also part of the CAC (Cecchini, 2003). Complex II converts succinate to fumarate and $FADH_2$ (flavin adenine dinucleotide) from this process is used for electron transfer to CoQ (Iverson, 2013; F. Sun et al., 2005). CoQ shuttles the electrons from complexes I and II to complex III (CoQ-cytochrome c reductase) which uses the donated electrons to transfer protons across the inner mitochondrial membrane (Trumpower, 2002). Complex III donates electrons to the electron carrier cytochrome c which shuttles the electrons to complex IV (cytochrome c oxidase). Complex IV uses the electrons to reduce oxygen to water and transfer protons across the inner mitochondrial membrane (Kadenbach & Huttemann, 2015; Wikstrom, 1977). The acceptance of protons by oxygen also contributes to the proton gradient across the inner mitochondrial membrane. The energy stored by the proton gradient allows for the regeneration of ATP by complex V (ATP synthase) through the phosphorylation of ADP (Hahn et al., 2016). The process of oxidative phosphorylation is depicted in **Figure 1.3**.

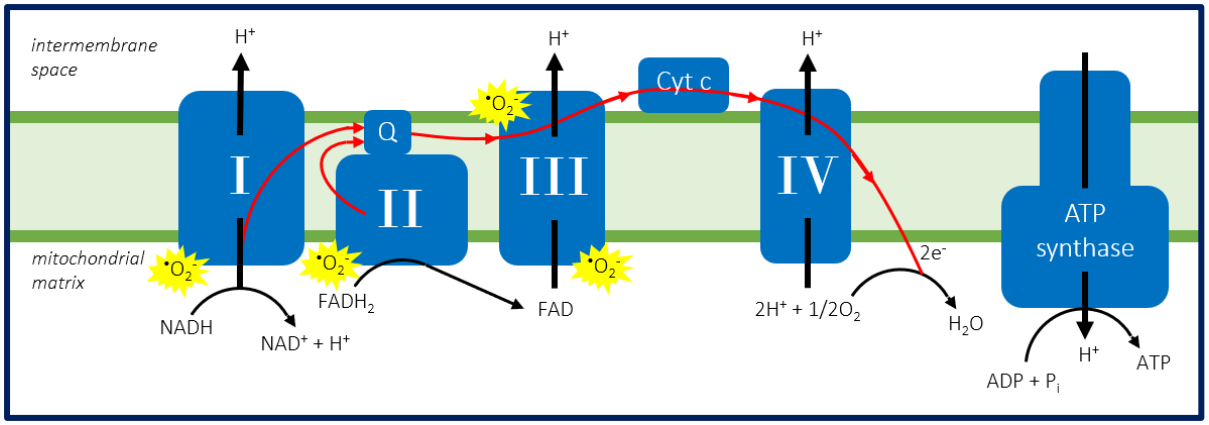

Figure 1.3: The mitochondrial electron transport chain.
The energy obtained from electrons donated to the complexes of the mETC (blue) from NADH and $FADH_2$ is used to pump protons into the intermembrane space, creating a proton gradient. The flow of protons back across the inner mitochondrial membrane is coupled with the generation of ATP. Red, electron flow; yellow, sites of electron leakage and production of superoxide. Adapted from Papa *et al.* (2012).

Although this process seems highly efficient, electron leak in the mETC means that oxygen can be reduced to produce reactive oxygen species (ROS), particularly superoxide and hydrogen peroxide. ROS are a main theme of this thesis and will be discussed in section 1.2. The altered metabolism seen in cancer cells also leads to changes in ROS handling inside the cells, highlighting the importance of understanding the role of ROS in cancer and its relationship with lipid metabolism.

1.2 Reactive oxygen species (ROS)

Reactive oxygen species (ROS) are a family of chemically reactive molecules or ions that are formed by the incomplete one-electron reduction of oxygen (O_2) (Chen, Azad, & Gibson, 2009).The major cellular ROS include the superoxide anion radical ($^{\bullet}O_2^-$), hydrogen peroxide (H_2O_2), and the hydroxyl radical ($^{\bullet}OH$) (Moloney & Cotter, 2018). ROS have important functions in the cell and are generated in different ways (Trachootham, Alexandre, & Huang, 2009).

1.2.1 Sources of ROS

The main source of ROS in the cell is the mETC. In addition, enzymes such as NADPH (nicotinamide adenine dinucleotide phosphate) oxidases, xanthine oxidase, and lipoxygenases are also large generators of ROS (Coyle & Puttfarcken, 1993; Harrison, 2002; Murphy, 2009). The most physiologically relevant sources of ROS will be discussed in this section.

Under physiological conditions, the mETC is one of the most physiologically and pathologically relevant sites of ROS production, with complex I and III being the major producers of superoxide

(Brand, 2010; Hamanaka & Chandel, 2010; Hirst, King, & Pryde, 2008; Kowaltowski, de Souza-Pinto, Castilho, & Vercesi, 2009; Sena & Chandel, 2012). Electron leakage and subsequent reduction of O_2 can occur during the transfer of electrons. In complex I, electrons can leak when transfer occurs between NADH and CoQ. This can also occur when complex III takes on CoQ (Turrens, Alexandre, & Lehninger, 1985). Similarly, electron leakage can occur from $FADH_2$ at complex II (Quinlan et al., 2012). Sites of electron leakage are shown in **Figure 1.3**. The superoxide produced in the mitochondria can be detoxified by the superoxide dismutase (SOD) family of enzymes which will be discussed in section 1.2.3.

Another cellular source of ROS is the NADPH oxidase family of enzymes whose primary role is to generate superoxide. In addition to these internal sources of ROS, external sources can also induce the generation of ROS, these include: ultraviolet light, ionising radiation, chemotherapeutics, inflammatory cytokines and environmental toxins (reviewed in (Finkel & Holbrook, 2000)).

1.2.2 Cellular roles of ROS

The past 30 years have seen an increased exploration of the cellular roles of ROS as they were initially believed to only be harmful species of no physiological importance (Kimura et al., 2005). It is now widely accepted that ROS are vital regulators in many cellular processes including, but not limited to cell signalling, cell growth and death, and gene expression (Ha & Lee, 2005; Zhang et al., 2016). This section will discuss the pathologically relevant roles of ROS.

1.2.2.1 ROS and the cell life cycle

Apoptosis is the process of programmed cell death where cells can actively 'choose' to self-destruct, and ROS and mitochondria play a central role in the initiation of apoptosis. ROS have a two-fold role in this process, whereby in addition to directly acting on the mitochondria, ROS can also activate pathways in the cytoplasm which lead to apoptosis. One example is cytochrome *c*, a key player in the apoptosis signalling cascade. Cytochrome *c* is anchored to the inner mitochondrial membrane by cardiolipin and is released after cardiolipin is oxidised by ROS. In response to ROS, mitochondrial pores open, allowing for the diffusion of cytochrome *c* into the cytoplasm which results in the activation of essential apoptotic proteins (Green & Reed, 1998; Orrenius, Gogvadze, & Zhivotovsky, 2007). Additionally, cytochrome *c* release is blocked by B-cell lymphoma (BCL)-xL and -w proteins which are suppressed when micro RNA (miR)-184 mismatches with BCL mRNA transcripts causing degradation (Wang et al., 2015). This mismatch is caused by the oxidation of miR-184 by ROS, and hence an increase in ROS promotes apoptosis.

Additionally, numerous studies have observed the importance of ROS in the induction of apoptosis by successfully using antioxidants as prevention (Cossarizza et al., 1995; Talley et al., 1995). Fas receptor-

mediated apoptosis is a mechanism where apoptosis is initiated through the binding of the Fas receptor on the surface of a cell to the Fas ligand on the surface of a T-cell (Chiba, Takahashi, Sato, Ishii, & Kikuchi, 1996; Um, Orenstein, & Wahl, 1996). This initiation is blocked in the presence of antioxidants, therefore implicating ROS as key players in this pathway. ROS have also been shown to be involved in the induction of both Fas receptor and Fas ligand gene transcription, and thus ROS play a role in inducing T-cell-mediated cytotoxicity (Bauer et al., 1998; Delneste, Jeannin, Sebille, Aubry, & Bonnefoy, 1996; Hug et al., 1997). In addition, ROS are involved in mediating apoptosis through the detection of ROS by thioredoxin. Thioredoxin is oxidised by ROS and is subsequently disassociated from apoptosis signal-regulating kinase 1 (ASK1), which results in the activation of apoptotic pathways (Saitoh et al., 1998). The role of ROS in cell death is depicted in **Figure 1.4**.

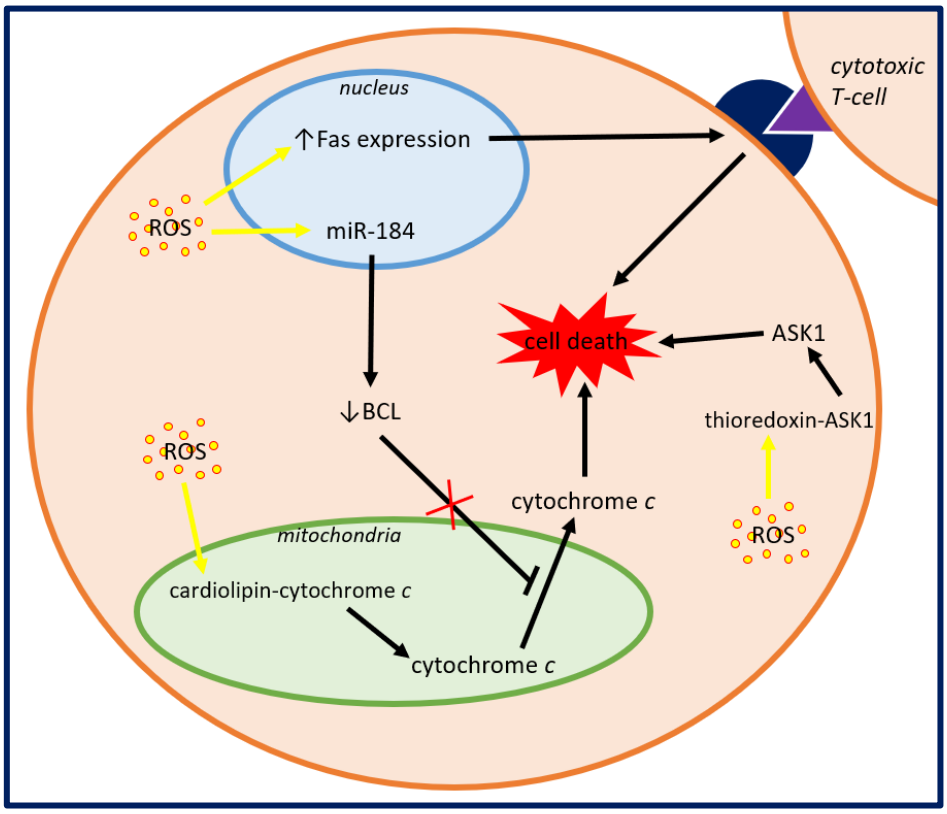

Figure 1.4: ROS play a vital role in cell death.
ROS oxidise cardiolipin allowing cytochrome *c* to be released from the mitochondria (green). ROS oxidise miR-184 causing a decrease in BCL proteins preventing BCL-mediated inhibition of cytochrome *c* release from the mitochondria. Cytochrome *c* activates apoptotic proteins causing cell death. ROS induce Fas gene transcription in the nucleus (blue) causing an increase in Fas ligand (purple) and receptor binding (dark blue) causing T-cell-mediated cell death. ROS oxidises thioredoxin causing its dissociation with ASK1 allowing ASK1 to activate apoptotic pathways.

ROS have also been implicated in cell growth and differentiation; in particular ROS are involved in balancing the regulation between proliferation and death through calcium signalling pathways (Sauer, Wartenberg, & Hescheler, 2001). Interactions between cells cause membrane-bound NADPH oxidases to produce superoxide, which stresses the endoplasmic reticulum causing calcium release that leads to mitochondrial depolarisation and opening of mitochondrial pores, initiating cell death (Baumgartner et al., 2009; Sauer et al., 2001). Additionally, the superoxide produced at complex III has been shown to be important for cellular proliferation through stabilisation of the transcription factor hypoxia-inducible factor (HIF)-1α which is responsible for inducing the transcription of genes associated with proliferation and survival under low-oxygen conditions (Lee, Bae, Jeong, Kim, & Kim, 2004).

Although ROS play a vital role in maintaining cellular homeostasis, they are capable of damaging important cellular components such as lipids, carbohydrates, proteins, and nucleic acids. ROS damage these molecules through oxidation, resulting in an alteration in function of the molecule or its destruction. However, alteration of these macromolecules leads to dysregulation of cell growth and differentiation, therefore playing an important role in the development and progression of cancerous cells (reviewed in (Valko, Rhodes, Moncol, Izakovic, & Mazur, 2006)) which, given the ubiquitous nature of ROS, would quickly result in cellular catastrophe. In order to reduce cellular damage caused by ROS, cellular defence mechanisms have evolved (Davies, 1986; Heffner & Repine, 1989).

1.2.3 Cellular defence against ROS

As mentioned previously, the main species of ROS are superoxide ($^{\bullet}O_2^-$), hydrogen peroxide (H_2O_2), and the hydroxyl radical ($^{\bullet}OH$). These ROS can go on to create more ROS as targets are oxidised. To prevent these targets from being damaged through oxidation, detoxification steps allow ROS to be converted to safer molecules, resulting in a constant flux of ROS. This detoxification is depicted in **Figure 1.5** (Chen et al., 2009; Suzuki, Forman, & Sevanian, 1997; Wood, Schroder, Robin Harris, & Poole, 2003).

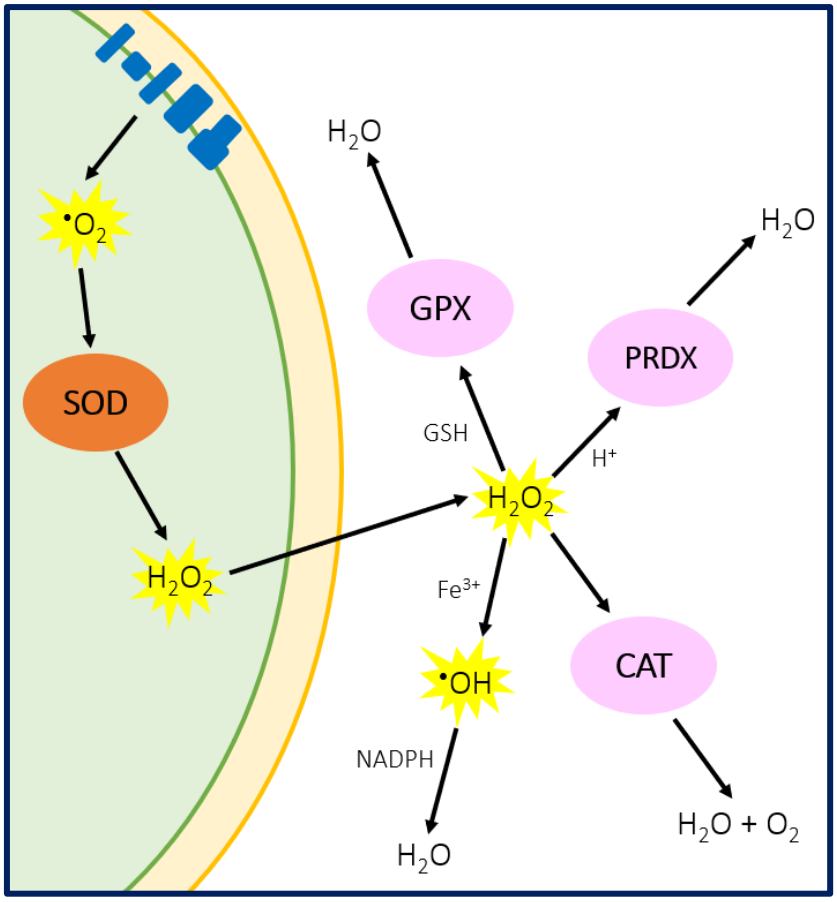

Figure 1.5: The detoxification of superoxide in the cell.
Superoxide is generated by the mETC (blue) and the superoxide dismutase (SOD) family of enzymes convert superoxide to hydrogen peroxide which can diffuse through the inner (green) and outer (yellow) mitochondrial membrane. Hydrogen peroxide can then be converted to water by glutathione (GSH) peroxidase (GPX), peroxiredoxin (PRDX), catalase (CAT), or to hydroxyl radical by ferrous iron (Fe^{3+}). The free radical scavenger NADPH then donates a proton to hydroxyl radical to form water.

An imbalance between ROS generation and antioxidant systems causes oxidative stress which has been linked to various diseases such as cancer, arteriosclerosis, and neurodegenerative diseases (Droge, 2002; Valko et al., 2007). This is potentially due to the dysregulation of important cellular pathways that ROS play vital roles in as mentioned in section 1.2.2.

1.2.3.1 ROS and expression of antioxidants

The Keap1/Nrf-2/ARE transcriptional system induces the expression of genes that are crucial for redox homeostasis. Nuclear factor erythroid 2-related factor 2 (Nrf-2) promotes the transcription of genes that have *cis*-regulatory antioxidant response elements (AREs), and hence promotes the expression of antioxidants (Rushmore, Morton, & Pickett, 1991). Under normal conditions Kelch-like ECH-

associated protein 1 (Keap1) ubiquinates Nrf-2 causing it to degrade, however, under oxidative stress cysteine residues on Keap1 are modified and it loses its ability to ubiquinate Nrf-2 and consequently the expression of antioxidants increases (Keum & Choi, 2014). The AREs are also a target for activator protein-1 (AP-1), a heterodimer of Fos and Jun transcription factors, and hence binding induces expression of antioxidants (Hernandez, Floyd, Weilbaecher, Green, & Boris-Lawrie, 2008; Shaulian, 2010).

A similar regulatory loop exists in the nuclear factor kappa-light-chain-enhancer of activated B-cells (NF-κB) canonical signalling pathway where NF-κB's DNA binding domain is blocked by NF-κB inhibitor proteins (IκB) until they are targeted for degradation (Schreck, Rieber, & Baeuerle, 1991). IκB is targeted for degradation through phosphorylation events that are triggered by ROS (Morgan & Liu, 2011). After degradation of IκB, NF-κB can move into the nucleus where it can act on its target genes (Morgan & Liu, 2011; Xu et al., 1999), one of particular interest is *SOD2* which has been shown to be expressed at a low level in chronic lymphocytic leukaemia and is a main focus of this thesis.

1.3 Chronic Lymphocytic Leukaemia (CLL)

Chronic Lymphocytic Leukaemia (CLL) is the most common form of leukaemia in the western world. CLL is clinically heterogeneous where some patients have an indolent disease course and may never require treatment in their natural life span, while others will suffer from an extremely aggressive disease which requires multiple episodes of treatment (reviewed in (Scarfò, Ferreri, & Ghia, 2016)). Heterogeneity is also represented in the varied progression-free survival time, where patients with a rapidly progressive disease may succumb and die within 3 years, but others may live with the disease for 20 years or longer and often die of non-CLL related causes (Rodriguez-Vicente, Diaz, & Hernandez-Rivas, 2013). CLL primarily affects the elderly, with a median age of 72 years at diagnosis, making this disease increasingly problematic for Australian society due to its aging population (Michallet et al., 2013).

1.3.1 B-lymphocyte biology

B-lymphocytes, like all other cellular components of the blood, are derived from the bone marrow, and mature cells reside within lymphoid follicles of the spleen and lymph nodes. B-lymphocytes are distinguished from T-cells and natural killer cells by the presence of a B-cell receptor (BCR). The BCR is a membrane bound immunoglobulin (Ig) which allows a B-lymphocyte to recognise a specific antigen (Mauri & Bosma, 2012). The major functions of B-lymphocytes are to secrete antibodies, act as antigen presenting cells, and develop immunological memory allowing the body to respond rapidly to subsequent infections (LeBien & Tedder, 2008). There are numerous sub-types of B-lymphocytes including plasma cells and memory cells, which can be segregated by their surface expression of cluster

of differentiation (CD) markers. The diagnosis of CLL and its clinical course, including therapy, will be discussed in this section.

1.3.1.1 CLL biology and symptoms

CLL is characterised by the accumulation of morphologically small, mature, and functionally impaired B-lymphocytes (Melo, Catovsky, & Galton, 1986; Watson, Wyld, & Catovsky, 2008). A peripheral blood lymphocyte count of $\geq 5x10^9$ cells/L sustained over three months with evidence of monoclonality of either kappa (κ) or lambda (λ) BCR surface expression light chains using flow cytometry, and a phenotype of CD5/19 dual positivity are the current diagnostic criteria for CLL (Hallek, Cheson, Catovsky, Caligaris-Cappio, Dighiero, Döhner, et al., 2018). Several haematological factors are used to differentiate between CLL and other leukaemias with similar morphologies such as mantle cell lymphoma: these factors include the characteristic co-expression of the antigens CD19, CD23, CD79b, CD200, CD20, and the aberrant expression of the T-cell antigen CD5 (Palumbo et al., 2009).

Defects in the B-lymphocyte population lead to symptomatic immune complications such as the immune deficiency hypogammaglobulinaemia, which is a reduction in the production of normal immunoglobulin and occurs through functional impairment of B-lymphocytes (Dearden, 2008). Other symptoms of CLL include enlarged lymph nodes, weight loss, and abdominal discomfort due to splenomegaly or enlarged abdominal lymph nodes. The 'crowding out' effect on other blood cell types by CLL B-lymphocytes in bone marrow and lymphatic organs, as well as functional impairment of other cell types (secondary immunoparesis of normal T- and B-lymphocytes), are the cause of many other symptoms in CLL. Overcrowding impairs many functions of T-cells including immune synapse formation and NK cell function as well as the bactericidal ability of neutrophils, cytotoxicity of macrophages, and process of chemotaxis (Dearden, 2008). Additionally, CLL B-lymphocytes functionally impair tumour surveillance by reducing antigen presentation to T-lymphocytes and disturbing the cytokine-induced response to the presence of the tumour cell itself (Riches, Ramsay, & Gribben, 2010). Also observed in CLL are a significant number of commonly reoccurring infectious complications which account for approximately 30-50 % of all deaths largely representing a failure of immunoglobulin production and bacterial pneumonias and T-lymphocyte dysfunction in the recurrence of herpes infections including Zoster and Simplex (Clifford & Schuh, 2012; Dearden, 2008; Francis et al., 2006).

The main tissue sites of CLL B-lymphocyte production are the bone marrow, lymph nodes, and spleen, of which the lymph nodes appear to be the predominant site of proliferation (Herishanu et al., 2011; Herreros et al., 2010). Homing surface molecules on and chemokines secreted by nodal accessory cells cause CLL B-lymphocytes in the circulation to infiltrate these sites and causes replication (Han, Fan, Li, & Xu, 2014).

1.3.2 CLL prognostication

CLL has different stages of clinical progression which are currently determined by clinicians using the Rai and Binet systems. These systems are based on lymphocyte count, the presence of anaemia and thrombocytopenia as well as various clinical features such as hepatomegaly, lymphadenopathy, and splenomegaly (Binet et al., 1977; Rai et al., 1975). At present, molecular markers are also incorporated, and are proving to assist in the prediction of disease course (Bulian et al., 2011; Sellner, Dietrich, Dreger, Glimm, & Zenz, 2012; Stamatopoulos et al., 2010). The range of biomarkers used for predicting disease course includes surface expression of CD49d and CD38 (section 1.3.2.3), immunoglobulin heavy chain variable gene (*IGHV*) mutational status (section 1.3.2.2), and serum parameters including β_2 microglobulin (B2M), thymidine kinase 1 (TK1), and lactate dehydrogenase (Bulian et al., 2011; Rai & Jain, 2011; Rodriguez-Vicente et al., 2013).

There are several serum parameters used to predict the disease course of CLL. B2M is a component of the major histocompatibility class I molecule and is constitutively released by CLL B-lymphocytes (Simonsson, Wibell, & Nilsson, 1980; Vilpo, Vilpo, Hurme, & Vuorinen, 1999). Serum B2M levels are therefore indicative of tumour load and can be used to predict disease course in the early stages of CLL with B2M-negative cases having a longer treatment-free survival (Gentile et al., 2009). TK1 is involved in DNA synthesis (He, Skog, Wang, Eriksson, & Tribukait, 1996), and hence serum TK1 is indicative of the proliferative capacity of CLL B-lymphocytes and is used to predict disease progression in CLL (Hallek et al., 1999; Hallek et al., 1996). LDH levels appear to have some prognostic significance in specific cases of CLL and have been reported as an independent prognostic factor in treatment-naïve trisomy 12 (Autore et al., 2019) and in a Chinese cohort (Liu et al., 2016). However, LDH is not prognostically significant generally in CLL. Elevations in LDH however, may predict Richter's transformation in CLL (Khan, Siddiqi, & Thompson, 2018).

1.3.2.1 Cytogenetic abnormalities in CLL

In addition to the molecular markers, there are several cytogenetic abnormalities that commonly occur in CLL. Chromosomal abnormalities are currently detected by fluorescence *in situ* hybridisation (FISH), a large-scale genetic visualisation tool, which was adapted and applied by Döhner *et al.* (2000), to investigate, identify, and quantify chromosomal abnormalities in CLL. Underlying biological effects and phenotypes have been identified through detection of chromosomal abnormalities, rendering these accurate predictive indicators for response to therapy. Chromosomal abnormalities are now primary prognostic indicators due to the relative ease of FISH analysis (Sagatys & Zhang, 2012). Australia is currently moving towards using single nucleotide polymorphism (SNP) arrays for the detection of chromosomal abnormalities, which can detect a wider number of genetic aberrations.

The most common chromosomal abnormality in CLL is a deletion in 13q14, which is found in approximately 50 % of patients. This lesion indicates an indolent disease course and a longer overall survival time (Dohner et al., 2000; Giertlova et al., 2011). The intermediate indicator, trisomy 12, occurs at a frequency of approximately 16 %, while del17p and del11q, occur at frequencies of approximately 8-15 %, depending on the patient cohort, and 19 %, respectively. Both del17p and del11q predict an aggressive disease course. **Figure 1.6** shows the survival probability of patients with the chromosomal abnormalities mentioned above.

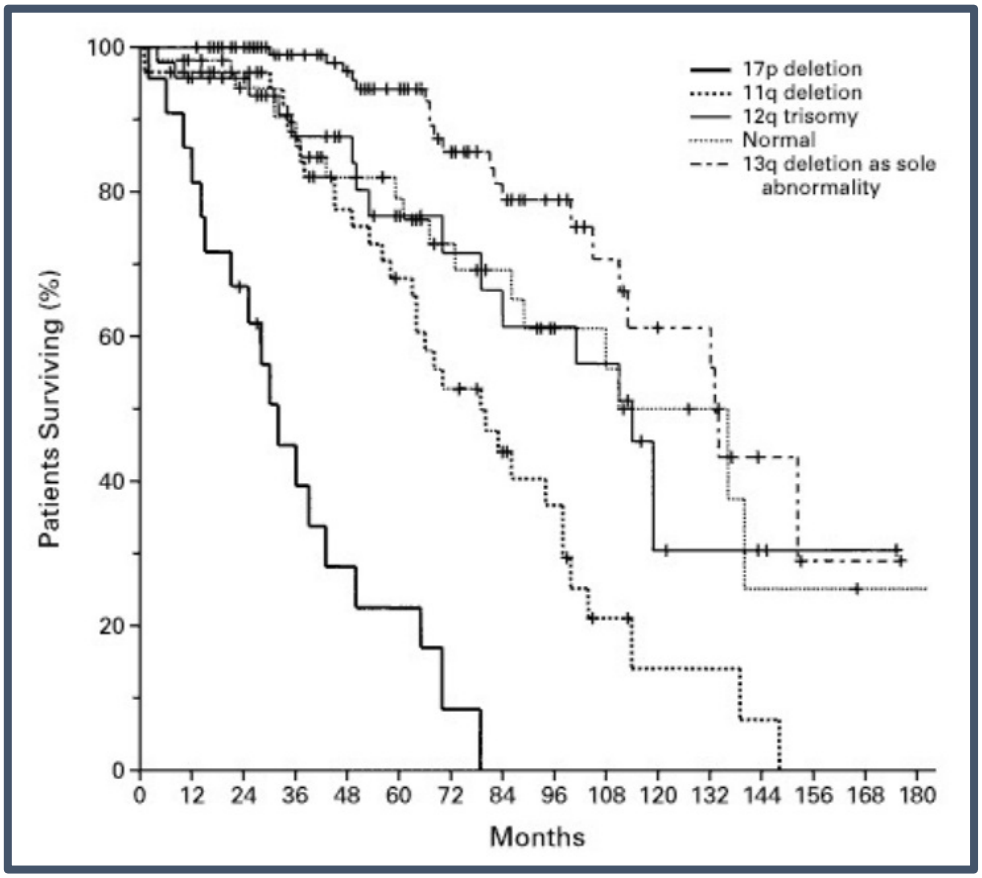

Figure 1.6: Probability of survival from the date of diagnosis among CLL patients with chromosomal abnormalities.
The Kaplan-Meier plot shows the overall survival, in months, of CLL patients with a chromosomal abnormality. Thick solid line, del17p; thick dotted line, del11q; thin solid line, trisomy 12; thin dotted line, normal karyotype; dashed line, single del13p as sole abnormality. Reproduced with permission from Döhner *et al.* (2000), copyright Massachusetts Medical Society.

1.3.2.1.1 Cytogenetic abnormalities that infer an indolent disease course

The minimum deleted region (MDR) for the del13q abnormality includes the first exon of *DLEU1*, the *DLEU2* locus, and the miR15a/16 cluster (Y. Liu et al., 1997). *DLEU1* and *DLEU2* are non-coding

RNAs, however, their function is unknown (Wolf et al., 2001). miR15a/16 act as a tumour suppressor by inhibiting the expression of the *BCL2* oncogene through RNA interference, and therefore a decrease in expression of these micro-RNAs leads to increased Bcl-2 expression and resistance to apoptosis (Calin et al., 2002). The tumour suppressor gene *RB1* can also be deleted in del13q CLL causing improper regulation of the cell cycle and hence cellular proliferation is promoted (Ouillette et al., 2011). The 13q14 deletion has also been associated with increased expression of several cell cycle-related genes which play a role in the transition of cells from the quiescent phase to the replicative phase (Klein & Dalla-Favera, 2010; Srivastava, Tsongalis, & Kaur, 2013). These appear to be early clonal mutations; however, mechanisms for this indolent disease course remain unclear.

It is also unclear as to why the trisomy 12 abnormality causes an intermediate disease course (Sellner et al., 2012). However, it is believed that an extra copy of the *MDM2* gene, encoding a negative regulator of the tumour suppressor p53, is responsible for the intermediate disease progression observed in these CLL patients (Watanabe et al., 1994).

1.3.2.1.2 Cytogenetic abnormalities that infer an aggressive disease course

In the del17p abnormality, a deletion in 17p13 causes the elimination of one *TP53* allele. The protein which is coded for by the *TP53* gene, p53, is involved in many cellular pathways such as apoptosis, autophagy, cellular metabolism, and DNA repair (Green & Kroemer, 2009; Sullivan, Gallant-Behm, Henry, Fraikin, & Espinosa, 2012; Vousden & Lane, 2007). A minority of del17p patients exhibit an indolent disease course due to the deletion of only one *TP53* allele whilst retaining some p53 function. However, approximately 80 % of del17p CLL patients experience a complete loss of p53 function due to a mutation in the remaining *TP53* allele rendering it non-functional (Dohner et al., 2000; Zenz, Benner, Dohner, & Stilgenbauer, 2008). These patients have an aggressive disease course with an overall survival of 32 months even with chemoimmunotherapy (**Figure 1.6** (Dohner et al., 2000). The incidence of *TP53* incompetence increases at relapse post-immunochemotherapy resulting in more aggressive and resistant disease. Chemoimmunotherapy is often avoided in this patient subset as new targeted therapies give more favourable responses (O'Brien et al., 2018; Stilgenbauer et al., 2016).

The del11q chromosomal abnormality occurs in 19 % of CLL patients at diagnosis, and the MDR includes the Ataxia-telangiectasia mutated (*ATM*) allele (Carter et al., 2006). The resulting protein coded for by the *ATM* gene, ATM, is a key player in the DNA damage response pathway, and therefore extremely important in cellular homeostasis (Harper & Elledge, 2007). The deletion of 11q associates in a bulky lymphadenopathy (BLA) disease phenotype with shortened response times to fludarabine-based therapy (Joshi et al., 2007). These patients have an overall survival time of 79 months (**Figure 1.6**) (Dohner et al., 2000). Interestingly, ATM has also been shown to respond to oxidative stress, a function that could be of great importance in CLL, as CLL B-lymphocytes have been shown to have higher intracellular ROS levels compared to normal B-lymphocytes (Z. Guo, Kozlov, Lavin, Person, &

Paull, 2010; Jitschin et al., 2014). This function may be key to the survival of CLL B-lymphocytes in a bulky, hypoxic microenvironment as hypoxia results in an increase in ROS generation at complex III of the mETC (Guzy et al., 2005). Also located on 11q is the *BIRC3* gene, a negative regulator of the non-canonical NF-κB pathway, and deletion or inactivating mutations in this gene are associated with a chemo-refractory phenotype irrespective of *IGHV* mutational status or *TP53* aberrations (Rossi, Fangazio, et al., 2012). In addition, mutations in the *SF3B1* gene are associated with del11q CLL (L. Wang et al., 2011) and are predictive of a shorter TTFT and overall survival (Nadeu et al., 2016).

Furthermore, activation of the Notch receptor 1 results in translocation of the intracellular subunit to the nucleus and induces the expression of genes associated with survival and proliferation (Kopan & Ilagan, 2009). In CLL, mutations in the *NOTCH1* gene (Sportoletti et al., 2010) prevent proteasome-dependent degradation of the intracellular subunit resulting in the constitutive activation of the NOTCH1 signalling pathway (Rosati et al., 2009) and occur in approximately 10 % of CLL cases at initial diagnosis. NOTCH1 mutations are associated with resistance to the anti-CD20 monoclonal antibody rituximab (Stilgenbauer et al., 2014), are enriched in chemo-refractory and unmutated *IGHV* cases (Del Poeta et al., 2013) and can are independent predictors of decreased overall survival (Rossi, Rasi, et al., 2012).

1.3.2.2 *IGHV* mutational status

The BCR, encompassing either IgM, IgD, IgG, IgA, or IgE monomers, is responsible for the recognition of foreign antigens through the Ig variable regions, which ultimately regulates cellular metabolism, survival, differentiation, proliferation, and migration (Brander, Allgood, Bond, Weinberg, & Lanasa, 2011; Efremov, Wiestner, & Laurenti, 2012; Wiestner, 2012). The primary function of the BCR in germinal centres is to capture and present antigens to T-lymphocytes, thereby initiating an immune response. The process of somatic hypermutation of the *IGHV* gene can alter the affinity of the BCR for antigens as the more mutated the V-region is, the more specific binding between antigen and BCR must be for activation. When B-lymphocytes are activated through the BCR, proliferation in the germinal centre of lymph nodes is promoted, and therefore an over-activated BCR leads to higher levels of proliferation of B-lymphocytes.

In 1999, Hamblin *et al.* reported that the presence of mutations in the *IGHV* gene is associated with stable disease and a better prognosis (Hamblin, Davis, Gardiner, Oscier, & Stevenson, 1999). As **Figure 1.7** shows, survival of CLL patients with unmutated *IGHV* was significantly lower (117 months) compared to CLL patients with mutated *IGHV* (293 months) (Hamblin et al., 1999). This is believed to be due to over-activation of the BCR signalling pathway which is vital for growth and survival of CLL B-lymphocytes (Rai & Jain, 2016; Stevenson, Krysov, Davies, Steele, & Packham, 2011).

In CLL, unmutated *IGHV* cases are associated with the expression of CD38 and ZAP-70, which are markers for poor prognosis and will be discussed in the next section (Damle et al., 1999; Hamblin et al., 1999).

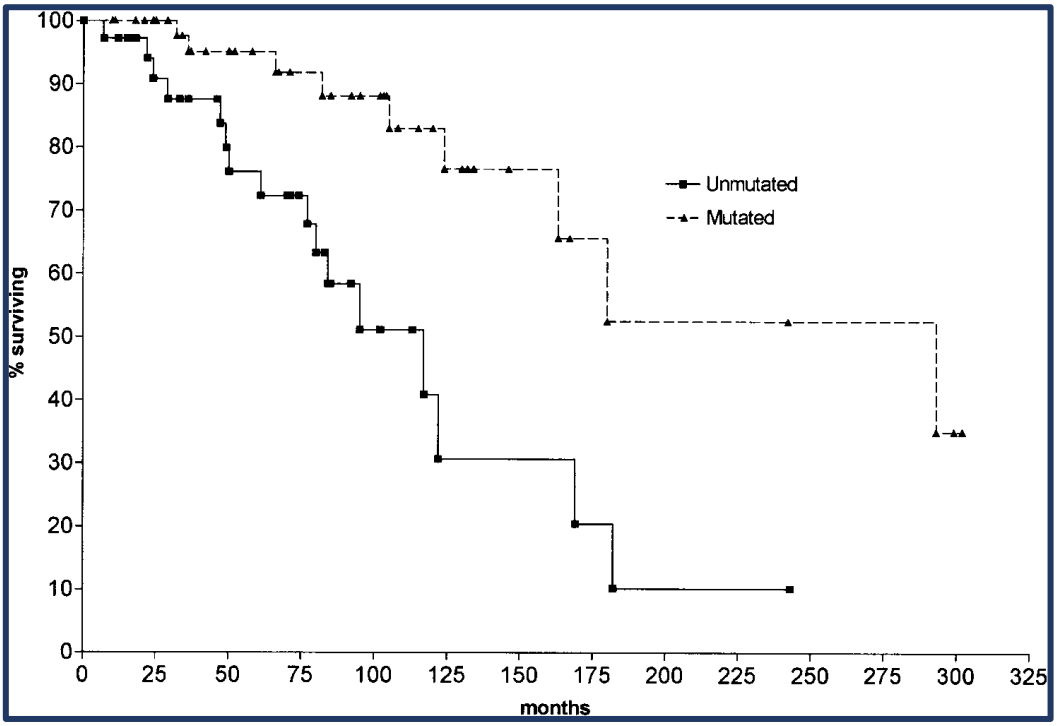

Figure 1.7: Probability of survival from the date of diagnosis among CLL patients with mutated and unmutated *IGHV*.
The Kaplan-Meier plot shows the overall survival, in months, of CLL patients based on their *IGHV* mutational status. Solid line, unmutated *IGHV*; dashed line, mutated *IGHV*. Reproduced with permission from Hamblin *et al.* (1999), copyright American Society of Hematology.

1.3.2.3 Prognostication using molecular markers

Homing of CLL cells to the microenvironment causes them to receive survival signals and therefore promotes proliferation. The CD marker CD44 is an important player in the crossing of CLL cells from the circulation into lymphoid organs, where they receive these survival signals (Gutjahr, Greil, & Hartmann, 2015). In addition, CD49d plays a role in adhesion, and implantation of cells, as well as homing of CLL cells to the microenvironment (Shahjahani et al., 2015). CD49d promotes proliferation and survival through interaction with stromal cells in the CLL microenvironment causing an upregulation of anti-apoptotic proteins (Hayashida, Shimaoka, Ochi, & Lipsky, 2000; Koopman et al., 1994; Shanafelt et al., 2008). CD49d expression is a strong predictor of overall survival with high expression associated with a poorer prognosis (Bulian et al., 2014). CD38 is a membrane-bound protein

responsible for signal transduction and proliferation during lymphocyte development (Funaro & Malavasi, 1999; Malavasi et al., 1994). This marker is not present on normal mature B-lymphocytes in the circulation; however, it can be present on the surface of CLL cells. Similarly, CD38 associates with surface homing molecules enhancing homing to lymphoid tissues (Vaisitti et al., 2010), and is able to induce intracellular calcium signalling promoting cellular proliferation through the conversion of NAD^+ and $NADP^+$ to ADP signalling mediators (Howard et al., 1993). The presence of these molecules on CLL cells can increase their survival capabilities and alter their interaction with other cells. This, therefore, with the aid of other cells, presumably allows CLL B-lymphocytes to proliferate and migrate and thereby conferring an aggressive disease.

Zeta-chain-associated protein kinase 70 (ZAP-70) is a member of the protein tyrosine kinase family and plays a role in T-cell antigen receptor signalling. This signal transduction mediates T-cell development and activation (Chu, Morita, & Weiss, 1998). The ZAP-70 gene is normally expressed in T and NK cells, and has been shown to be expressed in pro/pre B-lymphocytes, but not mature B-lymphocytes (Crespo et al., 2006). The expression of ZAP-70 in CLL causes an activation of pro-survival signals and increased migration due to an increased cellular response to chemokines (J. Burger, 2012; J. Burger & Chiorazzi, 2013). This enhanced migration of CLL B-lymphocytes and increase in pro-survival signals causes the disease to take on an aggressive form, and so ZAP-70 expression appears to be an ideal prognostic indicator, however measurement is technically difficult and so has not been widely adopted (Admirand et al., 2010; Mertens & Stilgenbauer, 2014).

Unfortunately, even with this large variety of prognostic molecular markers, any one or combination of markers is unable to provide an accurate prediction of disease course for the individual. This could be due to yet undiscovered abnormalities in CLL B-lymphocytes that allows the disease to behave unpredictably.

1.3.3 CLL treatment

After diagnosis, the primary approach to CLL treatment depends on the initial presentation of the disease. If the disease initially presents as aggressive, with severe cytopenia, then standard therapy is initiated (Hallek, Cheson, Catovsky, Caligaris-Cappio, Dighiero, Dohner, et al., 2018). The current agents used in the standard treatment of CLL include the chemotherapy agents fludarabine, a purine analogue, and cyclophosphamide, an alkylating agent; and the anti-CD20 antibody, rituximab (MabThera; RTX). For patients who initially present with non-aggressive disease, the primary response is to monitor blood lymphocyte counts and clinical disease behaviour in a ‘watch and wait’ manner. If the disease progresses, and patients become symptomatic, treatment is initiated. The treatment chosen must be suitable to the age and comorbidities of the patient and also the underlying biology of the disease.

1.3.3.1 Chemotherapy

Fludarabine is metabolised to the active F-ara-ATP, which blocks DNA synthesis and repair pathways (Ricci, Tedeschi, Morra, & Montillo, 2009). Cyclophosphamide also works to disturb nucleic acid metabolism and interferes with DNA replication by causing the addition of alkyl groups to DNA (Veal et al., 2016).

Both fludarabine and cyclophosphamide aim to disrupt DNA synthesis, leading to the initiation of apoptosis and cell death. The unwanted effects of exposure to these chemotherapeutic agents includes DNA damage in both myeloid and lymphoid cells. This increases the risk of myelodysplasia and of irreparable DNA damage in clonal CLL cells, particularly those with defective DNA damage repair mechanisms such as *ATM* deleted and *TP53* deleted CLL. It has long been presumed that the development of new, targeted therapies that do not rely on these pathways to initiate cell death may improve the disease course and outcome of patients with these aberrations.

1.3.3.2 Targeted therapy

New therapeutic strategies have been implemented in the last two decades following outstanding improvements in the treatment of other lymphoid malignancies with anti-CD20 monoclonal antibodies (mAbs).

The CD20 transmembrane cellular protein is a validated therapeutic target for the treatment of B-lymphocyte malignancies ((Marshall, Stopforth, & Cragg, 2017)) (Cragg, Walshe, Ivanov, & Glennie, 2005). CD20 is present on the cell surface from the initial pre-B-lymphocyte stage until their differentiation into plasma cells, however, is not expressed on haematopoietic stem cells (Stashenko, Nadler, Hardy, & Schlossman, 1980). CD20 predominantly exists as a tetramer on the cell surface and is neither shed nor internalised upon antibody binding. This indicates that immune effector cells are recruited, and sustained immunologic activity is mediated in response to antibody binding (Glennie, French, Cragg, & Taylor, 2007). Although the physiological function of CD20 remains unclear (Cragg et al., 2005), its involvement in calcium signalling downstream of BCR activation has been suggested (Polyak, Li, Shariat, & Deans, 2008). The development and use of anti-CD20 mAbs for the treatment of CLL has remarkably improved the clinical outcome of CLL patients (C. Tam et al., 2008).

RTX is a type I anti-CD20 monoclonal antibody used in first-line treatment of CLL. RTX binds to the large extracellular loop of the CD20 surface marker (**Figure 1.8**), and induces complement-dependent cytotoxicity (CDC) as a primary means of causing cell death (Huhn et al., 2001). RTX also causes antibody-dependent cellular cytotoxicity (ADCC) (Huhn et al., 2001). The combination of RTX with fludarabine and cyclophosphamide (FCR) is proving to be a successful therapy in both initial treatment of CLL (Tam et al., 2008) and relapse refractory CLL (Wierda et al., 2005), and it is effective at

prolonging progression-free survival (PFS) in CLL patients compared to fludarabine alone (Byrd et al., 2005) and a combination of fludarabine and cyclophosphamide (Hallek et al., 2010).

Ofatumumab (OFA) is a type I, humanised anti-CD20 monoclonal antibody, and was approved for treatment of CLL in 2009 (National Cancer Institute, 2014). OFA binds to the small and large extracellular loops of the CD20 surface marker (**Figure 1.8**), and subsequently induces ADCC and CDC (Klein et al., 2013). OFA has been shown to be a more potent mediator of CDC than RTX in preclinical studies (Pawluczkowycz et al., 2009), however, it has only been approved for the treatment of fludarabine-refractory CLL (Grosicki, 2015).

Obinituzumab (GA101) is a type II, humanised anti-CD20 monoclonal antibody, and was approved for treatment of CLL in 2013 (Institute, 2013). GA101 binds the large extracellular loop of the CD20 surface marker (**Figure 1.8**), and induces direct cell death, ADCC, and CDC (Mossner et al., 2010). GA101 is a more potent mediator of direct cell death and ADCC than type I anti-CD20 mAbs RTX and OFA, however, exhibits decreased CDC activity (Goede, Klein, & Stilgenbauer, 2015; Mossner et al., 2010; Niederfellner et al., 2011).

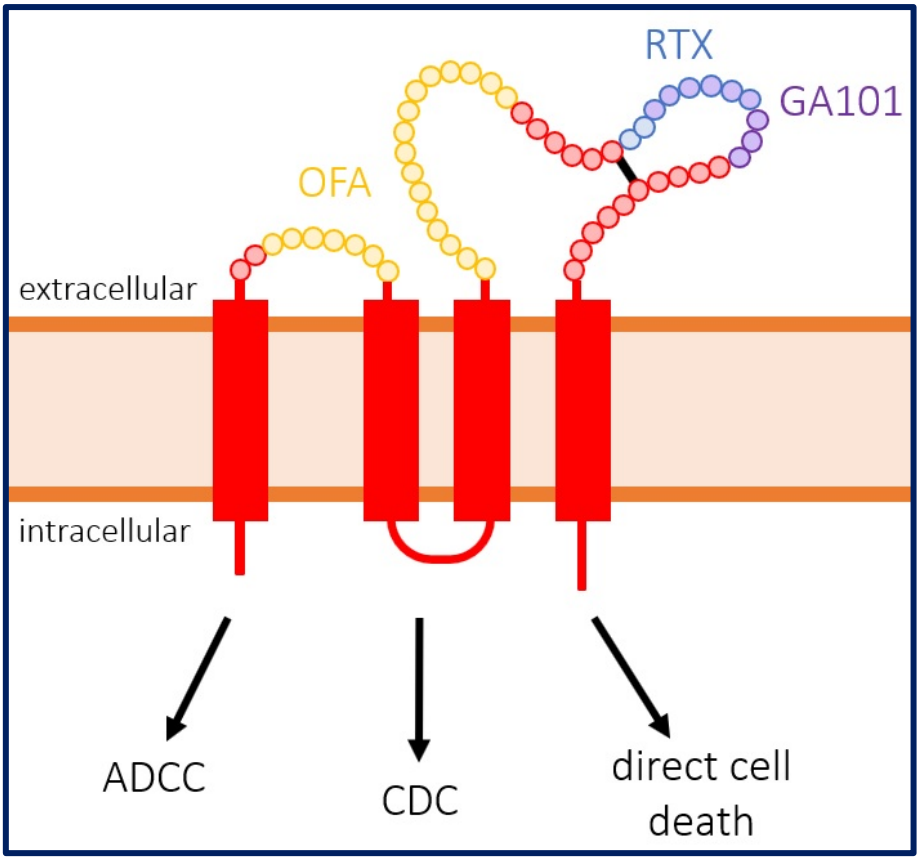

Figure 1.8: Schematic diagram of the CD20 surface receptor and the binding sites of anti-CD20 therapies; RTX, OFA, and GA101.
RTX and GA101 bind the large extracellular loop of the CD20 surface marker while OFA binds to both the large and small extracellular loops. Binding of these anti-CD20 mAbs to CD20 can lead to ADCC, CDC, and direct cell death. Red, CD20; orange, cell membrane; black, disulphide bond; yellow, OFA epitope; blue, RTX epitope; and purple, GA101 epitope. Modified from Klein *et al.* 2013.

Ibrutinib is a small molecular inhibitor of the BCR signalling kinase Bruton's tyrosine kinase (BTK) (Byrd et al., 2014) (**Figure 1.9**). As mentioned in section 1.3.2.2, the BCR is vital for the survival and growth of CLL B-lymphocytes. Ibrutinib binds irreversibly and blocks the BCR signalling cascade which is overactive in CLL (Honigberg et al., 2010). Not only does this drug inhibit downstream survival pathways but has also been shown to interrupt the migration of CLL B-lymphocytes to the microenvironment where proliferation occurs (Ponader et al., 2012). Ibrutinib also irreversibly binds to the T-cell interleukin (IL)-2-inducible kinase which results in T-cells increasing their tumour surveillance (Dubovsky et al., 2013). The success of ibrutinib in the treatment of CLL is reflected in the clinical trial data. The use of ibrutinib as first-line treatment has been shown to be more effective than cyclophosphamide and results in longer PFS regardless of disease stage, age, and several factors that infer poor prognostication (Burger et al., 2015). It was also shown to improve PFS when compared

to ofatumumab monotherapy in relapsed/refractory CLL (Byrd et al., 2014). Ibrutinib is also more effective in del11q and unmutated *IGHV* CLL than immunochemotherapy, which raises the question about how the specific biology of these subtypes of CLL differs to other subtypes, allowing ibrutinib to be effective.

Although ibrutinib is generally a successful therapy, mutation of a cysteine residue (C481S) in the binding site of BTK causes ibrutinib to bind reversibly, not irreversibly, and is thought to be one of the main causes of ibrutinib resistance (Woyach et al., 2014). Additionally, mutations (R665W and L845F) in phospholipase C γ2, which is important in B-lymphocyte development, have been identified in CLL (Woyach et al., 2014). Therefore, second and third generation BTK inhibitors have attempted to increase specificity and, in some cases, despite ibrutinib resistance (Tam et al., 2019).

Idelalisib also targets the BCR by inhibiting the delta isoform of phosphoinositol 3-kinase (PI3Kδ), and was approved for use in relapsed/refractory CLL in combination with RTX in 2014 (Furman et al., 2014) (**Figure 1.9**). Like ibrutinib, idelalisib has been shown to inhibit the homing and retention of CLL B-lymphocytes to the microenvironment and induces cell death (Davids et al., 2012; Hoellenriegel et al., 2011; Lannutti et al., 2011). Clinical trial data showed that a combination of idelalisib and RTX significantly increased the overall survival of patients compared to RTX alone (Furman et al., 2014). However, the side effect profile with this drug has limited its clinical application (Cuneo et al., 2019).

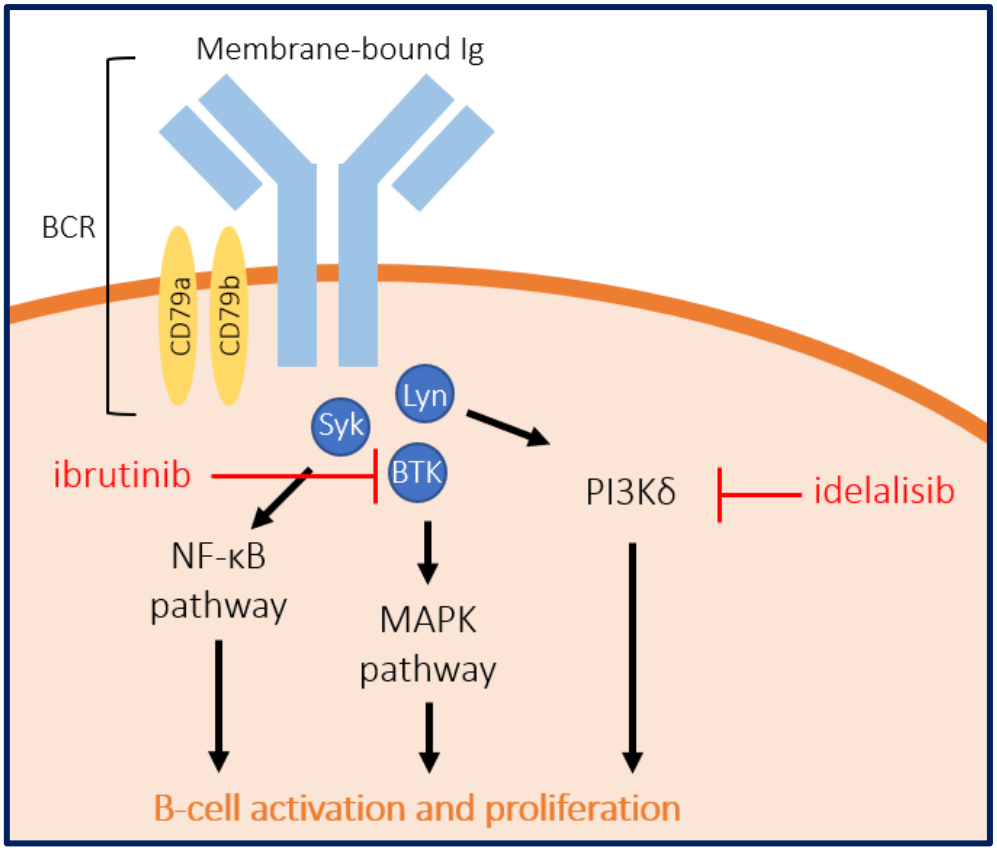

Figure 1.9: BCR signalling pathway targets by ibrutinib and idelalisib.
Ibrutinib and idelalisib prevent B-lymphocyte activation and proliferation. Ibrutinib inhibits BTK (dark blue) preventing mitogen-activated protein kinase (MAPK) signalling, and idelalisib inhibits PI3Kδ preventing PI3K signalling. BCR comprising membrane-bound immunoglobulin (light blue) and CD79a and b dimer (yellow). Signalling kinases Syk, Lyn and BTK (dark blue) with respective pathways. Modified from (Weinberg & Friedman, 2013).

1.4 Energy metabolism in CLL

Metabolic reprogramming is a hallmark of cancer and a promising target for therapeutic development. One of the most important changes in cancer cellular bioenergetics is the preferential use of glycolysis for ATP production – and this phenomenon was coined 'the Warburg effect' and is also referred to as 'aerobic glycolysis' (Warburg, 1956a, 1956b; Warburg, Posener, & Negelein, 1930). This metabolic change attracted the use of positron emission tomography (PET) scanning using radiolabelled glucose (fluorine-18 fluoro-deoxyglucose; FDG) to identify sites of cancer growth in the human body (Basu et al., 2011). An example of a FDG-PET scan in an individual with a lymphoma elevated glucose metabolism can be seen in **Figure 1.10 A**. Interestingly, FDG-PET scans in individuals with CLL fail to identify sites of rapid FDG uptake compared to individuals with other lymphoid malignancies (Karam et al., 2006). **Figure 1.10 B** shows the typical low level uptake of FDG observed in individuals with CLL which is measured by Standardised Uptake Values (SUV) which are characteristically <10 in CLL

compared to 30-40 in aggressive lymphomas including Richter's transformation of CLL (Falchi et al., 2014).

In the mid twentieth century it was found that CLL B-lymphocytes have decreased glucose metabolism compared to healthy controls and it has been observed that aerobic glycolysis it not overly active in CLL B-lymphocytes (Brody & Merlie, 1970; Brody, Oski, & Singer, 1969; Jitschin et al., 2014). Additionally, it was found that glycolytic end products had limited entry into the CAC (Tili et al., 2012). These findings suggest that CLL B-lymphocytes do not use glucose as their primary source of energy, and that there is another energy source that they utilise in order to meet energy demands. It is now widely accepted that CLL B-lymphocytes utilise lipids as their primary energy source and this will be discussed in the following section.

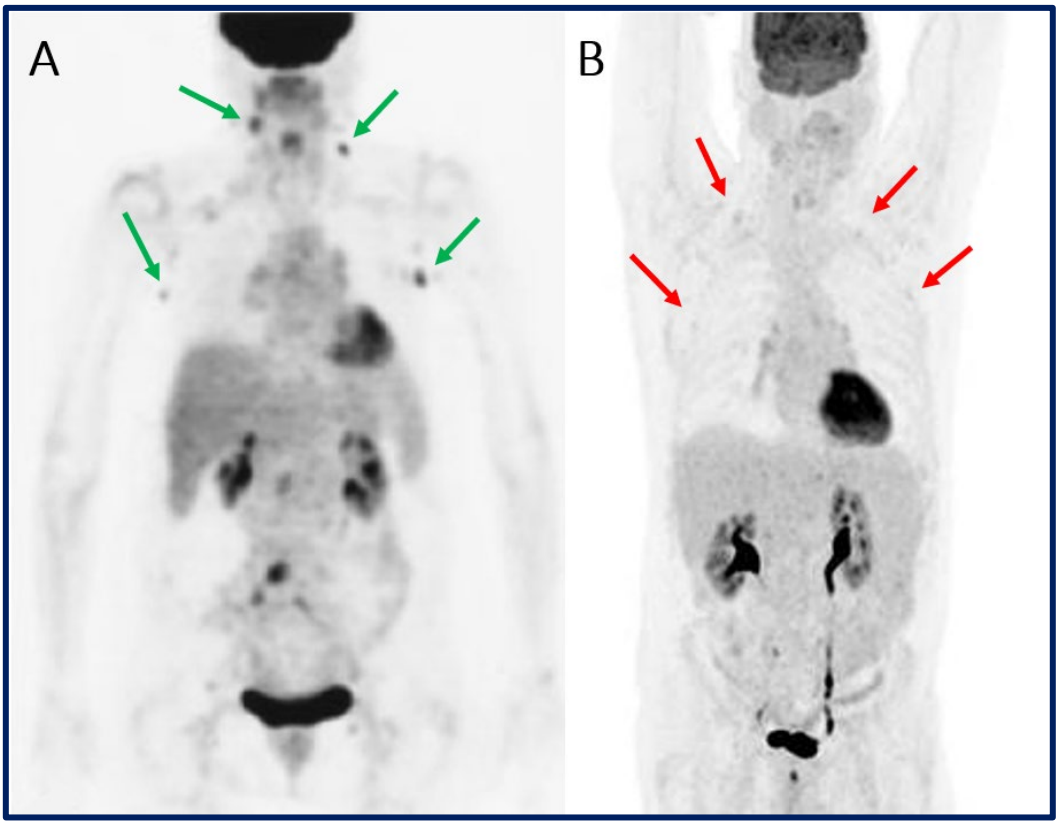

Figure 1.10: FDG-PET scans in individuals with CLL demonstrate low level uptake. Examples of FDG-PET of **A**, an individual with grade 1 follicular lymphoma, and **B**, an individual with CLL. Green arrows, high FDG uptake; red arrows, low FDG uptake. Note the non-pathological uptake of FDG into the heart and brain, and the excretion route through the kidneys and bladder. **A**, reproduced with permission from Karam *et al.* (2006), copyright of John Wiley and Sons. **B**, Molecular Medicine & Genetics, Flinders University clinical data.

1.4.1 Lipid metabolism in CLL

There are several lines of evidence that suggest that lipids are a critical energy source in CLL. The blood cholesterol lowering drugs statins, have previously been shown to induce apoptosis in CLL B-lymphocytes, and individuals with CLL taking statins at the time of diagnosis had a significantly reduced need for initial therapy (Chapman-Shimshoni, Yuklea, Radnay, Shapiro, & Lishner, 2003; Vitols, Angelin, & Juliusson, 1997). CLL B-lymphocytes oxidise more palmitate compared to healthy B-lymphocytes (Spaner et al., 2013), and additionally, orlistat, an inhibitor of fatty acid synthesis, has been shown to be toxic to CLL B-lymphocytes (Pallasch et al., 2008).

The rate of fatty acid oxidation in CLL B-lymphocytes is likely due to the availability of free fatty acids which serve as ligands of the nuclear receptor peroxisome proliferator-activated receptor-alpha (PPARα) which acts as a transcriptional regulator for oxidative phosphorylation genes (Kersten, 2014). Additionally, PPARα has been found to be overexpressed in CLL B-lymphocytes (Spaner et al., 2013). The high levels of free fatty acids found inside CLL B-lymphocytes have been attributed to high lipoprotein lipase (LPL) levels.

LPL is bound to the cell surface and is responsible for the hydrolysis of triglycerides from lipoproteins, allowing the lipid to be transported across the cell membrane (Chajek, Stein, & Stein, 1978; Felts, Itakura, & Crane, 1975). Expression of LPL is of prognostic significance in CLL and has been predictive of treatment-free survival (Nuckel et al., 2006; Oppezzo et al., 2005). High LPL levels in CLL are associated with CD38 and ZAP-70 expression and an unmutated *IGHV* mutational status, and associates with an aggressive disease (Heintel et al., 2005; Nuckel et al., 2006; Rosenwald et al., 2001). It has been shown that the CLL B-lymphocyte gene expression profile of those with high LPL mRNA levels is similar to that of fat and muscle tissue (Bilban et al., 2006). Interestingly, high LPL expressors had higher expression of *CPT1A* which is responsible for the modification of fatty acids allowing them to be transferred into the mitochondria for β-oxidation (Bilban et al., 2006). High LPL levels in CLL have been attributed to constitutive phosphorylation and hence activation of the transcription factor signal transducer and activator of transcription 3 (STAT3) (Hazan-Halevy et al., 2010; Rozovski et al., 2015). Additionally, RNA interference against *LPL* and *STAT3* induced apoptosis in CLL B-lymphocytes (Hazan-Halevy et al., 2010; Rozovski et al., 2015).

It is evident that CLL B-lymphocytes have an altered metabolism that pushes them towards the utilisation of fatty acids for energy production. Understanding lipid metabolism in CLL has the potential to unveil important players in these pathways that could be utilised for therapeutic regimen development. This, therefore, is a main focus of this thesis and will be explored in **Chapter 5**.

1.4.2 ROS in CLL

CLL B-lymphocytes have been shown to accumulate higher intracellular ROS levels compared to healthy B-lymphocytes, and they have increased mitochondrial biogenesis (Jitschin et al., 2014). A ROS-mitochondrial biogenesis feedback loop involving heme oxygenase-1 and mitochondrial transcription factor A has been identified as the main cause (Jitschin et al., 2014). CLL B-lymphocytes also have a high oxygen consumption rate, and therefore respiratory rate (Jitschin et al., 2014). CLL B-lymphocytes have adapted to oxidative stress by upregulating important molecules involved in detoxifying ROS including catalase, heme oxygenase-1, and the important proton donor NADPH, allowing CLL B-lymphocytes to have a higher antioxidant capacity (Jitschin et al., 2014). Interestingly, CLL B-lymphocytes have a lower level of MnSOD (SOD2) which most likely contributes to the elevated intracellular ROS levels observed in these cells (Jitschin et al., 2014). The reason for low SOD2 in CLL is another important research question addressed in this thesis and will be investigated in **Chapter 4**.

Stimulation of the BCR in mouse primary B-lymphocytes has been shown to increase intracellular ROS levels through NADPH oxidase and mitochondrial respiration, and antioxidant treatment of mouse splenic cells has been shown to inhibit BCR-induced activation and proliferation (Fedyk & Phipps, 1994; Wheeler & Defranco, 2012). This data could potentially translate to the contribution of elevated intracellular ROS in CLL B-lymphocytes as they have overactive BCR signalling (Duhren-von Minden et al., 2012; A. Guo et al., 2017). Additionally, Lee *et al.* (2007) demonstrated that redox pathways could be used to modulate B-lymphocyte activation and migration through activation of protein kinase B (R. L. Lee, Westendorf, & Gold, 2007).

The role of ROS is of importance in CLL as it has been shown that treatment of CLL B-lymphocytes with the anti-CD20 antibodies RTX and GA101 induces an increase in intracellular ROS and cell death and that cell death can be prevented through the use of antioxidants (Bellosillo et al., 2001; Honeychurch et al., 2012). However, it was demonstrated that superoxide and not H_2O_2 is involved in anti-CD20 mAb-induced cell death as antioxidants that quench H_2O_2 failed to prevent cell death (Honeychurch et al., 2012). NADPH oxidase was found to be responsible for ROS production in response to GA101 treatment and knock down of the NOX2 subunit prevented cell death, however it is not known if other NADPH oxidase isoforms are also responsible (Honeychurch et al., 2012). Additionally, the effects of anti-CD20 mAb treatment were dependent on surface CD20 expression (Bellosillo et al., 2001).

It is evident that elevated ROS are critical for CLL B-lymphocyte survival, mainly due to the second messenger effects of these molecules in activation and proliferation pathways. Additionally, CLL B-lymphocytes have an upregulated expression of various antioxidant molecules to help combat the

harmful effects of ROS. Understanding redox metabolism in CLL could identify prognostic factors that could inform therapeutic regimens, and this is a focus of this thesis.

1.5 Thesis Hypotheses and Objectives

Overarching hypothesis:

Reactive oxygen species and lipid metabolism are fundamental pathways of CLL pathophysiology. Abnormalities in these pathways result in intrinsic resistance of CLL B-lymphocytes to therapy.

Overall Aim:

To investigate energy metabolism pathways to identify novel therapeutic targets in CLL.

The broad aims of this study were:

1. To investigate the antioxidant capacity and therapeutic resistance of CLL B-lymphocytes from individuals with bulky lymphadenopathy (**Chapter 3**),

2. To investigate the reason for low superoxide dismutase 2 expression in CLL by sequencing and assessing methylation status of the *SOD2* promoter (**Chapter 4**),

3. To investigate lipid metabolic pathways in CLL (**Chapter 5**).

Chapter 2:

Common materials and methods

2.1 Common/miscellaneous procedures

Analytical or molecular biology grade chemicals and reagents were used for all methods unless specified otherwise. All incubation and centrifugation steps were carried out at room temperature unless specified otherwise. All methods using supplied kits were carried out as per manufacturer's instructions, unless otherwise noted.

2.1.1 RNA extraction

RNA was extracted using Trizol reagent. This method involved the addition of 1 mL Tri-Reagent (Sigma Aldrich, St Louis, USA) per 1 x10^7 cells, and incubated at room temperature for 5 minutes. Chloroform (Sigma Aldrich) was added at a ratio of 200 µL per 1 mL Tri-Reagent, and samples were shaken for 10 seconds to ensure thorough mixing. Samples were centrifuged at 1850 x *g* for 10 minutes at 4 °C to form a gradient, and the top layer containing the RNA was transferred to a sterile tube. Isopropanol (Sigma Aldrich) was added at 500 µL per 1 mL Tri-Reagent, and the tubes were inverted, incubated at room temperature for 10 minutes, and centrifuged at 1850 x *g* for 40 minutes at 4 °C. The supernatant was removed, and the pellet was washed with 4 mL of a 70 % ethanol solution (Sigma Aldrich). Following this, the sample was again centrifuged at 1850 x *g* for 10 minutes at 4 °C, the supernatant was discarded, and samples were air dried for approximately 8 minutes. The RNA pellet was resuspended in 100 µL diethyl pyrocarbonate (DEPC)-treated water (Sigma Aldrich), which has been treated to remove any contaminating RNases. Samples were stored at -80 °C until required. Gloves and pipettes were cleaned with RNase Zap® (Sigma Aldrich) prior to RNA extraction.

2.1.2 DNA degradation

The RNA was DNase I treated to degrade any residual DNA in the sample using a DNA-free kit (Life Technologies, VIC, Australia). 1x DNase I Buffer and 2 U of rDNase was added to the RNA sample and incubated at 37 °C for 30 minutes. 0.1x total volume DNase Inactivation Reagent was added and incubated at room temperature for 2 minutes. Samples were centrifuged at 10,000 x *g* for 90 seconds, and the supernatant was transferred to a sterile Eppendorf tube. Samples were stored at -80 °C until required.

2.1.3 Nucleic acid quantification and integrity analysis

2.1.3.1 Nanodrop

DNA and RNA concentrations were measured spectrophotometrically on a Nanodrop 1000 following manufacturer's instructions (Thermo-Fisher Scientific, Australia). In brief, the Nanodrop method

consisted of selecting the appropriate quantification assay, which measures the concentration of the RNA in solution based on optical density ratios. The machine was calibrated using DEPC-treated water followed by measuring 3 µL of the sample. Samples were assayed undiluted and 1 in 10 dilutions.

2.1.3.2 Bioanalyser

In order to quantify and assess RNA integrity, RNA was assessed using an RNA Nano Chip and analysed on the Agilent 2100 Bioanalyser as per manufacturer's instructions (protocol G2938-90037 Rev. D).

2.1.4 Complementary DNA (cDNA) generation

Each reaction contained 10 ng/µL random primers (Invitrogen, Life Technologies), 0.5 mM dNTPs (Fisher Biotechnologies, Australia), and a maximum of 2 µg total RNA in a total volume of 12 µL. Samples were incubated at 65 °C for 5 minutes, and snap frozen on ice for 2 minutes. 1x First Strand Buffer (Invitrogen, Life Technologies), 0.04 M dithiothreitol (DTT; Invitrogen, Life Technologies), and 40 U RNase Out (Invitrogen, Life Technologies) was added to achieve a total volume of 19 µL. Samples were incubated at 25 °C for 2 minutes, and 10 U of Superscript® II Reverse Transcriptase (Invitrogen, Life Technologies) was added. Samples were incubated at 25 °C for 10 minutes, 42 °C for 50 minutes, and 70 °C for 15 minutes. Absence of genomic DNA in RNA preps was verified by performing replicate reactions with omission of the reverse transcriptase and replaced with 1 µL DEPC-treated water.

2.1.5 Standard PCR

The glucuronidase β (*GUSB*) gene was used to confirm efficient cDNA production. Each PCR tube contained 5 µL cDNA template, 1x PCR Buffer (Applied Biosystems, Australia), 0.8 µM forward and reverse primers (Integrated DNA Technologies (IDT), IA, USA), 40 µM dNTPs (Fisher Biotechnologies, Australia), 5 U *Taq* Polymerase (Applied Biosystems), 1 mM Mg^{2+} (Applied Biosystems) in a final volume of 25 µL. All experiments were carried out under the cycling conditions detailed in **Table 2.1** unless noted otherwise. Genomic DNA and no template controls were also performed to check for primer specificity and reagent contamination, respectively.

Table 2.1: Standard PCR cycling method.

Stage (repeats)	Temperature (˚C)	Time
***Taq* activation**	95	7.5 minutes
Amplification (35x)	94	30 seconds
	55	30 seconds
	72	30 seconds
Final elongation phase	72	9 minutes
Incubation	25	2 minutes

2.1.6 Agarose gel electrophoresis

PCR products were visualised on a 1.5 % (w/v) agarose gel (Scientifix, VIC, Australia) in 1x Tris-acetate-EDTA (TAE) buffer (40 mM Tris, 20 mM acetic acid and 1 mM EDTA). Real-time qPCR products were visualised on a 2 % (w/v) agarose gel in 1x TAE buffer. Gels were stained with GelRed® (Biotium, Fremont, USA) to achieve a 0.75x concentration. Eight microlitres of sample was mixed with 2 µL 5x loading dye and loaded into the wells. 6 µL DMW-100L 100-1000 bp ladder (GeneWorks Pty Ltd., Australia) or 50 bp DNA Ladder (New England Biolabs Inc. (NEB), MA, USA) was added to determine product size. Gels were electrophoresed at 100 V for 60 minutes and visualised using a GeneGenius Gel Imaging System (Syngene, UK).

2.1.7 Standard real-time qPCR

Standard experiments were carried out using a ViiA 7 qPCR machine (Applied Biosystems) in the 384-well plate format (Applied Biosystems), and analysed using the Viia7 RUO software (Applied Biosystems). Real-time qPCR products were measured using SYBR Green (Applied Biosystems) intercalating dye, which was supplied as part of the 2x SYBR Green master mix. Primer and template master mixes were made up immediately prior to experiment, with final well concentrations of 1x SYBR Green Master Mix, 2 µM forward primer, 2 µM reverse primer, and various template concentrations in a total volume of 10 µL. All samples were amplified in triplicate, and genomic DNA and no template controls were also performed to confirm primer specificity and reagent contamination, respectively. All experiments were carried out under the conditions detailed in **Table 2.2** with reporter capture every 5 seconds.

Table 2.2: Standard real-time qPCR cycling method.

Stage (repeats)	Temperature (°C)	Time
UDG activation	50	2 minutes
UDG inactivation; *Taq* polymerase activation	95	2 minutes
Amplification (40x)	95	15 seconds
	60	1 minute
Melt curve	95	15 seconds
	60	Heat to 95 °C at 0.5 °C/s
	95	1 second

2.1.7.1 Standard real-time qPCR analysis

Individual threshold cycle (C_t) values were obtained by setting the threshold automatically by the ViiA 7 RUO software, and data from ViiA 7 were imported into Microsoft Excel.

Expression levels were calculated using the delta Ct method (Livak & Schmittgen, 2001). Genes that were undetected in samples were noted and excluded from analysis.

2.1.8 Gene Expression Omnibus (GEO) expression data mining

The Gene Expression Omnibus (GEO) database was used to assess the expression of genes of interest in CLL B-lymphocytes and healthy controls. Three data sets consisted of Genome-wide microarray expression data from B-lymphocytes from CLL and healthy individuals. The study by Vargova *et al.* (2011; GDS3902) consisted of 12 samples from individuals with CLL and 5 healthy controls. The study by Gutierrez *et al.* (2010; GDS4167 and GDS4168) consisted of 41 samples from individuals with CLL and 11 healthy controls.

2.1.9 Annexin-V/propidium iodide cell viability assay

In order to determine cell viability, cells were examined for their expression of Annexin-V and ability to be stained with propidium iodide (PI) using fluorescence-activated cell sorting (FACS). Cells were transferred to FACS tubes and centrifuged at 400 x *g* for 5 minutes at 4 °C. The cell pellet was washed twice with cold phosphate buffered saline (PBS; Sigma-Aldrich) supplemented with 1 % foetal calf serum (FCS; Bovogen Biologicals, VIC, Australia) and 1 % sodium azide. The final wash was carried out with 1 mL binding buffer (1 mM HEPES at pH 7.4, 140 mM $NaCl_2$, 2.5 mM $CaCl_2$), and the cells were centrifuged at 400 x *g* for 5 minutes at 4 °C. The supernatant was removed, and the cells were resuspended in the residual binding buffer (~100 µL). Five microlitres of fluorescein isothiocyanate (FITC) labelled Annexin-V (BD Biosciences Pharmingen, North Ryde, Australia), and PI (Sigma Aldrich) at a final concentration of 5 µg/mL, were added to tubes. Tubes were vortexed for 5 seconds and incubated in the dark for 15 minutes. Each sample was analysed using an Accuri C6 flow cytometer (BD Biosciences, CA, USA) equipped with a 488 nm argon blue laser as a light source. Green fluorescence was evaluated between 500 and 530 nm in the FL1 (FITC) channel, while red fluorescence was evaluated between 670 and 700 nm in the FL3 (PI) channel. Unstained control samples were used for comparison.

2.1.10 Cell culture

Lymphocytic cell lines were cultured in RPMI-1640 medium (Sigma Aldrich) supplemented with 15 µM 2-mercaptoethanol (2ME; Sigma Aldrich), 1 U/mL penicillin (Sigma Aldrich), 10 µg/mL

streptomycin (Sigma Aldrich), 400 µM L-Glutamine (Sigma Aldrich), and 10 % FCS. Cells were incubated at 37 °C in 5 % CO_2 and passaged every 2-3 days.

2.1.11 Cryopreservation of cells

Cells were resuspended at 2.5 x10^7/mL in freezing mixture containing 15 % dimethyl sulphoxide (DMSO; ChemSupply), 35 % FCS, and 50 % RPMI-1640.

2.1.12 Thawing of cells

Cells were rapidly thawed in a water bath at 37 °C. One millilitre RPMI-1640 media containing 10 % FCS was added dropwise through a syringe over 5 minutes. Cells were transferred to 9 mL RPMI-1640 media containing 10 % FCS and centrifuged at 860 x *g* for 5 minutes at room temperature. Supernatant was aspirated and cells were resuspended in 5 mL RPMI-1640 media containing 10 % FCS for cell counting.

2.1.13 Cell counting and viability by Trypan blue exclusion

Cells to be counted were diluted 1:1 in 0.4 % (w/v) trypan blue (Sigma-Aldrich) in PBS. Cells were added to a Neubauer chamber haematocytometer and the number of stained cells (dead cells) and total number of unstained cells (viable cells) were counted in four 1 mm^2 areas. This value was then divided by 4 to provide the average number of cells per 1 mm^2. The number of cells per mL was then calculated using: $c = n \times d \times 10^4$, where c = concentration (cells/mL), d = dilution, and n = average number of cells/mm^2.

2.1.14 Isolation of peripheral blood mononuclear cells (PBMCs)

Blood was diluted 1:2 in sterile PBS and was under laid with 10 mL Lymphoprep™ (Ficoll-Hypaque; AXIS-SHIELD, Oslo, Norway) and centrifuged at 500 x *g* for 40 minutes. Cells at the interphase (lymphocytes) were removed using a sterile transfer pipette, and a 5x volume of 50:50 RPMI-1640 media and FCS was added. The mixture was centrifuged at 500 x *g* for 5 minutes at room temperature.

2.1.15 CD19 magnetic bead purification

Eighty microlitres of Buffer B (PBS, pH 7.2 containing 0.5 % bovine serum albumin (BSA) and 2 mM EDTA (degassed)) was added per 1 x10^7 cells, and CD19 MicroBeads (Miltenyi Biotech, Germany) were diluted 1:4 in the cell suspension. Cell/magnetic bead mixture was incubated at 4 °C for 15 minutes before being centrifuged at 300 x *g* for 5 minutes at room temperature. Supernatant was removed, and 1.5 mL Buffer B was added. The mixture was centrifuged at 300 x *g* for 5 minutes at room temperature, and cells were resuspended in 500 µL buffer. Three millilitres buffer was added to a MACS® column (Miltenyi Biotech) set in a magnetic field and was allowed to drip through. The cell suspension was

then passed through. Three millilitres of Buffer B were passed through the column three times and then removed from the magnetic field. Five millilitres of Buffer B were added to the column and pressure was applied for 10 seconds to force the buffer through into a fresh collection tube to collect the $CD19^+$ cell fraction.

Chapter 3:

Redox pathways in the pathogenesis of and resistance to rituximab in CLL

The most significant adverse prognostic event in CLL is resistance to therapy. Anti-CD20 monoclonal antibodies, in particular rituximab (RTX), have continued to be keystones of current therapy in lymphoproliferative conditions for over 20 years (S. M. O'Brien et al., 2001). The combination of RTX with fludarabine and cyclophosphamide is currently one of the most successful therapies for CLL (Byrd et al., 2005; Hallek et al., 2010; Robak et al., 2010). Both immune-mediated and direct cell death play a part in the mechanism of action of RTX *in vitro*, however, despite this therapy being used to treat CLL for some time, it is unknown how important each of these mechanisms are *in vivo* for the anti-tumour response of RTX (Demidem et al., 1997; Engelberts et al., 2016; Golay et al., 2000; Reff et al., 1994). Despite the effectiveness of RTX in CLL, some individuals are or can become resistant to RTX (Huhn et al., 2001). Reactive oxygen species have previously been implicated in both RTX-mediated complement-mediated cytotoxicity (Bellosillo et al., 2001) and, antibody-dependent cellular cytotoxicity (Werlenius et al., 2016), RTX-induced ROS production has also been shown to be dependent on extracellular calcium (Jak, van Bochove, van Lier, Eldering, & van Oers, 2011). This presents an opportunity to explore a potential mode of RTX-resistance in CLL and is therefore the focus of this investigation.

In CLL, mitochondrial metabolism has been identified as the source of elevated intracellular ROS (Section 1.4.2). It has been shown that CLL B-lymphocytes have adapted to oxidative stress by upregulating important molecules involved in detoxifying ROS, allowing CLL B-lymphocytes to have a higher antioxidant capacity (Jitschin et al., 2014) (**Table 3.1**). This is further supported by work from our laboratory, where proteomic data showed that thioredoxin reductase 2, an essential player in the scavenging of mitochondrial ROS, to be expressed approximately 4.5 times higher in CLL B-lymphocytes compared to healthy controls (Thurgood, Dwyer, Lower, Chataway, & Kuss, 2019).

Table 3.1: Antioxidant molecules known to be increased in CLL B-lymphocytes.
Data from Jitschin *et al.* (2014) and Thurgood *et al.* (2019).

Molecule	Function
Catalase	Detoxification of H_2O_2
Heme-oxygenase 1	Availability of Fe^{2+}
Glutamate-cysteine ligase catalytic subunit	Glutathione synthesis
Glutathione S-transferase	Aids glutathione-mediated detoxification
Glucose-6-phosphate dehydrogenase	NADPH production
NADPH	Detoxification of ROS
Thioredoxin reductase 2	Antioxidant reduction maintenance

Given the elevated levels of ROS in CLL and the observation that antioxidant systems are strained in order to deal with these elevated levels, it has been hypothesised that RTX treatment may kill CLL B-lymphocytes by disrupting this balance. A study in 2001 found that RTX-induced complement-mediated cytotoxicity caused a loss of mitochondrial membrane potential, in addition to an increase in intracellular ROS levels (Bellosillo et al., 2001). Additionally, CLL B-lymphocytes with low expression of surface CD20 had a slower response to RTX with respect to intracellular ROS generation and phosphatidylserine exposure (a marker of early apoptosis). Conversely to these findings, previous work by Honeychurch *et al.* (2012) showed minimal levels of ROS and cell death (<10 %) in RTX-treated Raji cells (CD20-expressing Burkitt's lymphoma B-lymphocyte cell line) (Honeychurch et al., 2012). However, this may be explained by the fact that when RTX treatment was performed, a source of complement was not added and RTX was not cross-linked with anti-human IgG which has been shown to mimic cell-cell interactions that facilitate cell death *in vivo*; thus cross-linking enhances signal strength (Shan, Ledbetter, & Press, 2000).

Given the conflicting evidence in the literature and the importance of understanding RTX mechanisms, the link between ROS and RTX has been of interest to our group for some time. Previous work in our laboratory used two-dimensional differential in-gel electrophoresis (2D-DIGE) to profile proteomic changes in response to cross-linked RTX treatment in primary B-lymphocytes and characterised differences in expression in response to RTX treatment in RTX-resistant CLL and healthy B-lymphocytes (Sulda, 2009). Using mass spectrometry, expression of 21 cytoplasmic proteins changed in response to RTX treatment. Five of these proteins were identified as being involved in redox homeostasis (**Table 3.2**). These results further support the hypothesis that differential modulation of redox pathways occurs following RTX binding in resistant versus susceptible cells and the ability to increase antioxidant levels in response could determine cell fate.

Table 3.2: Proteins differentially expressed following cross-linked RTX treatment in RTX-resistant CLL and healthy B-lymphocytes.
Data from Sulda (2009).

Protein	Change	RTX-resistant CLL / healthy (RTX-susceptible)
Glutaredoxin-3	Decrease	Healthy (RTX-susceptible)
Peroxiredoxin-1	Decrease	Healthy (RTX-susceptible)
Peroxiredoxin-2	Decrease	Healthy (RTX-susceptible)
Superoxide dismutase 2	Increase	RTX-resistant CLL
Glutathione peroxidase-1	Increase	RTX-resistant CLL
Glutathione S-transferase	Increase	RTX-resistant CLL

In order to understand this mechanism further, a second cohort of CLL patients was analysed for baseline protein expression using unlabelled, quantitative mass spectrometry. Of the proteins identified in **Table 3.2**, glutathione S-transferase (**Table 3.1**) and superoxide dismutase 2 were expressed at a higher and lower level in CLL B-lymphocytes compared to healthy controls, respectively, indicating that redox pathways may be able to inform the disease course experienced by patients (Thurgood et al., 2019). These studies demonstrate that key differences in downstream signalling pathways occur between RTX-resistant and RTX-susceptible B-lymphocytes, and in CLL B-lymphocytes in general, implying that oxidative stress may be a key player in disease behaviour and response to RTX therapy.

Individuals with CLL can experience bulky lymphadenopathy (BLA) which results from large numbers of CLL B-lymphocytes to crowd in the lymph nodes. It is possible that this crowding causes low perfusion in the lymph nodes and thus BLA CLL B-lymphocytes must exist under hypoxic conditions. A similar appearance is apparent in bone marrow, which as CLL progresses becomes almost completely devoid of fat spaces and capillaries. Hypoxia causes an increase in superoxide production at complex III of the mETC, (Bell et al., 2007), and so it is possible that BLA CLL B-lymphocytes have developed higher antioxidant levels to combat this. As RTX-mediated cell death has previously been shown to be ROS-dependent, it was hypothesised that BLA CLL B-lymphocytes are resistant to RTX-induced cell death due to their enhanced antioxidant capacity (Bellosillo et al., 2001; Honeychurch et al., 2012). Therefore, this study aimed to understand the ability of CLL B-lymphocytes to withstand increased intracellular ROS.

The overarching hypothesis to this study is that maintaining redox homeostasis in a state of elevated ROS levels is critical for survival of CLL B-lymphocytes *in vivo*. Furthering our understanding of abnormal redox homeostasis in CLL could allow its exploitation in the development of novel therapeutic regimens. Therefore, further analysis of this potentially significant area is warranted.

This study has two aims related to elucidating the mechanisms behind abnormal redox homeostasis in CLL:

1) To assess intracellular ROS in a control lymphoblast cell line and CLL B-lymphocytes from individuals with and without bulky lymphadenopathy at baseline and in response to oxidative stress,
2) To establish whether cross-linked RTX treatment *in vitro* in Raji B-lymphocytes results in changes in intracellular ROS.

3.1 Materials and methods

3.1.1 Selection of individuals for inclusion into the RTX study

Individuals were selected from a South Australian cohort of patients of the Flinders Medical Centre, Department of Molecular Medicine & Genetics, who have CLL (HREC #216056). Informed consent was obtained from individuals for the use of their tissue in this study. Individuals were previously categorised as having or not having bulky lymphadenopathy (BLA) by Dr. James Cohen defined as a lymph node mass with a diameter of 5 cm or greater at any one site (Cohen, Thurgood, Lower, & Kuss, 2019). BLA was chosen as a potential marker of ROS tolerant disease. Circulating CLL cells were purified from these patients as per 2.1.15.

3.1.2 Rotenone treatment of lymphocyte cell lines

EBV-transformed B-lymphocytes were cultured as described in 2.1.10 until 90 % confluent. Cells were counted using the Trypan blue exclusion test as described in 2.1.13 and seeded at 5 x10^5/mL in T75 flasks (Sigma-Aldrich). Cells were treated with either 50 µM rotenone, vehicle (0.5 % DMSO) alone, or cells alone. Cells were incubated in 10 % CO_2 at 37 °C and intracellular ROS levels were assessed using the CellROX® Orange Indicator Assay as described in 3.1.5 at 1.5, 3, 7, and 25 hours post-treatment. Three biological replicates were performed.

3.1.3 Rotenone and RTX treatment of CLL B-lymphocytes

Cryopreserved PBMCs from individuals with CLL were thawed as in section 2.1.12 and resuspended in RPMI-1640 medium containing 10 % FCS. Cells were centrifuged at 1600 x *g* for 5 minutes and supernatant was aspirated. The cell pellet was resuspended in the same media and cells were counted using the Trypan blue exclusion test as outlined in section 2.1.13. Cells were seeded at 4 x10^6/mL in a 24-well plate and either rotenone was added to achieve final concentration of 50 µM, or RTX was added to achieve a final concentration of 10 µg/mL cross-linked with donkey anti-human IgG at a final concentration of 50 µg/mL. Untreated and vehicle (0.5 % DMSO) controls were also performed. Cells were incubated in 5 % CO_2 at 37 °C for 4 hours, and $CD19^+$ cells, intracellular ROS, mitochondrial mass, and cell death were assessed.

PBMCs were transferred to FACS tubes and centrifuged at 1600 x *g* for 5 minutes at room temperature. Supernatant was discarded and RPMI-1640 media containing 250 nM CellROX® Orange, 25 nM MitoTracker® Deep Red FM, and anti-CD19 conjugated to PE-Cy5 was added to PBMCs. PBMCs were vortexed for 5 seconds followed by incubation in 5 % CO_2 at 37 °C for 1 hour.

PBMCs were centrifuged at 1600 x *g* for 5 minutes, supernatant was discarded, and PBMCs were resuspended in 1 mL cold PBS supplemented with 1 % FCS and 1 % sodium azide. Cells were pelleted

for 5 minutes at 1600 x *g* and resuspension was repeated. A final centrifugation step was performed with 1 mL binding buffer (1 mM HEPES at pH 7.4, 140 mM $NaCl_2$, 2.5 mM $CaCl_2$). Supernatant was aspirated and PBMCs were resuspended in the residual binding buffer (~100 µL). Five microlitres of FITC labelled Annexin-V (BD Biosciences Pharmingen, North Ryde, Australia) was added to PBMCs. PBMCs were vortexed for 5 seconds and incubated in the dark for 15 minutes at room temperature. Each sample was analysed using a CytoFLEX flow cytometer (Beckman Coulter, CA, USA). Fluorophore detection information can be found in **Table 3.3**.

Table 3.3: CytoFLEX flow cytometric fluorophore detection information.

Label	Laser	Bandpass filter	Detector
Annexin-V	Blue: 488nm	525/40	FITC
CellROX® Orange	Yellow/Green: 561nm	585/42	PE
Anti-CD19	Yellow/Green: 561nm	690/50	Cy5.5
MitoTracker® Deep Red FM	Red: 633nm	660/20	APC

3.1.4 Rituximab treatment of Raji B-lymphocytes

Raji B-lymphocytes were cultured as described in 2.1.10 until 90 % confluent. Cells were counted using the Trypan blue exclusion test as described in 2.1.13 and seeded at 5 $x10^5$/mL in T25 flasks (Thermo-Fisher Scientific). One milligram per millilitre RTX was added to the treatment flasks to achieve a final concentration of 10 µg/mL, and 1.3 mg/mL $F(ab')_2$ fragment goat anti-human IgG was added to the treatment flasks to achieve a final concentration of 50 µg/mL. A no treatment control was also performed. Cells were incubated in 10 % CO_2 at 37 °C for 4 hours, and cell death and intracellular ROS levels were assessed using the Annexin-V/PI cell viability assay and CM-H_2DCFDA assay as described in 2.1.9 and 3.1.6, respectively.

3.1.5 CellROX® Indicator Assay

Cells were seeded at 5 $x10^5$/mL at 1 mL per well of a 24-well plate. CellROX® Orange was added to each well to achieve a final concentration of 250 nM, and cells were incubated in 10 % CO_2 at 37 °C for 1 hour. Cells were then transferred to FACS tubes (Corning) and washed three times with PBS. The cells were pelleted between each wash by centrifugation at 400 x *g* for 5 minutes. Each sample was analysed using an Accuri C6 flow cytometer (BD Biosciences, CA, USA) equipped with a 488 nm argon blue laser as a light source. Orange fluorescence was evaluated between 545 and 625 nm in the FL2 channel. Three technical replicates of each treatment were performed.

3.1.6 CM-H_2DCFDA Assay

Cells were seeded at 5 x10^5/mL at 1 mL per well of a 24-well plate in serum-free RPMI-1640 media. Fifty millimolar CM-H_2DCFDA was added to each well to achieve a final concentration of 50 µM, and cells were incubated in 10 % CO_2 at 37 °C for 30 minutes. Cells were then transferred to FACS tubes and centrifuged at 400 x *g* for 5 minutes at room temperature. Media was aspirated and 1 mL PBS was added to the FACS tubes followed by centrifugation at 400 x *g* for 5 minutes. This was repeated three times. Each sample was analysed using an Accuri C6 flow cytometer (BD Biosciences, CA, USA) equipped with a 400 nm argon blue laser as a light source. Green fluorescence was evaluated between 500 and 530 nm in the FL1 channel. Six technical replicates of each treatment were performed and mean fluorescent intensity values were recorded for analysis.

3.2 Results

3.2.1 Development of a positive control for evaluating elevated intracellular ROS resulting in cell death

As mentioned in section 3, the free radical superoxide is produced in response to RTX treatment (Bellosillo et al., 2001). Therefore, rotenone, a complex I inhibitor – which causes the production of superoxide, was selected for development of the required positive control (section 3.1.2) as it has previously been shown to induce cell death through elevation of intracellular ROS (Li et al., 2003).

The FH9 normal B-lymphocyte EBV-transformed cell line was used as a renewable source of cells for development of the positive control. FH9 B-lymphocytes were treated with 50 µM rotenone for 25 hours and intracellular ROS and cell death were analysed over this period using CellROX® Orange and the Annexin-V/PI assay, respectively.

Figure 3.1 shows that elevated intracellular ROS levels were maintained over 25 hours of rotenone treatment. There was a significant elevation in intracellular ROS after rotenone treatment at 1.5 hours ($p = 0.007$), 3 hours ($p = 0.002$), 7 hours ($p = 0.000005$), and 25 hours ($p = 0.00004$). There was also a significant ($p = 0.007$) elevation in intracellular ROS in the vehicle control at 7 hours.

Figure 3.2 shows that there was a significant increase in cell death after rotenone treatment at 1.5 hours ($p = 0.003$), 3 hours ($p = 0.01$), 7 hours ($p = 0.0002$), and 25 hours ($p = 0.001$), with no significant change in cell death in the vehicle control over this time period.

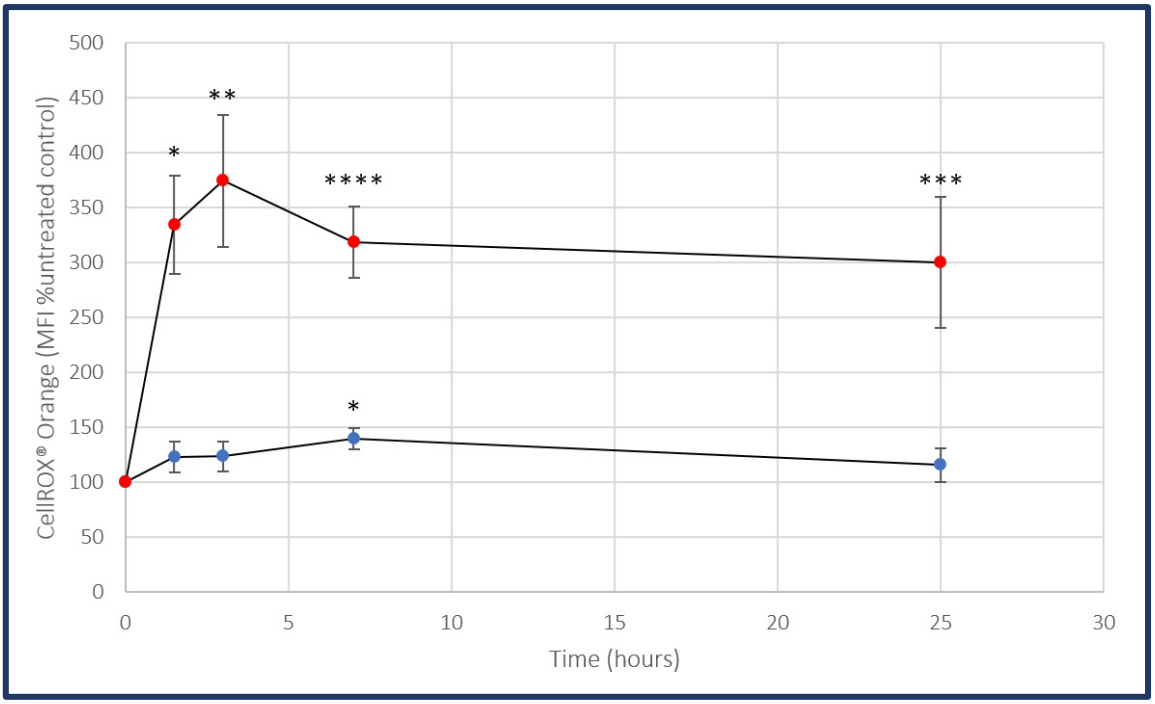

Figure 3.1: Elevated intracellular ROS levels are maintained over 25 hours of rotenone treatment.

FH9 B-lymphocytes were treated with vehicle (0.5 % DMSO; blue) or 50 µM rotenone (red) over 25 hours and intracellular ROS levels were assessed using CellROX® Orange and flow cytometry. n = 3; error bars, ±1 standard deviation; *, $p<0.05$; **, $p<0.005$; ***, $p<0.0005$; ****, $p<0.00005$ as calculated using t-test.

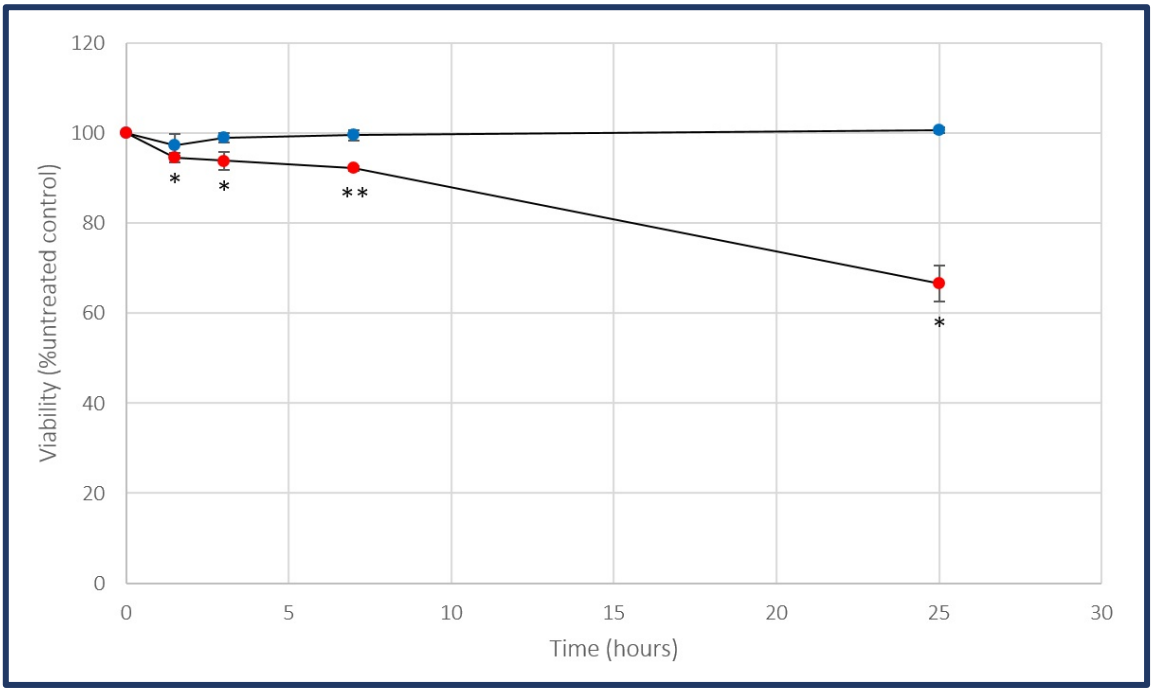

Figure 3.2: Rotenone induces cell death.

FH9 B-lymphocytes were treated with vehicle (0.5 % DMSO; blue) or 50 µM rotenone (red) over 25 hours and viability was assessed using the Annexin-V/PI assay and flow cytometry. n = 3; error bars, ±1 standard deviation; *, $p<0.05$; **, $p<0.005$ as calculated using t-test.

3.2.2 Investigating rituximab resistance in bulky lymphadenopathy

Clinical characterisation of the entire cohort was conducted by Dr. James Cohen and is as follows:

The mean nodal sizes were 85.91 mm (SD = 39.42) and 18.36 mm (SD = 12.18) for the BLA patients (n =23) and non-BLA patients (n =123), respectively. In the BLA cohort, 87 % were treated, with a median TTFT of 51 months (SE = 18.96). In the non-BLA cohort, 57 % were treated, with a median TTFT of 100 months (SE = 25.86; p = 0.012). There were no significant differences in the treatment chosen for each group and the majority of patients received RTX. The response to therapy in the BLA cohort (n = 17) showed 4 patients with complete remission and thirteen with partial remission. In the non-BLA cohort (n = 65) 27 showed complete remission and 38 showed partial remission. The difference in response was not significant (p = 0.173) between the BLA and non-BLA cohorts. The survival of BLA patients was significantly (p = 0.012) shorter; 48 % were deceased at the time of analysis (**Figure 3.3**). The estimated mean survival time was 96 months (SE = 42.22). In the non-BLA cohort, 27 % were deceased at the time of analysis with an estimated median survival time of 268 months (SE = 40.27; **Figure 3.3**). Frequency data for disease stage, treatment, and response to treatment can be seen in **Table 3.4**.

In this cohort there was a non-significant, weak propensity for BLA cases to have del11q and no association with any other chromosomal abnormality. In the BLA cohort (n =16) there were 6 patients with mutated *IGHV* and 11 with unmutated *IGHV*. In the non-BLA cohort (n =72) there were 48 patients with mutated *IGHV* and 24 with unmutated *IGHV* (p = 0.017) suggesting a significant, but weak, propensity for BLA patients to have unmutated *IGHV* and non-BLA patients to have mutated *IGHV*.

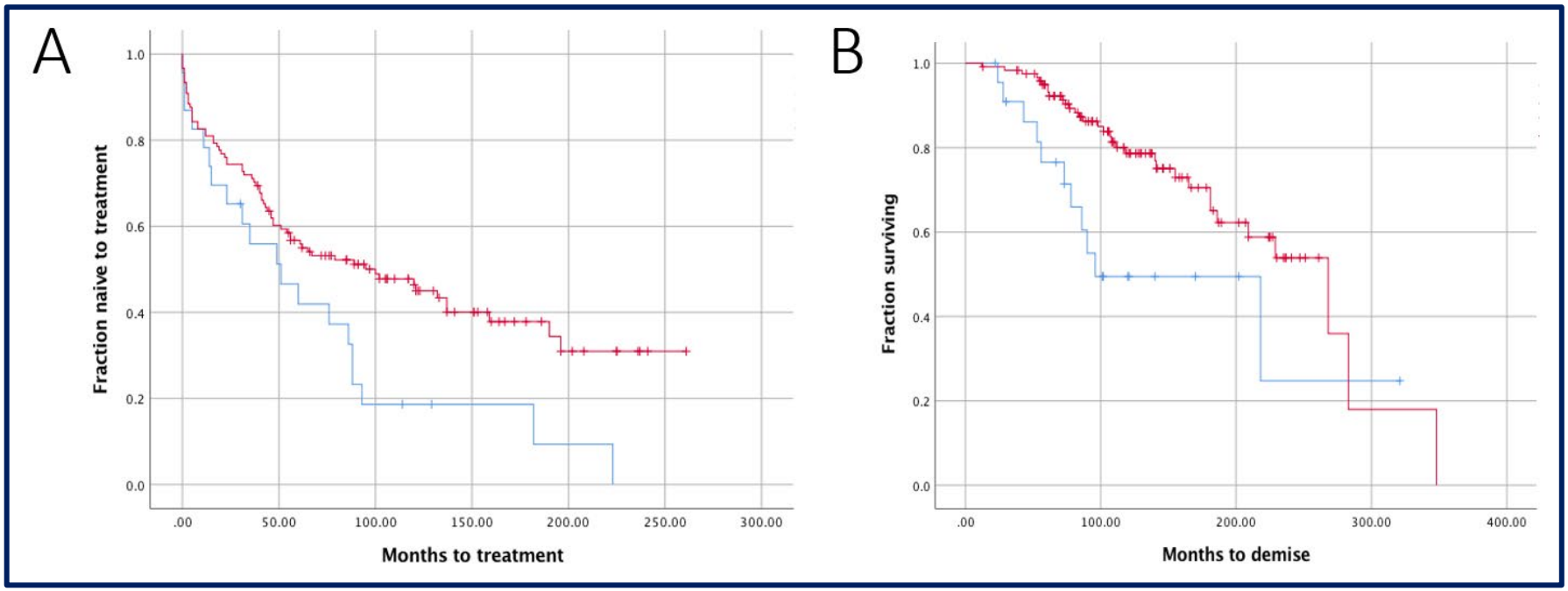

Figure 3.3: Kaplan-Meier curves for the entire BLA cohort.

A, TTFT and **B**, survival time of BLA (blue) and non-BLA (red) patient cohorts. Ticks along the curve represent a censored patient for whom no more treatment-free or survival time information is available. **A**, log rank (Mantel-Cox) analysis returned a chi-square value of 6.383, 1 degrees of freedom. **B**, log rank analysis returned a chi-square value of 6.317, 1 degrees of freedom.

Table 3.4: Frequency table for clinical characteristics of the entire BLA cohort.
Rai stage at diagnosis, choice of first-line therapy and response to treatment.

	BLA (% of cohort)	non-BLA (% of cohort)
Rai stage at diagnosis		
Rai 0	10 (43.48)	64 (52.03)
Rai I	6 (26.09)	19 (15.45)
Rai II	1 (4.35)	7 (5.69)
Rai III	2 (8.7)	4 (3.25)
Rai IV	0	8 (6.5)
Unknown	4 (17.39)	21 (17.07)
Treatment		
Chemotherapeutics	5 (25)	24 (34.29)
Chemotherapeutics + biologics	14 (70)	38 (54.29)
Biologics	0	1 (1.43)
Targeted inhibitors	1 (5)	4 (5.71)
Targeted inhibitors + biologics	0	2 (2.86)
Unknown	0	1 (1.43)
Response to treatment		
Clinical complete remission	3 (15.79)	13 (18.84)
Complete remission	1 (5.26)	8 (11.59)
Complete remission with incomplete count recovery	0	6 (8.7)
Partial remission	13 (68.42)	38 (55.07)
Stable disease	1 (5.26)	1 (1.45)
Progressive disease	2 (10.53)	3 (4.35)
Ongoing treatment	0	1 (1.45)

Individuals from the entire BLA cohort were selected for inclusion into the BLA study based on sample availability. Analysis of our cohort clinical data (**Table 3.4**) showed that individuals with BLA have a significantly ($p = 0.0089$) higher lymphocyte count (96.84×10^9 cells/L) compared to individuals without BLA (36.36×10^9 cells/L; **Figure 3.4 A**). Additionally, individuals with BLA have a shorter TTFT (36.9 months) compared to individuals without BLA implying early disease progression (91.6 months; **Figure 3.4 B**), although this was not significant ($p = 0.208$). TTFT is also represented in the Kaplan-Meier plot (**Figure 3.5**). The average age of individuals with BLA was 77.04 years compared to 73.92 years for individuals without BLA.

Table 3.5: Patient clinical information for the BLA investigation cohort.
Y, yes; N, no; C17, complex karyotype with 17p abnormalities; U, unmutated *IGHV*; M, mutated *IGHV*; N/A, data unavailable.

Sample	Bulky Y/N	Age (years)	Lymphocyte count (units)	TTFT (months)	Cytogenetics (FISH)	*IGHV*
FMC31	Y	65.33	25.96	23	C17	U
FMC34	N	79.69	No data	61	trisomy 12	U
FMC44	N	76.27	9.16	224	del13q, del11q	M
FMC63	Y	92.09	96.92	10	trisomy 12	N/A
FMC66	N	50.26	39.53	19	del11q	U
FMC74	N	93.74	30.62	46	normal	M
FMC82	N	55.71	44.46	Naïve	normal	M
FMC100	Y	83.69	29.6	14	del13q, del11q	U
FMC117	Y	87.99	137.88	76	del13q, del11q	U
FMC161	Y	86.25	61.59	47	del13q	N/A
FMC166	Y	77.07	135.22	49	normal	M
FMC170	Y	69.09	128.44	88	normal	U
FMC190	Y	58.81	66.1	Naïve	N/A	N/A
FMC232	N	87.87	58.02	108	trisomy 12	U
FMC236	Y	71.92	83.18	28	del17p	U
FMC248	Y	105.33	250.45	32	N/A	N/A
FMC279	Y	47.49	32.96	Naïve	trisomy 12	U
FMC285	Y	79.42	113.72	2	del13q	U

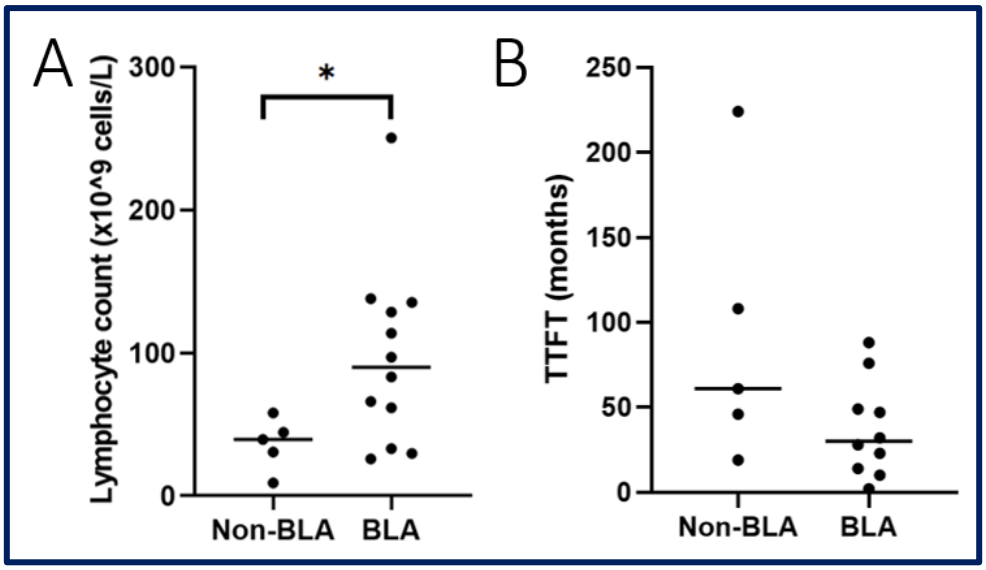

Figure 3.4: Patients with BLA have a higher lymphocyte count and shorter TTFT.
A, median lymphocyte count; **B**, median time to first treatment. Non-BLA, n = 5; BLA, n = 12; bars, median; **, $p<0.005$ as calculated using Welch's t-test.

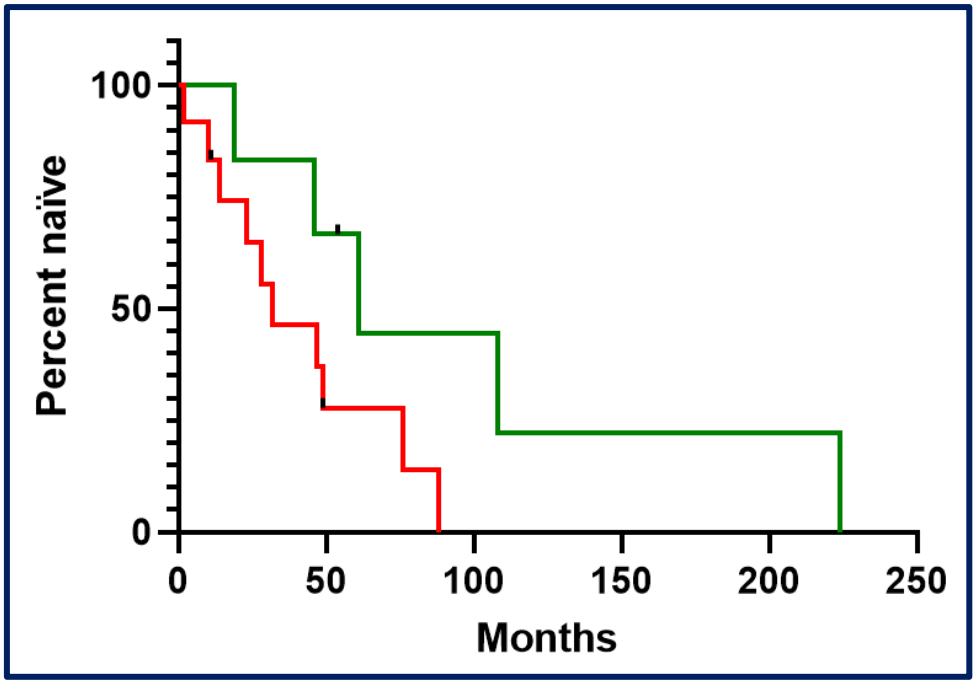

Figure 3.5: TTFT is shorter in patients with BLA.
Kaplan-Meier plot with time to first treatment in CLL patients with and without BLA. Red, BLA; green, non-BLA; ticks, patient naïve at point of sample collection. There was no statistically significant difference between these groups.

3.2.2.1 Basal intracellular ROS levels are lower in BLA CLL B-lymphocytes

PBMCs from individuals with CLL and healthy controls were treated with either 50 µM rotenone or 10 µg/mL RTX cross-linked with 50 µg/mL anti-human IgG for 4 hours as described in 3.1.3. Intracellular ROS, cell death, and mitochondrial mass were assessed using CellROX® Orange, Annexin-V, and MitoTracker® Deep Red FM, respectively. FMC63 and FMC190 were excluded from analysis due to high levels (>50 %) of spontaneous cell death.

As **Figure 3.6** shows, CLL B-lymphocytes from patients with BLA have lower intracellular ROS levels (mean = 2177) compared to both CLL B-lymphocytes from patients without BLA (mean = 3263) and healthy controls (mean = 3294), however this difference was not significant (control vs. BLA: $p = 0.2634$; non-BLA vs BLA: $p = 0.221$).

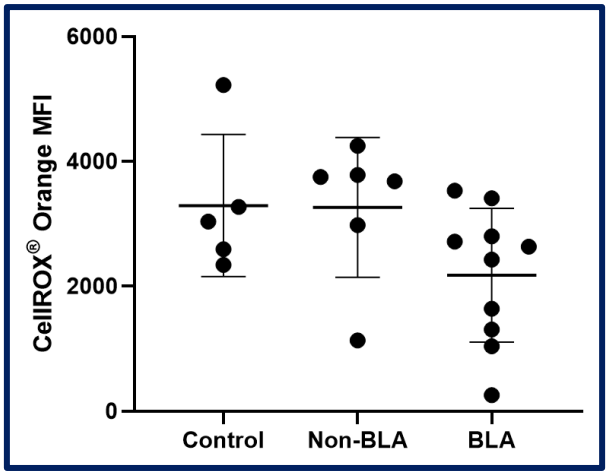

Figure 3.6: Basal intracellular ROS levels.
Basal intracellular ROS levels were detected using CellROX® Orange and flow cytometry. Control, n = 5; non-BLA, n = 6; BLA, n = 10; error bars, ±1 standard deviation. There was no statistically significant difference between these groups.

In order to determine whether mitochondrial mass affects the response to rotenone treatment, mitochondrial mass was measured as described in 3.1.3. As **Figure 3.7 A** shows, there was no significant difference in mitochondrial mass between CLL B-lymphocytes (non-BLA: mean = 7362, BLA: mean = 6582) and healthy controls (mean = 6359). There was also no correlation between mitochondrial mass and intracellular ROS levels ($R^2 = 0.0002317$).

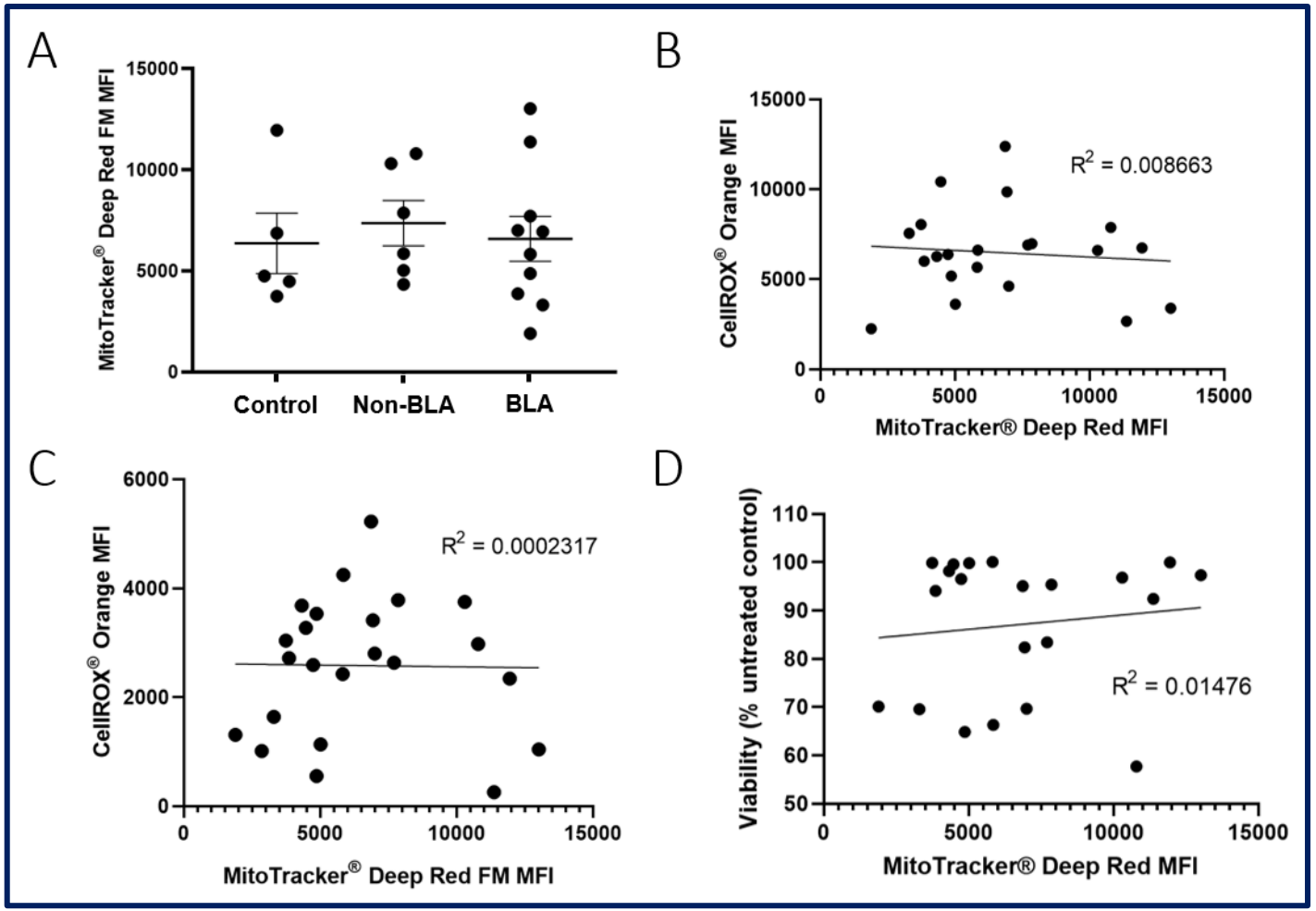

Figure 3.7: Mitochondrial mass does not influence intracellular ROS or cell death after rotenone treatment. PBMCs were treated with vehicle (0.5 % DMSO), 50 µM rotenone, or 10 µg/mL RTX cross-linked with 50 µg/mL IgG for 4 hours and **A**, mitochondrial mass was measured using MitoTracker® Deep Red FM and flow cytometry in untreated PBMCs; **B**, intracellular ROS was plotted against mitochondrial mass in untreated PBMCs; **C**, intracellular ROS was plotted against mitochondrial mass in rotenone-treated PBMCs; and **D**, viability after rotenone treatment was plotted against mitochondrial mass in untreated PBMCs. Control, n = 5; non-BLA, n = 6; BLA, n = 10; error bars; mean ±1 standard error of the mean.

Antioxidant expression was previously found to be different between resistant and susceptible B-lymphocytes (Sulda 2009). In these experiments, RTX was cross-linked with anti-human IgG to mimic *in vivo* interactions. Therefore, the relationship between intracellular ROS and cell death in response to cross-linked RTX treatment was explored by using conditions similar to Honeychurch *et al.* (2012) who did not cross-link RTX.

3.2.3 Cell death correlates with increased intracellular ROS after RTX treatment

Raji B-lymphocytes were treated with cross-linked RTX for 4 hours as described in section 3.1.4. Cell death and intracellular ROS levels were assessed as described in section 2.1.9 and 3.1.6, respectively. **Figure 3.8** shows that there was a correlation between intracellular ROS levels and cell death after treatment with cross-linked RTX. There was a significant ($p = 0.0325$) increase in intracellular ROS levels after treatment with cross-linked RTX compared to the untreated control (**Figure 3.8 A**). There was also an increase in intracellular ROS levels with cross-linking of RTX compared to RTX alone, although this was not significant ($p = 0.1$; **Figure 3.8 A**). The shift in carboxy-DCF fluorescence can be seen in **Figure 3.9**. **Figure 3.8 B** shows that there was a significant ($p = 0.000374$) decrease in viability after treatment with cross-linked RTX compared to the untreated control, and a significant ($p = 0.000743$) decrease in viability with cross-linking of RTX compared to RTX alone.

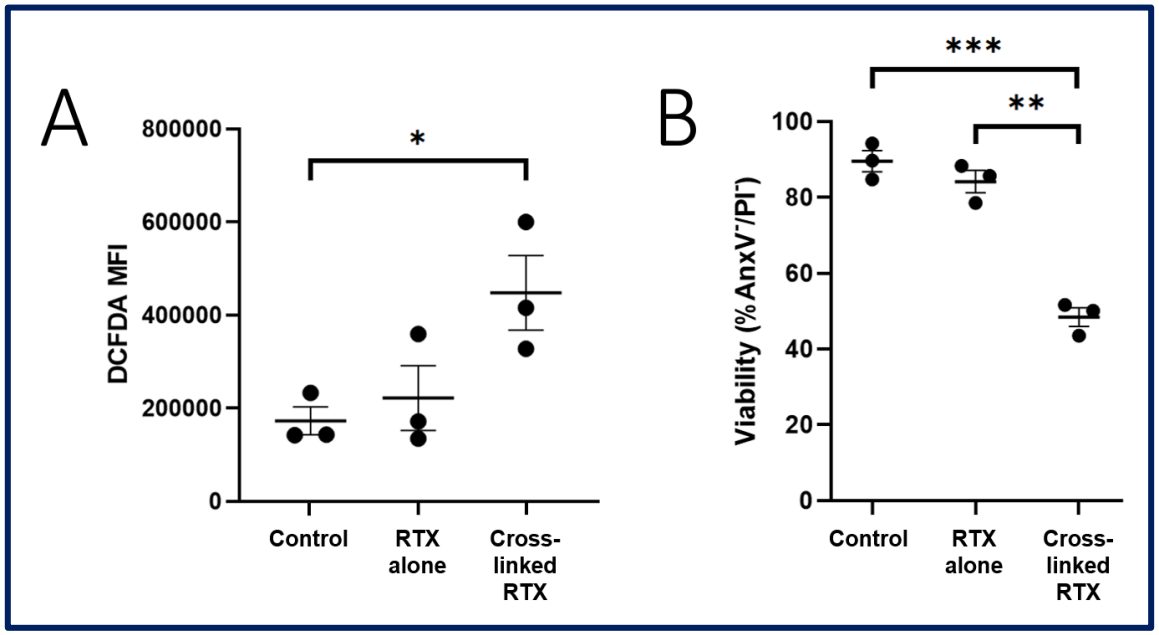

Figure 3.8: Cell death in cross-linked RTX-treated Raji cells correlates with an increase in intracellular ROS levels.

Raji B-lymphocytes were treated with cross-linked RTX for 4 hours and **A**, intracellular ROS were detected using CM-H_2DCFDA and flow cytometry, and **B**, cell death was assessed using the Annexin-V/PI assay and flow cytometry. n = 3; error bars, ±1 standard error of the mean; *, $p<0.05$; **, $p<0.005$; ***, $p<0.0005$ as calculated using t-test.

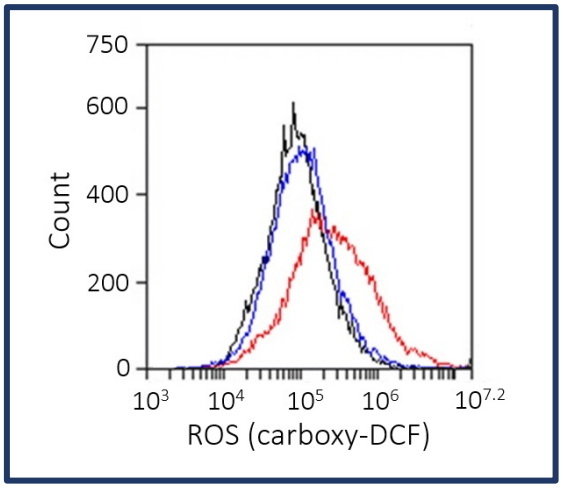

Figure 3.9: Representative histogram of an increase in intracellular ROS occurring after RTX treatment.
Raji B-lymphocytes were treated with cross-linked RTX for 4 hours and assayed for intracellular ROS using CM-H_2DCFDA. Black, untreated control; blue, RTX alone; red, cross-linked RTX.

These findings demonstrate that cross-linking of RTX with IgG elicits a response with respect to ROS in Raji cells. It was therefore decided that the next set of experiments would proceed to understand the effect of cross-linked RTX in CLL B-lymphocytes from individuals with BLA, and how antioxidant capacity may affect this.

3.2.3.1 CLL B-lymphocytes die in response to rotenone treatment

B-lymphocytes from individuals with CLL and healthy donors were treated with rotenone or cross-linked RTX as described in 3.1.3. As **Figure 3.10** shows, after treatment with rotenone, BLA CLL B-lymphocytes had significantly ($p = 0.021$) lower viability (82.4 %) compared to healthy controls (98.2 %). Non-BLA CLL B-lymphocytes also had lower viability (85.7 %) after treatment with rotenone compared to healthy controls, although this was not significant. After treatment with cross-linked RTX, healthy B-lymphocytes had significantly lower viability (85.2 %) compared to both non-BLA ($p = 0.029$; 98.2 %) and BLA ($p = 0.0179$; 99 %) CLL B-lymphocytes.

Figure 3.11 demonstrates that although intracellular ROS were lower in BLA CLL B-lymphocytes (mean = 2099) compared to non-BLA CLL B-lymphocytes (mean = 3054) and healthy controls (mean = 3461) after vehicle (05 % DMSO), there was no significant difference in intracellular ROS levels overall. After treatment with rotenone, intracellular ROS levels were significantly ($p = 0.0235$) lower

in BLA CLL B-lymphocytes (mean = 6332) compared to healthy controls (mean = 8793), however this was not significant. There was no difference in intracellular ROS levels between non-BLA CLL B-lymphocytes (mean = 2952) and healthy controls (mean = 2994) after treatment with cross-linked RTX. Intracellular ROS levels were lower in BLA CLL B-lymphocytes (mean = 2123) after cross-linked RTX treatment, however this was not significant.

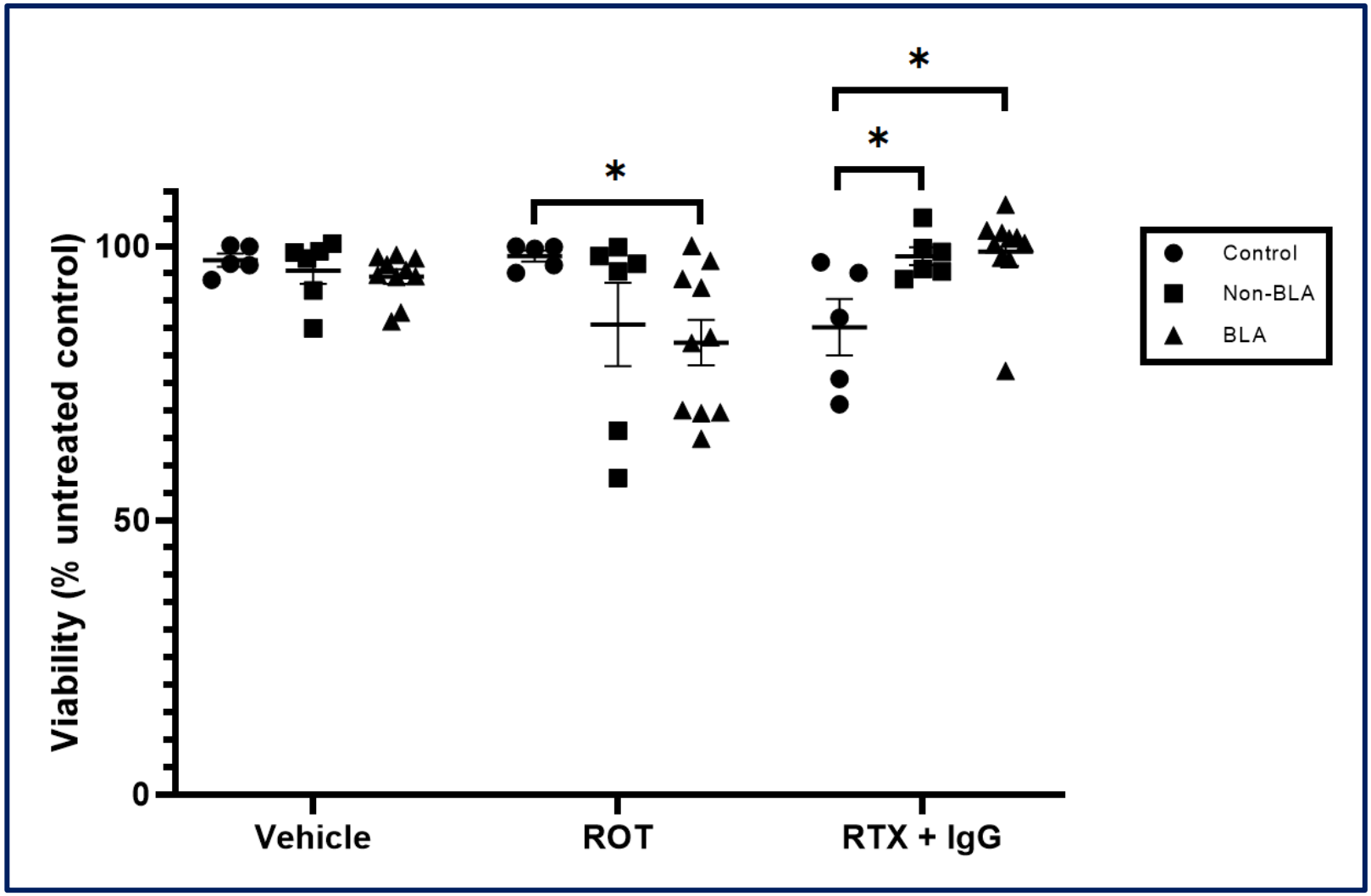

Figure 3.10: Rotenone causes cell death in CLL B-lymphocytes but not healthy controls.
PBMCs were treated with vehicle (0.5 % DMSO), 50 µM rotenone, or cross-linked RTX (10 µg/mL RTX + 50 µg/mL anti-human IgG) for 4 hours and cell death was assessed using Annexin-V. Circles, healthy controls (n = 5); squares, non-BLA (n = 6); triangles, BLA (n = 10); error bars, ±1 standard error of the mean; *, $p<0.05$ as calculated using t-test.

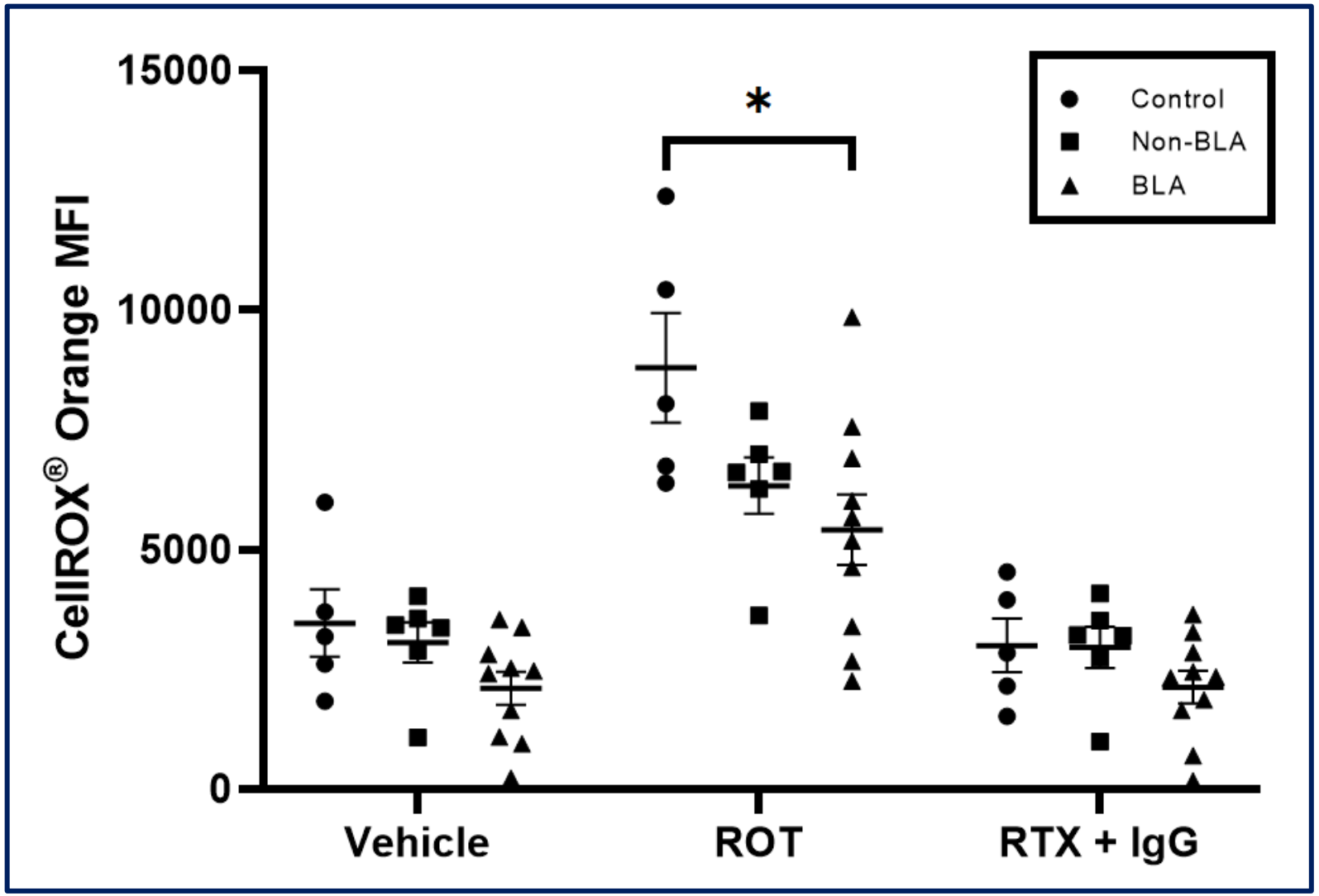

Figure 3.11: Intracellular ROS levels are consistently lower in BLA CLL B-lymphocytes across treatment groups.
PBMCs were treated with vehicle (0.5 % DMSO), 50 µM rotenone, or 10 µg/mL RTX cross-linked with 50 µg/mL IgG for 4 hours and intracellular ROS were detected using CellROX® Orange and flow cytometry. Control, n = 5; non-BLA, n = 6; BLA, n = 10; error bars, ±1 standard error of the mean; *, $p<0.05$ as calculated using t-test.

3.3 Discussion

3.3.1 Summary

This chapter investigated how RTX treatment affects intracellular ROS in CLL B-lymphocytes with a focus on patients with bulky lymphadenopathy. The patients with BLA were found to have a higher lymphocyte count and shorter time to first treatment and a lower overall survival. Most of the patients in each arm of the cohort received a biologic which was predominantly RTX. Hence, the biological course of disease appears to be more aggressive in the BLA disease cohort and there is intrinsic resistance to therapy *in vivo*.

Basal intracellular ROS levels of the circulating malignant lymphocytes were lower from individuals with BLA compared to non-BLA and healthy controls. Only healthy controls and not the selected CLL B-lymphocytes (non-BLA and BLA) responded to cross-linked RTX as evidenced by a reduction in cell viability, however no changes in intracellular ROS were detected in CLL cells or healthy B-lymphocytes. Healthy B-lymphocytes express CD20 at higher levels than CLL cells and rituximab treatment of patients is known to deplete healthy B-lymphocytes and is used in the treatment of rheumatoid arthritis (Ramwadhdoebe et al., 2019), therefore it was anticipated that ROS levels would rise in healthy B-lymphocytes. The opposite of this was observed after rotenone treatment with CLL B-lymphocytes (non-BLA and BLA) having lower viability than healthy controls despite higher ROS levels in healthy B-lymphocytes. Mitochondrial mass did not affect intracellular ROS or viability in untreated and rotenone-treated cells. These findings will now be discussed in detail.

3.3.2 Understanding antioxidant capacity and RTX resistance in bulky lymphadenopathy

The aim of this study was to investigate the antioxidant capacity of CLL B-lymphocytes from individuals with BLA and determine if this correlated with their ability to evade RTX-induced cell death which was demonstrated in the clinical outcomes of the patients. It was hypothesised that CLL B-lymphocytes from individuals with bulky disease have a higher antioxidant capacity due to their ability to survive in a hypoxic and hence ROS-abundant microenvironment.

3.3.2.1 Development of a positive control

Rotenone was selected as a way of generating superoxide which has been shown to be produced in response to RTX treatment (Bellosillo et al., 2001). Additionally, mitochondria are the main source of ROS in the CLL B-lymphocyte, and so the use of rotenone (a mETC complex I inhibitor) is a physiologically-relevant way of producing intracellular ROS (Jitschin et al., 2014). Intracellular ROS levels remained elevated in rotenone-treated B-lymphocytes (FH9 cell line) between 0.5 and 25 hours of treatment, and this caused cell death, indicating that these cells were under sustained oxidative stress (**Figures 3.1** and **3.2**). In hindsight, stimulation of NADPH oxidase as a means of ROS production

would have been the ideal option for the development of a positive control as this is responsible for ROS production in response to RTX (Honeychurch et al., 2012).

Ideally, the development of a positive control should have been performed in a CLL B-lymphocyte cell line as the phenotype would have resembled that of primary CLL B-lymphocytes, however, at the time, no CLL B-lymphocyte cell lines were available in our research laboratory. It would have been beneficial to establish a positive control in using primary patient samples; however, this would require a large number of samples to be tested due to the heterogeneity of the disease and was therefore impractical due to the invaluable nature of primary patient samples. This is further reflected in the observation that healthy B-lymphocytes did not die in response to rotenone after 4 hours of treatment, which suggests that oxidative stress-induced cell death may take longer in healthy B-lymphocytes compared to that observed in the immortalised FH9 B-lymphocyte cell line.

In addition to the above shortfalls of the development of a positive control was the use of CellROX® Orange to detect intracellular ROS. This probe was used as it had established in our research group to detect rotenone-induced ROS, however, as CellROX® Orange detects superoxide, hydrogen peroxide, and nitric oxide, this study cannot elucidate as to which ROS were detected at each timepoint and it is entirely possible that the ratio of superoxide and hydrogen peroxide changed throughout the time course. An alternative approach would be to use MitoSOX™ as it has previously been used to detect mitochondrial superoxide in CLL cells (Jitschin et al., 2014). Although the positive control could in future be better tailored to understanding RTX-mediated cell death, the use of rotenone therapy in understanding CLL cell's dependence on oxidative phosphorylation is still valid.

3.3.3 ROS and cell death non-BLA vs BLA

Individuals with CLL were selected based on the presence or absence of BLA and sample availability. The cohort consisted of 6 individuals without BLA and 12 with BLA. Those with BLA had evidence of earlier progressive disease compared to those without BLA (**Figures 3.3** and **3.4**). These results indicate that those with BLA have a poor prognosis which is supported by the literature (Joshi et al., 2007). Unfortunately, for many of the samples, the sample acquisition date was greater than 5 years after the date of diagnosis, particularly for those who were diagnosed before 2010, and was due to the BLA study and categorisation by Cohen *et al.* (2019) being retrospective and therefore having limited sample availability. Furthermore, samples that had been cryopreserved for more than 10 years had poor viability upon thawing and consequently only samples that were from 2012 onwards could be used for the purposes of studying in *in vitro* culture. Additionally, FMC63 and FMC190 were excluded from analysis for the remainder of this chapter due to high levels of spontaneous cell death, which has been reported in the literature to be common in *in vitro* culture of CLL B-lymphocytes (Oliveira, Pereira, Metze, & Lorand-Metze, 2001; Sanz et al., 2004).

Interestingly, basal intracellular ROS were on average lower in CLL B-lymphocytes from individuals with BLA compared to those without and healthy controls (**Figure 3.5**). This result supports the hypothesis that CLL B-lymphocytes arising from a crowded microenvironment may require higher levels of antioxidants because of higher ROS production due to hypoxic conditions. There were four samples from the BLA group that had low intracellular ROS levels (FMC100, FMC161, FMC285, and FMC31) three of which had an unmutated *IGHV* status and one unknown. B-cell receptor stimulation has been shown to increase the production of ROS, and CLL B-lymphocytes with unmutated *IGHV* have overactive B-cell receptor signalling (Cesano et al., 2013; Wheeler & Defranco, 2012). It is possible that these CLL B-lymphocytes have increased antioxidant levels to be able to handle the ROS produced in response to the overstimulated B-cell receptor, and hence have lower intracellular ROS levels. Also, del11q CLL are almost entirely have unmutated *IGHV* and it is this subtype of CLL that has been associated with BLA, even though our own cohort did not support that finding (Cohen et al., 2019) although unmutated *IGHV* trended to being associated with BLA in the larger cohort as stated. Therefore, CLL with unmutated *IGHV* with a higher chance of drug-resistant disease may have inherent ROS handling differences which would be an important avenue for future work. In addition, there was one non-BLA sample (FMC44) that also had low basal intracellular ROS and had a mutated *IGHV* status. However, as the *IGHV* for this individual was 6.3 % mutated, only 4.3 % above the 'mutated' classification cut off, discussion about the cut off for *IGHV* classification is warranted.

Loss of tumour suppressor genes has been associated with oxidative stress, and del17p and del11q CLL cases have higher levels of oxidative damage (Bensaad & Vousden, 2007; Collado et al., 2014; Watters, 2003). Therefore, samples with cytogenetic abnormalities affecting chromosomal regions containing tumour suppressor genes *ATM* (chromosome 11) and *TP53* (chromosome 17) were expected to have higher basal intracellular ROS levels. However, FMC100 (BLA), FMC44 (non-BLA), and FMC31 (BLA) had low intracellular ROS levels (<2000 CellROX® Orange MFI; **Figure 3.5**). These results suggest that these CLL B-lymphocytes have adapted to survive elevated intracellular ROS levels, that were generated through initial tumourigenesis, by increasing their antioxidant capacity. This indicates that these CLL B-lymphocytes may have a survival advantage when therapies that induce cell death through ROS signalling pathways, particularly anti-CD20 therapies, are used (Bellosillo et al., 2001; Honeychurch et al., 2012).

Jitschin *et al.* (2014) found that CLL B-lymphocytes have higher intracellular ROS levels compared to healthy controls. Although this was not the case in this study, there was a healthy control that had elevated basal intracellular ROS (**Figure 3.5**) that was most likely responsible for pushing the average up, and so it is debatable whether this sample should have been considered as an outlier and been removed from the analysis. More control samples would be required to confirm the statistical mean of a larger cohort. Regardless, the observation remains that CLL B-lymphocytes with low basal ROS levels exist and suggests a higher antioxidant capacity.

Understanding the antioxidant capacity of CLL B-lymphocytes would help to inform treatment regimens as these CLL B-lymphocytes are likely able to combat the ROS production that therapies cause as a means of inducing cell death and hence such therapeutics are likely to fail in these individuals. It would be of great benefit to explore this further by broadly assessing antioxidant levels in this cohort using mass spectrometry. Additionally, overall antioxidant capacity should be measured in the way that this has previously been performed in CLL using the Cayman Antioxidant Assay which measures the ability of cell lysates to prevent the oxidation of a fluorescent compound (Jitschin et al., 2014).

As the complex I inhibitor rotenone was used to increase intracellular ROS, mitochondrial mass was measured to determine whether this affected the response of CLL B-lymphocytes to rotenone treatment. It was expected that a higher mitochondrial mass would result in the production of more ROS by rotenone. However, there was no correlation between intracellular ROS or cell death with mitochondrial mass after rotenone treatment (**Figure 3.6**). This result suggests that mitochondrial mass did not impact the response of B-lymphocytes to rotenone treatment. Additionally, there was no difference in mitochondrial mass between non-BLA or BLA CLL B-lymphocytes and healthy controls, and there was no correlation between intracellular ROS and mitochondrial mass overall. However, the level of mitochondrially-produced ROS is also dependent on mETC activity. Therefore, mETC activity would be a better indication of the effect mitochondria could have on intracellular ROS levels. Analysis of mETC activity, by measuring oxygen consumption rate, in CLL B-lymphocytes has previously been performed by Lu *et al.* (2019) using an Extracellular Flux Analyser (Lu et al., 2019). Obtaining mETC activity data for samples in the current study would allow for a better understanding of the resting state of non-BLA and BLA CLL B-lymphocytes, and how this could impact their fate after treatment with rotenone.

The treatment of Raji B-lymphocytes with RTX was based on the work by Honeychurch *et al.* (2012) who showed that intracellular ROS levels and cell death did not change in response to RTX treatment. As mentioned previously, their study did not cross-link RTX with anti-human IgG which is required to elicit cell death *in vitro* (Shan et al., 2000). This study aimed to determine if intracellular ROS increased in response to cross-linked RTX treatment. It was observed that intracellular ROS levels significantly increased after treatment with cross-linked RTX whilst they did not increase after RTX alone, and this correlated with cell death in the malignant cell line (**Figure 3.7**).

To reproduce the work by Honeychurch *et al.* (2012), a 4-hour treatment period was selected, and, although this length of time allowed for the detection of cell death, generation of ROS in response to RTX treatment has been shown to occur as early as 10 minutes thereafter (Bellosillo et al., 2001). Therefore, it is highly likely that early increases in intracellular ROS levels were not detected. Additionally, intracellular ROS was only measured in viable cells as cells undergoing cell death have leaky membranes and cannot retain the carboxy-DCF, and therefore intracellular ROS cannot be

accurately measured in dead cells. It would have been beneficial to assess intracellular ROS at earlier time points to not only be able to detect early increases in intracellular ROS, but to include those cells that were dead at 4 hours. Earlier timepoints were not included in this study as enough cells were not available to perform this.

Four hours was selected as a treatment time point for future experiments as both intracellular ROS and cell death were significantly elevated after rotenone and cross-linked RTX treatment at this time, and these were both the desired measurable outcomes for experiments with primary CLL B-lymphocytes.

3.3.3.1 CLL B-lymphocytes die in response to rotenone

Unexpectedly, rotenone treatment had no effect on cell death in healthy B-lymphocytes (**Figure 3.9**) regardless of the increase in intracellular ROS levels that were detected (**Figure 3.10**). The way in which rotenone causes cell death through inhibition of complex I is two-fold: 1) electron leakage causes the formation of superoxide, generating elevated intracellular ROS levels and subsequent damage to important macromolecules; and 2) there is a significant reduction in proton transfer into the intermembrane space which in turn reduces ATP regeneration through oxidative phosphorylation. Cellular damage together with bioenergetic dysfunction cause the cell to undergo programmed cell death (Giordano, Lee, Darley-Usmar, & Zhang, 2012). It is possible that the 4-hour time point was not long enough to observe cell death, however it is also likely that healthy B-lymphocytes can regenerate ATP through glycolysis and the citric acid cycle and hence delay cell death through the ability to use alternative means of ATP regeneration. In contrast, rotenone caused cell death in CLL B-lymphocytes (**Figure 3.9**) along with an increase in intracellular ROS (**Figure 3.10**). However, intracellular ROS after rotenone treatment was lower in both non-BLA and BLA CLL B-lymphocytes compared to healthy controls suggesting that CLL B-lymphocytes have a higher antioxidant capacity. These results indicate that this enhanced antioxidant capacity did not assist in preventing cell death in CLL B-lymphocytes after rotenone treatment and it is highly likely that high levels of cell death were due to the blocking of oxidative phosphorylation which CLL B-lymphocytes are highly dependent on for energy production (Chowdhury et al., 2020). Perhaps the most important observation from these results is the distinct difference in response to rotenone treatment in the CLL cohort with six samples that undergo cell death and ten samples that seem resistant. However, future work should investigate later timepoints and dose response of CLL B-lymphocytes to rotenone treatment. Samples that had >10 % decrease in viability were FMC170, FMC236, FMC285, FMC31, FMC82, and FMC34. Five of these 6 samples had an unmutated *IGHV* status, suggesting that the use of therapeutics that take advantage of metabolic dysfunction may be more successful in individuals with an unmutated *IGHV* status.

Treatment of CLL B-lymphocytes with a direct inducer of oxidative stress such as hydrogen peroxide should be performed to determine which property of rotenone, increasing ROS or blocking of oxidative phosphorylation, caused cell death in the subgroup of CLL. Determining this could potentially reveal a

mechanism that may be able to be utilised for the development of personalised therapeutic regimens. These results present an opportunity to explore the use of such small molecules in combination with other CLL therapies.

As expected, healthy B-lymphocytes were susceptible to cross-linked RTX-mediated cell death, while CLL B-lymphocytes did not show signs of cell death following a 4-hour incubation with cross-linked RTX (**Figure 3.9**). In one CLL B-lymphocyte sample (FMC285) the response was similar to the healthy controls suggesting heterogeneity in ROS response in this disease, an effect that can only be resolved by a larger sample size. Interestingly, there was no increase in intracellular ROS observed across CLL B-lymphocytes and healthy controls following cross-linked RTX treatment which may have been due to the timing of ROS analysis (**Figure 3.10**). Previous work measured intracellular ROS in CLL B-lymphocytes after RTX treatment has only been measured up to 60 minutes post-treatment, and so it is unknown how superoxide generation is affected after this time (Bellosillo et al., 2001). The results from the current study suggest that superoxide generation is not sustained. Although the current study detected an increase in intracellular ROS levels in Raji B-lymphocytes after a 4-hour incubation with cross-linked RTX, it is possible that at this timepoint other ROS species that are a product of superoxide detoxification are elevated and this would have been detected in these experiments due to CM-H_2DCFDA being a general oxidative stress indicator. The experiments on CLL B-lymphocytes and healthy controls should therefore be repeated either using CellROX® Orange at a timepoint prior to 60 minutes or using CM-H_2DCFDA at the 4-hour timepoint to be able to detect increases in intracellular ROS after cross-linked RTX treatment. Additionally, the success of RTX treatment *in vitro* depends on surface CD20 expression and CLL B-lymphocytes have lower CD20 surface expression compared to healthy B-lymphocytes (Bellosillo et al., 2001). This suggests that the 4-hour timepoint in this study was inappropriate as an increase in intracellular ROS levels should have been observed in the healthy controls.

It was unexpected that some CLL samples exhibited low intracellular ROS levels, and this is grounds to explore how this is managed despite CLL B-lymphocytes relying heavily on oxidative phosphorylation for energy production. Nrf-2 overexpression is associated with poor prognosis in several cancers. If Nrf-2 were highly expressed and the Nrf-2 pathway continuously activated as suggested by Wu *et al.* (2010), the continuous induction of expression of antioxidants may explain the presence of CLL with low basal ROS (Ohta et al., 2008; Rushworth et al., 2012; Shibata et al., 2008; Solis et al., 2010). Additionally, low Keap1, which targets Nrf-2 for proteasome degradation, has been associated with cancer (Solis et al., 2010), and has been shown to be highly expressed in CLL (Wu et al., 2010). It would therefore be of great interest to assess the levels of Nrf-2 and Keap1 in CLL cases with low basal intracellular ROS. The Nrf-2 pathway could therefore be of therapeutic interest in CLL. The pro-oxidant Malabaricone-A is effective at causing cell death in lymphoblastic leukaemia cell lines through inhibition of Nrf-2 (Manna et al., 2015). If Nrf-2 is overexpressed in CLL cases with low

intracellular ROS levels, the effectiveness of Malabaricone-A should be tested in these cells. Additionally, such therapy could be beneficial in cases with high intracellular ROS levels by pushing these cells past their sustainable limit. Additionally, PEITC depletes the antioxidant glutathione and has previously been shown to elicit cell death in CLL but not healthy B-lymphocytes (Trachootham et al., 2008; Wu et al., 2010). Therapies that target redox homeostasis are therefore being investigated in CLL and thus the observation that some CLL B-lymphocytes have low basal ROS levels must be further explored in order to understand which cellular antioxidants are responsible for maintaining low ROS levels as this could inform the use of such therapeutics. Moreover, the use of rotenone to therapeutically target CLL B-lymphocytes is promising as it elicited cell death in CLL B-lymphocytes but not healthy controls.

As mentioned previously, the only other study to date that evaluated intracellular ROS levels of CLL (n = 10) and healthy B-lymphocytes (n = 8) found that CLL B-lymphocytes had elevated intracellular ROS levels (Jitschin et al., 2014). The number of healthy controls used in the study further supports the need for more healthy controls to be assessed and added to our dataset. Additionally, there was no mention of whether any patients included into their study had BLA, and, if no BLA cases were included, this may explain the absence of cases with low basal ROS. In addition, the study by Linley *et al.* (2015) found that individuals with unmutated *IGHV* had lower basal intracellular ROS levels compared to those with mutated *IGHV*, however did not disclose the presence of BLA in their cohort (Linley et al., 2015). Our results reflect this finding as the BLA cohort had lower basal ROS levels (**Figure 3.5**) and the majority had unmutated *IGHV* (7/8 with known *IGHV* mutational status; (**Table 3.7**). Of note, both studies used CM-H_2DCFDA to measure ROS levels suggesting that the cases identified in the current study as having low basal ROS as an artefact of the CellROX® Orange probe, however investigating the reason behind this would not be worthwhile, and instead basal ROS in our cohort should be re-measured using CM-H_2DCFDA as this method has already been established for use in our laboratory. The lack of identified cases with intracellular ROS levels lower than that of healthy controls in other studies warrants further investigation with more samples being added to our dataset.

Nevertheless, the results obtained from these experiments strengthen the need for therapeutic development and implementation in CLL that target the unique metabolic profile of CLL B-lymphocytes.

3.4 Conclusions

This chapter demonstrated that cross-linked RTX increases intracellular ROS and correlates with cell death in Raji B-lymphocytes. However, the relationship between ROS and primary CLL cells is less clear. Treatment of CLL B-lymphocytes with cross-linked RTX showed that most were resistant to cell death and did not demonstrate a significant increase in ROS. However, induction of oxidative stress in CLL B-lymphocytes using rotenone revealed that CLL B-lymphocytes are highly susceptible to inhibition of oxidative phosphorylation, suggesting that watershed events may occur is the cells are adequately stressed by ROS generation. These findings support what is known about the reduced ability of single agent anti-CD20 antibody RTX to induce cell death in the malignant CLL B-lymphocytes. While work from this chapter suggests that CLL B-lymphocytes from individuals with BLA may have higher basal antioxidant capacity compared to those without, the experimental work on BLA versus non-BLA CLL and their microenvironment ROS responses requires more data. The ROS data warrants further investigation into the reliance of BLA CLL B-lymphocytes on oxidative phosphorylation to potentially improve clinical response to RTX, particularly given the predictive effect of BLA on response to RTX-based therapy as seen here in the larger cohort and similar reduced response seen with bulky disease in new therapies such as venetoclax. Skewed metabolic responses and ROS handling presents an opportunity for therapeutic intervention that may assist with eradicating intrinsically resistant subclones in CLL, hiding in hypoxic under-perfused microenvironments that ultimately cause disease relapse and therapeutic failure.

Chapter 4:

Investigating low SOD2 expression in CLL

As mentioned in Section 1.2.1, the mETC is the main source of intracellular ROS through oxidative phosphorylation, therefore, antioxidants located in the mitochondria are required to protect important proteins and metabolic molecules in this organelle. There are two main antioxidants located at the mitochondria: superoxide dismutase 1 (SOD1) and superoxide dismutase 2 (SOD2). Both SOD1 and SOD2 work to convert superoxide to hydrogen peroxide, and are located in the intermembrane space and mitochondrial matrix, respectively (Kim, Gupta Vallur, Phaeton, Mythreye, & Hempel, 2017) (**Figure 4.1**).

Gene expression of *SOD2* in CLL has previously been shown to be significantly lower than in healthy B-lymphocytes, and proteomic data from our laboratory confirms this – SOD2 was found to be expressed approximately 5 times lower in CLL compared to healthy controls (Jitschin et al., 2014; Thurgood et al., 2019). Interestingly, not only is SOD2 expression lower, but the expression of its activating protein, sirtuin 3, is reduced in CLL which may further add to this effect by limiting the activity of the already reduced level of SOD2 available (Yu et al., 2016).

The antioxidant action of SOD2 also means that SOD2 has potential tumour suppressor activity through prevention of DNA damage by ROS (Bravard et al., 1992; Huang, He, & Domann, 1999). In support of this, decreased SOD2 has been shown to be associated with cancer development (Czeczot et al., 2005; G. G. Sun et al., 2011; Van Driel et al., 1997; Xu et al., 1999). Interestingly, CLL genotypes with unfavourable prognosis, del17p and del11q, show more oxidative damage with respect to the markers of oxidative stress: 8-oxo-2'-deoxyguanosine (DNA) and malondialdehyde (lipid), compared to the more favourable genotype del13q (Collado et al., 2014). Therefore, we hypothesised that low SOD2 expression in CLL could implicate SOD2 as an early driver of mutagenesis and disease progression, by allowing elevated basal intracellular ROS levels in the CLL cells and increasing the risk of mutagenesis favouring disease progression. Consequently, it is possible that low basal SOD2 expression in CLL may reflect a resetting of the ROS rheostat in this disease. Our prior work did however suggest that its expression is able to be increased in response to RTX therapy which we believe is driven by increasing potentially lethal ROS levels. Therefore, this chapter will further investigate SOD2 expression in samples from different CLL patients, to better understand this phenomenon and specifically investigate the mechanism of regulation of SOD2 in CLL, looking for genetic events which could downregulate basal levels yet allow response to lethal ROS challenges.

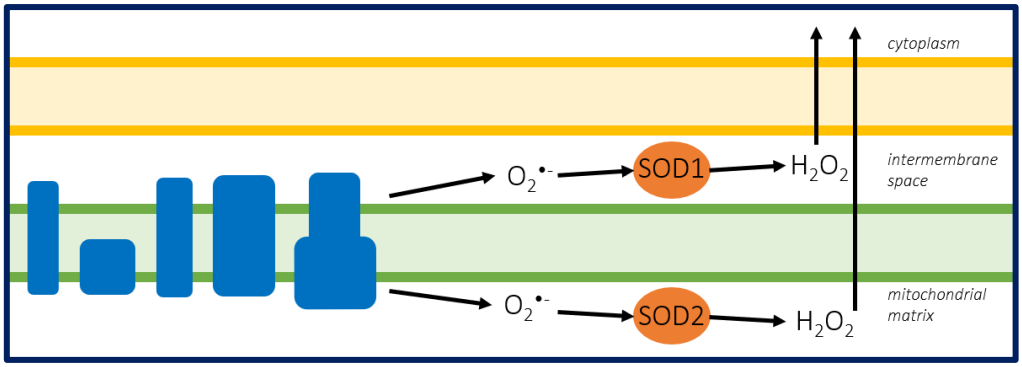

Figure 4.1: Detoxification of superoxide by superoxide dismutases.
Superoxide is produced by the mETC (blue) and detoxification is catalysed by SOD1 and SOD2 (orange) to form hydrogen peroxide which is converted to water by other cellular antioxidants.

The expression of *SOD2* is regulated by the transcription factors activating protein-2 (AP-2) and specificity protein 1 (Sp1). Through binding to GC-rich regions in the *SOD2* promoter, AP-2 and Sp1 inhibit and promote expression of *SOD2*, respectively (Xu, Porntadavity, & St Clair, 2002). A 70 bp stretch of the *SOD2* promoter (-150 bp – -80 bp) has been shown to be crucial for transcription factor binding and includes a region that forms an 11-guanine unpaired loop. Loss of this region has been shown to reduce *SOD2* transcriptional activity (Xu et al., 1999). In addition, it has been observed that methylation of the *SOD2* promoter can result in low SOD2 expression (Hodge et al., 2005; Huang, Peng, Oberley, & Domann, 1997; Hurt, Thomas, Peng, & Farrar, 2007b). Transcription factor binding sites in the *SOD2* promoter can be seen in **Figure 4.2**.

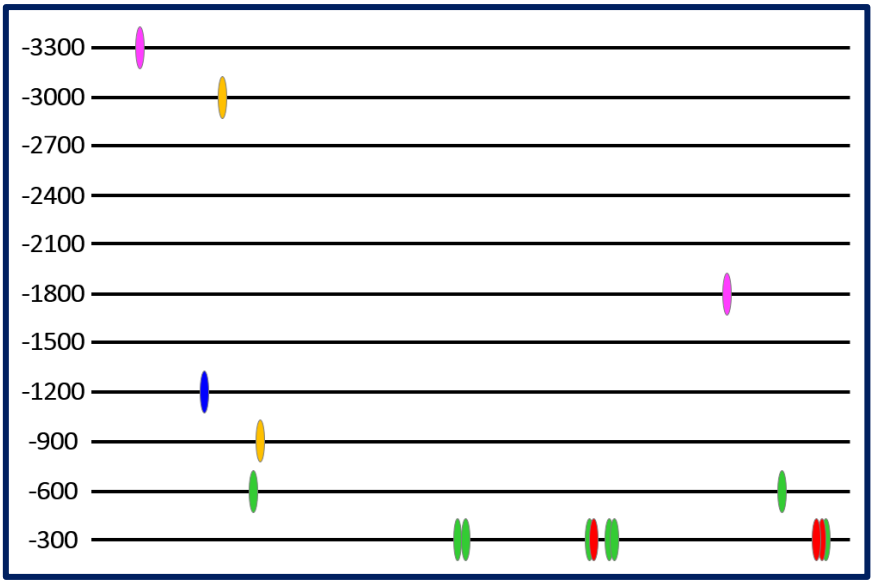

Figure 4.2: Schematic representation of transcription factor binding sites in the *SOD2* promoter.
Base position before the transcription start site is shown by numbers. Pink, NFκB; orange, AP-1; blue, antioxidant response element; green, Sp1; and red, AP-2 binding sites. Created using data from Xu *et al.* (1999).

Our previous work has shown that ROS handling in the advent of RTX exposure may be a critical factor in the cellular response to RTX. The literature and our own studies demonstrate that of the ROS handling machinery, SOD2 expression was lower than anticipated for CLL B-lymphocytes compared with healthy controls, but that it may be upregulated in drug-resistant CLL as potentially part of the mechanism for RTX and other drug resistance in this disease. ROS handling would appear to be highly important in the survival of CLL B-lymphocytes in the harsh microenvironments of the bulky expanded lymph nodes and grossly overcrowded bone marrow of the advanced CLL patient, who will require treatment of their disease. If RTX in part effects killing by generation of ROS, and individuals with BLA have disease cells that have mutated to withstand high ROS generation environments, then it is important to understand what drives their ability to withstand ROS and what mechanisms they possess to survive high ROS generation states. Taking into account our previous data as per Table 3.2, low SOD2 expression does not fit this particular hypothesis and is a standout in the normal ROS handling machinery. Therefore, this study aimed to explore the potential mechanism behind the downregulation of SOD2 in CLL.

4.1 Materials and methods

4.1.1 Selection of individuals for inclusion into the *SOD2* study

Individuals were selected from a South Australian cohort of treatment naïve individuals with CLL as a pilot study for this aim. Due to the heterogeneous nature of CLL, the cohort for this study consisted of patients that covered a broad range of important prognostic factors associated with CLL. Clinical characteristics for the cohort can be seen in **Table 4.1**. Normal B-lymphocytes were isolated from patients with haemochromatosis (which requires regular venesection of the patient for therapeutic purposes on a regular basis) and these served as the healthy controls. Peripheral blood pictures were assessed as otherwise normal.

Table 4.1: Patient clinical information for CLL PBMC samples used in the *SOD2* study.
U, unmutated *IGHV*; M, mutated *IGHV*.

Sample	Age (years)	TTFT (months)	Cytogenetics	*IGHV*
CLL1	47.17	Naïve	trisomy 12	U
CLL2	64.65	Naïve	del13q	M
CLL3	72.86	Naïve	normal	M
CLL4	65.2	Naïve	del11q	U
CLL5	67.84	Naïve	del17p	U
CLL6	76.69	Naïve	del13q	M

4.1.2 DNA extraction

Cell pellets were thawed followed by refreezing in liquid nitrogen with subsequent thawing at 95 °C. A total of three freeze-thaw cycles were performed. DNA extraction was performed using the Wizard® Genomic DNA Purification Kit (Promega, WI, USA) as per manufacturer's instructions (protocol TM050). Six hundred microlitres nuclei lysis solution was added to the cell pellet and cell lysate was passed through a needle until no visible cell clumps remained. Two hundred microlitres protein precipitation solution was added and the mixture was vigorously vortexed for 20 seconds before being placed on ice for 5 minutes. Lysates were centrifuged at 16000 x *g* for 4 minutes at room temperature and supernatant was transferred to a new 1.5 mL Eppendorf tube containing 600 µL isopropanol. The mixture was inverted until visible DNA strings were observed and the mixture was centrifuged at 16000 x *g* for 1 minute at room temperature. The supernatant was discarded, and the DNA pellet was washed with 600 µL 70 % ethanol and centrifuged at 16000 x *g* for 1 minute at room temperature. The

supernatant was discarded, and DNA pellets were allowed to air dry for 10 minutes. One hundred microlitres DNA rehydration buffer was added to the DNA pellet and DNA was incubated at 65 °C for 1 hour. DNA was stored at 4 °C until required.

4.1.3 PCR amplification of the *SOD2* promoter region (-3322 to -242 bp; PCR-1, PCR-2 and PCR-3)

Each PCR tube contained 50 ng DNA template, 1x PCR Buffer (Applied Biosystems), 0.8 µM forward and reverse primers (IDT), 200 µM dNTPs (Fisher Biotechnologies), 5 U *Taq* Polymerase (Applied Biosystems), 1 mM Mg^{2+} (Applied Biosystems), and 6 % DMSO (ChemSupply) in a final volume of 25 µL. Experiments were carried out under the cycling conditions detailed in **Table 4.2**. A no template control was also performed to check for reagent contamination.

Table 4.2: Amplification of the *SOD2* promoter region (-3322 to -242 bp) PCR cycling method.

Stage (repeats)	Temperature (°C)	Time
***Taq* activation**	95	5 minutes
Amplification (35x)	94	30 seconds
	58 (PCR-3); 60 (PCR-1 & PCR-2)	30 seconds
	72	30 seconds
Final elongation phase	72	7 minutes
Incubation	25	2 minutes

4.1.4 PCR amplification of the *SOD2* promoter region (-321 bp to +70 bp; PCR-4)

Each PCR tube contained 50 ng DNA template, 1x PCR buffer (Applied Biosystems), 0.8 µM forward and reverse primers (IDT), 200 µM dNTPs (Fisher Biotechnologies), 5 U *Taq* Polymerase (Applied Biosystems), 1.5 mM Mg^{2+}, 5 % DMSO, and 1.3 M betaine (Sigma-Aldrich). Reactions contained 150 µM 7-deaza-dGTP (C7-dGTP) (NEB) and dGTP was added to achieve a final concentration of 50 µM (3:1 ratio). Experiments were carried out under the cycling conditions detailed in **Table 4.3**. A no template control was also performed to check for reagent contamination.

Table 4.3: Amplification of the *SOD2* promoter region (-321 to +70 bp) PCR cycling method.

Stage (repeats)		Temperature (°C)	Time
***Taq* polymerase activation**		95	5 minutes
Primer annealing (5x)		95	45 seconds
		72	1 minute
Amplification (35x)	**Denaturing**	95	30 seconds
		98	10 seconds
	Annealing	60	30 seconds
	Extension with heat pulses (7x)	78	5 seconds
		85	2 seconds
	Extension with heat pulses (7x)	78	5 seconds
		90	2 seconds
Final elongation phase		72	10 minutes
Incubation		4	1 minute

4.1.5 Gel extraction and purification of PCR products

PCR products were visualised on a 0.8 % (w/v) agarose gel as described in 2.1.6. Bands were excised using a scalpel and weighed. PCR products were purified using the GenElute™ Gel Extraction Kit (Sigma-Aldrich) as per manufacturer's instructions (protocol TD, JC, PHC 06/11-1). Centrifugation steps were performed at 16,000 x *g*.

4.1.6 Sodium bisulphite conversion

DNA was sodium bisulphite treated using the EpiTect Bisulfite kit (QIAGEN, Netherlands) as per manufacturer's instructions (protocol 1090269 12/2014). Centrifugation steps were performed at 17,000 x *g*.

4.1.7 PCR of the *SOD2* promoter region (bisulphite-treated – short product)

Two rounds of PCR were performed to amplify the *SOD2* promoter region. Each PCR tube contained 25 ng bisulphite-treated DNA template, 1x PCR Buffer (Applied Biosystems), 0.8 µM forward and reverse primers (IDT), 200 µM dNTPs (Fisher Biotechnologies), 5U *Taq* polymerase (Applied Biosystems), 1.5 mM Mg^{2+} (Applied Biosystems) in a final volume of 25 µL. All experiments were carried out under the cycling conditions detailed in **Table 4.4**. No template control was also performed to check for reagent contamination.

Table 4.4: PCR cycling method for stunted amplification of the *SOD2* promoter region.

Stage (repeats)	Temperature (˚C)	Time
***Taq* polymerase activation**	95	5 minutes
Amplification (35x)	94	30 seconds
	55 (round 1) 60 (round 2)	30 seconds
	72	30 seconds
Final elongation phase	72	7 minutes
Incubation	25	2 minutes

4.1.8 PCR of the *SOD2* promoter region (bisulphite-treated – full-length product)

Two rounds of PCR were performed to amplify the *SOD2* promoter region. Each PCR tube contained 25 ng bisulphite-treated DNA template, 1x AmpliTaq™ 360 Buffer (ThermoFisher Scientific, Australia), 10 % 360 GC-enhancer (ThermoFisher Scientific), 0.8 µM forward and reverse primers (IDT), 200 µM dNTPs (Fisher Biotechnologies, Australia), 5 U AmpliTaq 360 DNA Polymerase (ThermoFisher Scientific), 1.5 mM Mg^{2+} (Applied Biosystems) in a final volume of 25 µL. For the second round of PCR, 2 µL of first round product was used as template DNA. All experiments were carried out under the cycling conditions detailed in **Table 4.5**. No template control was also performed to check for reagent contamination.

Table 4.5: PCR cycling method for full-length amplification of the *SOD2* promoter region.

Stage (repeats)	Temperature (˚C)	Time
***Taq* polymerase activation**	95	5 minutes
Amplification (35x)	95	30 seconds
	55	30 seconds
	72	30 seconds
Final elongation phase	72	7 minutes
Incubation	25	2 minutes

4.1.9 Enzymatic purification of PCR products

PCR products were purified by treatment with Shrimp Alkaline Phosphatase (SAP; GE Healthcare, Australia) to degrade residual dNTPs, and exonuclease I (NEB) to degrade single stranded DNA such as residual PCR primers. In brief, 5 U exonuclease I (NEB), 1 U SAP and 1x SAP reaction buffer (GE Healthcare) were added to 5 µL of PCR product and the reaction was incubated at 37 °C for 60 minutes. Enzymes were heat inactivated by incubation to 80 °C for 20 minutes.

4.1.10 Sanger sequencing

PCR product concentration was determined through agarose gel electrophoresis and compared to that of known standards. PCR products were diluted to 10 ng/100 bp of product, forward and reverse primers were diluted to 5 μM, and these were provided to the SA Pathology Sequencing Facility for Sanger sequencing.

4.2 Results

Superoxide dismutase 2 RNA and protein expression levels have been shown to be lower in CLL B-lymphocytes compared to healthy B-lymphocytes (Jitschin et al., 2014; Thurgood et al., 2019). Gene promoters are crucial for proper regulation of gene expression as they contain regulatory elements that recruit transcription factors. In order to understand *SOD2* gene regulation and promoter dynamics in CLL, this study posed three specific questions addressing the aim: To explore the potential mechanism behind the downregulation of SOD2 in CLL.

1. Are there mutations in transcription factor binding sites that prevent the binding of transcription factors to the *SOD2* promoter in CLL?
2. Is the *SOD2* promoter methylated, and hence 'switched off', in CLL?
3. Are the 'on' and 'off' transcription factors Sp1 and AP-2 abnormally expressed in CLL?

4.2.1 *SOD2* gene expression in selected cohort

The cohort selected for this study consisted of three healthy controls and six CLL patients with a range of prognostic indicators (**Table 4.1**). As **Figure 4.3** shows, *SOD2* transcripts were expressed at a significantly ($p = 0.00194$) lower level in CLL B-lymphocytes compared to healthy controls. Therefore, this cohort was appropriate for use in a pilot study to address the aims of this study.

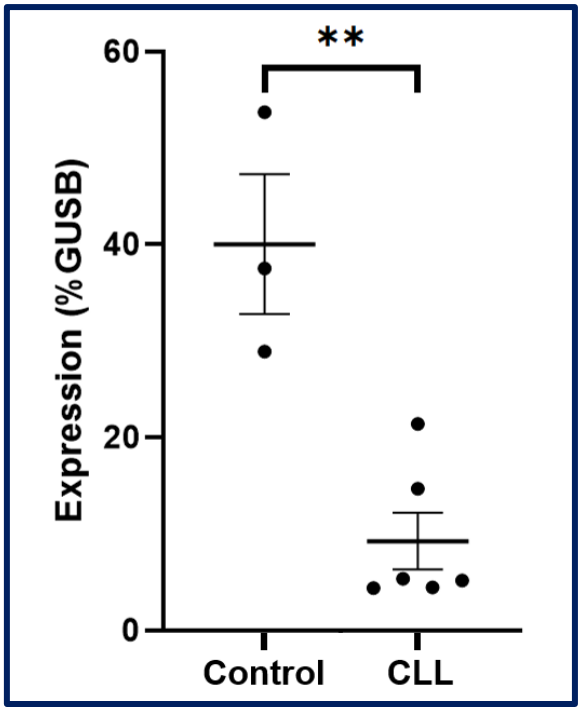

Figure 4.3: *SOD2* is expressed at a lower level in CLL B-lymphocytes compared to healthy controls.
SOD2 transcripts were assessed using real-time qPCR. Error bars, ±1 standard error of the mean; n = 3 for healthy controls; n = 6 for CLL B-lymphocytes; **, $p<0.05$ as calculated using a t-test.

4.2.2 Sequencing the *SOD2* promoter

The *SOD2* promoter was previously sequenced in the low SOD2-expressing HT29 human colon adenocarcinoma cell line and mutations in AP-2 and Sp1 transcription factor binding sites were identified (St Clair & Holland, 1991; Xu et al., 1999). These mutations were found to be present in additional colon cancer cell lines, the U87 human glioblastoma cell line and HT-1080 human fibrosarcoma cell line. Transcription factor binding sites in the *SOD2* promoter can be seen in **Figure 4.2**. In order to understand why SOD2 expression is lower in CLL, the promoter was sequenced to determine if CLL individuals had acquired mutations which could explain the observed reduction in expression.

Initial attempts to amplify the GC-rich region of the *SOD2* promoter (PCR-4: -321 to +70 bp) using conditions specified by Xu *et al.* (1999) were unsuccessful. This region of the promoter sequence is extremely GC-rich (76.5 % GC with a 52 bp-long stretch of 100 % GC), and therefore a comprehensive literature search on amplification of GC-rich regions was performed. A combination of 7-deaza-dGTP (C7-dGTP), DMSO, betaine, and heat pulses during the extension phase of PCR were used to

successfully amplify through this region of the *SOD2* promoter (Musso, Bocciardi, Parodi, Ravazzolo, & Ceccherini, 2006; Orpana, Ho, & Stenman, 2012) (**Figure 4.4**). Although successful amplification was achieved, only low quantities of product of the correct size were produced. Therefore, products were excised from the agarose gel in order to be sequenced (as described in 4.1.5). Sequencing of this region was unable to be performed for two CLL samples (CLL4 and CLL5) due to unsuccessful amplification (**Table 4.8**). In addition, the sequence of the first NF-κB binding site (**Figure 4.2**) could not be determined due to chromatogram traces being unable to be resolved.

Despite these difficulties, no mutations were detected within the predicted transcription factor binding sites nor within the *SOD2* promoter (-3332 to +70 bp) in the CLL B-lymphocytes compared to the healthy controls (**Table 4.8**).

Methylation of gene promoters can also result in the suppression of gene expression (reviewed in Moore *et al.* (2013)), and *SOD2* has previously been shown to be epigenetically silenced (Hodge et al., 2005). Therefore, methylation of the *SOD2* promoter in CLL was investigated as a potential cause for its downregulation in CLL.

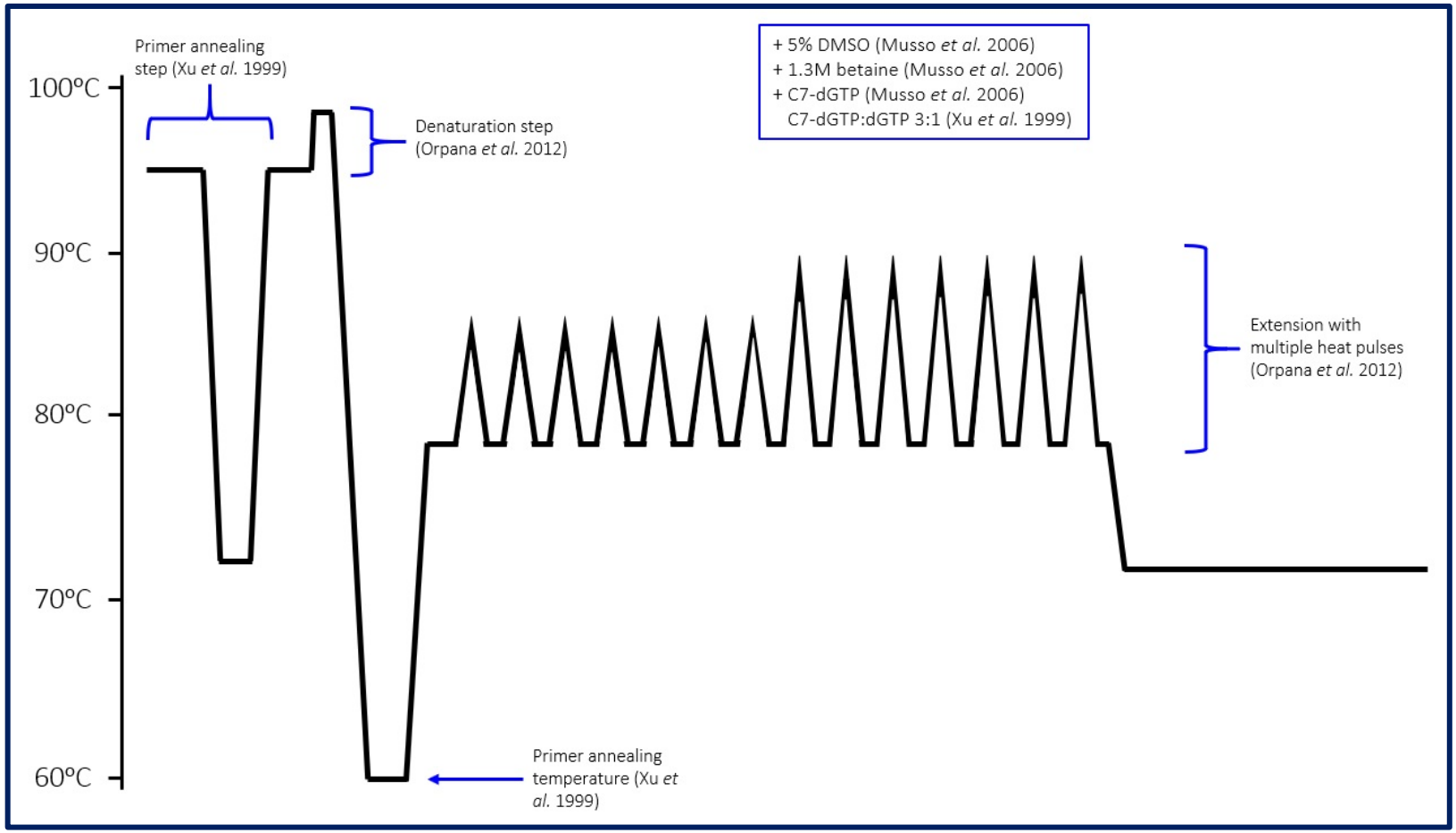

Figure 4.4: Customised PCR conditions used to amplify through the GC-rich region of the *SOD2* promoter.
PCR conditions were modified based on the literature. Modifications are identified in blue.

4.2.3 Determining the methylation status of the *SOD2* promoter

Xu *et al.* (1999 & 2002) showed that a GC-rich region of the *SOD2* promoter is crucial for transcriptional activity, and several studies have shown that hypermethylation of the *SOD2* promoter is associated with low SOD2 expression in diseased tissues (Hodge et al., 2005; Hurt, Thomas, Peng, & Farrar, 2007a; Hurt et al., 2007b). Therefore, this section investigated the methylation status of this region in CLL B-lymphocytes.

Amplification of a region of the *SOD2* promoter was performed using nested PCR on bisulphite treated genomic DNA as described in 4.1.7 (Hodge et al., 2005). Surprisingly, initial amplification produced a product 99 bp shorter than the expected size and was confirmed by Sanger sequencing (missing region is indicated by the box in **Figure 4.5**). The GC-rich region of the *SOD2* promoter that had been shown to be crucial for the expression of *SOD2* was absent in the chromatogram traces from both healthy and CLL B-lymphocytes. Thorough examination of the literature revealed that this region was also absent from the study conducted by Hodge *et al.* (2005), however *was* present in studies conducted by Xu *et al.* (1999 & 2002).

The inconsistency of these results led to the hypothesis that these findings were not biological, but instead that this region was being spliced out during PCR due to the nature of the G-rich region being able to form secondary structure(s). Secondary structures allow for the phenomenon of '*Taq* jumping' to occur around this site, and this phenomenon has previously been reported (Viswanathan, Krcmarik, & Cianciotto, 1999). Figure **4.6** depicts the proposed physical structure that occurred during amplification of the *SOD2* promoter, leading to the deletion of this 99 bp G-rich region.

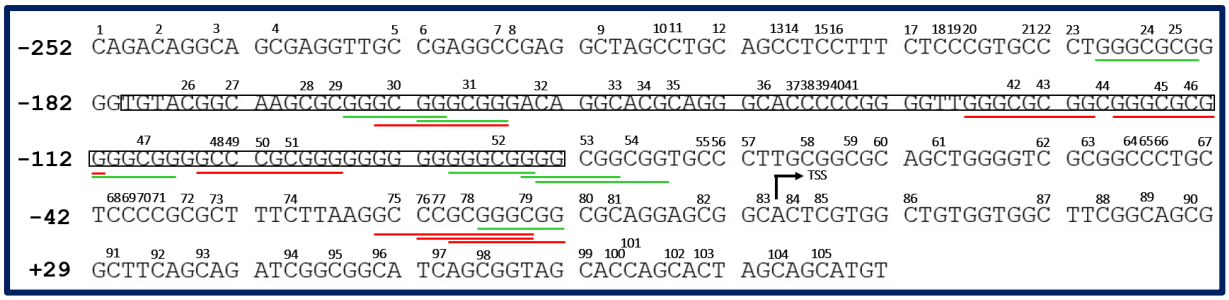

Figure 4.5: Sequence surrounding the *SOD2* transcription start site.
Numerical designation shows cytosine residues. Green, Sp1 binding site; red, AP-2 binding site; arrow, transcription start site; black box, missing sequence.

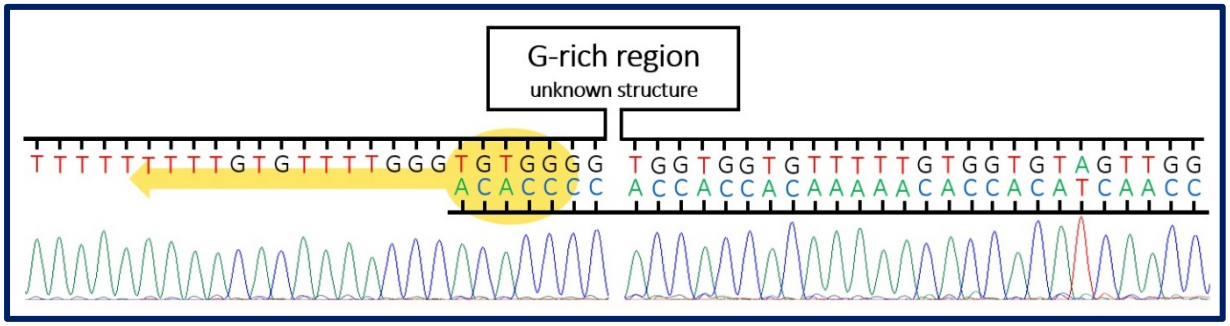

Figure 4.6: '*Taq* jumping' occurs across an unknown structure during amplification of the *SOD2* promoter using bisulphite-treated DNA.
From top to bottom: G-rich region unknown secondary structure of template strand (bisulphite treated); strand synthesised by *Taq* (yellow); chromatogram trace of *Taq* polymerase-synthesised strand.

Combinations of DMSO, betaine, and C7-dGTP with heat pulses during the extension phase of PCR were unsuccessful in resolving the secondary structure(s). Therefore, higher fidelity *Taq* polymerase and a GC-rich buffer were tested (as described in 4.1.8) and proved to be successful at amplifying the correct sized product.

As **Figure 4.8** shows, the *SOD2* promoter was largely unmethylated. Where methylation was detected, only limited methylation was observed (**Figure 4.7**). The methylation status of cytosine residues in a region spanning -195 to -100 in samples NOR1, CLL1, CLL3, and CLL6 were unable to be determined due to polythymine and polycytosine runs causing frame shifts in the forward and reverse chromatograms, respectively. Sequencing of samples that could sequence through the polycytosine run were because of the insertion of a thymine between C5 and C6 of the polycytosine sequence (**Figure 4.9**), and this was believed to be an artefact of sequencing through the G-rich region and will be discussed in section 4.3.4.

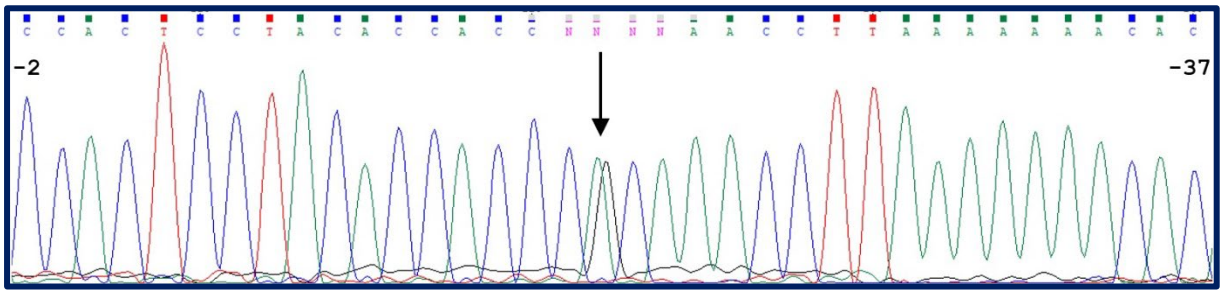

Figure 4.7: Cytosine methylation detection example.
Chromatogram trace of CLL1 annotated with base number with respect to the transcription start site. Arrow, limited methylation.

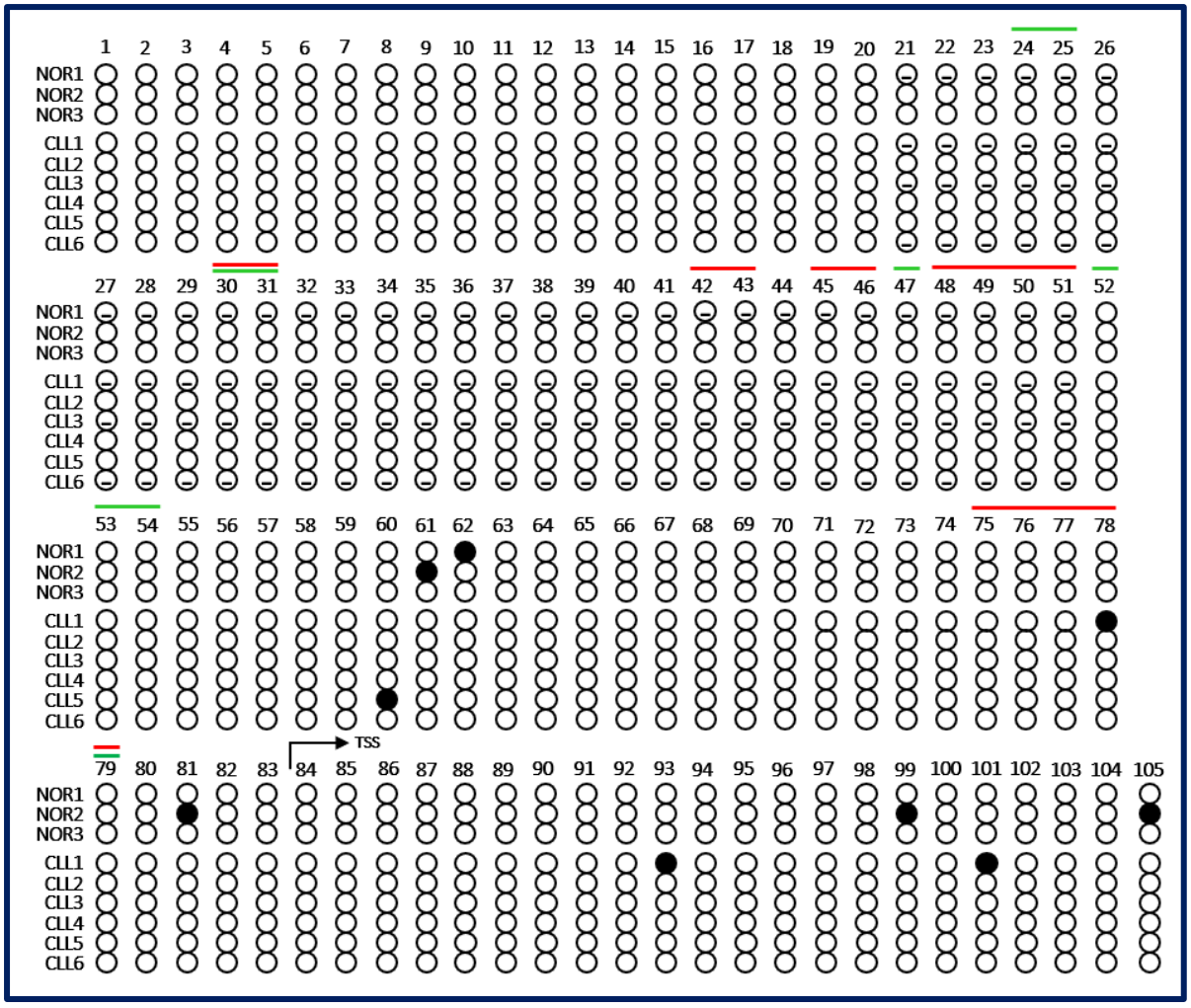

Figure 4.8: Methylation status of cytosine residues surrounding the *SOD2* transcription start site in CLL and healthy B-lymphocytes.

Numerical designation corresponds to cytosine residue in **Figure 3.15**. Blank, unmethylated; black, methylation detected; – , undetermined; green, Sp1 binding site; red, AP-2 binding site; arrow, transcription start site.

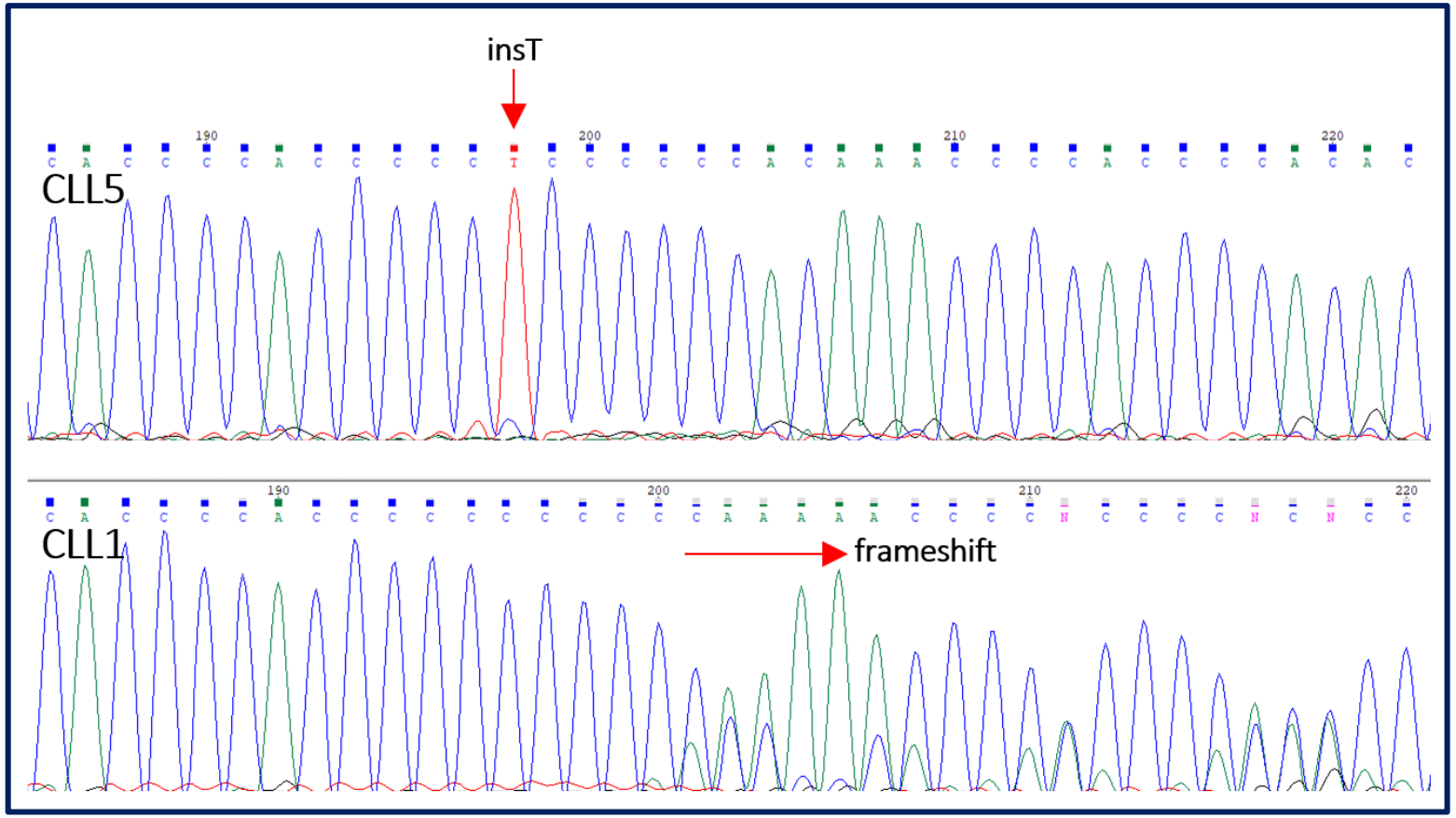

Figure 4.9: Thymine insertion prevents a frameshift caused by the 11 bp-long cytosine sequence.
Top to bottom: insertion of thymine in polycytosine run between C5 and C6 in CLL5; no insertion of thymine in CLL1 causing frameshift and sequence unable to be resolved.

As these results indicated that SOD2 downregulation in CLL B-lymphocytes is not due to either mutations in or methylation of the promoter, the final step was to analyse the expression of transcription factors responsible for *SOD2* expression.

4.2.4 Expression of transcription factors responsible for regulating SOD2 gene expression

As mentioned in section 3, there are two main transcription factors responsible for the regulation of *SOD2* transcription – Sp1 which promotes *SOD2* expression and AP-2 which inhibits *SOD2* expression. To determine if downregulation of *SOD2* expression is due to abnormal gene expression of these transcription factors, real-time qPCR amplicons targeting expression of the components of these transcription factor complexes were designed (**Table 4.6**). Although 2 out of 5 AP-2 variants have not been detected in blood cells, they were included into the panel since AP-2 inhibits *SOD2* gene expression, any non-physiological expression could explain the absence of *SOD2* transcription.

Table 4.6: Transcription factor gene panel.
Transcription factors with their designated gene symbol and protein expression in blood (from the Human Integrated Protein Expression Database in GeneCards).

Transcription factor	Gene	Expressed in whole blood?
Sp1	*SP1*	Monocyte, B-lymphocyte, CD4 T-cell, CD8 T-cell, lymph node
AP-2	*TFAP2A*	Not detected
	TFAP2B	Platelet
	TFAP2C	Platelet
	TFAP2D	Not detected
	TFAP2E	Platelet

Standard curves for each primer set were generated using serial 10-fold dilutions of control cDNA. Primer sets were successfully optimised for *TFAP2A*, *TFAP2C*, and *SP1* (**Table 4.7**). Primer sets for *TFAP2B*, *TFAP2D*, and *TFAP2E* could not be used due to non-specific amplification and suboptimal M-values. Therefore, publicly available GEO expression data was mined to assess the expression of these genes as an alternative and comparison with our own generated data.

Expression of *TFAP2A* and *TFAP2C* was not detected in CLL B-lymphocytes or healthy controls by real-time qPCR. However, this is discordant with proteomic data from our laboratory, which previously identified TFAP2A, TFAP2B, TFAP2C, and TFAP2E expression in CLL B-lymphocytes. **Figure 4.10 A** shows that mean *SP1* expression was 28 % lower in CLL B-lymphocytes compared to healthy

controls, however this difference was not significant (p = 0.356). **Figure 4.10 B** shows that there was no correlation between *SP1* and *SOD2* expression (R^2 = 0.0212).

Table 4.7: M and R^2 values of transcription factor primer sets.

Gene symbol	M-value	R^2-value
SP1	3.228	0.9999
TFAP2A	3.2813	1
TFAP2C	3.1019	0.999

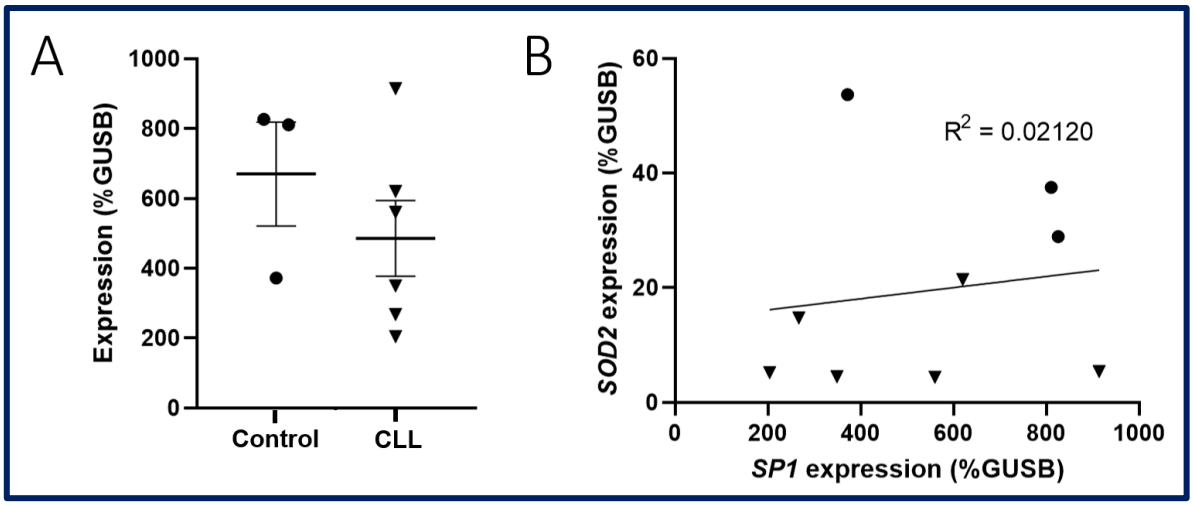

Figure 4.10: *SP1* gene expression does not correlate with *SOD2* gene expression.
SP1 gene expression was measured using real-time qPCR. **A**, expression of *SP1* in CLL B-lymphocytes and healthy controls; **B**, individual expression data for *SP1* and *SOD2* expression with trendline. Error bars, ± 1 standard error of the mean; circles, healthy controls; triangles, CLL B-lymphocytes.

In the absence of primary data generated in this study, the GEO database was utilised to assess the expression of *TFAP2B*, *TFAP2D*, and *TFAP2E* in CLL and healthy B-lymphocytes. Three RNA datasets that compared CLL and healthy B-lymphocytes were available. Of the three datasets available, only one dataset (GDS3902) detected gene expression of both *SOD2* and *TFAP2* transcription factors, however, in this cohort *SOD2* was expressed at a higher level in CLL B-lymphocytes compared to healthy controls, although not significantly (Vargova et al., 2011). Regardless, the dataset was used to determine whether there was a correlation between *SOD2* and *SP1* expression. **Figure 4.11 A** shows that there was no difference in expression of either *TFAP2B* and *TFAP2E* between CLL B-lymphocytes and healthy controls. There was also no correlation between the expression of either *TFAP2B* or

TFAP2E compared to *SOD2* as indicated by the R^2 values (**Figure 4.11 C & D**). In addition, *SP1* was detected and although expressed at a higher level in CLL B-lymphocytes compared to healthy controls (**Figure 4.11 A**), this was not significant and there was no correlation between *SOD2* and *SP1* expression (**Figure 4.11 B**). *TFAP2D* was not detected in this cohort.

This data indicates that expression of these transcription factors alone is not responsible for abnormal *SOD2* expression observed in CLL. Although a clear regulator of *SOD2* gene expression was not elucidated from these studies, several possibilities have been eliminated.

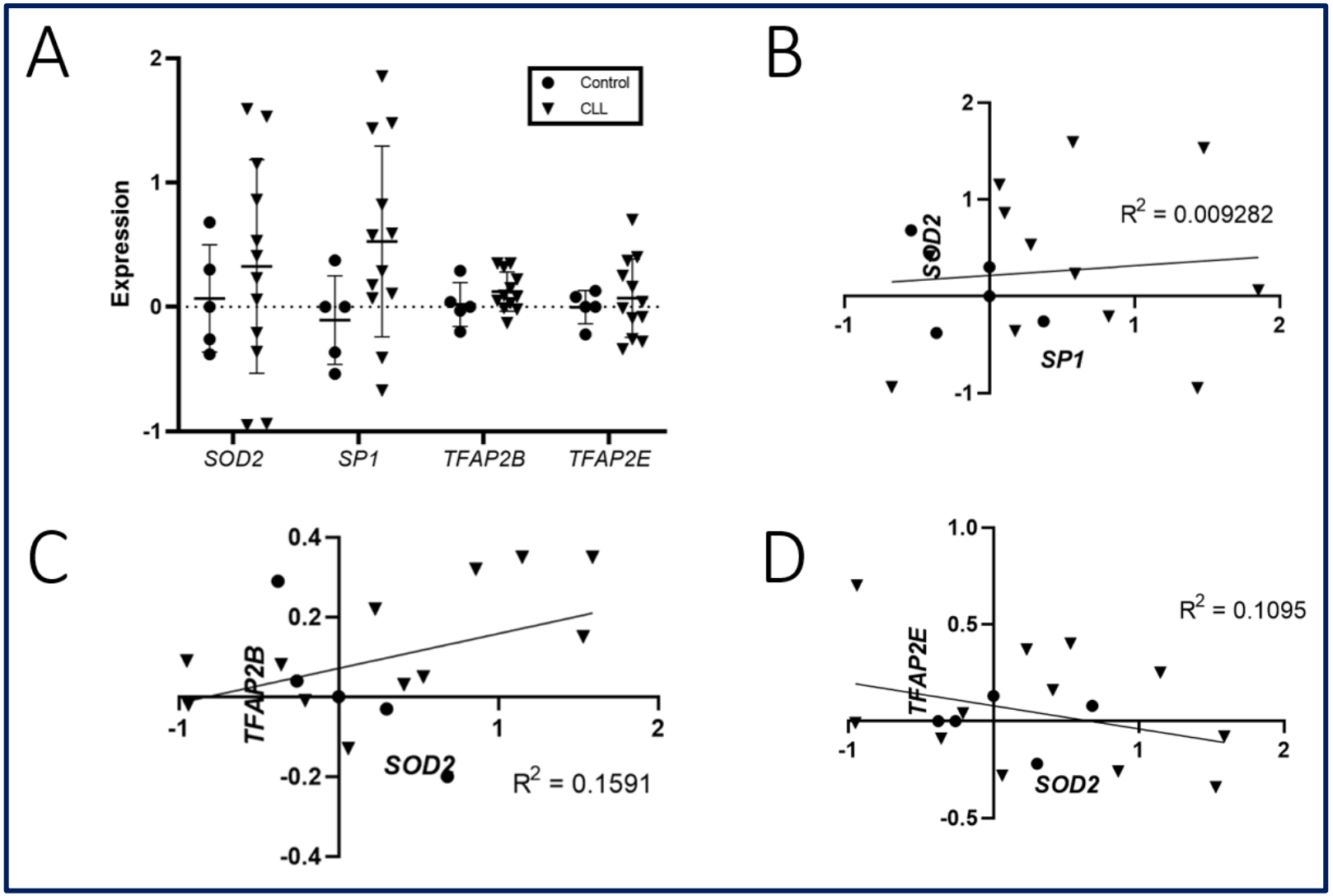

Figure 4.11: *SOD2* and transcription factor gene expression from GEO expression data mining.
A, *SOD2* and transcription factor expression in CLL B-lymphocytes (triangles) and healthy controls (circles); and individual expression data for: **B**, *SP1* and *SOD2*; **C**, *SOD2* and *TFAP2B*; and **D**, *SOD2* and *TFAP2E* with trendlines. Error bars, ± 1 standard deviation. Data from Vargova *et al.* (2011).

Table 4.8: Summary data of *SOD2* promoter sequencing status and identification of mutations.

Expression of *SOD2* and *SP1*; amplicons sequenced with identified mutations (-, none identified); bisulphite sequencing with number of methylated cytosines (C^m) identified.

	Expression (%*GUSB*)		Sequencing		Methylation	
Sample	***SOD2***	***SP1***	**Amplified**	**Mutations**	**Sequenced**	**C^m**
NOR1	53.7	372	1-4	-	Yes	2
NOR2	37.5	811	1-4	-	Yes	4
NOR3	28.9	826	1-4	-	Yes	0
CLL1	5.37	914	1-4	-	Yes	3
CLL2	14.7	267	1-4	-	Yes	0
CLL3	21.4	600	1-4	-	Yes	0
CLL4	4.4	560	1-3	-	Yes	0
CLL5	5.18	204	1-3	-	Yes	1
CLL6	4.45	349	1-4	-	Yes	0

4.3 Discussion

4.3.1 Summary

Antioxidant and reactive oxygen species have a two-faced role in the development and progression of cancer: loss of antioxidant activity leads to damage of cellular macromolecules that facilitate tumorigenesis, and the ability of antioxidants to scavenge harmful ROS in cancerous cells promotes their survival (Cockfield & Schafer, 2019). One such antioxidant is superoxide dismutase 2 (SOD2/MnSOD) which is localised to the mitochondrial matrix and is responsible for detoxifying superoxide to hydrogen peroxide.

In CLL, SOD2 has been shown to be expressed at a lower level compared to healthy B-lymphocytes (Jitschin et al., 2014). It is apparent that CLL B-lymphocytes have increased expression of other antioxidant molecules (**Table 3.1**) to counteract high mitochondrial activity and presumably compensate for low SOD2 levels. If SOD2 suppression were an early evolutionary event in the development of CLL and there were a non-reversible mechanism for low SOD2 expression, such as DNA mutations or promoter methylation, there would be an opportunity for therapeutic development that can take advantage of this dysregulation. Therefore, this study aimed to understand why SOD2 is expressed at a low level in CLL and what the pathophysiology behind this could be.

This chapter tested in detail, several possible causes for decreased SOD2 expression in CLL but found none of them able to provide plausible explanation. No mutations were identified in transcription factor binding sites of the *SOD2* promoter; however, one NF-κB binding site was missed due to the inability of chromatogram traces to be resolved. There were no similarities in the methylation pattern of the *SOD2* promoter between CLL B-lymphocytes, and no remarkable differences between CLL B-lymphocytes and healthy controls. Methylation of a region of the *SOD2* promoter could not be determined due to polyadenine and polyguanine runs causing frameshifts in chromatogram traces. RNA expression of transcription factors Sp1 and AP-2 involved in promoting and inhibiting *SOD2* expression, respectively, were not found to be responsible for the lower *SOD2* gene expression in CLL compared with healthy controls.

4.3.2 *SOD2* gene expression in selected cohort

The questions posed in section 4.2 were addressed using a pilot cohort of six individuals with CLL and three healthy controls. The CLL cohort consisted of three individuals with mutated *IGHV* and three with unmutated *IGHV* (**Table 4.1**). Two of the individuals with mutated *IGHV* had a deletion of 13q whilst the third had a normal karyotype, and individuals with unmutated *IGHV* had trisomy 12, deletion of 11q and deletion of 17p (**Table 4.1**). These factors confer a range of prognoses as seen in **Figures 1.6** and **1.7**. Although the pilot cohort was small, the range of prognostic indicators within the cohort

represents the heterogeneity seen in this disease, and thus provides an opportunity for SOD2 commonalities between CLL individuals to be identified in a pilot cohort. SOD2 expression was significantly lower in CLL B-lymphocytes compared to healthy controls ($p = 0.00194$; **Figure 4.3**) which supports the literature and proteomic data from our laboratory. The cohort was therefore deemed appropriate for the investigation.

Of note, the four CLL B-lymphocyte samples with the lowest *SOD2* expression (CLL1, CLL4, CLL5, and CLL6; **Figure 4.3**) correspond to the prognostic factors: deletion of 13q with mutated *IGHV*, trisomy 12 with unmutated *IGHV*, deletion of 11q with unmutated *IGHV*, and deletion of 17p with unmutated *IGHV*. As mentioned previously, del13q and mutated *IGHV* confer an indolent disease course, trisomy 12 infers an intermediate disease course, and del11q, del17p and unmutated *IGHV* infer an aggressive disease course. It may be beneficial to track the progression of the disease in these individuals and determine if *SOD2* expression levels change over time or correlate with disease progression to assess its use as a predictive marker. Additionally, it would be beneficial to perform such tracking in a larger number of individuals in a prospective cohort to provide conclusive statistical evaluation.

In this pilot study, the cohort consisted of individuals who were treatment naïve so that founding mutations or abnormalities in the regulation of *SOD2* expression could be identified. However, if time permitted, it would be of great benefit to assess SOD2 dynamics in individuals with relapse/refractory CLL as SOD2 expression is increased in advanced cancers and the response of SOD2 to various ROS-enhancing challenges (Dhar, Tangpong, Chaiswing, Oberley, & St Clair, 2011; Hempel, Carrico, & Melendez, 2011; Hempel, Ye, Abessi, Mian, & Melendez, 2009). Tracking SOD2 expression over the disease course presents an opportunity to investigate if and how SOD2 expression changes in CLL and could be used to demonstrate disease progression in particular the increase in BLA and changing metabolism of the cells, in individuals with this disease.

4.3.3 Sequencing the *SOD2* promoter

The *SOD2* promoter has binding sites for transcription factors that promote and inhibit *SOD2* expression. NF-κB, AP-1, Sp1, and the antioxidant response element promote *SOD2* expression while AP-2 inhibits *SOD2* expression (**Figure 4.2**; (Xu et al., 2002)). A region approximately 150 bp upstream of the transcription start site containing overlapping Sp1 and AP-2 binding sites has been shown to be crucial for the regulation of *SOD2* expression (Xu et al., 2002). Therefore, this region and up to -3300 bp upstream of the transcription start site was sequenced in order to investigate the possibility of mutations in transcription factor binding sites, or the introduction of transcription factor binding sites that could inhibit *SOD2* transcriptional activity.

The *SOD2* promoter was sequenced in four parts (Appendix 1 Table A1). The GC-rich nature of the PCR-4 region of the *SOD2* promoter proved difficult to sequence, and this is most likely due to DNA superstructures forming during PCR. The modified C7-dGTP has been widely used for the amplification of G-rich sequences as it has a weaker bond between bases compared to dGTP, preventing the formation of secondary structures (Fernandez-Rachubinski, Eng, Murray, Blajchman, & Rachubinski, 1990).

Initial attempts at replicating PCR conditions outlined in Xu *et al.* (1999) using a mixture of C7-dGTP and dGTP to amplify the GC-rich region of the *SOD2* promoter (PCR-4) failed. A comprehensive literature search identified two additional compounds (DMSO and betaine) that could be used to prevent the formation of hydrogen bonds between bases during PCR, and thus the formation of DNA superstructures (Bhagya, Wijesundera Sulochana, & Hemamali, 2013; Jensen, Fukushima, & Davis, 2010). Musso *et al.* (2006) found that a combination of DMSO, betaine and 7-deaza-dGTP can be used to successfully amplify GC-rich regions of DNA, however, attempts at using all three of these compounds to amplify the GC-rich region of the *SOD2* promoter failed. Orpana *et al*. (2012) found that using heat pulses during the extension phase of PCR helped to resolve DNA superstructures in GC-rich templates. This method was therefore incorporated into amplification of the GC-rich region of the SOD2 promoter as outlined in **Figure 4.4** and was successful. Although the correct size product was produced, and many attempts were made, Sanger sequencing of this region failed in CLL4 and CLL5 (**Table 4.8**) and it is unclear why this is the case. No mutations were identified in this region in CLL B-lymphocytes suggesting that the lower expression was not due to inherent genetic abnormalities in the promoter and therefore must relate either to the balance of ROS handling proteins within the cell or to other aspects of CLL homeostasis for ROS (**Table 4.8**).

There were no mutations identified in the *SOD2* promoter in CLL and there was no difference in the sequence between CLL B-lymphocytes and healthy controls (**Table 4.8**). However, the first NF-κB binding site could not be sequenced. Although it is highly unlikely that a mutation in this one NF-κB binding site is responsible for low *SOD2* gene expression in all samples tested, future work should be performed to sequence this site. Additionally, Xu *et al.* (1999b) found that an intronic NF-κB element is crucial for the promotion of *SOD2* gene expression by TNFα and IL-1β. Unfortunately, time did not permit investigation into this region in CLL and therefore this NF-κB element should also be sequenced to determine if there are mutations that could be responsible for low SOD2 expression. Interestingly, IL-1β levels in CLL are lower than in healthy controls, and lower in progressive disease compared to non-progressive (Hulkkonen, Vilpo, Vilpo, Koski, & Hurme, 2000). Therefore, low IL-1β levels could be responsible for low SOD2 expression in CLL through the intronic enhancer being under stimulated. It would therefore be of great benefit to conduct an experiment that assesses whether IL-1β treatment can restore normal SOD2 levels in CLL in order to understand if this is responsible.

4.3.4 Methylation of the *SOD2* promoter

Hypermethylation of the *SOD2* promoter has previously been shown to be responsible for low SOD2 expression in diseased tissues (Hodge et al., 2005; Hurt et al., 2007a, 2007b). Therefore, the bisulphite sequencing method established by Hodge *et al.* (2005) was used to determine the methylation status of cytosines in the *SOD2* promoter in CLL samples.

This method was not initially successful at amplifying the entire region of interest and 99 bp of sequence was found to be missing (**Figure 4.5**). After some investigation, it was discovered that this region was absent from the results of the three publications that had used this method, and its absence was not acknowledged or explained (Hodge et al., 2005; Hurt et al., 2007a, 2007b). Interestingly, this region contains the 70 bp that has been shown to be crucial for *SOD2* promoter activity – including the 11-guanine unpaired loop (Xu et al., 1999). It was hypothesised that the G-rich nature of this region of the *SOD2* promoter allowed for the formation of secondary structures, which are more likely to form due to the single-stranded nature of bisulphite-treated DNA, and that *Taq* polymerase was able to 'skip' this structure during the first round of PCR (**Figure 4.6**) (Darst, Pardo, Ai, Brown, & Kladde, 2010). After interrogating the literature, an article was found that reported the phenomenon of '*Taq* jumping', where *Taq* polymerase had missed a hairpin structure that formed due to inverted repeats (Viswanathan et al., 1999). Therefore, alternative methods to resolve secondary structures during PCR amplification were pursued. It is intriguing that the '*Taq* jumping' phenomenon has not been reported more often and in studies sequencing GC-rich promoters, raising the possibility that incomplete sequencing reports exist.

As shown in section 4.1.4, a combination of DMSO, betaine, and C7-dGTP with heat pulses during the extension phase of PCR were successful at resolving DNA superstructures when sequencing the GC-rich region of the *SOD2* promoter. This method was tested on bisulphite-treated DNA but was unsuccessful. Communications with the Australian Genome Research Facility suggested that a high-fidelity *Taq* polymerase and GC-enhancer be tested. The use of AmpliTaq Gold™ 360 with 360 GC enhancer (ThermoFisher Scientific) proved successful in producing the correct size product. The *SOD2* promoter was largely unmethylated in both CLL and healthy controls (**Figure 4.8**). Additionally, the methylation status of a region including 31 cytosines could not be determined in one healthy control and three CLL due to frameshifts in both forward and reverse chromatogram traces. The frameshift in the reverse strand was caused by a 12-cytosine run located between cytosines 51 and 52 (**Figure 4.5**), which included the 11-unpaired guanine loop sequence. The frameshift in the forward strand was caused by a 13-thymine run located between cytosines 13 and 20 (**Figure 4.5**), where all cytosines in this region had been converted to thymine during bisulphite treatment.

Interestingly, from a technical perspective, successful sequencing through the 12-cytosine run was due to the insertion of a thymine between G6 and G7 of the 11-unpaired guanine loop sequence (-93 bp; **Figure 4.9**). This insertion was unexpected and consistent across all five samples that successfully

sequenced through this region. It is believed that this is an artefact of sequencing through a region with such low variation, and not a true insertion as this was not observed in previous sequencing of the corresponding genomic DNA for the same individuals. The insertion of the thymine on the reverse strand could be due to the nature of the *Taq* polymerase used during PCR. It is possible that during an early round of PCR, *Taq* polymerase encounters a DNA superstructure created by the G-rich sequence at the 11-unpaired guanine loop site, causing it to fall off and add a 3' adenine overhang. This fragment would then be preferentially amplified causing the resulting sequence to show this insertion. Interestingly, an adenine insertion at this site (-93 bp) was previously reported in tumour cell lines by Xu *et al.* (1999) who believed the insertion interferes with the G-loop structure and recruitment of transcription factors, thus preventing *SOD2* transcription. Evidence from the current study supports the fact that the result reported by Xu *et al.* (1999) is an artefact of sequencing this G-rich region.

The intronic enhancer was not investigated in this study, however methylation of this region is associated with decreased SOD2 levels (Huang et al., 1999). It has also been suggested that there is an interaction between the intronic enhancer and core promoter that promotes *SOD2* expression (Guo, Boekhoudt, & Boss, 2003; Maehara, Uekawa, & Isobe, 2002). Although investigating the intronic enhancer was beyond the scope of this study, it is of great interest to investigate this region in CLL to determine if its functionality is impaired.

It is also possible that RNA surveillance pathways are responsible for low *SOD2* transcripts in CLL. Nonsense-mediated decay of tumour suppressor gene transcripts has previously been reported in cancer, however this has not been previously reported for *SOD2* (Anczuków et al., 2008; R. Karam et al., 2008; Perrin-Vidoz, Sinilnikova, Stoppa-Lyonnet, Lenoir, & Mazoyer, 2002; Pinyol et al., 2007; Ware et al., 2006). The entire *SOD2* gene should be sequenced in CLL B-lymphocytes to identify any premature stop codons that could cause transcript decay, and hence be responsible for low *SOD2* in CLL. Additionally, micro-RNA expression could be responsible for the degradation of *SOD2* RNA transcripts, and future work should assess the level of the micro-RNA miR-146a, which has previously been shown to interact with the 3' untranslated region of *SOD2* to decrease translational activity (Ji et al., 2013).

4.3.5 Expression of transcription factors in CLL

As there were no mutations and no consistent methylation identified in the *SOD2* core promoter, expression of *SP1* and *TFAP2* genes were assessed to determine if abnormal expression of one or both could be responsible for low *SOD2* levels observed in CLL. As mentioned previously, Sp1 promotes *SOD2* transcription while AP-2 inhibits *SOD2* transcription (Xu et al., 2002).

SP1 expression was lower in CLL B-lymphocytes compared to healthy controls, however *SP1* expression did not correlate with *SOD2* expression levels in the cohort (**Figure 4.10**). Although *SP1*

expression did not correlate with *SOD2* expression in this study, Sp1 binding to the *SOD2* promoter has been shown to be p53-dependent, and therefore, it would be interesting to assess the expression of p53 in this cohort (Dhar et al., 2011).

Primer sets could not be selected for *TFAP2B*, *TFAP2D*, and *TFAP2E* due to non-specific amplification. As primer sequences were checked for specificity *in silico*, this is most likely due to low transcript availability forcing amplification of non-specific sites.

Therefore, expression of these genes in CLL was assessed using a dataset from GEO (GDS3902). This dataset consisted of Genome-wide microarray expression data of B-lymphocytes from CLL and healthy individuals (Vargova et al., 2011). The dataset indicated that there was no correlation between *TFAP2B* or *TFAP2E* with *SOD2* expression (**Figure 4.11 C** & **D**). *TFAP2D* was not detected in this dataset. In addition, *SP1* was detected and was higher in CLL compared to healthy controls, and expression varied greatly among the CLL cohort (**Figure 4.11 A**). However, there was no correlation between *SP1* and *SOD2* expression (**Figure 4.11 B**). Interestingly, *SOD2* expression varied greatly within the CLL cohort and on average was not lower in CLL compared to healthy controls (**Figure 4.11 A**). Unfortunately, the corresponding publication did not include any clinical information for the individuals in the CLL cohort (Vargova et al., 2011). It would be interesting to correlate the clinical data to SOD2 expression, as *SOD2* dynamics have been shown to change between the early stages of carcinogenesis, where it is expressed at a low level, to aggressive disease, where it is expressed at a higher level and this may explain the difference in SOD2 expression in these cohorts (Dhar et al., 2011; Hempel et al., 2011).

Additionally, the level of AP-2 and Sp1 proteins should also be assessed to determine if low transcription factor levels are responsible for low *SOD2* transcripts in CLL. Interestingly, Sp1 requires phosphorylation at Thr278/739 by c-Jun N-terminal kinase 1 (JNK1) to maintain its stability during mitosis (Chuang et al., 2008). It is possible that a defect exists in this mechanism causing Sp1 to undergo ubiquitin-dependent degradation when CLL B-lymphocytes are proliferating in the tumour microenvironment. It would therefore be beneficial to assess Thr278/739 phosphorylation of Sp1 in CLL B-lymphocytes from bone marrow aspirates. Vincristine has been shown to activate JNK in CLL (Bates, Lewis, Eastman, & Danilov, 2015) presenting this drug as being able to restore Sp1 protein stability and SOD2 expression, thus potentially rescuing CLL B-lymphocytes from the tumorigenic effects of high superoxide levels.

Regulation of *SOD2* expression is obviously a complex process that involves regulatory DNA elements and their interacting proteins, as well as downstream RNA surveillance, all of which could have impaired functioning in CLL. A deeper investigation into *SOD2* transcription is required in order to fully understand this mechanism in CLL.

4.4 Conclusions

Through the sequencing of the *SOD2* promoter in six individuals with CLL and three healthy controls, this chapter revealed that mutations in and methylation of the *SOD2* promoter are not responsible for low SOD2 expression in CLL. Additionally, gene expression of transcription factors Sp1 and AP-2 were found to not correlate with *SOD2* gene expression suggesting another mechanism at play and requires further exploration including investigating the intronic enhancer and RNA interference.

Chapter 5:

Understanding lipid metabolism in CLL

Glycolysis is the generation of pyruvate from the catabolism of glucose and results in the production of two molecules of ATP. Many types of cancer rely on high glucose uptake and aerobic glycolysis as a means of energy production (Warburg, 1956a). This high glucose uptake is exploited by imaging techniques and forms the basis of PET scanning (Basu et al., 2011). In CLL, aerobic glycolysis is not overly active, however mitochondrial oxidative phosphorylation is significantly higher than in healthy B-lymphocytes (Jitschin et al., 2014). Oxidative phosphorylation has also been identified as the predominant means of energy production in other cancers, with prostate cancer being the prime example (Deep & Schlaepfer, 2016; Tamura et al., 2009). Previous work in our research laboratory further supports elevated oxidative phosphorylation in CLL by identifying proteins involved in lipid metabolism to be expressed at higher levels in CLL B-lymphocytes compared to healthy B-lymphocyte controls (Thurgood et al., 2019) (**Figure 5.1**).

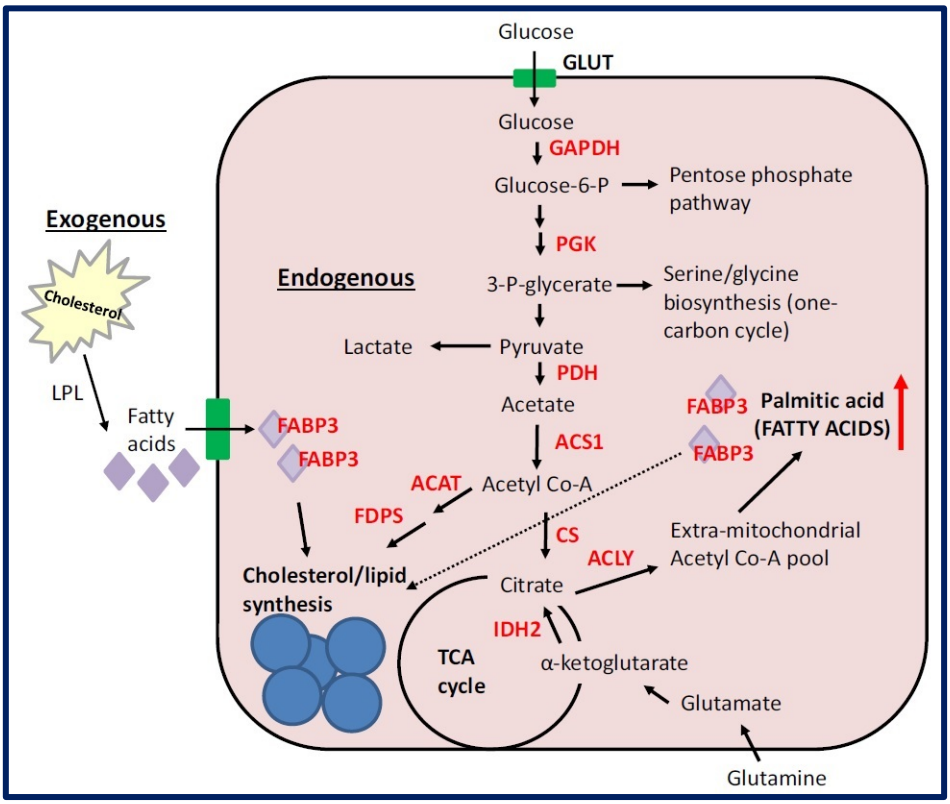

Figure 5.1: Model depicting the upregulation of proteins involved in lipid metabolism in CLL.

Red, proteins expressed at higher levels in CLL B-lymphocytes compared to healthy controls; pink, cell; purple, fatty acids; blue, lipid storage droplets; green, transport proteins. Reproduced with permission from Thurgood *et al.* (2019), copyright Wiley and Sons.

As discussed in section 1.4.1, lipoprotein lipase (LPL), is expressed at a substantially higher level in CLL compared to healthy B-lymphocytes, and is associated with poor outcome (Prieto & Oppezzo, 2017). LPL is bound to the cell surface, and is responsible for the hydrolysis of triglycerides within circulating chylomicrons and lipoproteins allowing the lipid to be transported across the cell membrane (Chajek et al., 1978; Felts et al., 1975). LPL is predominantly found on tissues that require fatty acids for energy production or storage such as myocytes and adipocytes. In CLL, LPL can be overexpressed and is responsible for making fatty acids free to be transported into the cell and contributes to the unique metabolic nature of CLL B-lymphocytes. Fatty acids can traverse the cell membrane by either receptor-mediated uptake, endocytosis, or diffusion (Buckley & King, 2017; Meshulam, Simard, Wharton, Hamilton, & Pilch, 2006; Pilch & Liu, 2011; Schwenk, Holloway, Luiken, Bonen, & Glatz, 2010). Work performed by this research laboratory has shown that free fatty acid uptake is remarkably increased in CLL B-lymphocytes compared to healthy controls (**Figure 5.2**) and that CLL B-lymphocytes prefer long-chain over short- and medium-chain fatty acids (unpublished laboratory data).

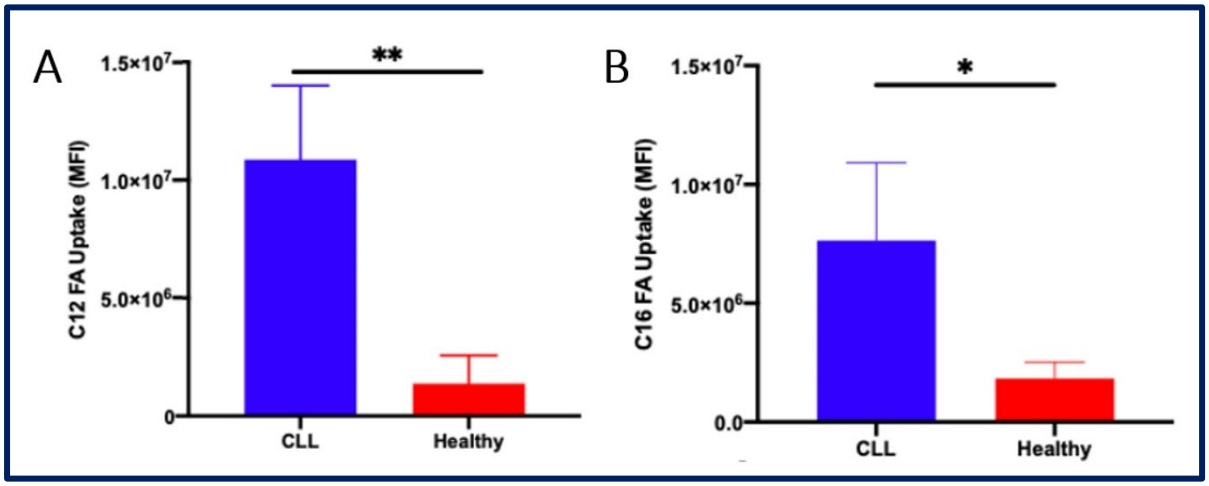

Figure 5.2: Free fatty acid uptake is significantly higher in CLL B-lymphocytes compared to healthy controls.
B-lymphocytes were exposed to 5 µM BODIPY-labelled C12 (**A**) and C16 (**B**) fatty acids for 15 minutes and uptake was assessed using flow cytometry. Blue, CLL B-lymphocytes; red, healthy controls; n = 3, error bars, ±1 standard deviation; *, $p<0.05$; **, $p<0.005$ calculated using an unpaired t-test.

Once in the cell, fatty acids are either utilised immediately or stored in lipid droplets which are specialised vesicles that are required to protect the cell from lipotoxicity, where excess fatty acids cause cellular dysfunction and death (Ke, Bao, & Chen, 2019). Previous work by Rozovski *et al.* (2015) showed the presence of lipid storage droplets in CLL B-lymphocytes which were not present in healthy B-lymphocytes (**Figure 5.3**). This finding has also been confirmed in our laboratory (unpublished laboratory data).

Although it is known that CLL B-lymphocytes source lipids exogenously (**Figure 5.2**), little is known about endogenously derived lipids (*de novo* synthesis) in CLL. Current therapeutics for CLL are predominantly palliative as CLL remains an incurable disease. Interestingly, in prostate cancer both fatty acid uptake and *de novo* lipid synthesis have been identified as being responsible for the observed fatty acid phenotype, and dual blocking of these pathways prevented tumour growth *in vivo* (Deep & Schlaepfer, 2016; Tamura et al., 2009; Watt et al., 2019). Therefore, exploring the dynamics of lipid metabolism in CLL will help us better understand how CLL B-lymphocytes meet their energy requirements and will assist in identifying novel therapeutic targets that can exploited to essentially starve CLL cells. Therapeutics that target crucial metabolic steps in CLL could be used in combination with current therapeutics presenting a unique opportunity to improve outcomes. Therefore, investigating lipid metabolic pathways in CLL is the focus of this chapter.

It is hypothesised that dysregulation of lipid metabolic pathways is responsible for the fatty acid-dependent phenotype observed in CLL.

Therefore, the aims of this investigation are:

1. To assess lipid metabolic pathways in healthy and CLL B-lymphocytes using real-time qPCR, and
2. To identify novel genes in lipid metabolic pathways that may play a role in CLL pathogenesis.

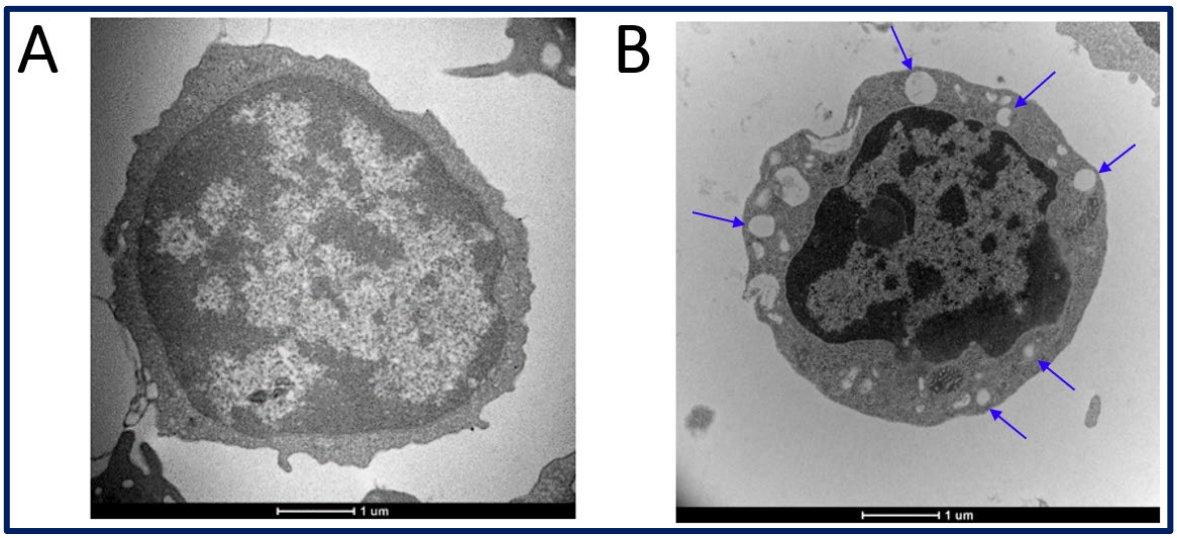

Figure 5.3: Lipid storage droplets identified in the cytoplasm of CLL B-lymphocytes using transmission electron microscopy.
A, healthy B-lymphocyte; **B**, CLL B-lymphocyte. Arrows indicate lipid droplets.

5.1 Materials and methods

5.1.1 Selection of patients for inclusion into this study

Samples were selected from a South Australian cohort of treatment naïve individuals (HREC #216056). Due to the heterogeneous nature of CLL, the cohort for this study consisted of patients that had a broad range of prognostic factors associated with CLL. Clinical characteristics for the cohort can be seen in **Table 5.1**. Normal B-lymphocytes were isolated from patients with haemochromatosis, a red blood cell disorder which requires venesection of blood from the patient on a regular basis. These samples served as the healthy controls. Whilst these patients have excess red blood cells, their B-lymphocytes are considered to be healthy.

Table 5.1: Patient clinical information for CLL PBMC samples used in PrimePCR™ real-time qPCR.
U, unmutated *IGHV*; M, mutated *IGHV*.

Sample	Age (years)	TTFT (months)	Cytogenetics	*IGHV*
FMC279	47.17	Naïve	trisomy 12	U
FMC124	64.65	Naïve	del13q	M
FMC292	72.86	Naïve	normal	M
FMC10	65.2	Naïve	del11q	U
FMC297	67.84	Naïve	del17p	U
FMC234	76.69	Naïve	del13q	M

5.1.2 cDNA synthesis (iScript method)

Each reaction contained 1x iScript Reverse Transcription Supermix (containing reverse transcriptase, RNase inhibitor, dNTPs, oligo(dT), random primers, buffer, $MgCl_2$, and stabilisers; Bio-Rad, Australia), 1x PrimePCR RT Control RNA Template (Bio-Rad), and a maximum of 1 µg RNA sample. Samples were incubated at 42 °C for 30 minutes followed by 85 °C for 5 minutes.

5.1.3 PrimePCR™ real-time qPCR

Primers were pre-lypophilised to the wells of the PrimePCR™ 384-well plates (Bio-Rad). Template master mixes were prepared immediately prior to addition to plates, with final well concentrations containing 0.6 ng cDNA template and 1x SsoAdvanced™ Universal SYBR® Green Supermix (Bio-Rad). All experiments were carried out under the conditions detailed in **Table 5.2** with reporter capture every 5 seconds. PrimePCR™ 384-well plate real-time qPCR experiments were carried out using a ViiA 7 qPCR machine (Applied Biosystems), and analysed using the ViiA 7 RUO software (Applied Biosystems).

Table 5.2: Real-time qPCR cycling method for PrimePCR™ real-time qPCR.

Stage (repeats)	Temperature (°C)	Time
***Taq* polymerase activation**	95	2 minutes
Amplification (40x)	95	5 seconds
	60	30 seconds
Melt curve	65	1 minute
	65	Heat to 95 °C at 0.5 °C/5 s
	95	15 seconds

5.1.3.1 Quality control and real-time qPCR analysis for PrimePCR™ Round 1

Individual threshold cycle (C_t) values were obtained by setting the threshold automatically by the ViiA 7 RUO software, and data from ViiA 7 were imported into Microsoft Excel.

Because only technical duplicates were performed, many of the genes did not pass initial quality control where duplicates must reach the threshold within 0.5 cycles of each other. Therefore, the average of the technical duplicates was calculated and expression levels were calculated using the delta Ct method (Livak & Schmittgen, 2001). As the technical stringency was decreased, only genes where expression was ≥10-fold in at least one CLL sample compared to the mean of normal B-lymphocytes were selected for further investigation.

5.1.3.2 Quality control and real-time qPCR analysis for PrimePCR™ Round 2

Genes were selected for re-analysis based on expression in all three healthy controls with a minimum of 7/9 samples (6 CLL and 3 healthy controls) meeting strict quality control standards. The significance threshold was increased to $p<0.01$ to account for decreased technical stringency.

5.1.4 Sodium dodecyl sulphate polyacrylamide gel electrophoresis (SDS-PAGE) and western blotting

To confirm the translation of RNA expression data at the protein level, western blotting was used.

5.1.4.1 Preparation of total cell lysates for SDS-PAGE

To prepare a total cell lysate for analysis of protein expression by western blot, 1 x10^7 cells were placed in a sterile microfuge tube, washed twice in 1 mL PBS (1600 x *g*, 5 minutes) then resuspended in 1 mL Pierce's RIPA Buffer (ThermoFisher Scientific) and 1x Halt™ Protease Inhibitor (ThermoFisher Scientific). Cells were incubated on ice for 10 minutes and then lysed using 3 cycles of sonication (75

% power; 5 second bursts with a 1-minute rest on ice between bursts) using a Branson B12 Sonifier (Branson Sonic Power, Danbury USA). Lysate was incubated for 15 minutes then centrifuged at 13,000 x *g* for 5 minutes at 4 °C to remove debris. Supernatant (containing cell lysate) was removed and transferred to a sterile microfuge tube.

5.1.4.2 Protein quantification

The protein concentration of individual samples was determined using the EZQ™ Protein Quantitation kit (ThermoFisher Scientific) as per the manufacturers' instructions. A standard curve using ovalbumin (ThermoFisher) was used to determine the sample concentration.

5.1.4.3 1D SDS-PAGE

Total protein from each sample (10 µg) was combined with 1x Reducing Laemmli Buffer +0.05 % 2ME. Samples were heated to 95 °C for 5 minutes in a heating block and were centrifuged at 13,300 x *g* for 5 minutes. The supernatant was loaded into a Mini-PROTEAN SDS-PAGE stain free gel (Bio-Rad) and electrophoresed in 1x SDS-PAGE running buffer. A broad range (10-250 kDa) Precision Plus Protein standard (Bio-Rad) was used to estimate the size of protein bands. The gel was electrophoresed at 220 V for 30 minutes in a Mini Protean II gel electrophoresis system (Bio-Rad). Gels were removed from the support and visualised using the ChemiDoc™ Touch (Bio-Rad) prior to transfer.

5.1.4.4 Transfer of protein and western blotting

A 0.2 µm PVDF-transfer membrane (Bio-Rad) was soaked in methanol and the membrane and blotting pads were soaked in 1x transfer buffer (Bio-Rad) for 3 minutes before beginning transfer. The polyacrylamide gel was placed over the PVDF membrane within the transfer cassette and was sandwiched between two transfer stacks (Bio-Rad). Excess buffer, overhanging gel and any bubbles were removed prior to locking the cassette and placing it in the Trans-Blot® Turbo™ Transfer system (Bio-Rad). Transfer was performed at 25 V, 1 A for 30 minutes. Once transferred, both the gel and membrane were visualised using the ChemiDoc™ Touch to ensure successful transfer had occurred.

Following transfer, the membrane was placed in blocking buffer (PBS containing 0.1 % Tween-20 (Sigma-Aldrich) and 1 % skim milk powder (Foodland, South Australia)) and was incubated at 4 °C overnight with shaking. The blocking buffer was subsequently removed, and the membrane was incubated with anti-CD36 rabbit monoclonal primary antibody (AbCam; ab124763) diluted 1 in 10,000 in antibody-diluent (PBS containing 0.1 % Tween-20 and 0.5 % skim milk powder). The membrane was incubated overnight at 4 °C with shaking then washed 3x 10 minutes in wash buffer (PBS containing 0.1 % Tween-20) and incubated with donkey anti-rabbit horseradish peroxidase-conjugated secondary antibody (Sigma-Aldrich) diluted 1 in 10,000 in antibody-diluent for 1 hour with rocking at room temperature. The membrane was then washed with wash buffer (1x 15 minute and 2x 5 minutes)

followed by a 5-minute wash in PBS. Following the final wash, the membrane was incubated with 2 mL SuperSignal West Pico Chemiluminescent substrate (ThermoFisher Scientific) for 5 minutes in the dark. Antibody-antigen complexes were visualised on the ChemiDoc™ Touch System and analysed using the ImageLab software (Bio-Rad).

5.1.5 Detection of surface markers and fatty acid uptake in CLL fractions

Cryopreserved CLL PBMCs were thawed into Hank's balanced salt solution (HBSS) with 1 % (w/v) fatty acid-free BSA before being counted using Trypan blue exclusion as described in 2.1.13. PBMCs were seeded at 5 x10^5 cells/mL and incubated with 2 µM BODIPY-labelled C12 at 37 °C for 15 minutes before being added to stop buffer (PBS containing 0.25 % BSA) at 4 °C. PBMCs were centrifuged at 1600 x *g* for 5 minutes and incubated with the antibody cocktail (**Table 5.3**) for 20 minutes in the dark at room temperature. Two millilitres PBS was added, and the cells were centrifuged at 1600 x *g* for 5 minutes. Fluorescence was analysed on a CytoFLEX S flow cytometer (Beckman Coulter, CA, USA).

Table 5.3: Antibodies used for the detection of surface markers using flow cytometry.

Antibody/marker	Fluorophore	Concentration	Target
Anti-CD45	V450	1/8 dilution	T- and B-lymphocytes (Nakano, Harada, Morikawa, & Kato, 1990)
Anti-CD38	PE Cy5	¼ dilution	Lymphocytes entering circulation (Awan & Byrd, 2018)
Anti-CD5	PE	¼ dilution	T-lymphocytes (Lydyard, Jamin, & Youinou, 1998), aberrantly expressed on CLL B-lymphocytes (Friedman, Guadeloupe, Volkheimer, & Weinberg, 2016)
Anti-CD19	PE Cy7	¼ dilution	B-lymphocytes – excluding plasma cells (Schroeder, Imboden, & Torres, 2019)
Anti-CD184 (CXCR4)	APC	½ dilution	Chemokine receptor, proliferative compartment homing marker (To, Levesque, & Herbert, 2011)
C12 fatty acid	BODIPY	2 µM	Fatty acids internalised by the cell (Kolahi, Louey, Varlamov, & Thornburg, 2016)

5.2 Results

5.2.1 Lipid gene expression analysis

A panel of 89 genes involved in lipid metabolism were assembled and curated in conjunction with Dr. Lauren Thurgood. Three genes (*GUSB*, *HPRT1*, and *B2M*) previously shown to be stably expressed in CLL B-lymphocytes were selected as the reference genes for normalisation of genes of interest (Valceckiene, Kontenyte, Jakubauskas, & Griskevicius, 2010). **Table 5.4** categorises each gene (except for reference genes) into 1 of 5 key lipid metabolic pathways. Twenty-one genes were categorised as associated with *lipolysis*, 9 as *regulation of transcription*, 15 as *lipid biosynthesis*, 15 as *extracellular/membrane*, 9 as *intracellular*, and 16 as *other*.

Table 5.4: Gene panel categorisation into lipid metabolic pathways.

Lipolysis		Regulation of transcription	Lipid biosynthesis	Extracellular/membrane	Intracellular	Other
ACAA1	*LIPE*	*PPARG* (β-oxidation)	*GAPDH*	*APOC2*	*LPL*	*HMOX1*
ADIPOQ	*PLA2G4A*	*NR1H3* (cholesterol homeostasis)	*FADS1*	*ANGPTL4*	*APOA1*	*MAPK14*
ADIPOR1	*LIPC*	*SREBF1* (lipid homeostasis)	*FADS2*	*LCAT*	*LMF1*	*GOT1*
HADH	*LIPG*	*NR1H4* (bile acid homeostasis)	*GCK*	*APOC3*	*NPC1*	*PDGFRB*
CPT1A	*ACAD8*	*PPARGC1A* (lipid metabolism)	*ACACB*	*PON1*	*FABP1*	*MAPK3*
CROT	*ALOX5*	*VDR* (calcium homeostasis)	*SCD5*	*LEP*	*FABP2*	*PTEN*
ACOX1	*PLA2G2A*	*PPARA* (β-oxidation)	*PRKAB1*	*APOA4*	*PLIN1*	*PIK3CG*
DECR1	*PNPLA3*	*PPARD (*β-oxidation)	*SCD*	*CETP*	*PLIN2*	*PIK3CA*
ACAT1	*FAAH*	*SIRT1* (lipid metabolism)	*C3*	*APOC1*	*ABCA1*	*TNFRSF1A*
ACSL5	*PLA2G7*		*PRKAA2*	*PCSK9*		*PRKCB*
MGLL	*APOE*		*ACLY*	*SORL1*		*MTHFR*
	CEL		*FASN*	*CD36*		*PIK3R1*
			LPIN1	*APOB*		*IL6R*
			HMGCR	*SLC27A1*		*MAPK1*
				LDLR		*GGT1*
						HPSE

5.2.1.1 Exclusion of *B2M* for expression analysis

As mentioned previously in section 1.3.2.3, β-2 microglobulin is used as a serum marker for CLL. The gene that codes for this protein (*B2M*) has previously been shown to be a suitable reference gene for use in CLL gene expression studies (Valceckiene et al., 2010). However, as this study compared CLL B-lymphocytes to healthy B-lymphocytes, and little is known about the stability of *B2M* expression in healthy B-lymphocytes, the stability of *B2M* across all samples was evaluated.

It was found that *B2M* expression had high variation in healthy B-lymphocytes (**Figure 5.4**). *B2M* expression in healthy B-lymphocytes had a range of 5.44 cycles, compared to 2.3 and 3.2 cycles for *GUSB* and *HPRT1*, respectively.

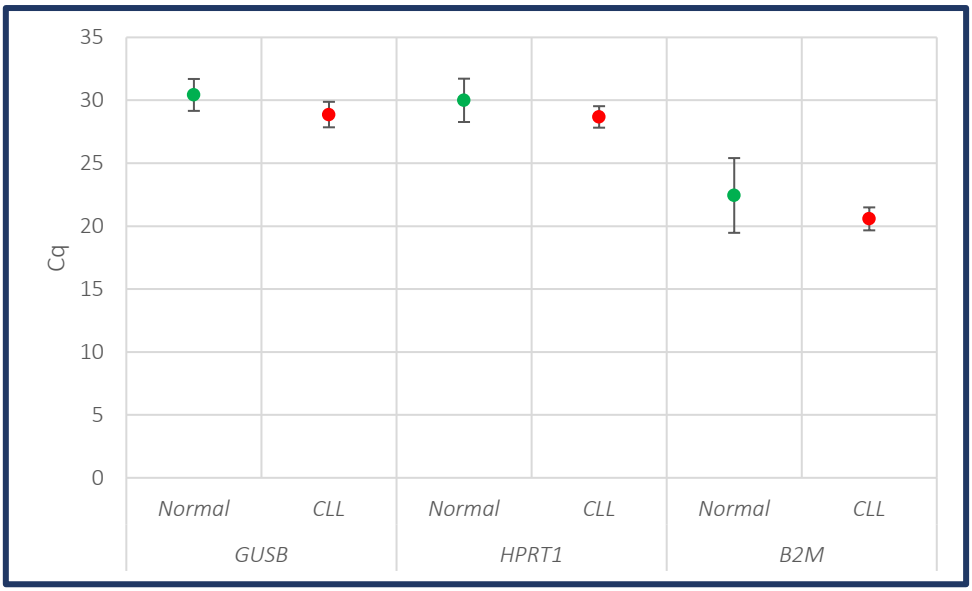

Figure 5.4: *B2M* gene expression has high variation in healthy B-lymphocytes.
RNA was isolated from normal and CLL B-lymphocytes. cDNA was generated, and expression levels of reference genes were determined using real-time qPCR. Green, healthy B-lymphocytes; red, CLL B-lymphocytes; error bars, ±1 standard deviation; n = 3 for normal B-lymphocytes; n = 6 for CLL B-lymphocytes.

5.2.1.2 Twenty-five genes were found to be differentially expressed in CLL B-lymphocytes compared to healthy controls (analysis round 1)

As mentioned in section 5.1.3.1, quality control was modified due to results not passing initial strict quality control criteria. Only genes where expression was ≥10-fold in at least one CLL sample compared to the mean of normal B-lymphocytes were selected for further investigation. **Tables 5.5-5.10** identify genes that were differently expressed in CLL B-lymphocytes compared to healthy controls.

Expression levels were found to be highly variable across all CLL samples, with five genes (*ANGPTL4*, *APOA4*, *APOB*, *CEL*, and *PNPLA3*) not detected in any samples. *ADIPOQ* was only detected in CLL B-lymphocytes (**Table 5.5**).

Nine genes (*LPIN1*, *APOC2*, *LPL*, *PCSK9*, *ADIPOQ*, *LCAT*, *TNFRSF1A*, *GGT1*, and *MTHFR*) were denoted 'undetected' for analysis in three samples (NOR2, CLL5, and CLL6) due to the amplification of genomic DNA in these samples and the primer sets for these genes being exonic.

Seven genes categorised as *lipolysis* associated (*ALOX5*, *APOE*, *LIPC*, *LIPG*, *MGLL*, *PLA2G2A*, and *PLA2G7*) were differentially expressed in CLL B-lymphocytes compared to healthy controls (**Table 5.5**). Four genes categorised as *regulation of transcription* (*PPARG*, *PPARGC1A*, *SREBF1*, and *VDR*) were expressed at a lower level in CLL B-lymphocytes compared to healthy controls (**Table 5.6**). Four

genes categorised as *lipid biosynthesis* (*C3*, *FADS2*, *PRKAA2*, and *SCD5*) were expressed at a lower level in CLL B-lymphocytes compared to healthy controls (**Table 5.7**). Four genes categorised as *extracellular/membrane* (*APOC1*, *APOC3*, *CD36*, and *PON1*) were expressed at a lower level in CLL B-lymphocytes compared to healthy controls (**Table 5.8**). Four genes categorised as *intracellular* (*FABP1*, *FABP2*, *LPL*, and *PLIN1*) were differentially expressed between CLL B-lymphocytes and healthy controls (**Table 5.9**). One gene categorised as *other* (*PDGFRB*) was expressed at a higher level in CLL B-lymphocytes compared to healthy controls (**Table 5.10**).

Table 5.5: Expression data for genes classed as associated with *lipolysis*.
Expression (relative to reference genes) of 86 genes was assessed using real-time qPCR. Differential expression assessed as 10-fold higher or lower than mean of healthy controls. Blue, decreased in CLL B-lymphocytes; orange, increased in CLL B-lymphocytes; yellow, only detected in CLL B-lymphocytes; UND, undetected. Expression values transformed to 3 significant figures.

Gene Symbol	NOR1	NOR2	NOR3	NOR Mean	CLL1	CLL2	CLL3	CLL4	CLL5	CLL6	CLL Mean
ACAA1	29.7	11.5	89.2	**43.5**	27.6	74.3	45.5	66.4	11.3	31.5	**42.8**
ACAD8	13.2	8.82	33.7	**18.6**	4.59	38.9	14.5	59.8	8.61	22.4	**24.8**
ACAT1	29.6	15.3	20.8	**21.9**	22.8	114	49.4	55.4	33.2	107	**63.6**
ACOX1	23.2	13.7	UND	**18.5**	13.1	52.0	22.2	63.6	40.6	27.1	**36.4**
ACSL5	40.4	28.0	73.4	**47.3**	52.6	135	83.3	145	86.3	69.7	**95.3**
ADIPOQ	UND	UND	UND	**N/A**	3.43	UND	3.39	0.640	UND	UND	**N/A**
ADIPOR1	284	51.0	152	**162**	316	151	152	117	45.0	53.1	**139**
ALOX5	138	191	487	**272**	220	1108	9.84	764	389	326	**469**
APOE	5.20	2.19	7.48	**4.96**	3.19	3.68	3.00	3.31	0.179	1.08	**2.4**
CEL	UND	UND	UND	**N/A**	UND	UND	UND	UND	UND	UND	**N/A**
CPT1A	16.5	8.26	18.0	**14.2**	13.5	69.9	29.4	128	28.1	21.0	**48.3**
CROT	11.1	11.6	1.23	**8.01**	3.77	26.0	9.26	22.3	10.7	29.1	**16.9**
DECR1	87.1	206	9.78	**101**	51.9	197	124	202	217	206	**166**
FAAH	1.64	2.44	16.3	**6.81**	7.78	5.47	UND	4.50	0.765	1.37	**4**
HADH	39.8	104	111	**85.2**	63.5	108	48.3	276	91.1	159	**124**
LIPC	2.46	UND	10.6	**6.58**	2.96	1.15	UND	1.12	UND	0.225	**1.36**
LIPE	2.59	6.47	22.8	**10.6**	1.58	25.1	5.01	42.9	5.57	10.1	**15**
LIPG	1.06	0.191	21.2	**7.51**	1.43	0.539	6.14	0.818	0.961	0.196	**1.68**
MGLL	83.3	0.559	41.3	**41.7**	17.3	20.7	1.93	9.87	8.21	2.97	**10.2**
PLA2G2A	6.17	UND	UND	**6.17**	6.39	0.414	0.132	2.14	UND	UND	**2.27**
PLA2G4A	9.48	0.887	3.60	**4.65**	9.38	0.959	UND	2.47	2.16	0.798	**3.15**
PLA2G7	5.49	2.20	UND	**3.84**	1.72	0.505	8.51	2.11	5.78	45.5	**10.7**
PNPLA3	UND	UND	UND	**N/A**	UND	UND	UND	UND	UND	UND	**N/A**

Table 5.6: Expression data for genes classed as *regulation of transcription*.
Expression (relative to reference genes) of 86 genes was assessed using real-time qPCR. Differential expression assessed as 10-fold higher or lower than mean of healthy controls. Blue, decreased in CLL B-lymphocytes; orange, increased in CLL B-lymphocytes; UND, undetected. Expression values transformed to 3 significant figures.

Gene Symbol	NOR1	NOR2	NOR3	NOR Mean	CLL1	CLL2	CLL3	CLL4	CLL5	CLL6	CLL Mean
NR1H3	1.14	2.36	9.20	**4.23**	21.9	26.0	3.82	4.93	13.2	6.38	**12.7**
PPARA	12.8	14.7	21.9	**16.5**	17.5	41.2	13.6	29.3	7.39	8.07	**19.5**
PPARD	49.4	UND	61.8	**55.6**	21.5	64.7	35.9	82.4	UND	UND	**51.1**
PPARG	12.0	4.97	112	**43.2**	13.8	1.95	10.4	4.01	4.82	9.09	**7.35**
PPARGC1A	5.14	2.67	17.1	**8.32**	2.82	1.05	7.81	0.674	1.31	2.29	**2.66**
SIRT1	170	219	UND	**195**	118	215	102	124	98.7	134	**132**
SREBF1	29.9	3.17	15.4	**16.1**	86.8	33.8	49.6	26.3	1.34	2.03	**33.3**
VDR	4.26	UND	10.9	**7.59**	2.09	1.63	UND	3.60	0.713	0.959	**1.8**

Table 5.7: Expression data for genes classed as *lipid biosynthesis*.

Expression (relative to reference genes) of 86 genes was assessed using real-time qPCR. Differential expression assessed as 10-fold higher or lower than mean of healthy controls. Blue, decreased in CLL B-lymphocytes; orange, increased in CLL B-lymphocytes; UND, undetected. Expression values transformed to 3 significant figures.

Gene Symbol	NOR1	NOR2	NOR3	NOR Mean	CLL1	CLL2	CLL3	CLL4	CLL5	CLL6	CLL Mean
ACACB	1.39	6.29	14.1	**7.26**	16.4	41.0	6.92	27.7	9.28	8.38	**18.3**
ACLY	16.4	12.8	73.4	**34.2**	39.6	59.0	23.2	151	14.4	16.7	**50.7**
C3	0.569	UND	27.8	**14.2**	UND	0.814	0.319	2.85	1.49	0.747	**1.24**
FADS1	3.18	2.42	26.6	**10.7**	7.19	5.91	34.4	7.42	1.49	3.36	**9.96**
FADS2	2.09	UND	28.6	**15.3**	7.81	2.15	11.6	103	0.591	0.643	**21**
FASN	8.66	2.62	UND	**5.64**	4.09	8.68	2.46	11.6	1.67	2.40	**5.15**
GAPDH	6140	2406	2121	**3556**	4063	3296	3416	1513	2195	2278	**2794**
GCK	2.02	1.27	17.9	**7.07**	0.737	2.37	5.71	3.55	3.29	3.24	**3.15**
HMGCR	60.2	16.7	7.95	**28.3**	22.4	32.7	31.7	54.2	10.6	16.2	**28**
LPIN1	29.1	UND	50.6	**39.8**	36.4	28.6	44.9	51.3	UND	UND	**40.3**
PRKAA2	0.261	UND	2.37	**1.31**	0.121	UND	UND	UND	UND	0.250	**0.186**
PRKAB1	25.4	32.1	14.3	**23.9**	22.6	71.2	32.5	68.2	11.4	27.8	**39**
SCD	UND	3.38	9.24	**6.31**	0.491	7.32	UND	1.58	8.16	7.49	**5**
SCD5	10.6	1.56	32.9	**15.0**	3.44	1.29	11.5	3.92	1.02	1.16	**3.72**

Table 5.8: Expression data for genes classed as *extracellular/membrane*.

Expression (relative to reference genes) of 86 genes was assessed using real-time qPCR. Differential expression assessed as 10-fold higher or lower than mean of healthy controls. Blue, decreased in CLL B-lymphocytes; orange, increased in CLL B-lymphocytes; UND, undetected. Expression values transformed to 3 significant figures.

Gene Symbol	NOR1	NOR2	NOR3	NOR Mean	CLL1	CLL2	CLL3	CLL4	CLL5	CLL6	CLL Mean
ANGPTL4	UND	UND	UND	**N/A**	UND	UND	UND	UND	UND	UND	**N/A**
APOA4	UND	UND	UND	**N/A**	UND	UND	UND	UND	UND	UND	**N/A**
APOB	UND	UND	UND	**N/A**	UND	UND	UND	UND	UND	UND	**N/A**
APOC1	9.77	UND	57.4	**33.6**	UND	1.49	14.3	0.596	0.987	3.77	**4.23**
APOC2	0.611	UND	3.21	**1.91**	1.07	0.739	UND	1.07	UND	UND	**0.96**
APOC3	1.14	UND	3.43	**2.28**	UND	0.100	0.720	0.568	0.488	0.097	**0.395**
CD36	101	7.22	116	**74.9**	23.6	12.8	4.73	32.5	36.4	47.7	**26.2**
CETP	5.93	9.27	UND	**7.59**	2.27	4.28	2.36	3.26	5.52	1.08	**3.13**
LCAT	2.12	UND	7.89	**5.00**	8.54	10.4	4.24	9.35	UND	UND	**8.13**
LDLR	11.7	4.15	9.97	**8.62**	4.61	10.2	32.4	3.78	3.29	3.29	**9.6**
LEP	0.197	UND	UND	**0.197**	UND	UND	0.400	UND	0.0723	UND	**0.236**
PCSK9	0.218	UND	0.440	**0.329**	UND	UND	UND	0.0426	UND	UND	**0.0426**
PON1	1.75	UND	UND	**1.75**	2.20	UND	0.625	0.357	0.441	0.0695	**0.739**
SDC1	2.99	0.770	UND	**1.88**	3.60	UND	UND	0.756	0.414	UND	**1.59**
SLC27A1	7.61	3.05	8.42	**6.36**	2.97	3.81	8.95	6.74	7.55	4.94	**5.83**
SORL1	133	17.7	46.8	**66.0**	78.2	104	42.5	55.7	27.5	30.5	**56.4**

Table 5.9: Expression data for genes classed as *intracellular*.

Expression (relative to reference genes) of 86 genes was assessed using real-time qPCR. Differential expression assessed as 10-fold higher or lower than mean of healthy controls. Blue, decreased in CLL B-lymphocytes; orange, increased in CLL B-lymphocytes; UND, undetected. Expression values transformed to 3 significant figures.

Gene Symbol	NOR1	NOR2	NOR3	NOR Mean	CLL1	CLL2	CLL3	CLL4	CLL5	CLL6	CLL Mean
ABCA1	32.5	11.1	14.5	**19.4**	44.2	56.6	15.2	24.7	29.1	32.4	**33.7**
APOA1	0.118	2.72	UND	**1.42**	UND	3.04	0.762	0.577	0.199	0.680	**1.05**
FABP1	5.14	1.51	34.8	**13.8**	5.91	1.07	5.19	2.36	1.16	2.08	**2.96**
FABP2	2.08	0.138	10.5	**4.24**	5.71	0.292	3.53	0.792	1.72	0.360	**2.07**
LMF1	10.8	13.7	4.01	**9.53**	10.2	30.6	4.47	20.9	31.2	13.6	**18.5**
LPL	0.170	2.35	UND	**1.26**	1.65	133	2.86	90.4	20.9	15.4	**44**
NPC1	27.5	11.6	6.07	**15.1**	33.5	50.0	22.0	54.9	15.0	17.5	**32.2**
PLIN1	0.714	UND	UND	**0.714**	UND	0.873	4.21	0.743	14.7	0.099	**3.44**
PLIN2	391	136	56.9	**194**	66.5	33.3	146	37.9	45.9	32.7	**60.4**

Table 5.10: Expression data for genes classed as *other*.

Expression (relative to reference genes) of 86 genes was assessed using real-time qPCR. Differential expression assessed as 10-fold higher or lower than mean of healthy controls. Blue, decreased in CLL B-lymphocytes; orange, increased in CLL B-lymphocytes; UND, undetected. Expression values transformed to 3 significant figures.

Gene Symbol	NOR1	NOR2	NOR3	NOR Mean	CLL1	CLL2	CLL3	CLL4	CLL5	CLL6	CLL Mean
HMOX1	34.8	22.1	15.6	**24.2**	142	96.5	50.8	96.8	35.0	47.5	**78.1**
MAPK1	79.2	45.6	45.9	**56.9**	45.6	241	43.4	381	122	94.5	**155**
MAPK14	47.1	17.6	19.5	**28.1**	38.1	112	22.5	90.6	31.7	49.9	**57.5**
GOT1	40.2	31.8	UND	**36.0**	15.8	32.9	22.4	27.7	41.0	36.3	**29.4**
PDGFRB	0.081	0.758	UND	**0.420**	UND	7.04	3.17	7.98	10.6	0.821	**5.92**
MAPK3	48.5	55.1	48.0	**50.5**	22.5	130	36.8	150	39.3	65.8	**74.1**
PTEN	44.5	UND	UND	**44.5**	13.8	163	11.5	175	UND	UND	**90.8**
PIK3CA	338	208	13.9	**186**	121	144	122	167	82.8	79.8	**119**
PIK3CG	63.6	28.7	0.596	**31.0**	33.7	71.5	24.9	95.0	44.8	35.7	**50.9**
TNFRSF1A	32.0	UND	9.51	**20.7**	33.9	58.5	5.56	65.0	UND	UND	**40.7**
PRKCB	183	416	242	**280**	219	930	216	651	400	493	**485**
MTHFR	21.6	UND	24.0	**22.8**	13.3	55.4	19.5	83.1	UND	UND	**109**
PIK3R1	603	73.9	3.65	**227**	372	269	346	1016	52.2	81.9	**356**
IL6R	8.38	3.02	9.35	**6.92**	7.20	20.0	19.7	42.7	5.07	14.6	**109**
GGT1	0.794	UND	0.660	**0.72**	3.52	0.177	0.299	3.53	UND	UND	**1.88**
HPSE	16.2	0.957	8.52	**8.57**	15.8	4.34	10.1	11.4	6.06	16.1	**10.6**

Due to the nature of the data not meeting high quality control criteria where technical replicates must meet the threshold within 0.5 cycles of each other, confirmation of the identified changes was performed using in-laboratory methods. In addition, further investigation of the refined gene panel requires the use of self-designed primer sets and normalisation to the reference gene *GUSB*. Therefore, confirmation of gene expression changes was performed using self-designed primer sets and standard in-laboratory real-time qPCR methods using the same samples.

5.2.1.3 Reproducibility of real-time qPCR results is inconsistent between PrimePCR™ and in-laboratory methods

Standard curves for each primer set were generated using serial 10-fold dilutions of control cDNA. Primer sets were successfully optimised for 20 out of 25 genes (**Table 5.11**). The primer set for *CD36* was designed and optimised by Dr. Lauren Thurgood. Primer sets for *C3*, *FABP2*, *PRKAA2*, *SCD5*, and *VDR* could not be selected due to non-specific amplification.

Table 5.11: M and R^2 values for standard curves of each primer set for selected genes (analysis round 1).

Gene symbol	M value	R^2 value
ADIPOQ	2.919	0.9999
ALOX5	3.1812	0.9999
APOC1	3.5394	0.9999
APOC3	3.4089	0.9989
APOE	3.5769	0.9997
CD36	3.5619	0.9975
FABP1	3.4255	0.999
FADS2	3.3391	0.9973
LIPC	3.2849	1
LIPG	3.068	0.999
LPL	3.3302	0.9981
MGLL	3.304	0.9991
PDGFRB	3.3134	0.9992
PLA2G2A	3.5003	0.9996
PLA2G7	3.4031	0.9946
PLIN1	3.2753	0.999
PON1	3.2661	0.9988
PPARG	3.5483	0.9975
PPARGC1A	3.3268	0.9999
SREBF1	3.0131	0.9997

APOC3, *LIPG*, *PPARG*, and *PPARGC1A* were undetected in almost all CLL B-lymphocyte and healthy control samples. Also, *FABP1*, *PLA2G2A*, *PLA2G7*, and *PON1* were non-specific when used on CLL cDNA. Therefore, these genes were not included in the comparison of real-time qPCR methods.

Comparison of in-laboratory real-time qPCR data with PrimePCR™ real-time qPCR data showed that reproducibility is inconsistent between methods as observations in expression trends could not be replicated (**Table 5.12**). PrimePCR™ expression data was confirmed in a sample when it followed the same pattern when in-lab real-time qPCR methods were used. PrimePCR™ expression data was

contradicted in a sample when it did not follow the same pattern when in-lab real-time qPCR methods were used. Expression of *APOC1* and *ALOX5* was higher in CLL B-lymphocyte samples compared to healthy controls which contradicted PrimePCR™ expression data. *PLIN1* was expressed at a lower level in CLL B-lymphocyte samples compared to healthy controls which also contradicted PrimePCR™ expression data. PrimePCR™ expression data for *LPL* and *PDGFRB* was both confirmed and contradicted in CLL B-lymphocyte samples using in-laboratory methods. *MGLL*, *APOE*, *FADS2*, *SREBF1*, and *LIPC* were expressed at lower levels in CLL B-lymphocyte samples compared to healthy controls which confirmed PrimePCR™ expression data. **Table 5.12** also shows that *ADIPOQ* was undetected in healthy controls and CLL B-lymphocytes which contradicts PrimePCR™ expression data.

Table 5.12: Reproducibility of real-time qPCR data is inconsistent between PrimePCR™ and in-laboratory methods.

Expression of 12 genes was assessed using real-time qPCR (relative to *GUSB*). Genes identified as being expressed at ≥10-fold of healthy controls using PrimePCR™ methods (blue, decreased expression; orange, increased expression) were either confirmed (green), or contradicted (red) using in-laboratory methods.

		NOR1	NOR2	NOR3	NOR Mean	CLL1	CLL2	CLL3	CLL4	CLL5	CLL6
ADIPOQ	**PrimePCR™**	UND	UND	UND	**N/A**	0.0343	UND	0.0339	0.0064	UND	UND
	In-lab	UND	UND	UND	**N/A**	UND	UND	UND	UND	UND	UND
APOC1	**PrimePCR™**	9.77	UND	57.4	**33.5**	UND	1.49	14.3	0.596	0.987	3.77
	In-lab	0.323	0.342	UND	**0.332**	2.54	0.732	1.77	0.341	0.379	0.133
CD36	**PrimePCR™**	101	7.22	116	**74.7**	23.6	12.8	4.73	32.5	36.4	47.7
	In-lab	205	1500	905	**870**	16.1	76.7	11.6	14.6	113	77.8
LPL	**PrimePCR™**	0.17	2.35	UND	**1.26**	1.65	133	2.86	90.4	20.9	15.4
	In-lab	UND	11.4	34.2	**22.8**	451	4.59	UND	275	23.1	UND
ALOX5	**PrimePCR™**	138	191	487	**272**	220	1108	9.84	764	389	326
	In-lab	44.8	103	257	**135**	190	58.2	181	130	98.5	134
MGLL	**PrimePCR™**	83.3	0.559	41.3	**41.7**	17.3	20.7	1.93	9.87	8.21	2.97
	In-lab	48.9	357	243	**216**	17.6	25.6	UND	6.99	2.79	4.52
PLIN1	**PrimePCR™**	0.714	UND	UND	**0.714**	UND	0.873	4.21	0.743	14.7	0.099
	In-lab	0.263	1.83	2.86	**1.65**	5.99	0.728	0.167	1.49	1.23	1.46
PDGFRB	**PrimePCR™**	0.081	0.758	UND	**0.419**	UND	7.04	3.17	7.98	10.6	0.821
	In-lab	2.79	16.1	14.5	**11.1**	61.5	2.29	35.2	36.0	8.60	9.30
APOE	**PrimePCR™**	5.2	2.19	7.48	**4.95**	3.19	3.68	3	3.31	0.179	1.08
	In-lab	992	UND	602	**797**	455	912	1859	191	243	351
FADS2	**PrimePCR™**	2.09	UND	28.6	**15.3**	7.81	2.15	11.6	103	0.591	0.643
	In-lab	1961	7113	8048	**5707**	4216	2124	2094	13829	6.14	632
SREBF1	**PrimePCR™**	29.9	3.17	15.4	**16.1**	86.8	33.8	49.6	26.3	1.34	2.03
	In-lab	98.7	65.8	66.1	**76.9**	198	171	674	82.6	18.5	26.0
LIPC	**PrimePCR™**	2.46	UND	10.6	**6.53**	2.96	1.15	UND	1.12	UND	0.225
	In-lab	65.2	466	452	**328**	73.2	58.9	138	UND	UND	14.1

Real-time qPCR data using standard in-laboratory methods was plotted and can be seen in **Figure 5.5**. *MGLL* ($p = 0.021$) and *CD36* ($p = 0.0127$) were expressed at significantly lower levels in CLL B-lymphocytes compared to healthy controls. Cost analysis of PrimePCR™ versus in-lab real-time qPCR methods can be found in Appendix B (**Table B4**).

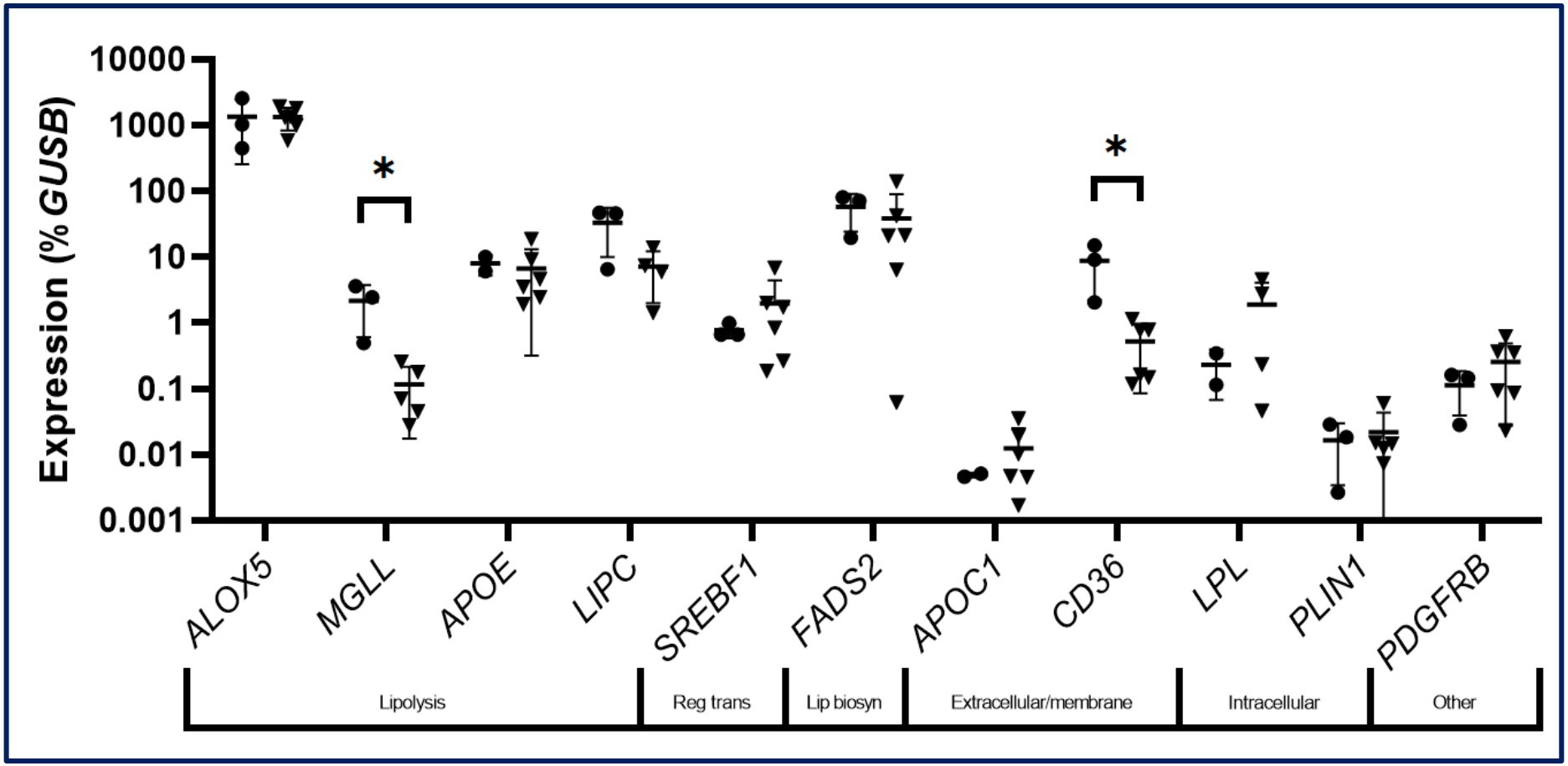

Figure 5.5: Expression data of selected genes in CLL B-lymphocytes compared to healthy controls.
Expression of 11 genes was assessed using in-laboratory real-time qPCR methods. Error bars, ±1 standard deviation; n = 3 for healthy controls (circles); n = 6 for CLL B-lymphocytes (triangles); *, $p<0.05$ calculated using t-test.

5.2.1.4 Five genes were found to be differentially expressed in CLL B-lymphocytes compared to healthy controls (analysis round 2)

Although the 5/11 genes assessed using in-laboratory methods confirmed expression changes observed using PrimePCR™ methods, the inconsistent nature of real-time qPCR data reproducibility from PrimePCR™ plates raised the question of effective data analysis. Therefore, it was decided that re-analysis of raw PrimePCR™ real-time qPCR data would be performed. Genes were selected for re-analysis based on expression in all three healthy controls (to ensure an average could be calculated) and a minimum of 7/9 samples (out of 6 CLL and 3 healthy controls) meeting strict quality control standards (5.1.3.2).

As **Figure 5.6** shows, 22 genes were included in re-analysis of raw PrimePCR™ real-time qPCR data. *MGLL* ($p = 0.00936$), *CD36* ($p = 0.00852$), and *PLIN2* ($p = 0.01$) were expressed at a lower level in CLL B-lymphocytes compared to healthy controls. *HMOX1* ($p = 0.00654$) and *ACSL5* ($p = 0.00827$) were expressed at a significantly higher level in CLL B-lymphocytes compared to healthy controls.

Genes identified as being expressed at a significantly different level in CLL B-lymphocytes compared to healthy controls were included for confirmation of real-time qPCR data with standard in-laboratory methods. As **Figure 5.5** shows, *MGLL* and *CD36* expression data from PrimePCR™ have been confirmed using standard in-laboratory methods. Therefore, standard curves for *ACSL5*, *HMOX1*, and *PLIN2* were generated using serial 10-fold dilutions of control cDNA (**Table 5.13**).

Figure 5.7 shows that there was no difference in expression of *ACSL5*, *HMOX1*, and *PLIN2* between CLL B-lymphocytes and healthy controls, contradicting PrimePCR™ real-time qPCR data.

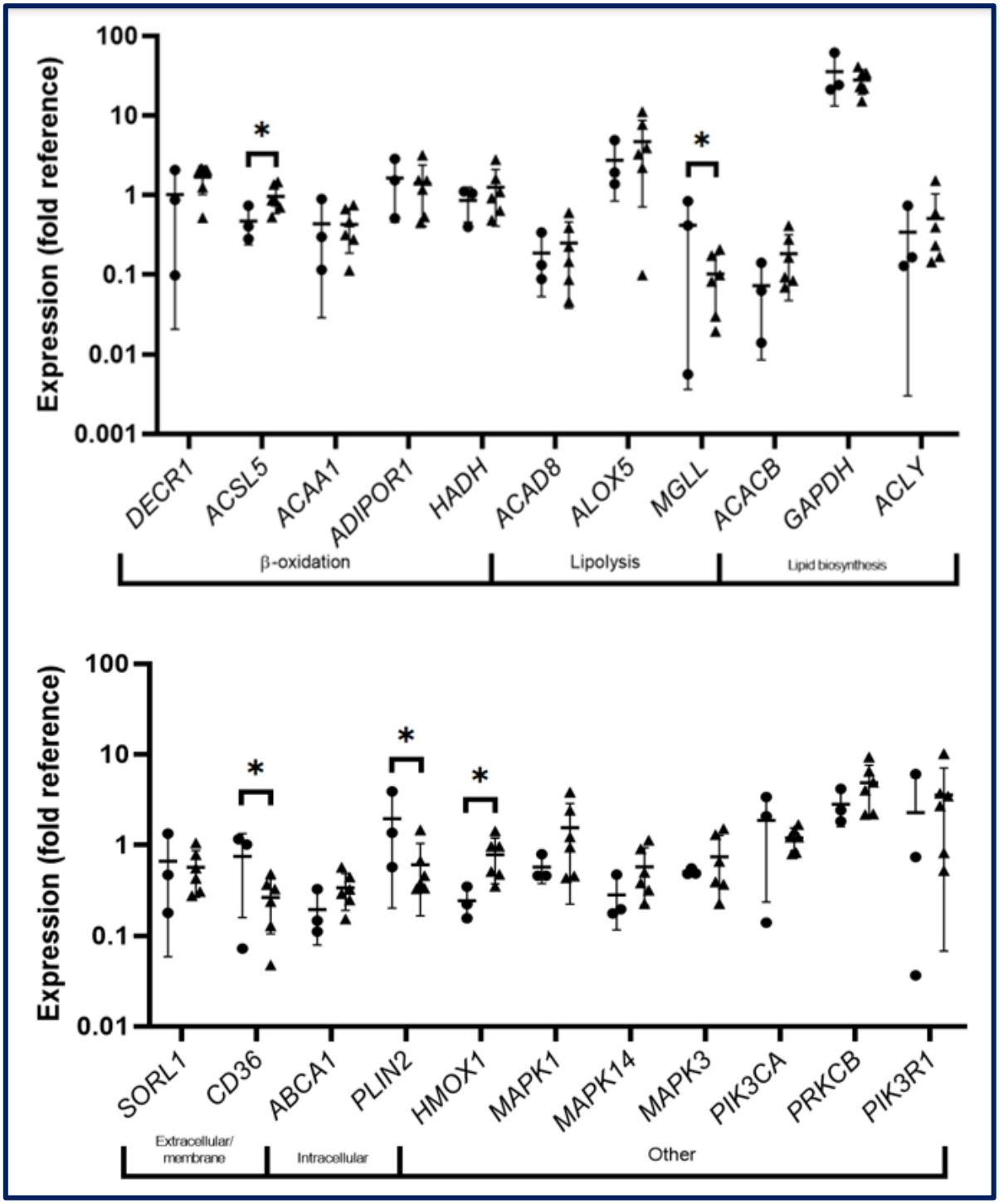

Figure 5.6: Expression data from second-round analysis of PrimePCR™ real-time qPCR.
Expression of 22 genes was assessed using PrimePCR™ real-time qPCR data and calculated relative to the reference genes *GUSB* and *HPRT1*. Error bars, ±1 standard deviation; n = 3 for healthy controls (circles); n = 6 for CLL B-lymphocytes (triangles); *, $p<0.01$ as calculated using t-test.

Table 5.13: M and R^2 values for standard curves of each primer set for selected genes (analysis round 2).

Gene symbol	M value	R^2 value
ACSL5	3.3375	0.9999
HMOX1	3.3293	1
PLIN2	3.3401	0.9999

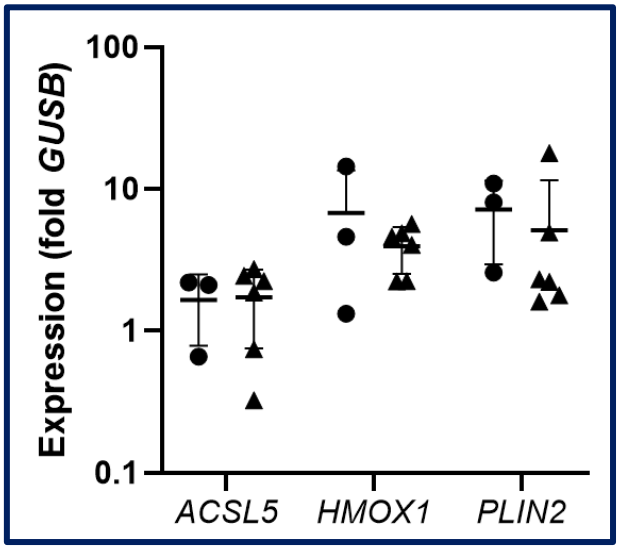

Figure 5.7: Expression data of selected genes in CLL B-lymphocytes compared to healthy controls.
Error bars, ±1 standard deviation; n = 3 for healthy controls (circles); n = 6 for CLL B-lymphocytes (triangles).

Based on the real-time qPCR data from **Figure 5.5**, two genes (*CD36* and *MGLL*) were selected for expression assessment in a larger cohort of CLL patients and healthy controls. In addition, *ACSL5* was included as a negative control as expression was previously shown to not be significantly different between CLL B-lymphocytes and healthy controls.

5.2.2 Assessing the expression of the refined lipid gene panel in a larger cohort

Previous real-time qPCR data identified *CD36* and *MGLL* as being significantly differentially expressed between CLL B-lymphocytes and healthy controls. In order to determine whether these differences in expression can be observed across the disease, assessment of expression in a larger cohort of CLL patients and healthy controls was performed (**Table 5.14**).

Table 5.14: Patient clinical information for CLL PBMC samples used in the larger cohort.
U, unmutated *IGHV*; M, mutated *IGHV*; N/A, data not available.

Sample	Age (years)	TTFT (months)	Cytogenetics	*IGHV*
FMC279	47.17	Naïve	trisomy 12	U
FMC124	64.65	Naïve	del13q	M
FMC292	72.86	Naïve	normal	M
FMC10	65.2	Naïve	del11q	U
FMC297	67.84	Naïve	del17p	U
FMC234	76.69	Naïve	del13q	M
FMC207	68.98	Naïve	del13q	M
FMC206	87.59	Naïve	N/A	N/A
FMC272	38.05	N/A	del13q	M
FMC194	65.15	121	del13q	M
FMC121	55.02	49	del13q	M
FMC278	72.08	N/A	del13q	M
FMC11	81.42	56	del11q	U
FMC281	47.88	N/A	N/A	M
FMC174	81.8	2	trisomy 12	U
FMC293	56.9	Naïve	del13q	M

Figure 5.8 shows that *CD36* ($p = 0.013$) and *MGLL* ($p = 0.0175$) were expressed at significantly lower levels in CLL B-lymphocytes compared to healthy controls. There was no significant difference in the expression of *ACSL5* (negative control) between CLL B-lymphocytes and healthy controls. In addition, the GEO database was used to compare the expression of *CD36*, *MGLL* and *ACSL5* gene expression in studies comparing CLL and healthy B-lymphocytes. *CD36* was expressed at a lower level in CLL B-lymphocytes compared to healthy controls in all three datasets. There was no difference in both *MGLL* and *ACSL5* gene expression between CLL B-lymphocytes and healthy controls in all three datasets.

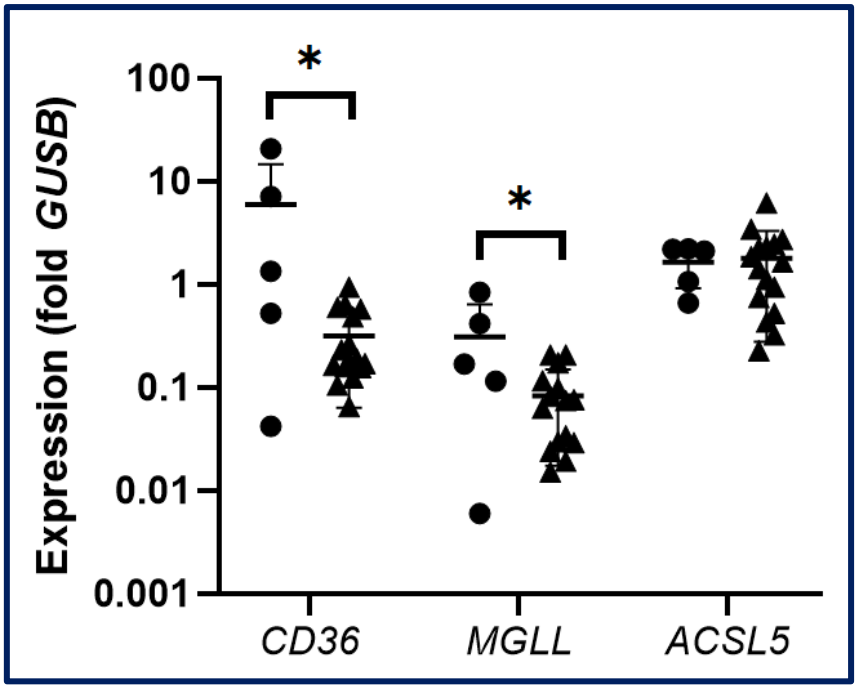

Figure 5.8: Expression data of the refined gene panel in CLL B-lymphocytes and healthy controls.
Error bars, ±1 standard deviation; n = 5 for healthy controls (circles); n = 16 for CLL B-lymphocytes (triangles); *, $p<0.05$ as calculated using t-test.

Expression of these genes in CLL was also assessed using three datasets from the GEO database (GDS3902, GDS4168 and GDS4167). These datasets consisted of Genome-wide microarray expression data of B-lymphocytes from CLL and healthy individuals (Gutierrez et al., 2010; Vargova et al., 2011). CD36 gene expression was found to be lower in CLL B-lymphocytes compared to healthy controls in all three datasets and *ACSL5* gene expression was no different in CLL B-lymphocytes compared to healthy controls, which mirrored our finding. However, *MGLL* gene expression was no different in CLL B-lymphocytes compared to healthy controls in the GEO datasets. Despite this, as monoglyceride lipase (*MGLL*) hydrolyses monoacylglycerol in lipid droplets to produce fatty acids (Zechner et al., 2012), it was hypothesised that monoglyceride lipase is required for hydrolysis of CLL lipid stores in the CLL microenvironment where there is low perfusion, and hence low nutrient availability. Therefore, expression of this gene was further explored in matched peripheral blood and bone marrow samples from individuals with CLL. Additionally, lymph node proteomic data from the research laboratory was interrogated to determine whether the monoglyceride lipase protein was detected.

Figure 5.9 A shows that *MGLL* expression was lower in bone marrow compared to peripheral blood in six individuals, and higher in bone marrow compared to peripheral blood in three individuals. As **Figure 5.9 B** shows, there was no difference in the expression of *MGLL* between matched peripheral blood and

bone marrow samples. Proteomic analysis of lymph node tissue showed that monoglyceride lipase was not detected in CLL or healthy individuals. Therefore, further investigation into this lipase was ceased.

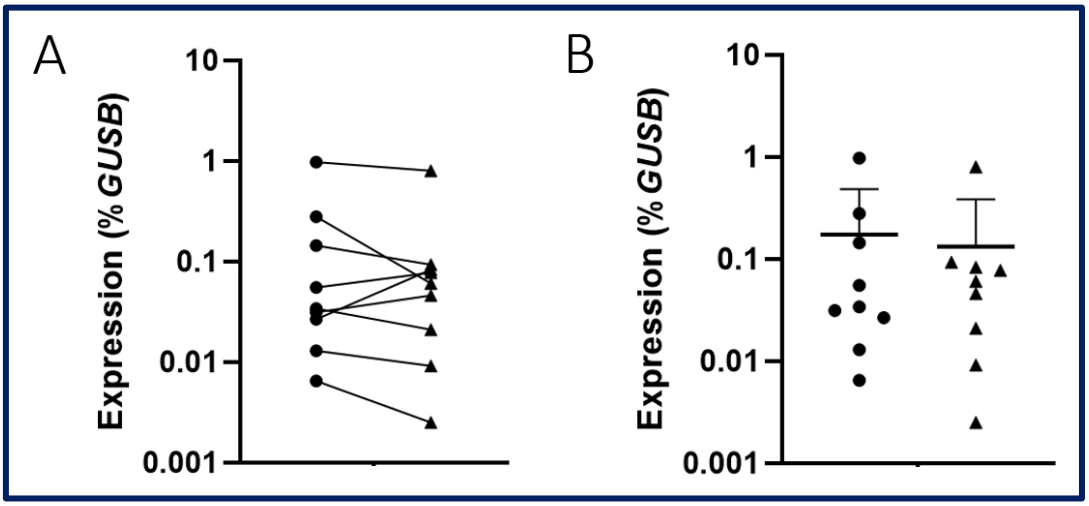

Figure 5.9: *MGLL* gene expression in matched peripheral blood and bone marrow. Expression in matched peripheral blood (circles) and bone marrow (triangles) samples was assessed using real-time qPCR. **A**, *MGLL* gene expression in matched samples; **B**, mean *MGLL* gene expression for each group. Error bars, ±1 standard deviation.

The fatty acid translocase CD36 is a major importer of fatty acids into the cell, and, as the results above show that CD36 is significantly lower in CLL compared to healthy controls, this does not fit the fatty acid phenotype observed in CLL. Therefore, in order to confirm that RNA expression data translates to protein expression of CD36, western blotting was performed on protein lysates from CLL B-lymphocytes and healthy controls. Gels used for normalisation of protein loading can be seen in Appendix B **Figure B2**. This work was performed by Dr. Lauren Thurgood.

As **Figure 5.11** shows, CD36 was expressed at a significantly ($p = 0.037$) lower level in CLL B-lymphocytes compared to healthy controls. **Figure 5.10** shows loading of protein lysates obtained from CLL B-lymphocytes into the polyacrylamide gel. Samples which exhibited protein degradation could not be repeated due to sample unavailability.

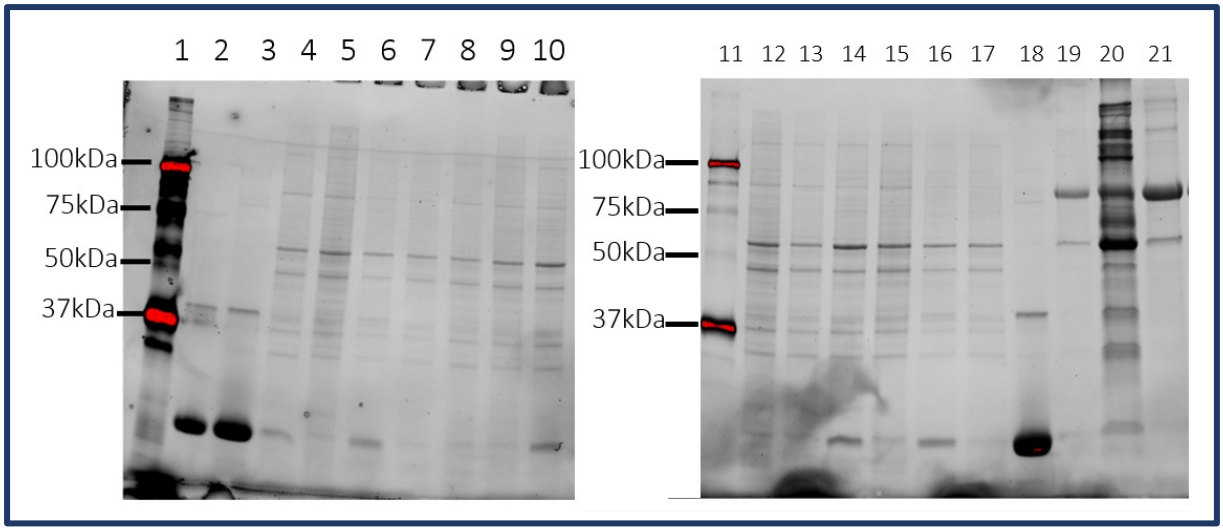

Figure 5.10: SDS-PAGE images used for protein loading normalisation.
Lanes 1 and 11, protein standard; lanes 2-5 and 12-18, CLL B-lymphocyte samples; lanes 6-10 and 19-21, healthy controls. Lanes 2, 3, and 18 were excluded from analysis due to sample degradation. Using stain-free gels, the total protein load for each lane was determined. Data generated by Dr. Lauren Thurgood.

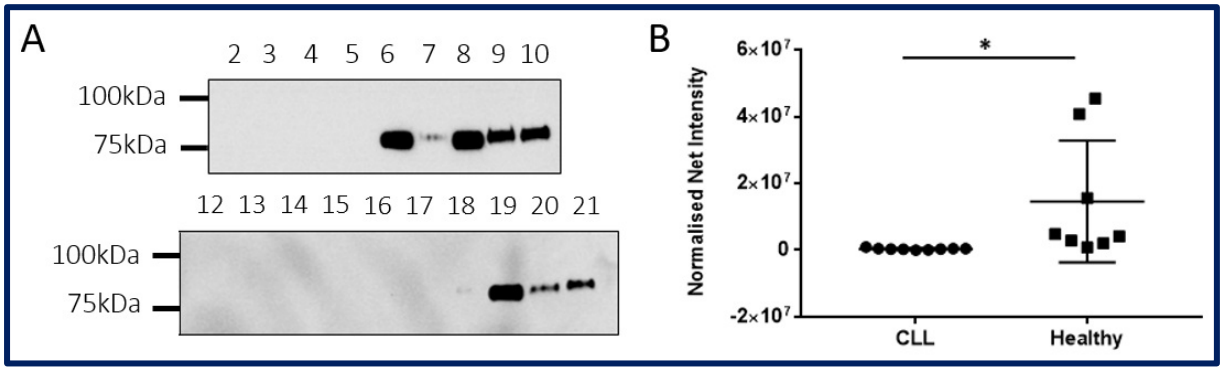

Figure 5.11: The CD36 protein is expressed at a significantly lower level in CLL B-lymphocytes compared to healthy controls.
A, lanes 2-5 and 12-18, CLL B-lymphocyte samples; lanes 6-10 and 19-21, healthy controls. Samples 2, 3, and 18 were excluded from analysis due to sample degradation. **B**, the total protein load was used to normalise net intensity of antibody signal for each sample. n = 9 for CLL; n = 8 for healthy controls; *, $p<0.05$ calculated using t-test. Data generated by Dr. Lauren Thurgood.

The data from this section shows that the fatty acid translocase CD36 is absent from CLL B-lymphocytes. Consequently, there must be other fatty acid importers responsible for regulating the uptake of fatty acids across the plasma membrane into CLL B-lymphocytes. Investigation into the mechanism of fatty acid import in CLL is the focus of the next section.

5.2.3 Fatty acid import

CD36 expression data showed that this translocase is absent in CLL B-lymphocytes compared to healthy controls. As this molecule is one of the predominant importers of fatty acids across the plasma membrane, experiments to understand how and if receptor-mediated fatty acid import occurs in CLL and if this is different to healthy B-lymphocytes was performed (Nickerson et al., 2009).

The term 'fatty acid import' was searched for in the *Human Cyc: Encyclopedia of Human Genes and Metabolism* database (humancyc.org). Proteins identified in the fatty acid import pathways were included into the gene panel. The literature was also interrogated for key players in fatty acid import, and *FABP3* was included as a positive control as fatty acid binding protein 3 has previously been shown to be elevated in CLL B-lymphocytes (Thurgood et al., 2019).

Table 5.15 shows the fatty acid import gene panel. Standard curves for each primer set were generated using serial 10-fold dilutions of control cDNA. Primer sets were successfully optimised for all genes (**Table 5.16**). The primer sets for *FATP1-6* were designed and optimised by Dr. Lauren Thurgood.

Table 5.15: Fatty acid import gene panel.

Gene	Function	Source
ACSL1	Conversion of long-chain fatty acids to acyl-CoA, direct transport of long-chain fatty acids across plasma membrane through binding	HumanCyc, (Schwenk, Luiken, Bonen, & Glatz, 2008)
ACSL3	Conversion of long-chain fatty acids to acyl-CoA	HumanCyc
CAV1	Scaffolding in caveolae formation	(Eyre, Cleland, & Mayrhofer, 2008)
CAV2	Scaffolding in caveolae formation	(Eyre et al., 2008)
FABP3	Direct transport of long-chain fatty acids across plasma membrane	Positive control ↑ in CLL (Thurgood et al., 2019), Human Cyc
FATP1	Direct transport of long-chain fatty acids across plasma membrane, conversion of long-chain fatty acids to acyl-CoA	(Schaffer & Lodish, 1994; Schwenk et al., 2008)
FATP2	Involved in transport of long-chain fatty acids across plasma membrane, conversion of long-chain fatty acids to acyl-CoA	HumanCyc, (Hirsch, Stahl, & Lodish, 1998)
FATP3	Conversion of long-chain fatty acids to acyl-CoA	(Schaffer & Lodish, 1994)
FATP4	Direct transport of long-chain fatty acids across plasma membrane, conversion of long-chain fatty acids to acyl-CoA	HumanCyc
FATP5	Transport of long-chain fatty acids across plasma membrane, conversion of long-chain fatty acids to acyl-CoA	(Doege et al., 2006; Schaffer & Lodish, 1994)
FATP6	Transport of long-chain fatty acids across plasma membrane, conversion of long-chain fatty acids to acyl-CoA	(Gimeno et al., 2003; Schaffer & Lodish, 1994)
GOT2	Facilitates transport of long-chain fatty acids across plasma membrane	(Clarke et al., 2004; Holloway et al., 2007; Schwenk et al., 2008)
SLC22A9	Direct transport of short-chain fatty acids across plasma membrane	HumanCyc

Table 5.16: M and R^2 values for standard curves of each primer set for the fatty acid import gene panel.

Gene symbol	M value	R^2 value
ACSL1	3.25	0.999
ACSL3	3.0954	1
CAV1	3.1402	0.9996
CAV2	3.41	0.9991
FABP3	2.9617	0.9985
FATP1	3.46	0.9988
FATP2	3.26	0.9904
FATP3	3.24	0.9959
FATP4	3.173	0.9965
FATP5	3.414	0.9982
FATP6	3.53	0.9913
GOT2	3.3657	1
SLC22A9	3.1632	0.9992

SLC22A9 gene expression was not detected in CLL or healthy B-lymphocytes. GEO was utilised to assess the expression of *SLC22A9* in CLL compared to healthy B-lymphocytes. One of three datasets comparing CLL to healthy B-lymphocytes detected *SLC22A9* gene expression (GDS4168), however there was no difference between the groups. In addition, data for *FABP3* was unable to be generated due to non-specific amplification encountered in CLL and healthy B-lymphocytes. However, proteomic data from our laboratory detected fatty acid binding protein 3 in CLL B-lymphocytes and was found to be 3.26-fold higher in CLL B-lymphocytes compared to healthy controls (**Figure 5.1**).

As **Figure 5.12** shows, *CAV2* was expressed at a significantly lower ($p = 0.0179$) level in CLL B-lymphocytes compared to healthy controls. However, *CAV2* was only detected in 4/5 healthy controls and 6/16 CLL. *CAV1* was expressed 2.4 times higher in CLL B-lymphocytes compared to healthy controls and detected in 1/5 healthy controls and 3/16 CLL. *FATP2* was expressed 4.9 times higher in CLL B-lymphocytes compared to healthy controls, however, was only detected in 4/5 healthy controls and 11/16 CLL. Similarly, *FATP5* was expressed 4 times higher in CLL B-lymphocytes compared to healthy controls and was detected in 3/5 healthy controls and 12/16 CLL. *FATP6* was expressed 9.4 times higher in CLL B-lymphocytes compared to healthy controls, however, was detected in 2/5 healthy controls and 11/16 CLL.

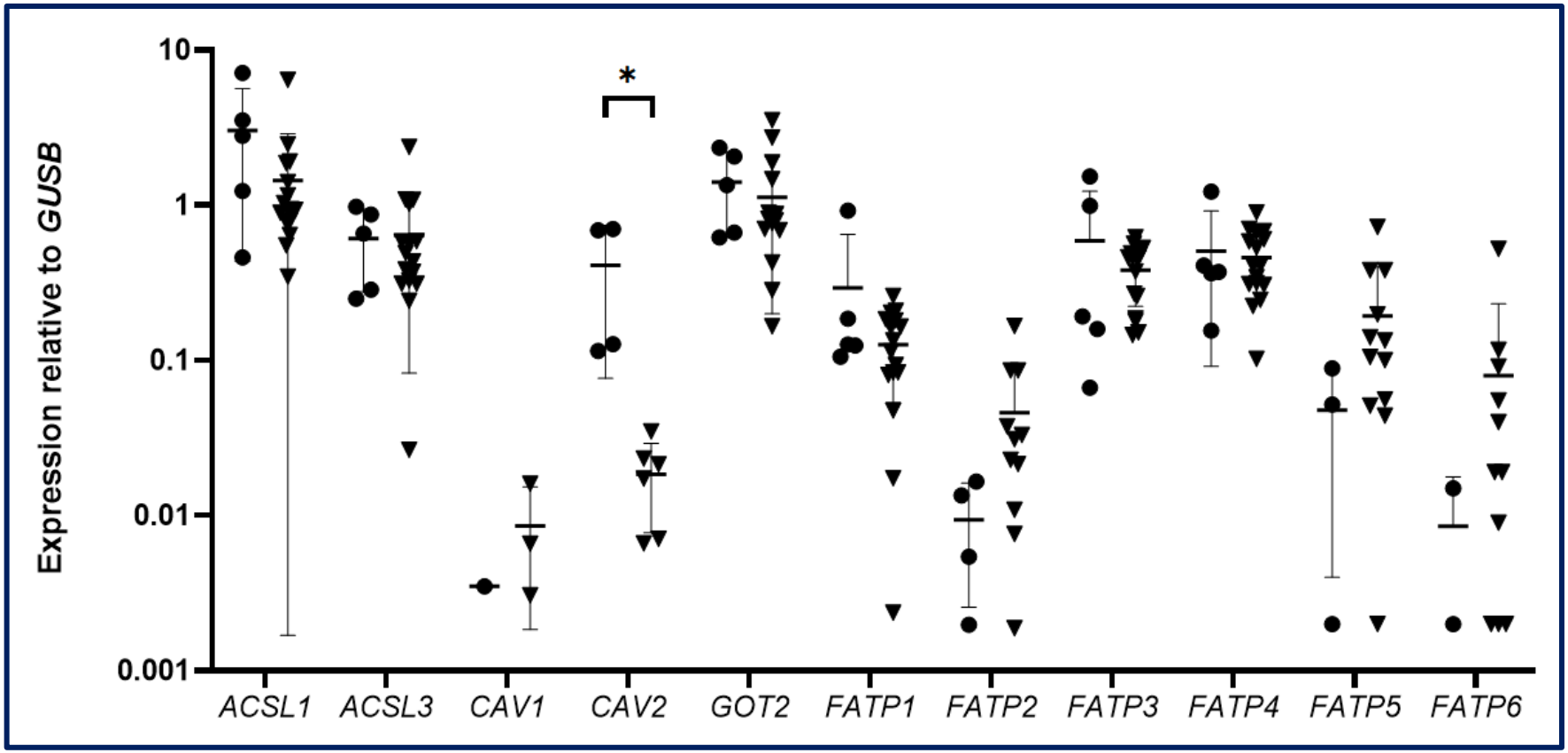

Figure 5.12: Expression data of the fatty acid import gene panel in CLL B-lymphocytes and healthy controls.
Circles, healthy controls (n = 5); triangles, CLL B-lymphocytes (n = 16); error bars, ±1 standard deviation; *, $p<0.05$ as calculated using unpaired t-test.

Work undertaken by the research group aimed to identify the method of fatty acid import using small molecular inhibitors against players from the fatty acid import panel as well as pinocytosis, a form of fluid phase endocytosis (**Table 5.17**).

It was found that fatty acid uptake was decreased after treatment with triascin C, an inhibitor of long-chain fatty acid-CoA ligases 1 and 3 (*ACSL1* and *ACSL3* genes, respectively). Similarly, fatty acid uptake was decreased after treatment with aminooxyacetic acid (AOA), an inhibitor of mitochondrial aspartate aminotransferase. The decrease in fatty acid uptake caused by triascin C and AOA was not, however, significant. Interestingly, inhibitors of macropinocytosis (ethylisopropyl amiloride (EIPA) and LY294002) and micropinocytosis (filipin and nystatin) significantly decreased fatty acid uptake.

Results from this section show that pinocytosis is the primary method of fatty acid uptake into CLL B-lymphocytes as inhibitors of both macro and micropinocytosis caused significant decreases in fatty acid uptake in HG-3 CLL B-lymphocytes.

Table 5.17: Collated protein expression and inhibition data in CLL B-lymphocytes.
Protein description with corresponding gene; *, RNA expression significantly different between CLL B-lymphocytes and healthy controls; protein identified in CLL; PB, peripheral blood; LN, lymph node; inhibitor against protein; and if fatty acid uptake was affected in response to small molecular inhibitor; N/A, not applicable. Data produced in collaboration with Ashley Rowland and Dr. Lauren Thurgood.

Description	Gene	Identified in CLL?	Inhibitor	Uptake
Long-chain fatty acid-CoA ligase 1	*ACSL1*	Yes, PB	Triacsin C	Decreased
Long-chain fatty acid-CoA ligase 3	*ACSL3*	Yes, PB	Triacsin C	Decreased
Caveolin 1	*CAV1*	Yes, LN	Methyl β cyclodextrin	Not performed as inhibitor unsuitable for application
Caveolin 2	*CAV2**	No, LN	N/A	N/A
Plasma membrane-associated fatty acid binding protein (FABPpm; aspartate aminotransferase, mitochondrial)	*GOT2*	Yes, PB	AOA	Decreased
Long-chain fatty acid transport protein 1	*FATP1*	No, PB	N/A	N/A
Long-chain fatty acid transport protein 2	*FATP2*	No, PB	Lipofermata	Not performed as not detected in CLL
Long-chain fatty acid transport protein 3	*FATP3*	Yes, PB	N/A	N/A
Long-chain fatty acid transport protein 4	*FATP4*	No, PB	N/A	N/A
Long-chain fatty acid transport protein 5	*FATP5*	No, PB	N/A	N/A
Long-chain fatty acid transport protein 6	*FATP6*	Yes, PB	N/A	N/A
Macropinocytosis	N/A	N/A	EIPA LY294002	Significantly decreased in HG-3 CLL B-lymphocyte cell line EIPA: $p<0.05$ LY294002: $p<0.0001$
Micropinocytosis	N/A	N/A	Filipin Nystatin	Significantly decreased in HG-3 CLL B-lymphocyte cell line Filipin: $p<0.0001$ Nystatin: $p<0.0001$

5.2.4 Understanding lipid metabolism in CLL

Chemokine C-X-C motif receptor 4 (CXCR4) is a surface molecule, and high expression in CLL B-lymphocytes is associated with homing to proliferative compartments (Davids & Burger, 2012). Previous work in the department showed that CLL B-lymphocytes with high CXCR4 surface expression (entering the proliferative lymph nodes and bone marrow microenvironments) had higher levels of intracellular neutral lipids compared to low CXCR4 surface expression (exiting lymph nodes and bone marrow). This data suggests that CLL B-lymphocytes returning to proliferative compartments have scavenged fatty acids whilst in the peripheral blood and could be using these fatty acids as an energy source whilst in the proliferative compartments where perfusion is low. Therefore, this data warranted an investigation into the fatty acid uptake rate of CLL B-lymphocytes based on CXCR4 surface expression. This work was performed in collaboration with an Honours student, Ashley Rowland.

It was hypothesised that CLL B-lymphocytes that had recently left the proliferative compartments would be lipid depleted and would therefore have a higher uptake rate of fatty acids compared to those that were homing back to the proliferative compartments. CLL patient samples were selected based on >80 % viability upon thawing (clinical information can be seen in **Table 5.18**).

Table 5.18: Patient clinical information for CLL PBMC samples used in the assessment of free fatty acid uptake.
U, unmutated *IGHV*; M, mutated *IGHV*; N/A, data not available.

Sample	Age (years)	TTFT (months)	Cytogenetics	*IGHV*
FMC20	N/A	30	normal	U
FMC117	87.99	76	del13q, del11q	U
FMC207	N/A	N/A	del13q	M
FMC226	54.53	106	del13q	M
FMC240	77.54	121	N/A	M
FMC281	47.88	N/A	N/A	M
FMC330	48.9	92	complex karyotype	U

CLL B-lymphocytes were thawed and incubated with BODIPY-labelled C12 for 15 minutes as described in 5.1.5. **Figure 5.13** shows that fatty acid uptake was significantly ($p = 0.0362$) lower in the $CXCR4_{high}$ fraction compared to the $CXCR4_{low}$ fraction. This data shows that fatty acid uptake is inversely correlated to CXCR4 surface expression.

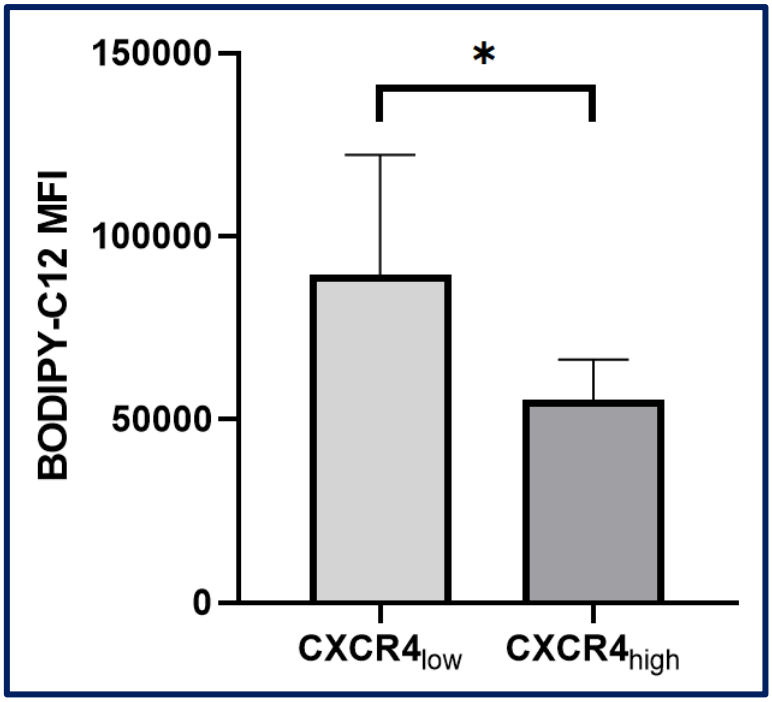

Figure 5.13: BODIPY-C12 uptake is higher in CLL B-lymphocytes leaving the microenvironment.
Error bars, ±1 standard deviation; *, $p<0.05$ assessed using a paired t-test; n = 7.

In addition, work in our laboratory showed that lipid droplet content was significantly higher in $CXCR4_{high}$ (entering the microenvironment) compared to $CXCR4_{low}$ (exiting the microenvironment) CLL B-lymphocytes suggesting that fatty acids imported in the periphery are being stored. Co-localisation studies of free fatty acid uptake and lipid droplet markers are currently being performed in our research laboratory.

5.3 Discussion

5.3.1 Summary

This chapter investigated lipid metabolic pathways in CLL using gene expression analysis. Due to technical issues, a complete picture of lipid-associated gene expression profiling was unable to be performed. However, despite limited sample size for the broad scope analysis, a more targeted analysis revealed that fatty acid translocase, *CD36* gene expression was significantly lower in CLL B-lymphocytes compared to healthy controls which was also reflected in the analysis of GEO datasets. Western blotting showed that CD36 was absent from CLL B-lymphocytes. As fatty acid translocase is a primary importer of fatty acids into the cell, this suggested that an alternative pathway for fatty acid uptake and the fatty acid replete phenotype of CLL, and hence shifted the focus of this investigation to understanding how fatty acid uptake occurs in CLL in the absence of CD36.

Consequently, the importation of fatty acids into the cell was assessed by RNA expression of major players in this process. *CAV2* was expressed at a significantly lower level in CLL B-lymphocytes compared to healthy controls. *FATP6* was expressed at higher levels in CLL B-lymphocytes compared to healthy controls and long-chain fatty acid transport protein 6 was detected in CLL B-lymphocytes. Inhibition of long-chain acyl-coA ligase 1, long-chain acyl-coA ligase 3, and plasma membrane-associated fatty acid binding protein all decreased the uptake of fatty acids in the HG-3 CLL B-lymphocyte cell line. However, only inhibition of macro and micropinocytosis caused a significant decrease in fatty acid uptake in HG-3 cells.

Due to the potential differences between peripheral blood lymphocytes versus those situated in a microenvironment, it was postulated that lymphocytes may differ in their ability to uptake and utilise fatty acids as the primary energy pathway. A model for nutrient uptake in CLL B-lymphocytes based on their location in the body was then further investigated based on their CXCR4 expression. This analysis demonstrated that fatty acid uptake was higher in CLL B-lymphocytes with low CXCR4 surface expression, an indicator of having recently left the microenvironment versus high CXCR4 seen in those cells about to return to the microenvironment. This suggests that in the hypoxic and crowded nodal or bone marrow environments, CLL cells preferentially metabolise lipids for an energy source requiring circulating blood lymphocytes, as they leave the microenvironment depleted of lipid, to scavenge lipids in the peripheral blood and store them for return to the microenvironment compartments where proliferation predominantly occurs. A model depicting the novel findings in this chapter can be seen in **Figure 5.14**.

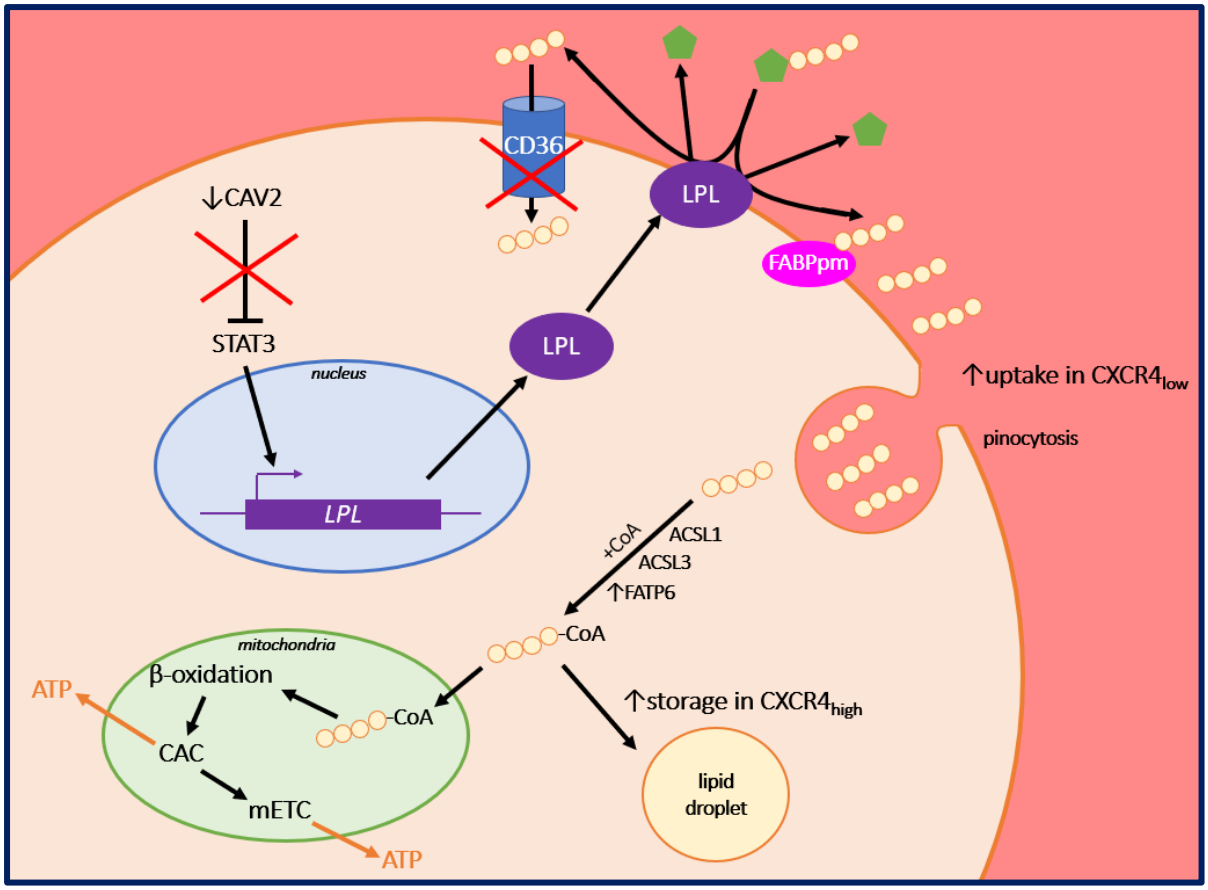

Figure 5.14: Fatty acid metabolism mechanisms at play in the CLL cell.
Low CAV2 may be responsible for constitutive STAT3 activation and high LPL expression. LPL (purple) cleaves lipoproteins into the protein (green) and fatty acid (yellow chains) components. Pinocytosis is largely responsible for fatty acid uptake in CLL. Fatty acid uptake is reliant on binding of fatty acids by FABPpm (pink) at the plasma membrane, and conversion of fatty acids to fatty acid-CoA by ACSL1, ACSL3 and FATP6 for use in energy production or storage in lipid droplets (yellow). Fatty acid transport does not depend on CD36 (blue) which is absent in CLL cells. Fatty acid uptake and storage occurs in the peripheral blood for use in the proliferative compartments. These mechanisms become druggable targets.

5.3.2 Gene expression

Previous work in our department identified proteins that were differentially expressed between normal and CLL B-lymphocytes using mass spectrometry (Thurgood et al., 2019). Proteins involved in fatty acid uptake and storage, and glycolysis were identified as being expressed at higher levels in CLL B-lymphocytes compared to normal B-lymphocytes. The results suggested that CLL B-lymphocytes have an increased exogenous uptake of free fatty acids for cellular storage. Therefore, a further aim of this study was to determine how CLL B-lymphocytes utilise lipids by assessing the expression of genes involved in lipid metabolism using real-time qPCR.

Individuals selected for use in this study were chosen for a range of representative cytogenetic abnormalities and *IGHV* mutational status as these factors are prognostic and able to distinguish CLL populations (Dohner et al., 2000; Hamblin et al., 1999). This would provide a range of CLL genetic backgrounds which could be specifically expanded once key lipid-related proteins were identified. The initial patient selection for use in PrimePCR^{TM} expression analysis included three healthy controls and six CLL patients (**Table 5.1**) to minimise costs of the assay whilst ensuring that a broad range of CLL populations were included.

The 89 genes selected included three reference genes (*GUSB*, *HPRT1*, and *B2M*) which were stably expressed in CLL B-lymphocytes (**Figure 5.4**), and this was supported by literature reports (Valceckiene et al., 2010). However, expression of *B2M* was highly variable across healthy controls, with a C_t value range of 5.4 cycles. Theoretically this range could skew the normalisation factor by 42-fold across healthy controls. Therefore, *B2M* was removed as a reference gene. To date, there are no publications that use *B2M* as a reference gene in healthy B-lymphocytes. It is advised that in future gene expression studies comparing CLL B-lymphocytes to healthy controls that *B2M* not be used as a reference gene.

Five genes (*ANGPTL4*, *APOA4*, *APOB*, *CEL*, and *PNPLA3*) were undetected in all samples, and so were excluded from further investigation. These genes were originally included due to their role in lipid metabolism, despite being known as lowly expressed in bone marrow, lymph nodes, and spleen, as cancer cell gene expression patterns often differ from their tissue of origin (Axelsen, Lotem, Sachs, & Domany, 2007). Genes undetected in samples were excluded from analysis to prevent biased inference of real-time qPCR data (McCall, McMurray, Land, & Almudevar, 2014).

ADIPOQ, which codes for adiponectin, has C1Q and collagen domains and is exclusively expressed in adipocytes, was detected in CLL B-lymphocytes with no detection in healthy controls. Adiponectin is predominantly secreted by adipose tissue and, depending on the protein form, elicits a number of cellular responses when it binds to its receptor including mitochondrial biogenesis and fatty acid oxidation (Achari & Jain, 2017; Ruan & Dong, 2016). It has been reported that CLL B-lymphocytes have a gene expression profile similar to that of fat and muscle tissue suggesting that *ADIPOQ* is a key player in the metabolic profile observed in CLL B-lymphocytes through stimulation of fatty acid oxidation and mitochondrial biogenesis, which has previously been reported to be elevated in CLL (Bilban et al., 2006; Jitschin et al., 2014). However, further investigation of *ADIPOQ* expression was inconclusive due to genomic DNA contamination of the qPCR reaction and the *ADIPOQ* amplicon being exonic, resulting in being unable to distinguish between amplification of genomic DNA or cDNA. Although expression of *ADIPOQ* was inconclusive, expression of the *ADIPOR1* gene was detected. This gene encodes the adiponectin receptor 1, and binding of adiponectin results in an increase in fatty

acid oxidation. As *ADIPOR1* RNA was detected in CLL (**Table 5.5**), it is possible that adiponectin plays a role in fatty acid oxidation in CLL and warrants further investigation.

5.3.2.1 Analysis Round 1

Data from the PrimePCR™ real-time qPCR plates did not meet the requirement of technical duplicates lying within 0.5 cycles of each other, and so the identification of genes of further interest was based on expression being ≥10-fold different in a CLL B-lymphocyte sample compared to the average of the healthy controls in an attempt to reduce the likelihood of pursuing false positives. The replicate discrepancy may have been due to pipetting variance which would have been eliminated by a 384-well plate robot, however this was not available at the time. Hence, this task was completed manually, and further verification of PrimePCR™ results by standard in-laboratory real-time qPCR was therefore essential.

Expression analysis using in-lab methods found that *MGLL* and *CD36* were expressed at a significantly lower level in CLL B-lymphocytes compared to healthy controls and will be discussed further in section 5.3.2.2(**Figure 5.5**).

Interestingly, in-lab real-time qPCR revealed that *LPL* was expressed at a higher level (8.26-fold; **Figure 5.5**) in CLL B-lymphocytes compared to healthy controls which supports the literature (Heintel et al., 2005; Rozovski et al., 2015). However, *LPL* was undetected in 2 of the 6 CLL samples analysed, and there was a distinct difference between *LPL* expression in the four samples where *LPL* was detected (approximately 26-fold; **Table 5.12**). Samples with high *LPL* expression correspond to trisomy 12 (unmutated *IGHV*) and del11q (unmutated *IGHV*). Although these represent sample sizes of one each and need to be tested in an expanded cohort, findings are consistent with published literature which associates high *LPL* expression with poorer prognosis and patient outcome (Bilous, Abramenko, Chumak, Dyagil, & Martina, 2019; Heintel et al., 2005; Mátrai et al., 2017). In addition, those with lower or undetected *LPL* expression corresponded to two del13q (mutated *IGHV*), and normal karyotype (mutated IGHV), which is also consistent with published literature. The isolated finding of del17p with an unmutated *IGHV* and low *LPL* demonstrated the heterogeneity of this disease and the value of an expanded cohort in future analysis.

5.3.2.2 Second round analysis – using higher stringency

Twenty-two genes were chosen from a second-round interrogation of the data, on the basis of meeting strict quality control criteria (5.1.3.2). From this round, gene expression of *MGLL*, *CD36* and *PLIN2* was found to be significantly lower, and *HMOX1* and *ACSL5* significantly higher in CLL B-lymphocytes compared to healthy controls (**Figure 5.6**). *MGLL*, *CD36*, *ACSL5*, *HMOX1*, and *PLIN2* expression differences were then assessed using in-lab real-time qPCR to confirm results (**Figure 5.5**). Using in-laboratory real-time qPCR contradicted the previous findings for *ACSL5*, *HMOX1* and *PLIN2*.

These results again question the reliability of the PrimePCR™ real-time qPCR data in this case, although previous publications have not reported similar issues with this assay (Memmert et al., 2019; Sarras et al., 2016). In retrospect, we suspect that the sensitivity of the assay was insufficient for very low-level expression genes for the amount of RNA added to each reaction. As a consequence of the verified analysis, *MGLL* and *CD36* expression was then assessed in a larger cohort to confirm the initial findings, using *ACSL5* as a control where gene expression did not differ from healthy B-lymphocytes.

The GEO data analysis proved consistent with these results for *CD36* but contradictory for *MGLL*. Given that this disease is so heterogeneous and that the GEO datasets are no larger than our own, we believe that *MGLL* remains a potential candidate for variation in lipid metabolism in CLL but ideally this would be confirmed in a much larger cohort (e.g. 400 samples) so that all prognostic groups are well represented and the dataset is appropriately powered to detect subtypes of CLL.

In terms of energy demands, monoglyceride lipase (MGL) has been shown to be associated with lipid storage droplets and is involved in the process of lipolysis where it is responsible for the breakdown of monoacylglycerol to free fatty acids which are used for subsequent energy production (Beilstein, Carriere, Leturque, & Demignot, 2016). This role of MGL is of interest in CLL as data from our laboratory shows the presence of lipid droplets in CLL B-lymphocytes, and low MGL expression indicates that lipolysis is not promoted in the peripheral blood. It was therefore hypothesised that MGL is required in the microenvironment, where perfusion and therefore nutrient availability is low, for the lipolysis of lipids stored in lipid droplets as a source of energy. There was however no difference in the expression of *MGLL* between matched peripheral blood and bone marrow samples (**Figure 5.9**) and lymph node proteomic data did not identify MGL in CLL B-lymphocytes or healthy controls. However, as research samples of bone marrow aspiration represent the second draw into the syringe which is a mixture of cells from the bone marrow and peripheral blood implying that the sample is contaminated with peripheral blood, and hence more closely representing CLL B-lymphocytes from the periphery. This may explain why there was no difference in *MGLL* gene expression between peripheral blood and bone marrow samples used in this study. Utilising fresh bone marrow biopsy trephines may help to eliminate this tissue and will be a method of study in future. Likewise, the absence of MGL protein in the lymph node samples may be due to the formalin-fixation and paraffin-embedded lymph node biopsy samples that were used in this analysis. Fresh, unfixed samples and bone marrow trephines will be required in the future to complete this analysis.

Interestingly, Liu et al. (2018) found that knock out of *MGLL* in mice caused elevated cyclooxygenase-2 levels which has previously been observed in CLL (R. Liu et al., 2018; Secchiero et al., 2005). Cyclooxygenase-2 overexpression is associated with apoptotic resistance, and induction of apoptosis in cancer cells has been achieved through inhibition of this protein (Hara, Yoshimi, Niwa, Ino, & Mori,

1997; Sawaoka et al., 1998; Tsujii & DuBois, 1995). This provides further evidence that *MGLL* downregulation in CLL warrants further investigation.

CD36 codes for fatty acid translocase and is responsible for translocating free fatty acids across the plasma membrane (Schwenk et al., 2008). RNA (**Figure 5.8**) and protein expression (**Figure 5.11**) data show that CD36 was expressed at a significantly lower level in CLL B-lymphocytes compared to healthy controls. The absence of CD36 detection using western blotting indicates that it is below the level of detection, however, does not eliminate the presence of surface CD36 expression. Flow cytometry should be used in future to determine surface CD36 expression in CLL. Expression of CD36 is regulated by CCAAT/enhancer-binding protein (CEBP) α and β, which directly enhance expression upon binding to the CD36 promoter (Qiao et al., 2008). The corresponding genes, *CEBPA* and *CEBPB*, were not included in the PrimePCR™ gene panel but it would be important to investigate their expression in CLL to determine if this is likewise abnormal and potentially responsible for low CD36 expression. Additionally, and importantly, mutations in the CD36 gene, with missense mutations being the most common, have been identified to be responsible for the absence of CD36 in heart tissue (Tanaka et al., 2001). Mutations in CD36 could be responsible for low expression in CLL, and future work should investigate this as a potential contributor to the low expression of CD36.

The lack of CD36 despite high LPL means that the CLL cells must have another mechanism for the import of locally-available lipids, and as our data showed that fatty acid uptake was elevated in CLL B-lymphocytes compared to healthy controls (Figure 4.2), an alternative mechanism for fatty acid uptake in CLL must be at play. As a consequence of these findings, other forms of fatty acid import were investigated.

5.3.3 Fatty acid import

Uptake of fatty acids across the plasma membrane is dependent on three steps: increasing the local concentration of fatty acids at the plasma membrane through binding, direct transport across the lipid bilayer, and acylation of internalised fatty acids (Black & DiRusso, 2007; Pepino, Kuda, Samovski, & Abumrad, 2014; Schwenk et al., 2008). As CD36/fatty acid translocase, a primary transporter of fatty acids across the plasma membrane, was absent from CLL B-lymphocytes, and CLL B-lymphocytes have a significantly elevated fatty acid uptake compared to healthy B-lymphocytes, a gene panel was constructed to include the main players in fatty acid import into the cell to determine how fatty acid uptake occurs in CLL (**Table 5.15**). Understanding fatty acid uptake and regulation in CLL could reveal druggable targets which could be blocked to essentially starve CLL B-lymphocytes of the fatty acid energy source that they depend on. Alternative pathways including direct transport across the plasma membrane by solute carriers and endocytosis were explored.

ACSL1 and *ACSL3* gene expression were not different between CLL B-lymphocytes and healthy controls. However, inhibition of these proteins with triacsin C showed decreased uptake of fatty acids in HG-3 CLL cells (**Table 5.17**). This is most likely due to the fact that fatty acid uptake is dependent on vectorial acylation, a process where fatty acids are metabolically activated during transport by long-chain fatty acid-CoA ligases i.e. ACSL1 and ACSL3 (Black & DiRusso, 2007). Fatty acids undergo esterification with coenzyme A forming fatty acid-CoA, allowing fats to be able to enter various metabolic pathways including lipid signalling, storage, and β-oxidation (Arias-Barrau, Dirusso, & Black, 2009). Inhibition of this activation process stalls the preceding fatty acid uptake step and most likely explains why uptake was decreased (Black & DiRusso, 2007). Interestingly, ACSL3 is also required for lipid droplet formation, the presence of which has been confirmed in CLL in our laboratory and others, presenting itself as a potential therapeutic target allowing for the inhibition of important import and storage steps in fatty acid metabolism (Kassan et al., 2013; Rozovski et al., 2015). However, as these proteins are required in other fatty acid-metabolising organs such as the heart, this would need to be carefully tested in an animal model.

Similarly, the observed reduction in fatty acid uptake after inhibition of plasma membrane-associated fatty acid binding protein (FABPpm) with AOA is most likely due to fatty acid uptake being dependent on local binding of fatty acids to the plasma membrane (Schwenk et al., 2008). As such, inhibition of local fatty acid binding, conversion to acyl-CoA, and formation of lipid droplets are pathways of potential therapeutic intervention for CLL. Although *FABP3* expression could not be measured due to non-specific amplification, proteomic data from our laboratory showed higher FABP3 expression in CLL (Thurgood et al., 2019).

Fatty acid transport proteins (FATP) 1-6 regulate the import of exogenous fatty acids with variable expression across human tissues (Black & DiRusso, 2007). *FATP2* was expressed 5 times higher in CLL B-lymphocytes compared to healthy controls, although did not reach statistical significance in this analysis due to high variation in the CLL cohort (**Figure 4.12**). While increased expression of this transporter/acyl-CoA ligase could be responsible for an increased rate in fatty acid uptake into the cell, proteomic data from our laboratory did not confirm this increase and FATP2 was not detected (**Table 5.17**).

Although *FATP5* was expressed 4 times higher in CLL B-lymphocytes compared to healthy controls (**Figure 5.12**), the proteomic data did not support this as FATP5 was not detected in CLL (**Table 5.17**). Similar discordance was seen for FATP2. Although primers were optimised to detect individual family members, and were checked with the UCSC genome browser, it remains possible that the amplification of another family member was occurring. The FATP6 protein, however, was detected in CLL B-lymphocytes (**Table 5.17**) and gene expression was 9.4 times higher in CLL B-lymphocytes compared to healthy controls (**Figure 5.12**). Interestingly, FATP6 is primarily expressed in the heart, which is the

tissue with the highest LPL expression (Gimeno et al., 2003; Schulze, Drosatos, & Goldberg, 2016). In CLL, cases with high LPL expression exhibit a dysregulation of muscle genes (Bilban et al., 2006). It would therefore be beneficial to assess LPL expression in this cohort to determine whether FATP6 expression is associated with high LPL expression and to investigate FATP6 as a therapeutic target for such CLL cases. However, therapeutic targeting of FATP6 would need to be tissue specific due to its reliance in the heart. Interestingly, FATP6 colocalises with CD36 at the plasma membrane in mouse heart (Gimeno et al., 2003) and long-chain fatty acid-CoA ligase activity and not transport of fatty acids by murine FATP6 has previously been observed (DiRusso et al., 2005). The absence of CD36 in this study therefore suggests that the long-chain fatty acid-CoA ligase activity of FATP6 is the sole function of FATP6 in CLL. Inhibition of FATP6 and assessment of fatty acid uptake was not performed in the current study as a FATP6 inhibitor is not commercially available.

Endocytosis allows extracellular fluid to be internalised by the cell and types of endocytosis can be categorised by their mediating proteins, two of which were of particular interest in this study: clathrin-mediated endocytosis (pinocytosis) and caveolar-mediated endocytosis (Sandvig & van Deurs, 1994; van Deurs, Petersen, Olsnes, & Sandvig, 1989). Additionally, adipose tissue has the highest expression of both caveolin 1 and 2 indicating that caveolae-mediated endocytosis is important for the functioning of fat-storing cells and the role of these proteins in fatty acid uptake were therefore investigated in CLL (Scherer et al., 1996).

Caveolin 1, a structural scaffolding protein found as homodimers on membrane invaginations called caveolae, was detected in CLL lymph node material, and RNA expression of *CAV1* was higher in CLL B-lymphocytes compared to healthy controls (**Figure 5.12**; (Eyre et al., 2008)). However, *CAV1* gene expression was detected in a small number in both CLL and healthy controls, most likely due to low transcript availability. Additionally, measurement of fatty acid uptake with inhibition of this protein was not performed as the methyl-β cyclodextrin also prevents the formation of clathrin-coated invaginations, hence inhibition is not specific to caveolae and therefore, conclusions about the importance of caveolin 1 in CLL fatty acid uptake cannot be made (Rodal et al., 1999). However, caveolin 1 has been shown to enhance mitochondrial function and reduce apoptosis and as caveolin 1 was detected in CLL lymph nodes the role of caveolin 1 in CLL cell survival and metabolism in the CLL microenvironment may be of more interest than its role in the uptake of fatty acids (Y. H. Chen et al., 2014; Fridolfsson et al., 2012; Niesman et al., 2013). Interestingly, caveolin 1 is considered an oncogenic protein, is overexpressed in a number of cancers, and has been reported to be responsible for the glycolytic phenotype observed in advanced colon cancer through stimulation of glucose transporter 3 expression (Burgermeister, Liscovitch, Röcken, Schmid, & Ebert, 2008; T. K. Ha et al., 2012). Glucose transporter 3 expression is believed to be increased by BCR signalling as treatment of CLL cells with ibrutinib blocked an IgM-stimulated increase in glucose transporter 3 (Clear et al., 2018). It would therefore be beneficial to assess the expression of caveolin 1 in ibrutinib-resistant CLL and

advanced CLL and investigate its potential as a driver of Richter's transformation where CLL transforms to an aggressive lymphoma with a glycolytic phenotype (Bruzzi et al., 2006).

Caveolin 2 can form hetero-oligomers with caveolin 1 at caveolae, however its function is not well understood (Scherer et al., 1997). Caveolin 2 was not detected in CLL lymph node material and RNA was expressed at a significantly lower level in CLL B-lymphocytes compared to healthy controls ($p = 0.0179$; **Figure 5.12**). Relevant to current findings in this study, Lee *et al.* (2011) showed that re-expression of caveolin 2 in HepG2 hepatocellular carcinoma cells decreased proliferation and growth rate. This group also showed that re-expression inhibited the cell cycle in HepG2 cells and concluded that caveolin 2 acts as a tumour suppressor in this case (S. Lee, Kwon, Jeong, & Pak, 2011). Interestingly, caveolin 2 re-expression in HepG2 cells also showed a decrease in STAT3 transcriptional activation (S. Lee et al., 2011). In CLL, STAT3 is constitutively activated and is responsible for elevated LPL expression (Rozovski et al., 2015). The finding from this study suggests a potential link between caveolin 2 and the altered metabolism observed in CLL. Re-expression of caveolin 2 in CLL is warranted to further understand its role in CLL cell survival, mRNA-based therapeutics that deliver *CAV2* mRNA through endocytosis and re-introduce caveolin 2 expression can be used in this context (Kowalski, Rudra, Miao, & Anderson, 2019). The tumour suppressing function and role of caveolin 2 in high LPL expression is perhaps of more interest in CLL as caveolin 2 expression is not a requirement for the formation of caveolae, and hence it most likely does not play a direct role in fatty acid uptake in CLL but rather through other regulating mechanisms (Razani et al., 2002).

Pinocytosis is a form of fluid-phase endocytosis where clathrin-coated pits in the cell membrane form invaginations allowing extracellular fluid to be internalised through the eventual formation of vesicles (Lin et al., 2018). Inhibitors and the concentration used in this study were selected by Ms Ashley Rowland based on the presence of non-necrotic lymphocytes at the selected time point. Inhibition of macro and micropinocytosis in the HG-3 CLL B-lymphocyte cell line significantly reduced fatty acid uptake suggesting that this is the major means of fatty acid uptake in CLL (**Table 5.17**). LY294002, successfully used in this study to inhibit macropinocytosis, is an inhibitor of all PI3K isoforms (Araki, Johnson, & Swanson, 1996). In CLL, idelalisib inhibits PI3Kδ effectively preventing cellular proliferation signalling (**Figure 1.9**) (Zirlik & Veelken, 2018). Interestingly, permanent activation of PI3K in rat fibroblasts resulted in constitutive macropinocytosis (Amyere et al., 2000) indicating that, in CLL, macropinocytosis and hence fatty acid uptake is at least partly dependent on PI3K activity and hence BCR stimulation, and that higher BCR activity results in higher macropinocytosis. It would be of great benefit to conduct an experiment blocking PI3Kδ in CLL B-lymphocytes using idelalisib and measuring fatty acid uptake, hence determining whether the therapeutic benefits of idelalisib are also due to a reduction in macropinocytosis. If this is the case, then inhibitors of fatty acid synthase, the major enzyme responsible for *de novo* synthesis of fatty acids from acetyl-CoA, could be used in combination with idelalisib to inhibit both fatty acid uptake and synthesis simultaneously essentially

starving CLL B-lymphocytes and causing cell death. The novel fatty acid synthase inhibitor TVB-2640 is currently being tested in a phase I clinical trial for its effectiveness in colon cancer and therefore has potential for therapeutic use in CLL (ClinicalTrials.gov, 2018). Additionally, ND-646 an inhibitor of acetyl-CoA carboxylase, a crucial enzyme in fatty acid synthesis, has been shown to inhibit fatty acid synthesis in the A549 non-small-cell lung carcinoma cell line (Svensson et al., 2016) and future work should test the effectiveness of this drug on inducing cell death in CLL B-lymphocytes to reveal the importance of fatty acid synthesis in their survival. In addition, due to higher BCR stimulation in unmutated versus mutated *IGHV* CLL, and hence higher PI3K activity, it can be assumed that macropinocytosis is higher in unmutated *IGHV* CLL (Kienle et al., 2006). Therefore, comparing fatty acid uptake in these groups will elucidate whether unmutated *IGHV* CLL is likely to benefit from therapeutic inhibition of pinocytosis, and can lead to the development of novel therapeutic regimens for this group.

The transcription factor PPARγ is activated by unsaturated fatty acids and is responsible for regulating metabolic pathways including fatty acid oxidation and lipid storage (Bogacka, Ukropcova, McNeil, Gimble, & Smith, 2005; Bogacka, Xie, Bray, & Smith, 2005; Desvergne & Wahli, 1999; Tontonoz, Hu, & Spiegelman, 1994). In CLL, inhibition of PPARγ with CDDO caused cell death indicating a reliance on PPARγ activity in the survival of CLL (Inoue, Snowden, Dyer, & Cohen, 2004; Pedersen et al., 2002). PPARγ inhibition-induced cell death may be explained by CLL cell's reliance on fatty acid oxidation for energy. Additionally, activation of PPARγ has been shown to increase mitochondrial biogenesis and the expression of antioxidants (Bogacka, Xie, et al., 2005; X. Wang et al., 2011). Therefore, elevated fatty acid uptake and subsequent activation of PPARγ could be responsible for increased mitochondrial biogenesis and elevated antioxidant levels observed in CLL (Jitschin et al., 2014). Blocking of pinocytosis in CLL is therefore of great importance as it potentially has many downstream effects that contribute to the pathogenicity of CLL.

5.3.4 Understanding lipid import in CLL

The CLL microenvironment plays an important role in CLL disease pathogenesis by providing stimulation for survival and proliferation (Caligaris-Cappio, Bertilaccio, & Scielzo, 2014). As mentioned previously, a portion of the CLL load circulates in the peripheral blood – if the microenvironment is an ideal location for CLL B-lymphocytes to proliferate, why do they exit into the blood stream? Although CLL B-lymphocytes secrete vascular endothelial growth factor to promote neovascularisation in the tumour microenvironment, the CLL-dense nature of the microenvironment indicates that these sites have low perfusion, and low perfusion and oxygenation of bone marrow has previously been reported in acute myeloid leukaemia xenografts (Badoux et al., 2011; Lutzny et al., 2013; Suzuma et al., 2002). It was therefore hypothesised that CLL B-lymphocytes 'choose' to leave

the microenvironment when energy stores are low and unavailable due to low perfusion and subsequently go on to scavenge lipids in the periphery for return to the microenvironment.

In order to test this hypothesis, CLL B-lymphocytes were cultured with BODIPY-labelled C12 for 15 minutes to assess fatty acid uptake, and surface CXCR4 was labelled to identify CLL B-lymphocytes homing to the microenvironment, with low CXCR4 an indicator of having recently exited the microenvironment (Calissano et al., 2011; To et al., 2011). The results indicate that CLL B-lymphocytes entering the circulation from the microenvironment have a higher uptake rate of fatty acids, are nutrient depleted and therefore have a higher demand for an energy source than those homing to secondary lymphoid organs. This result also fits with our previous observation that CLL B-lymphocytes with high CXCR4 surface expression, and hence homing to the microenvironment, having a greater lipid load compared to those exiting the microenvironment (Thurgood, unpublished).

In this study, fatty acid uptake assessment was performed on cryopreserved CLL B-lymphocytes. The process of cryopreservation involves the incubation of CLL B-lymphocytes in a 50:50 RPMI 1640:FCS mixture, a source of fatty acids at high concentrations. Therefore, it could be that the true uptake of fatty acids in the $CXCR4_{low}$ fraction is much higher than demonstrated in **Figure 5.13**. This work could be repeated in CLL B-lymphocytes from fresh blood samples to determine the true fatty acid uptake rate in CLL B-lymphocytes.

Interestingly, hypoxia has been shown to induce the accumulation of lipid droplets in a hypoxia-inducible factor-1α (HIF-1α)-dependent manner in glioblastoma cells (Bensaad et al., 2014). HIF-1α is a transcription factor responsible for regulating cellular pathways in response to low oxygen availability (Mole et al., 2009). Additionally, hypoxia has been shown to repress *de novo* fatty acid synthesis (Bensaad & Vousden, 2007). Since the CLL microenvironment is believed to be hypoxic, and there are reports of high HIF-1α gene expression in CLL, it is plausible that the microenvironmental conditions stimulate the accumulation of exogenously-derived fatty acids into lipid droplets, which cannot be created through *de novo* fatty acid synthesis, and hence there is a need for fatty acids to be imported into the cell (Kontos et al., 2017). However, due to the ability of CLL B-lymphocytes to move freely around the body, unlike other solid tumours, an adaptive mechanism may have developed whereby CLL cells can exit the nutrient-poor microenvironment, where proliferation takes place, and enter the circulation to scavenge lipids for use on return to the proliferation centres. To test how such a mechanism might work, it would be of great benefit to investigate intracellular lipid content and CXCR4 surface expression in CLL B-lymphocytes from bone marrow aspirates to determine if CXCR4 expression decreases in response to low lipid storage levels. This could be easily performed using a neutral lipid stain such as LipidTOX™ (ThermoFisher) or BODIPY® 493/503 (ThermoFisher) together with an anti-CXCR4 antibody and flow cytometry.

The CLL lipid droplet presents itself as a potential therapeutic target in CLL. Inhibition of lipid droplet formation using pyrrolidine-2 has previously been reported to improve the effectiveness of therapeutics in the U251N glioblastoma cell line (I. Zhang et al., 2016). This should also be tested in CLL as it could lead to the development of novel therapeutic regimens including the combination of inhibitors of lipid droplet formation with therapeutics currently used to treat CLL. Additionally, it would be of great benefit, and interest, to characterise the CLL lipid droplet proteome to reveal novel therapeutic targets that either prevent the formation of lipid droplets or the ability of them to be metabolised, essentially starving the cell and causing cell death. Furthermore, the origin of CLL lipid droplets should be investigated to determine whether they originate from vesicles formed through pinocytosis or from the endoplasmic reticulum where they are associated with a number of lipid droplet-specific proteins (Robenek et al., 2006). Characterisation of the CLL lipid droplet proteome will aid in understanding this and is currently being performed in our research laboratory.

5.4 Conclusions

Through gene expression analysis of 89 genes involved in lipid metabolic pathways, this chapter revealed that CD36/fatty acid translocase is absent in CLL B-lymphocytes. Gene expression was assessed in a panel comprising importers of fatty acids and discovered that *CAV2* gene expression was lower in CLL B-lymphocytes compared to healthy controls. This finding presents caveolin 2 as a modulator in CLL as in a range of other cancers as well as affecting STAT3 activity, which is constitutively active in CLL and responsible for high LPL levels. CAV2 is a positive regulator of cellular mitogenesis and required for nuclear translocation and activation of MAPK1 and STAT3. Further investigation into the role caveolin 2 plays in CLL is therefore warranted. Through inhibition of fatty acid import pathways, it was discovered that pinocytosis is responsible for the import of fatty acids into CLL B-lymphocytes and presents this mechanism as a therapeutic target. Additionally, inhibition of ACSL1 and ACSL3 decreased fatty acid uptake. These results suggest that the ability of CLL B-lymphocytes to take up large quantities of fatty acids is also due to the rapid conversion of imported fatty acids into fatty acyl-CoA.

Additionally, the ability of CLL B-lymphocytes to import free fatty acids which associates with expression of the CXCR4 homing surface marker indicates that CLL B-lymphocytes likely enter the peripheral blood circulation for the scavenging and storage of fatty acids. Furthermore, this discovery fits with the observation in our research laboratory that CLL B-lymphocytes returning to the proliferative compartments have a higher lipid load. This chapter is the first to present pinocytosis and lipid droplet storage as therapeutic targets in CLL.

Chapter 6:

Final discussion and future directions

This thesis aimed to understand how energy metabolism pathways could be responsible for disease pathogenesis and resistance to therapy in CLL and explored redox homeostasis and lipid metabolism in hopes of finding defects in these pathways that could be exploited by novel therapeutics and therapeutic regimens. Firstly, how and if antioxidant capacity enables CLL B-lymphocytes to evade RTX-mediated cell death was investigated and it was found that CLL B-lymphocytes did not respond to cross-linked RTX with either ROS induction or increased cell death, did respond to the blocking of oxidative phosphorylation using rotenone, however the response was mixed, consistent with the known biological heterogeneity of the disease. A number of genes involved in ROS handling were shown to have altered expression in primary CLL cells which lead to investigating the reason for low SOD2 expression in CLL which would otherwise be elevated when high ROS levels are experienced. No cause thus far for the low expression of SOD2 was determined although additional routes for discovery were identified. This thesis then went on to explore lipid metabolic pathways and CD36/fatty acid translocase, which transports fatty acids in normal B-lymphocytes, was identified as being absent in CLL B-lymphocytes despite a propensity for CLL cells to store and utilise fatty acids. Following this, pinocytosis was identified as the primary mechanism of fatty acid uptake in CLL. The final discovery from this thesis was that CLL B-lymphocytes recently having left the proliferative compartments had a higher rate of fatty acid uptake compared to those returning. Whilst further investigation is required, this thesis presents multiple candidates for improved understanding of the fundamental biological processes altered in CLL which lead to proliferative and survival advantage; and which may assist in disease prognostication and potential for therapeutic development.

6.1 Exploring antioxidant pathways in CLL

6.1.1 Antioxidant capacity in CLL (Chapter 3)

This thesis showed that CLL B-lymphocytes die in response to the uncoupling of electron transfer at complex I of the mETC using rotenone. Although cell death was assessed at 4 hours post-treatment, this was dramatically different from the response elicited by RTX where the majority of CLL B-lymphocyte samples exhibited resistance. Unfortunately, an increase in intracellular ROS could not be detected in response to RTX treatment and this may be due to the timing of measurement. Further experimentation of the response to RTX treatment with respect to intracellular ROS is needed and this should be performed at an earlier timepoint preferentially between 10 and 60 minutes post-treatment. The antioxidant capacity of CLL B-lymphocytes from individuals with and without BLA demonstrated a reduction in ROS species in the BLA associated lymphocytes. However, how this affected the ability to resist ROS-induced cell death was unable to be elucidated in this thesis due to the blocking of

oxidative phosphorylation effectively causing cell death in CLL B-lymphocytes. However, it did demonstrate the heterogeneous dependence of CLL on adequate ROS handling machinery and the potential of therapeutic manipulation of ROS in CLL. CLL B-lymphocytes from individuals with BLA had consistently lower intracellular ROS levels at both pre- and post-treatment. This result could indicate one of two things: these cells have a lower metabolic rate and hence lower ROS production, or they have a greater ability to respond to ROS with increased antioxidants allowing for the detoxification of ROS. The rate of oxidative phosphorylation and levels of antioxidants should therefore be measured in the samples used in this study. In addition, as mentioned previously, high ROS levels in early stages of disease indicate a more favourable prognosis (Linley et al., 2015). It is possible that CLL B-lymphocytes from individuals with BLA are able to increase antioxidant levels and along with low CD20 expression are able to evade RTX-induced cell death. Further work is required to explore the findings from our research group and to further investigate ROS handling in CLL as a druggable pathway and predictor of disease response.

Additionally, not only does the inhibition of complex I cause an increase in superoxide generation, but it blocks the ability of the mETC to effectively carry out oxidative phosphorylation. The results from this study therefore also indicate this process as being crucial for CLL B-lymphocyte survival and presents the reliance of CLL B-lymphocytes on oxidative phosphorylation as a vulnerability and potential therapeutic target. Interestingly, in acute myeloid leukaemia, inhibition of the anti-apoptotic protein Bcl-2 using venetoclax has been shown to inhibit complex II of the mETC resulting in the blocking of oxidative phosphorylation (Pollyea et al., 2018). In CLL, venetoclax has demonstrated therapeutic superiority over immunochemotherapy in both initial treatment and treatment of relapsed/refractory CLL (Jain et al., 2019; Roberts et al., 2016). The success of venetoclax in CLL may therefore be partially due to the blocking of oxidative phosphorylation which CLL B-lymphocytes are so heavily reliant upon as well as its anti-Bcl-2 effects. Confirmation of inhibition of complex II using venetoclax is therefore suggested in CLL.

6.1.2 SOD2 expression in CLL (Chapter 4)

This thesis was unable to elucidate the reason for low SOD2 levels in CLL, however made some interesting technical discoveries regarding amplification of the GC-rich *SOD2* promoter. Firstly, it is possible for the phenomenon of '*Taq* jumping' to occur in bisulphite-treated DNA templates that create DNA secondary structures. Secondly, the use of agents that prevent the formation of hydrogen bonds between bases in combination with heat pulses during the extension phase of PCR to resolve DNA secondary structures can be used to successfully amplify the promoter of the *SOD2* gene. Thirdly, when highly homogenous sequences are being amplified, like that of the *SOD2* promoter which includes a run of 11 guanines, insertions at these sites may be false positives and due to *Taq* polymerase becoming dissociated at sites of DNA secondary structure formation and adding a 3' overhang upon dissociation.

All these observations from this thesis must be considered in future investigations of the *SOD2* promoter and further work is required to establish the reason for low SOD2 expression in CLL.

As SOD2 expression has been shown to change with disease stage, with low levels observed in tumourigenesis and high levels in late stage aggressive cancer, it would be beneficial to assess SOD2 expression in CLL at different stages of the disease. The presence of such a 'switch' in CLL may be able to be used to predict the disease course if this is monitored over time. In this thesis, SOD2 expression was assessed in a small cohort of treatment-naïve individuals to determine if there was a founding mutation in the SOD2 promoter of CLL B-lymphocytes that could result in low SOD2 expression and hence higher levels of DNA-damaging intracellular ROS. Although beyond the scope of this study, intracellular ROS levels of the CLL and healthy B-lymphocytes used in this study should be assessed to determine if low SOD2 expression does indeed correlate with high intracellular ROS, or whether other antioxidant molecules have been upregulated in order to combat this. Interestingly, high intracellular ROS in early stages of CLL have been shown to be associated with mutated *IGHV* status and a longer TTFT (Linley et al., 2015), compared with the non-BLA patients in our cohort and it would therefore be of interest to assess SOD2 expression in a larger cohort of individuals with CLL to determine if its expression is associated with any clinical parameters in particular its expression in bulky and non-bulky lymph nodes. Additionally, it is possible that sub-clonal variation in SOD2 expression exists. As such, a high SOD2-expressing subclone, initially repressed by the dominant clone, could, upon treatment and eradication of the dominant clone, proliferate and add to the biological aggressiveness seen in relapsed CLL. The existence of high SOD2-expressing subclones could be tested using fluorescence-activated cell sorting of high and low SOD2-expressing cells. In addition, superoxide levels may also distinguish high and low SOD2 expressors in CLL, and sorting of CLL B-lymphocytes with either high or low levels of superoxide could be assessed for SOD2 expression. Clearly, ROS handling and superoxide levels would also be dependent on the activity of the mETC and other proteins as well as enzymes such as NADPH oxidases and these should also be assessed in future work.

6.2 Exploiting lipid metabolism in CLL (Chapter 5)

6.2.1 Fatty acid import

Although technical difficulties were encountered when exploring lipid metabolic pathways, the most interesting finding from this study was the absence of CD36/fatty acid translocase expression in CLL. This result was surprising as CD36 is a primary importer of fatty acids. Additionally, high LPL expression in CLL suggests high fatty acid availability at the plasma membrane. Therefore, it was of great interest to elucidate how fatty acids enter CLL cells and this became the subsequent focus of the thesis.

Gene expression data revealed two potentially important players in CLL, *CAV2* and *FATP6*. The high *FATP6* gene expression compared to healthy controls indicated that this transport protein is important in CLL for the import of fatty acids across the plasma membrane and presents a novel target for therapeutic development. However, the effects of FATP6 inhibition on fatty acid uptake could not be assessed by our research group as an inhibitor of this protein does not currently exist. The importance of FATP6 on fatty acid metabolism in CLL could be investigated by targeting *FATP6* mRNA transcripts with siRNA in either CLL B-lymphocyte cell lines or primary patient samples and measuring outcomes such as fatty acid uptake, cell death and mitochondrial (oxidative phosphorylation) activity.

Additionally, *CAV2* gene expression was significantly lower in CLL B-lymphocytes compared to healthy controls. Caveolin 2 is not required for the formation of caveolae and hence fatty acid uptake, and it is the tumour suppressor function of caveolin 2 which is of more interest in CLL. Interestingly, a previous study found that activation of the transcription factor STAT3 decreased with caveolin 2 re-expression (S. Lee et al., 2011). In CLL, constitutive activation of STAT3 through phosphorylation of serine 727 results in the expression of pro-survival and anti-apoptotic genes including the aberrant expression of the *LPL* gene (Hazan-Halevy et al., 2010; Rozovski et al., 2015). High LPL expression is associated with a shorter treatment-free progression and indicators that infer a poor prognosis including unmutated *IGHV*, CD38 expression and ZAP-70 expression (Heintel et al., 2005; Nuckel et al., 2006; Oppezzo et al., 2005). This strongly implicates caveolin 2 in CLL pathogenesis and the disease experienced by some patients with high LPL expression and suggests that re-expression of caveolin 2 could be used therapeutically in CLL. Firstly, caveolin 2 and LPL gene and protein expression should be assessed in a cohort of individuals with CLL to determine if low caveolin 2 is associated with high LPL levels. Secondly, the effects of caveolin 2 re-expression should be tested in CLL to determine if this can prevent constitutive STAT3 activation, and hence overcome elevated expression of pro-survival and anti-apoptotic genes. The reverse should also be tested – STAT3 activation and LPL expression should be assessed after knocking down caveolin 2 using siRNA in healthy B-lymphocytes. This study presents caveolin 2 as a novel therapeutic target in CLL and further investigation of the role of caveolin 2 in CLL is essential.

Pinocytosis was identified as being responsible for free fatty acid uptake and this should be confirmed in primary patient samples. Interestingly, LY294002, used to block macropinocytosis and reduce free fatty acid uptake, is an inhibitor of PI3K which strongly implicates the BCR in free fatty acid uptake as it is upstream of PI3K signalling (Werner, Hobeika, & Jumaa, 2010). Since *IGHV* gene mutational status determines BCR signalling activity and is an accurate indicator of prognosis in CLL, fatty acid uptake through pinocytosis may also have potential as a prognostic indicator. Further investigation into *IGHV* gene mutational status, BCR signalling and fatty acid uptake is therefore warranted. Additionally, this thesis presents pinocytosis as a therapeutic target in CLL, however the effects of inhibition will

need to be tested in an animal model to ensure that other tissues that require fatty acids for an energy source, such as the heart, are not negatively affected.

Additionally, if elevated pinocytosis in CLL is due to BCR activation, blocking of this pathway may result in alternative fatty acid uptake pathways being utilised. It is possible that CD36 is not present on the surface of CLL B-lymphocytes due to the sheer magnitude of fatty acids being imported into the cell through pinocytosis rendering CD36 expression unnecessary. Long-term treatment of CLL B-lymphocytes with inhibitors of pinocytosis should therefore be conducted to assess upregulation of alternative fatty acid import pathways including CD36.

6.2.2 Fatty acid storage

Of great interest from this thesis was that CLL B-lymphocytes returning to the proliferative compartments had a lower fatty acid uptake rate compared to those having recently left. This presents a model of CLL B-lymphocyte survival where CLL cells leave the microenvironment due to low nutrient availability and scavenge fatty acids in the periphery for return to the microenvironment and subsequent proliferation. This work further supports the importance of exploring the blocking of fatty acid uptake as a therapeutic means of eradicating CLL and also how it may work in conjunction with blockade of the BCR. It should be considered, however, that glycolytic subclones in CLL exist and successfully eradicating those with a fatty acid phenotype may make way for the development of a B-cell lymphoma such as Richter's transformation, and so development of such therapeutics requires careful testing. Additionally, exploring the effects of blocking fatty acid uptake on the expression of homing surface markers is important in understanding if low nutrient availability is indeed the reason that CLL B-lymphocytes leave the microenvironment. This could be tested by assessing intracellular lipid content and the expression of the homing surface marker CXCR4 in CLL B-lymphocytes from bone marrow aspirates. As mentioned previously, it is important that this is performed using PBMCs from the first pull of aspiration to avoid any contamination with peripheral blood.

Our research group also showed that neutral lipid content is higher in CLL B-lymphocytes returning to the microenvironment compared to those that had recently left. It is highly likely that these lipids are stored in lipid droplets and our research group is currently characterising the CLL lipid droplet proteome in hope of identifying therapeutic targets. One important class of lipid droplet-associated proteins are perilipins which are scaffolding proteins and are responsible for mediating lipolysis of lipid droplets through binding of the lipolytic complex (Sztalryd & Brasaemle, 2017). This investigation identified the expression of both *PLIN1* and *PLIN2* genes in CLL B-lymphocytes, and it is therefore likely that these play a role in regulating the CLL lipid droplet.

Lipid uptake and storage may be responsible for the ability of CLL B-lymphocytes to accumulate and proliferate in the secondary lymphoid organs and cause bulky lymphadenopathy. If these cells have an

enhanced ability to import and store lipids, this may result in being able to reside in the secondary lymphoid organs for a greater length of time. This enhanced ability could be due to the hypoxic nature of the microenvironment which our group believes to be worse in bulky lymphadenopathy. Hypoxia stabilises HIF-1α which has previously been shown to increase lipid uptake.

The importance of fatty acid uptake and storage in the proliferation and survival of CLL B-lymphocytes invokes the question: should low-fat diets and a reduction of body-fat content be recommended to patients? Although previous findings found no correlation between dietary factors and the development of CLL (Tsai et al., 2010), the effects of low-fat diets have not been previously investigated. Interestingly, in 2018, the first account of improving the outcome from a haematological malignancy by switching to a low-fat diet was reported in obese mice (Tucci et al., 2018), warranting such an investigation in CLL. Additionally, statin use has been shown to reduce the need for initial therapy in individuals with CLL. Therefore, the use of fatty acid uptake and evidence of CLL dependence on fatty acids could be used to personalise medical advice.

6.3 Exploiting energy metabolism pathways in CLL

Although lipid metabolism and the oxidative capacity of CLL B-lymphocytes were assessed separately in this thesis, the two are very much intertwined. With elevated lipid metabolism in CLL comes higher mETC activity and hence higher intracellular ROS levels. We believe that low basal ROS in BLA CLL B-lymphocytes is due to the hypoxic nature of the microenvironment causing an increase in mitochondrially-produced ROS resulting in intrinsically higher antioxidant levels. Additionally, results showed that CLL B-lymphocytes returning to the secondary lymphoid organs have higher lipid levels and low fatty acid uptake presumably for use in the proliferative microenvironment-supported compartments of CLL. In BLA, large numbers of CLL B-lymphocytes exist in the secondary lymphoid organs. The results from this thesis suggest that BLA CLL B-lymphocytes may be better able to import and store fatty acids and are thus able to reside in the secondary lymphoid organs for a greater length of time and due to intrinsically better ROS handling are less affected by the hypoxic environment. Interestingly, in Drosophilia, lipid droplets have previously been shown to work as antioxidants (Bailey et al., 2015). This could also be the case in CLL, and, in BLA CLL B-lymphocytes, this may result in them having a higher antioxidant capacity. However, as mentioned previously, the levels of antioxidant molecules should be measured and compared between BLA and non-BLA CLL. Additionally, the study by Bailey *et al.* (2015) found that hypoxia increased lipid droplet accumulation. It would therefore be of great benefit to investigate this phenomenon in CLL B-lymphocytes especially those from individuals with BLA as the microenvironment is believed to be more hypoxic than in those without BLA. The ability of CLL B-lymphocytes to scavenge lipids may also affect their ability to quench ROS in response to chemoimmunotherapy, and therefore impact their ability to evade treatment-mediated cell death. It would therefore be beneficial to assess fatty acid uptake, subsequent formation of lipid

droplets, and the ability to resist chemoimmunotherapy-induced cell death in CLL. This mechanism therefore presents an opportunity to develop an assay that may aid in predicting the response to therapy in CLL.

Interestingly, the study by Bailey *et al.* (2015) also found that SOD2 overexpression inhibits the induction of lipid droplet formation by hypoxia. In addition to this observation, Gao *et al.* (2013) found that HIF-1α inhibited SOD2 expression in renal carcinoma and concluded that a positive feedback mechanism allows HIF-1α to be stabilised through elevated superoxide as a result of decreased SOD2 through blocking of transcription by HIF-1α (Gao et al., 2013). Together, these observations implicate hypoxia, and therefore the nature of the CLL microenvironment, in the decreased expression of SOD2 in CLL. It would therefore be of great interest to explore this mechanism in CLL B-lymphocytes. Healthy B-lymphocytes, with normal SOD2 expression levels, should be cultured under hypoxic conditions and SOD2 expression should be assessed over time. Additionally, HIF-1α should be targeted using siRNA in CLL B-lymphocytes to determine whether SOD2 expression can be restored. Being able to restore SOD2 expression in CLL may therefore aid in the prevention of lipid droplet formation which would be therapeutically beneficial.

Lastly, lipid peroxides have previously been shown to mediate cell cycle arrest and suppress proliferation in leukaemic cells (Barrera et al., 1987; Barrera et al., 1994; Barrera et al., 1996a; Barrera et al., 1996b; Pizzimenti et al., 2006). As CLL B-lymphocytes have elevated mitochondrial activity and hence intracellular ROS levels, this suggests that the rapid storage of lipids is of utmost importance to the survival and proliferative capacity of CLL B-lymphocytes. This emphasises the importance of being able to therapeutically target the lipid droplet by inhibiting its formation in CLL. Additionally, there is an opportunity to develop therapeutic regimens that inhibit lipid droplet formation in conjunction with increasing intracellular ROS levels resulting in the formation of lipid peroxides. This would be particularly important in CLL cases that present with low intracellular ROS levels like those from individuals with BLA observed in this thesis. Furthermore, the bax proapoptotic gene has been shown to be increased in response to treatment with 4-hydroxynonenal, the product of polyunsaturated fatty acid peroxidation, in a p53-independent manner (Cerbone et al., 2007). In CLL, the *TP53* gene can be deleted and results in aggressive disease. Additionally, the ratio of the anti-apoptotic Bcl-2 and proapoptotic bax proteins can be used to identify resistance to chemotherapy and Bcl-2 inhibitors (Del Principe et al., 2016; Williamson, Kelly, Hamilton, McManus, & Johnston, 1998). Investigation into the effects of 4-hydroxynonenal treatment in CLL B-lymphocytes is therefore necessary as being able to initiate cell death through lipid peroxides could be beneficial, particularly in those that are *TP53* deleted and/or resistant to current therapeutics.

Chapter 7:
References

Achari, A. E., & Jain, S. K. (2017). Adiponectin, a Therapeutic Target for Obesity, Diabetes, and Endothelial Dysfunction. *Int J Mol Sci, 18*(6). doi:10.3390/ijms18061321

Admirand, J. H., Knoblock, R. J., Coombes, K. R., Tam, C., Schlette, E. J., Wierda, W. G., . . . Abruzzo, L. V. (2010). Immunohistochemical detection of ZAP70 in chronic lymphocytic leukemia predicts immunoglobulin heavy chain gene mutation status and time to progression. *Mod Pathol, 23*(11), 1518-1523. doi:10.1038/modpathol.2010.131

Amyere, M., Payrastre, B., Krause, U., Van Der Smissen, P., Veithen, A., & Courtoy, P. J. (2000). Constitutive macropinocytosis in oncogene-transformed fibroblasts depends on sequential permanent activation of phosphoinositide 3-kinase and phospholipase C. *Mol Biol Cell, 11*(10), 3453-3467. doi:10.1091/mbc.11.10.3453

Anczuków, O., Ware, M. D., Buisson, M., Zetoune, A. B., Stoppa-Lyonnet, D., Sinilnikova, O. M., & Mazoyer, S. (2008). Does the nonsense-mediated mRNA decay mechanism prevent the synthesis of truncated BRCA1, CHK2, and p53 proteins? *Hum Mutat, 29*(1), 65-73. doi:10.1002/humu.20590

Araki, N., Johnson, M. T., & Swanson, J. A. (1996). A role for phosphoinositide 3-kinase in the completion of macropinocytosis and phagocytosis by macrophages. *J Cell Biol, 135*(5), 1249-1260. doi:10.1083/jcb.135.5.1249

Arias-Barrau, E., Dirusso, C. C., & Black, P. N. (2009). Methods to monitor Fatty Acid transport proceeding through vectorial acylation. *Methods Mol Biol, 580*, 233-249. doi:10.1007/978-1-60761-325-1_13

Autore, F., Strati, P., Innocenti, I., Corrente, F., Trentin, L., Cortelezzi, A., . . . Laurenti, L. (2019). Elevated Lactate Dehydrogenase Has Prognostic Relevance in Treatment-Naïve Patients Affected by Chronic Lymphocytic Leukemia with Trisomy 12. *Cancers (Basel), 11*(7). doi:10.3390/cancers11070896

Awan, F., & Byrd, J. (2018). *Chapter 77 - Chronic Lymphocytic Leukaemia* (Seventh Edition ed.): Elsevier.

Axelsen, J. B., Lotem, J., Sachs, L., & Domany, E. (2007). Genes overexpressed in different human solid cancers exhibit different tissue-specific expression profiles. *Proc Natl Acad Sci U S A, 104*(32), 13122-13127. doi:10.1073/pnas.0705824104

Badoux, X., Bueso-Ramos, C., Harris, D., Li, P., Liu, Z., Burger, . . . Estrov, Z. (2011). Cross-talk between chronic lymphocytic leukemia cells and bone marrow endothelial cells: role of signal transducer and activator of transcription 3. *Hum Pathol, 42*(12), 1989-2000. doi:10.1016/j.humpath.2011.02.027

Bailey, A. P., Koster, G., Guillermier, C., Hirst, E. M., MacRae, J. I., Lechene, C. P., . . . Gould, A. P. (2015). Antioxidant Role for Lipid Droplets in a Stem Cell Niche of Drosophila. *Cell, 163*(2), 340-353. doi:10.1016/j.cell.2015.09.020

Barrera, G., Martinotti, S., Fazio, V., Manzari, V., Paradisi, L., Parola, M., . . . Dianzani, M. U. (1987). Effect of 4-hydroxynonenal on c-myc expression. *Toxicol Pathol, 15*(2), 238-240. doi:10.1177/019262338701500219

Barrera, G., Muraca, R., Pizzimenti, S., Serra, A., Rosso, C., Saglio, G., . . . Dianzani, M. U. (1994). Inhibition of c-myc expression induced by 4-hydroxynonenal, a product of lipid peroxidation, in the HL-60 human leukemic cell line. *Biochem Biophys Res Commun, 203*(1), 553-561. doi:10.1006/bbrc.1994.2218

Barrera, G., Pizzimenti, S., Muraca, R., Barbiero, G., Bonelli, G., Baccino, F. M., . . . Dianzani, M. U. (1996a). Effect of 4-Hydroxynonenal on cell cycle progression and expression of differentiation-associated antigens in HL-60 cells. *Free Radic Biol Med, 20*(3), 455-462. doi:10.1016/0891-5849(95)02049-7

Barrera, G., Pizzimenti, S., Serra, A., Ferretti, C., Fazio, V. M., Saglio, G., & Dianzani, M. U. (1996b). 4-hydroxynonenal specifically inhibits c-myb but does not affect c-fos expressions in HL-60 cells. *Biochem Biophys Res Commun, 227*(2), 589-593. doi:10.1006/bbrc.1996.1550

Basu, S., Kwee, T. C., Surti, S., Akin, E. A., Yoo, D., & Alavi, A. (2011). Fundamentals of PET and PET/CT imaging. *Ann N Y Acad Sci, 1228*, 1-18. doi:10.1111/j.1749-6632.2011.06077.x

Bates, D. J., Lewis, L. D., Eastman, A., & Danilov, A. V. (2015). Vincristine activates c-Jun N-terminal kinase in chronic lymphocytic leukaemia in vivo. *Br J Clin Pharmacol, 80*(3), 493-501. doi:10.1111/bcp.12624

Bauer, M. K., Vogt, M., Los, M., Siegel, J., Wesselborg, S., & Schulze-Osthoff, K. (1998). Role of reactive oxygen intermediates in activation-induced CD95 (APO-1/Fas) ligand expression. *J Biol Chem, 273*(14), 8048-8055. doi:10.1074/jbc.273.14.8048

Baumgartner, H. K., Gerasimenko, J. V., Thorne, C., Ferdek, P., Pozzan, T., Tepikin, A. V., . . . Gerasimenko, O. V. (2009). Calcium elevation in mitochondria is the main Ca2+ requirement for mitochondrial permeability transition pore (mPTP) opening. *J Biol Chem, 284*(31), 20796-20803. doi:10.1074/jbc.M109.025353

Beilstein, F., Carriere, V., Leturque, A., & Demignot, S. (2016). Characteristics and functions of lipid droplets and associated proteins in enterocytes. *Exp Cell Res, 340*(2), 172-179. doi:10.1016/j.yexcr.2015.09.018

Bell, E. L., Klimova, T. A., Eisenbart, J., Moraes, C. T., Murphy, M. P., Budinger, G. R., & Chandel, N. S. (2007). The Qo site of the mitochondrial complex III is required for the transduction of hypoxic signaling via reactive oxygen species production. *J Cell Biol, 177*(6), 1029-1036. doi:10.1083/jcb.200609074

Bellosillo, B., Villamor, N., Lopez-Guillermo, A., Marce, S., Esteve, J., Campo, E., . . . Montserrat, E. (2001). Complement-mediated cell death induced by rituximab in B-cell lymphoproliferative disorders is mediated in vitro by a caspase-independent mechanism involving the generation of reactive oxygen species. *Blood, 98*(9), 2771-2777. doi:10.1182/blood.v98.9.2771

Bensaad, K., Favaro, E., Lewis, C. A., Peck, B., Lord, S., Collins, J. M., . . . Harris, A. L. (2014). Fatty acid uptake and lipid storage induced by HIF-1α contribute to cell growth and survival after hypoxia-reoxygenation. *Cell Rep, 9*(1), 349-365. doi:10.1016/j.celrep.2014.08.056

Bensaad, K., & Vousden, K. H. (2007). p53: new roles in metabolism. *Trends Cell Biol, 17*(6), 286-291. doi:10.1016/j.tcb.2007.04.004

Berrisford, J. M., & Sazanov, L. A. (2009). Structural basis for the mechanism of respiratory complex I. *J Biol Chem, 284*(43), 29773-29783. doi:10.1074/jbc.M109.032144

Bhagya, C. H., Wijesundera Sulochana, W. S., & Hemamali, N. P. (2013). Polymerase chain reaction optimization for amplification of Guanine-Cytosine rich templates using buccal cell DNA. *Indian J Hum Genet, 19*(1), 78-83. doi:10.4103/0971-6866.112898

Bilban, M., Heintel, D., Scharl, T., Woelfel, T., Auer, M. M., Porpaczy, E., . . . Jager, U. (2006). Deregulated expression of fat and muscle genes in B-cell chronic lymphocytic leukemia with high lipoprotein lipase expression. *Leukemia, 20*(6), 1080-1088. doi:10.1038/sj.leu.2404220

Bilous, N., Abramenko, I., Chumak, A., Dyagil, I., & Martina, Z. (2019). Analysis of LPL gene expression in patients with chronic lymphocytic leukemia. *Exp Oncol, 41*(1), 39-45.

Binet, J. L., Leporrier, M., Dighiero, G., Charron, D., D'Athis, P., Vaugier, G., . . . Follezou, J. Y. (1977). A clinical staging system for chronic lymphocytic leukemia: prognostic significance. *Cancer, 40*(2), 855-864. doi:10.1002/1097-0142(197708)40:2<855::aid-cncr2820400239>3.0.co;2-1

Black, P. N., & DiRusso, C. C. (2007). Vectorial acylation: linking fatty acid transport and activation to metabolic trafficking. *Novartis Found Symp, 286*, 127-138; discussion 138-141, 162-123, 196-203. doi:10.1002/9780470985571.ch11

Bogacka, I., Ukropcova, B., McNeil, M., Gimble, J. M., & Smith, S. R. (2005). Structural and functional consequences of mitochondrial biogenesis in human adipocytes in vitro. *J Clin Endocrinol Metab, 90*(12), 6650-6656. doi:10.1210/jc.2005-1024

Bogacka, I., Xie, H., Bray, G. A., & Smith, S. R. (2005). Pioglitazone induces mitochondrial biogenesis in human subcutaneous adipose tissue in vivo. *Diabetes, 54*(5), 1392-1399. doi:10.2337/diabetes.54.5.1392

Brand, M. D. (2010). The sites and topology of mitochondrial superoxide production. *Exp Gerontol, 45*(7-8), 466-472. doi:10.1016/j.exger.2010.01.003

Brander, D., Allgood, S., Bond, K., Weinberg, J., & Lanasa, M. (2011). The Role of Surface Immunoglobulin Isotype in Chronic Lymphocytic Leukemia Disease Biology and Clinical Outcome. *Blood, 118*(21).

Bravard, A., Sabatier, L., Hoffschir, F., Ricoul, M., Luccioni, C., & Dutrillaux, B. (1992). SOD2: a new type of tumor-suppressor gene? *Int J Cancer, 51*(3), 476-480. doi:10.1002/ijc.2910510323

Brody, J. I., & Merlie, K. (1970). Metabolic and biosynthetic features of lymphocytes from patients with diabetes mellitus: similarities to lymphocytes in chronic lymphocytic leukaemia. *Br J Haematol, 19*(2), 193-201. doi:10.1111/j.1365-2141.1970.tb01616.x

Brody, J. I., Oski, F. A., & Singer, D. E. (1969). Impaired pentose phosphate shunt and decreased glycolytic activity in lymphocytes of chronic lymphocytic leukemia. Metabolic pathway. *Blood, 34*(4), 421-429.

Bruzzi, J. F., Macapinlac, H., Tsimberidou, A. M., Truong, M. T., Keating, M. J., Marom, E. M., & Munden, R. F. (2006). Detection of Richter's transformation of chronic lymphocytic leukemia by PET/CT. *J Nucl Med, 47*(8), 1267-1273.

Buckley, C. M., & King, J. S. (2017). Drinking problems: mechanisms of macropinosome formation and maturation. *Febs j, 284*(22), 3778-3790. doi:10.1111/febs.14115

Bulian, P., Shanafelt, T. D., Fegan, C., Zucchetto, A., Cro, L., Nückel, H., . . . Gattei, V. (2014). CD49d is the strongest flow cytometry-based predictor of overall survival in chronic lymphocytic leukemia. *J Clin Oncol, 32*(9), 897-904. doi:10.1200/jco.2013.50.8515

Bulian, P., Tarnani, M., Rossi, D., Forconi, F., Del Poeta, G., Bertoni, F., . . . Laurenti, L. (2011). Multicentre validation of a prognostic index for overall survival in chronic lymphocytic leukaemia. *Hematol Oncol, 29*(2), 91-99. doi:10.1002/hon.959

Burger, Tedeschi, A., Barr, P. M., Robak, T., Owen, C., Ghia, P., . . . Kipps, T. J. (2015). Ibrutinib as Initial Therapy for Patients with Chronic Lymphocytic Leukemia. *N Engl J Med, 373*(25), 2425-2437. doi:10.1056/NEJMoa1509388

Burger, J. (2012). Inhibiting B-cell receptor signaling pathways in chronic lymphocytic leukaemia. *Curr Haematol Malig Rep, 7*, 8.

Burger, J., & Chiorazzi, N. (2013). B-cell receptor signaling in chronic lymphocytic leukaemia. *Trends Immunol, 34*, 9.

Burgermeister, E., Liscovitch, M., Röcken, C., Schmid, R. M., & Ebert, M. P. (2008). Caveats of caveolin-1 in cancer progression. *Cancer Lett, 268*(2), 187-201. doi:10.1016/j.canlet.2008.03.055

Byrd, J. C., Brown, J. R., O'Brien, S., Barrientos, J. C., Kay, N. E., Reddy, N. M., . . . Hillmen, P. (2014). Ibrutinib versus ofatumumab in previously treated chronic lymphoid leukemia. *N Engl J Med, 371*(3), 213-223. doi:10.1056/NEJMoa1400376

Byrd, J. C., Rai, K., Peterson, B. L., Appelbaum, F. R., Morrison, V. A., Kolitz, J. E., . . . Larson, R. A. (2005). Addition of rituximab to fludarabine may prolong progression-free survival and overall survival in patients with previously untreated chronic lymphocytic leukemia: an updated retrospective comparative analysis of CALGB 9712 and CALGB 9011. *Blood, 105*(1), 49-53. doi:10.1182/blood-2004-03-0796

Caligaris-Cappio, F., Bertilaccio, M. T., & Scielzo, C. (2014). How the microenvironment wires the natural history of chronic lymphocytic leukemia. *Semin Cancer Biol, 24*, 43-48. doi:10.1016/j.semcancer.2013.06.010

Calin, G., Dumitru, C., Shimizu, M., Bichi, R., Zupo, S., Noch, E., . . . Croce, C. (2002). Frequent deletions and down-regulation of micro-RNA genes miR15 and miR16 at 13q14 in chronic lymphocytic leukaemia. *Proceedings of the National Academy of Sciences, 99*, 5.

Calissano, C., Damle, R. N., Marsilio, S., Yan, X. J., Yancopoulos, S., Hayes, G., . . . Chiorazzi, N. (2011). Intraclonal complexity in chronic lymphocytic leukemia: fractions enriched in recently born/divided and older/quiescent cells. *Mol Med, 17*(11-12), 1374-1382. doi:10.2119/molmed.2011.00360

Carter, A., Lin, K., Sherrington, P. D., Atherton, M., Pearson, K., Douglas, A., . . . Pettitt, A. R. (2006). Imperfect correlation between p53 dysfunction and deletion of TP53 and ATM in chronic lymphocytic leukaemia. *Leukemia, 20*(4), 737-740. doi:10.1038/sj.leu.2404120

Cecchini, G. (2003). Function and structure of complex II of the respiratory chain. *Annu Rev Biochem, 72*, 77-109. doi:10.1146/annurev.biochem.72.121801.161700

Cerbone, A., Toaldo, C., Laurora, S., Briatore, F., Pizzimenti, S., Dianzani, M. U., . . . Barrera, G. (2007). 4-Hydroxynonenal and PPARgamma ligands affect proliferation, differentiation, and apoptosis in colon cancer cells. *Free Radic Biol Med, 42*(11), 1661-1670. doi:10.1016/j.freeradbiomed.2007.02.009

Cesano, A., Perbellini, O., Evensen, E., Chu, C. C., Cioffi, F., Ptacek, J., . . . Scupoli, M. T. (2013). Association between B-cell receptor responsiveness and disease progression in B-cell chronic lymphocytic leukemia: results from single cell network profiling studies. *Haematologica, 98*(4), 626-634. doi:10.3324/haematol.2012.071910

Chajek, T., Stein, O., & Stein, Y. (1978). Lipoprotein lipase of cultured mesenchymal rat heart cells. II. Hydrolysis of labeled vary low density lipoprotein triacylglycerol by membrane-supported enzyme. *Biochim Biophys Acta, 528*(3), 466-474. doi:10.1016/0005-2760(78)90036-x

Chapman-Shimshoni, D., Yuklea, M., Radnay, J., Shapiro, H., & Lishner, M. (2003). Simvastatin induces apoptosis of B-CLL cells by activation of mitochondrial caspase 9. *Exp Hematol, 31*(9), 779-783. doi:10.1016/s0301-472x(03)00192-9

Chen, Azad, & Gibson. (2009). Superoxide is the major reactive oxygen species regulating autophagy. *Cell Death Differ, 16*(7), 1040-1052. doi:10.1038/cdd.2009.49

Chen, Y. H., Lin, W. W., Liu, C. S., Hsu, L. S., Lin, Y. M., & Su, S. L. (2014). Caveolin-1 provides palliation for adverse hepatic reactions in hypercholesterolemic rabbits. *PLoS One, 9*(1), e71862. doi:10.1371/journal.pone.0071862

Chiba, T., Takahashi, S., Sato, N., Ishii, S., & Kikuchi, K. (1996). Fas-mediated apoptosis is modulated by intracellular glutathione in human T cells. *Eur J Immunol, 26*(5), 1164-1169. doi:10.1002/eji.1830260530

Chowdhury, S., Bouchard, E. D. J., Saleh, R., Nugent, Z., Peltier, C., Mejia, E., . . . Banerji, V. (2020). Mitochondrial Respiration Correlates with Prognostic Markers in Chronic Lymphocytic Leukemia and Is Normalized by Ibrutinib Treatment. *Cancers (Basel), 12*(3). doi:10.3390/cancers12030650

Chu, D. H., Morita, C. T., & Weiss, A. (1998). The Syk family of protein tyrosine kinases in T-cell activation and development. *Immunol Rev, 165*, 167-180. doi:10.1111/j.1600-065x.1998.tb01238.x

Chuang, J. Y., Wang, Y. T., Yeh, S. H., Liu, Y. W., Chang, W. C., & Hung, J. J. (2008). Phosphorylation by c-Jun NH2-terminal kinase 1 regulates the stability of transcription factor Sp1 during mitosis. *Mol Biol Cell, 19*(3), 1139-1151. doi:10.1091/mbc.e07-09-0881

Clarke, D. C., Miskovic, D., Han, X. X., Calles-Escandon, J., Glatz, J. F., Luiken, J. J., . . . Bonen, A. (2004). Overexpression of membrane-associated fatty acid binding protein (FABPpm) in vivo increases fatty acid sarcolemmal transport and metabolism. *Physiol Genomics, 17*(1), 31-37. doi:10.1152/physiolgenomics.00190.2003

Clear, A., D'Avola, A., Agrawal, S., Rassenti, L., Kipps, T., Gribben, J., & Riches, J. (2018). B-Cell Receptor Signaling Drives Glycolysis in Chronic Lymphocytic Leukemia Cells. *Blood, 132*(Supplement 1).

Clifford, R., & Schuh, A. (2012). State-of-the-Art Management of Patients Suffering from Chronic Lymphocytic Leukemia. *Clin Med Insights Oncol, 6*, 165-178. doi:10.4137/cmo.s6201

ClinicalTrials.gov. (2018). Identifier NCT02980029, TVB 2640 for Resectable Colon Cancer Other Resectable Cancers ; a Window Trial. Retrieved from https://clinicaltrials.gov/ct2/show/NCT02980029

Cockfield, J. A., & Schafer, Z. T. (2019). Antioxidant Defenses: A Context-Specific Vulnerability of Cancer Cells. *Cancers (Basel), 11*(8). doi:10.3390/cancers11081208

Cohen, J., Thurgood, L., Lower, K., & Kuss, B. (2019). *Identification of the frequency and characteristics of bulky versus non-bulky lymphomatous disease in chronic lymphocytic leukaemia (CLL)*. Paper presented at the iwCLL, Edinburgh, Scotland.

Collado, R., Ivars, D., Oliver, I., Tormos, C., Egea, M., Miguel, A., . . . Carbonell, F. (2014). Increased oxidative damage associated with unfavorable cytogenetic subgroups in chronic lymphocytic leukemia. *Biomed Res Int, 2014*, 686392. doi:10.1155/2014/686392

Cossarizza, A., Franceschi, C., Monti, D., Salvioli, S., Bellesia, E., Rivabene, R., . . . Malorni, W. (1995). Protective effect of N-acetylcysteine in tumor necrosis factor-alpha-induced apoptosis in U937 cells: the role of mitochondria. *Exp Cell Res, 220*(1), 232-240. doi:10.1006/excr.1995.1311

Coyle, J. T., & Puttfarcken, P. (1993). Oxidative stress, glutamate, and neurodegenerative disorders. *Science, 262*(5134), 689-695. doi:10.1126/science.7901908

Cragg, M. S., Walshe, C. A., Ivanov, A. O., & Glennie, M. J. (2005). The biology of CD20 and its potential as a target for mAb therapy. *Curr Dir Autoimmun, 8*, 140-174. doi:10.1159/000082102

Crespo, M., Villamor, N., Giné, E., Muntañola, A., Colomer, D., Marafioti, T., . . . Bosch, F. (2006). ZAP-70 expression in normal pro/pre B cells, mature B cells, and in B-cell acute lymphoblastic leukaemia. *Clinical Cancer Research, 12*(3 Pt 1), 8.

Cullis, P. R., & de Kruijff, B. (1979). Lipid polymorphism and the functional roles of lipids in biological membranes. *Biochim Biophys Acta, 559*(4), 399-420. doi:10.1016/0304-4157(79)90012-1

Cuneo, A., Barosi, G., Danesi, R., Fagiuoli, S., Ghia, P., Marzano, A., . . . Zinzani, P. L. (2019). Management of adverse events associated with idelalisib treatment in chronic lymphocytic leukemia and follicular lymphoma: A multidisciplinary position paper. *Hematol Oncol, 37*(1), 3-14. doi:10.1002/hon.2540

Czeczot, H., Skrzycki, M., Podsiad, M., Gawryszewska, E., Nyckowski, P., & Porembska, Z. (2005). [Antioxidant status of patients with primary colorectal cancer and liver metastases of colorectal cancer]. *Pol Merkur Lekarski, 18*(103), 58-61.

Damle, R. N., Wasil, T., Fais, F., Ghiotto, F., Valetto, A., Allen, S. L., . . . Chiorazzi, N. (1999). Ig V gene mutation status and CD38 expression as novel prognostic indicators in chronic lymphocytic leukemia. *Blood, 94*(6), 1840-1847.

Darst, R. P., Pardo, C. E., Ai, L., Brown, K. D., & Kladde, M. P. (2010). Bisulfite sequencing of DNA. *Curr Protoc Mol Biol, Chapter 7*, Unit 7.9.1-17. doi:10.1002/0471142727.mb0709s91

Davids, M. S., & Burger, J. A. (2012). Cell Trafficking in Chronic Lymphocytic Leukemia. *Open J Hematol, 3*(S1). doi:10.13055/ojhmt_3_s1_03.120221

Davids, M. S., Deng, J., Wiestner, A., Lannutti, B. J., Wang, L., Wu, C. J., . . . Letai, A. (2012). Decreased mitochondrial apoptotic priming underlies stroma-mediated treatment resistance in chronic lymphocytic leukemia. *Blood, 120*(17), 3501-3509. doi:10.1182/blood-2012-02-414060

Davies, K. J. (1986). Intracellular proteolytic systems may function as secondary antioxidant defenses: an hypothesis. *J Free Radic Biol Med, 2*(3), 155-173.

Dearden, C. (2008). Disease-specific complications of chronic lymphocytic leukemia. *Hematology Am Soc Hematol Educ Program*, 450-456. doi:10.1182/asheducation-2008.1.450

Deep, G., & Schlaepfer, I. R. (2016). Aberrant Lipid Metabolism Promotes Prostate Cancer: Role in Cell Survival under Hypoxia and Extracellular Vesicles Biogenesis. *Int J Mol Sci, 17*(7). doi:10.3390/ijms17071061

DeFilippis, R. A., Chang, H., Dumont, N., Rabban, J. T., Chen, Y. Y., Fontenay, G. V., . . . Tlsty, T. D. (2012). CD36 repression activates a multicellular stromal program shared by high mammographic density and tumor tissues. *Cancer Discov, 2*(9), 826-839. doi:10.1158/2159-8290.cd-12-0107

Del Poeta, G., Dal Bo, M., Del Principe, M. I., Pozzo, F., Rossi, F. M., Zucchetto, A., . . . Gattei, V. (2013). Clinical significance of c.7544-7545 delCT NOTCH1 mutation in chronic lymphocytic leukaemia. *Br J Haematol, 160*(3), 415-418. doi:10.1111/bjh.12128

Del Principe, M. I., Dal Bo, M., Bittolo, T., Buccisano, F., Rossi, F. M., Zucchetto, A., . . . Del Poeta, G. (2016). Clinical significance of bax/bcl-2 ratio in chronic lymphocytic leukemia. *Haematologica, 101*(1), 77-85. doi:10.3324/haematol.2015.131854

Delneste, Y., Jeannin, P., Sebille, E., Aubry, J. P., & Bonnefoy, J. Y. (1996). Thiols prevent Fas (CD95)-mediated T cell apoptosis by down-regulating membrane Fas expression. *Eur J Immunol, 26*(12), 2981-2988. doi:10.1002/eji.1830261225

Demidem, A., Lam, T., Alas, S., Hariharan, K., Hanna, N., & Bonavida, B. (1997). Chimeric anti-CD20 (IDEC-C2B8) monoclonal antibody sensitizes a B cell lymphoma cell line to cell killing by cytotoxic drugs. *Cancer Biother Radiopharm, 12*(3), 177-186. doi:10.1089/cbr.1997.12.177

Deng, F., Fang, Y., Shen, Z., Gong, W., Liu, T., Wen, J., . . . Nie, B. (2017). Use of confocal laser endomicroscopy with a fluorescently labeled fatty acid to diagnose colorectal neoplasms. *Oncotarget, 8*(35), 58934-58947. doi:10.18632/oncotarget.19515

Desvergne, B., & Wahli, W. (1999). Peroxisome proliferator-activated receptors: nuclear control of metabolism. *Endocr Rev, 20*(5), 649-688. doi:10.1210/edrv.20.5.0380

Dhar, S. K., Tangpong, J., Chaiswing, L., Oberley, T. D., & St Clair, D. K. (2011). Manganese superoxide dismutase is a p53-regulated gene that switches cancers between early and advanced stages. *Cancer Res, 71*(21), 6684-6695. doi:10.1158/0008-5472.Can-11-1233

DiRusso, C. C., Li, H., Darwis, D., Watkins, P. A., Berger, J., & Black, P. N. (2005). Comparative biochemical studies of the murine fatty acid transport proteins (FATP) expressed in yeast. *J Biol Chem, 280*(17), 16829-16837. doi:10.1074/jbc.M409598200

Doege, H., Baillie, R. A., Ortegon, A. M., Tsang, B., Wu, Q., Punreddy, S., . . . Stahl, A. (2006). Targeted deletion of FATP5 reveals multiple functions in liver metabolism: alterations in hepatic lipid homeostasis. *Gastroenterology, 130*(4), 1245-1258. doi:10.1053/j.gastro.2006.02.006

Dohner, H., Stilgenbauer, S., Benner, A., Leupolt, E., Krober, A., Bullinger, L., . . . Lichter, P. (2000). Genomic aberrations and survival in chronic lymphocytic leukemia. *N Engl J Med, 343*(26), 1910-1916. doi:10.1056/nejm200012283432602

Droge, W. (2002). Aging-related changes in the thiol/disulfide redox state: implications for the use of thiol antioxidants. *Exp Gerontol, 37*(12), 1333-1345.

Dubovsky, J. A., Beckwith, K. A., Natarajan, G., Woyach, J. A., Jaglowski, S., Zhong, Y., . . . Byrd, J. C. (2013). Ibrutinib is an irreversible molecular inhibitor of ITK driving a Th1-selective pressure in T lymphocytes. *Blood, 122*(15), 2539-2549. doi:10.1182/blood-2013-06-507947

Duhren-von Minden, M., Ubelhart, R., Schneider, D., Wossning, T., Bach, M. P., Buchner, M., . . . Jumaa, H. (2012). Chronic lymphocytic leukaemia is driven by antigen-independent cell-autonomous signalling. *Nature, 489*(7415), 309-312. doi:10.1038/nature11309

Efremov, D. G., Wiestner, A., & Laurenti, L. (2012). Novel Agents and Emerging Strategies for Targeting the B-Cell Receptor Pathway in CLL. *Mediterr J Hematol Infect Dis, 4*(1), e2012067. doi:10.4084/mjhid.2012.067

Engelberts, P. J., Voorhorst, M., Schuurman, J., van Meerten, T., Bakker, J. M., Vink, T., . . . Beurskens, F. J. (2016). Type I CD20 Antibodies Recruit the B Cell Receptor for Complement-Dependent Lysis of Malignant B Cells. *J Immunol, 197*(12), 4829-4837. doi:10.4049/jimmunol.1600811

Eyre, N. S., Cleland, L. G., & Mayrhofer, G. (2008). FAT/CD36 expression alone is insufficient to enhance cellular uptake of oleate. *Biochem Biophys Res Commun, 370*(3), 404-409. doi:10.1016/j.bbrc.2008.02.164

Falchi, L., Keating, M. J., Marom, E. M., Truong, M. T., Schlette, E. J., Sargent, R. L., . . . Ferrajoli, A. (2014). Correlation between FDG/PET, histology, characteristics, and survival in 332 patients with chronic lymphoid leukemia. *Blood, 123*(18), 2783-2790. doi:10.1182/blood-2013-11-536169

Fedyk, E. R., & Phipps, R. P. (1994). Reactive oxygen species and not lipoxygenase products are required for mouse B-lymphocyte activation and differentiation. *Int J Immunopharmacol, 16*(7), 533-546. doi:10.1016/0192-0561(94)90105-8

Felts, J. M., Itakura, H., & Crane, R. T. (1975). The mechanism of assimilation of constituents of chylomicrons, very low density lipoproteins and remnants - a new theory. *Biochem Biophys Res Commun, 66*(4), 1467-1475. doi:10.1016/0006-291x(75)90524-0

Fernandez-Rachubinski, F., Eng, B., Murray, W. W., Blajchman, M. A., & Rachubinski, R. A. (1990). Incorporation of 7-deaza dGTP during the amplification step in the polymerase chain reaction

procedure improves subsequent DNA sequencing. *DNA Seq, 1*(2), 137-140. doi:10.3109/10425179009016041

Finkel, T., & Holbrook, N. J. (2000). Oxidants, oxidative stress and the biology of ageing. *Nature, 408*(6809), 239-247. doi:10.1038/35041687

Francis, S., Karanth, M., Pratt, G., Starczynski, J., Hooper, L., Fegan, C., . . . Delgado, J. (2006). The effect of immunoglobulin VH gene mutation status and other prognostic factors on the incidence of major infections in patients with chronic lymphocytic leukemia. *Cancer, 107*(5), 1023-1033. doi:10.1002/cncr.22094

Fridolfsson, H. N., Kawaraguchi, Y., Ali, S. S., Panneerselvam, M., Niesman, I. R., Finley, J. C., . . . Patel, H. H. (2012). Mitochondria-localized caveolin in adaptation to cellular stress and injury. *Faseb j, 26*(11), 4637-4649. doi:10.1096/fj.12-215798

Friedman, D., Guadeloupe, E., Volkheimer, A., & Weinberg, J. (2016). Surface CD5 Protein Risk Stratifies Chronic Lymphocytic Leukaemia. *Blood, 128*(22), 3212.

Fujiwara, R., Takenaka, S., Hashimoto, M., Narawa, T., & Itoh, T. (2014). Expression of human solute carrier family transporters in skin: possible contributor to drug-induced skin disorders. *Sci Rep, 4*, 5251. doi:10.1038/srep05251

Funaro, A., & Malavasi, F. (1999). Human CD38, a surface receptor, an enzyme, an adhesion molecule and not a simple marker. *J Biol Regul Homeost Agents, 13*(1), 54-61.

Furman, R. R., Sharman, J. P., Coutre, S. E., Cheson, B. D., Pagel, J. M., Hillmen, P., . . . O'Brien, S. M. (2014). Idelalisib and rituximab in relapsed chronic lymphocytic leukemia. *N Engl J Med, 370*(11), 997-1007. doi:10.1056/NEJMoa1315226

Gao, Y. H., Li, C. X., Shen, S. M., Li, H., Chen, G. Q., Wei, Q., & Wang, L. S. (2013). Hypoxia-inducible factor 1α mediates the down-regulation of superoxide dismutase 2 in von Hippel-Lindau deficient renal clear cell carcinoma. *Biochem Biophys Res Commun, 435*(1), 46-51. doi:10.1016/j.bbrc.2013.04.034

Gentile, M., Cutrona, G., Neri, A., Molica, S., Ferrarini, M., & Morabito, F. (2009). Predictive value of beta2-microglobulin (beta2-m) levels in chronic lymphocytic leukemia since Binet A stages. *Haematologica, 94*(6), 887-888. doi:10.3324/haematol.2009.005561

Giertlova, M., Hajikova, M., Vaskova, J., Kafkova, A., Stecova, N., Mirossay, L., . . . Sarissky, M. (2011). Cytogenetic abnormalities predict treatment-free interval and response to therapy in previously untreated chronic lymphocytic leukemia patients. *Neoplasma, 58*(1), 82-88. doi:10.4149/neo_2011_01_82

Gimeno, R. E., Ortegon, A. M., Patel, S., Punreddy, S., Ge, P., Sun, Y., . . . Stahl, A. (2003). Characterization of a heart-specific fatty acid transport protein. *J Biol Chem, 278*(18), 16039-16044. doi:10.1074/jbc.M211412200

Giordano, S., Lee, J., Darley-Usmar, V. M., & Zhang, J. (2012). Distinct effects of rotenone, 1-methyl-4-phenylpyridinium and 6-hydroxydopamine on cellular bioenergetics and cell death. *PLoS One, 7*(9), e44610. doi:10.1371/journal.pone.0044610

Glatz, J. F., Luiken, J. J., & Bonen, A. (2010). Membrane fatty acid transporters as regulators of lipid metabolism: implications for metabolic disease. *Physiol Rev, 90*(1), 367-417. doi:10.1152/physrev.00003.2009

Glennie, M. J., French, R. R., Cragg, M. S., & Taylor, R. P. (2007). Mechanisms of killing by anti-CD20 monoclonal antibodies. *Mol Immunol, 44*(16), 3823-3837. doi:10.1016/j.molimm.2007.06.151

Goede, V., Klein, C., & Stilgenbauer, S. (2015). Obinutuzumab (GA101) for the treatment of chronic lymphocytic leukemia and other B-cell non-hodgkin's lymphomas: a glycoengineered type II CD20 antibody. *Oncol Res Treat, 38*(4), 185-192. doi:10.1159/000381524

Golay, J., Zaffaroni, L., Vaccari, T., Lazzari, M., Borleri, G. M., Bernasconi, S., . . . Introna, M. (2000). Biologic response of B lymphoma cells to anti-CD20 monoclonal antibody rituximab in vitro: CD55 and CD59 regulate complement-mediated cell lysis. *Blood, 95*(12), 3900-3908.

Green, D. R., & Kroemer, G. (2009). Cytoplasmic functions of the tumour suppressor p53. *Nature, 458*(7242), 1127-1130. doi:10.1038/nature07986

Green, D. R., & Reed, J. C. (1998). Mitochondria and apoptosis. *Science, 281*(5381), 1309-1312. doi:10.1126/science.281.5381.1309

Grosicki, S. (2015). Ofatumumab for the treatment of chronic lymphocytic leukemia. *Expert Rev Hematol, 8*(3), 265-272. doi:10.1586/17474086.2015.1037736

Guo, Boekhoudt, G. H., & Boss, J. M. (2003). Role of the intronic enhancer in tumor necrosis factor-mediated induction of manganous superoxide dismutase. *J Biol Chem, 278*(26), 23570-23578. doi:10.1074/jbc.M303431200

Guo, A., Lu, P., Lee, J., Zhen, C., Chiosis, G., & Wang, Y. L. (2017). HSP90 stabilizes B-cell receptor kinases in a multi-client interactome: PU-H71 induces CLL apoptosis in a cytoprotective microenvironment. *Oncogene, 36*(24), 3441-3449. doi:10.1038/onc.2016.494

Guo, Z., Kozlov, S., Lavin, M. F., Person, M. D., & Paull, T. T. (2010). ATM activation by oxidative stress. *Science, 330*(6003), 517-521. doi:10.1126/science.1192912

Gutierrez, A., Jr., Tschumper, R. C., Wu, X., Shanafelt, T. D., Eckel-Passow, J., Huddleston, P. M., 3rd, . . . Jelinek, D. F. (2010). LEF-1 is a prosurvival factor in chronic lymphocytic leukemia and is expressed in the preleukemic state of monoclonal B-cell lymphocytosis. *Blood, 116*(16), 2975-2983. doi:10.1182/blood-2010-02-269878

Gutjahr, J. C., Greil, R., & Hartmann, T. N. (2015). The Role of CD44 in the Pathophysiology of Chronic Lymphocytic Leukemia. *Front Immunol, 6*, 177. doi:10.3389/fimmu.2015.00177

Guzy, R. D., Hoyos, B., Robin, E., Chen, H., Liu, L., Mansfield, K. D., . . . Schumacker, P. T. (2005). Mitochondrial complex III is required for hypoxia-induced ROS production and cellular oxygen sensing. *Cell Metab, 1*(6), 401-408. doi:10.1016/j.cmet.2005.05.001

Ha, & Lee. (2005). Reactive oxygen species amplify glucose signalling in renal cells cultured under high glucose and in diabetic kidney. *Nephrology (Carlton), 10 Suppl*, S7-10. doi:10.1111/j.1440-1797.2005.00448.x

Ha, T. K., Her, N. G., Lee, M. G., Ryu, B. K., Lee, J. H., Han, J., . . . Chi, S. G. (2012). Caveolin-1 increases aerobic glycolysis in colorectal cancers by stimulating HMGA1-mediated GLUT3 transcription. *Cancer Res, 72*(16), 4097-4109. doi:10.1158/0008-5472.Can-12-0448

Hahn, A., Parey, K., Bublitz, M., Mills, D. J., Zickermann, V., Vonck, J., . . . Meier, T. (2016). Structure of a Complete ATP Synthase Dimer Reveals the Molecular Basis of Inner Mitochondrial Membrane Morphology. *Mol Cell, 63*(3), 445-456. doi:10.1016/j.molcel.2016.05.037

Hallek, M., Cheson, B. D., Catovsky, D., Caligaris-Cappio, F., Dighiero, G., Dohner, H., . . . Kipps, T. J. (2018). iwCLL guidelines for diagnosis, indications for treatment, response assessment, and supportive management of CLL. *Blood, 131*(25), 2745-2760. doi:10.1182/blood-2017-09-806398

Hallek, M., Cheson, B. D., Catovsky, D., Caligaris-Cappio, F., Dighiero, G., Döhner, H., . . . Kipps, T. J. (2018). iwCLL guidelines for diagnosis, indications for treatment, response assessment, and supportive management of CLL. *Blood, 131*(25), 2745-2760. doi:10.1182/blood-2017-09-806398

Hallek, M., Fischer, K., Fingerle-Rowson, G., Fink, A. M., Busch, R., Mayer, J., . . . Stilgenbauer, S. (2010). Addition of rituximab to fludarabine and cyclophosphamide in patients with chronic lymphocytic leukaemia: a randomised, open-label, phase 3 trial. *Lancet, 376*(9747), 1164-1174. doi:10.1016/s0140-6736(10)61381-5

Hallek, M., Langenmayer, I., Nerl, C., Knauf, W., Dietzfelbinger, H., Adorf, D., . . . Emmerich, B. (1999). Elevated serum thymidine kinase levels identify a subgroup at high risk of disease progression in early, nonsmoldering chronic lymphocytic leukemia. *Blood, 93*(5), 1732-1737.

Hallek, M., Wanders, L., Ostwald, M., Busch, R., Senekowitsch, R., Stern, S., . . . Emmerich, B. (1996). Serum beta(2)-microglobulin and serum thymidine kinase are independent predictors of progression-free survival in chronic lymphocytic leukemia and immunocytoma. *Leuk Lymphoma, 22*(5-6), 439-447. doi:10.3109/10428199609054782

Hamanaka, R. B., & Chandel, N. S. (2010). Mitochondrial reactive oxygen species regulate cellular signaling and dictate biological outcomes. *Trends Biochem Sci, 35*(9), 505-513. doi:10.1016/j.tibs.2010.04.002

Hamblin, T. J., Davis, Z., Gardiner, A., Oscier, D. G., & Stevenson, F. K. (1999). Unmutated Ig V(H) genes are associated with a more aggressive form of chronic lymphocytic leukemia. *Blood, 94*(6), 1848-1854.

Han, T. T., Fan, L., Li, J. Y., & Xu, W. (2014). Role of chemokines and their receptors in chronic lymphocytic leukemia: function in microenvironment and targeted therapy. *Cancer Biol Ther, 15*(1), 3-9. doi:10.4161/cbt.26607

Hanahan, D., & Weinberg, R. A. (2011). Hallmarks of cancer: the next generation. *Cell, 144*(5), 646-674. doi:10.1016/j.cell.2011.02.013

Hara, A., Yoshimi, N., Niwa, M., Ino, N., & Mori, H. (1997). Apoptosis induced by NS-398, a selective cyclooxygenase-2 inhibitor, in human colorectal cancer cell lines. *Jpn J Cancer Res, 88*(6), 600-604. doi:10.1111/j.1349-7006.1997.tb00424.x

Harper, J. W., & Elledge, S. J. (2007). The DNA damage response: ten years after. *Mol Cell, 28*(5), 739-745. doi:10.1016/j.molcel.2007.11.015

Harrison, R. (2002). Structure and function of xanthine oxidoreductase: where are we now? *Free Radic Biol Med, 33*(6), 774-797.

Hayashida, K., Shimaoka, Y., Ochi, T., & Lipsky, P. E. (2000). Rheumatoid arthritis synovial stromal cells inhibit apoptosis and up-regulate Bcl-xL expression by B cells in a CD49/CD29-CD106-dependent mechanism. *J Immunol, 164*(2), 1110-1116. doi:10.4049/jimmunol.164.2.1110

Hazan-Halevy, I., Harris, D., Liu, Z., Liu, J., Li, P., Chen, X., . . . Estrov, Z. (2010). STAT3 is constitutively phosphorylated on serine 727 residues, binds DNA, and activates transcription in CLL cells. *Blood, 115*(14), 2852-2863. doi:10.1182/blood-2009-10-230060

He, Q., Skog, S., Wang, N., Eriksson, S., & Tribukait, B. (1996). Characterization of a peptide antibody against a C-terminal part of human and mouse cytosolic thymidine kinase, which is a marker for cell proliferation. *Eur J Cell Biol, 70*(2), 117-124.

Heffner, J. E., & Repine, J. E. (1989). Pulmonary strategies of antioxidant defense. *Am Rev Respir Dis, 140*(2), 531-554. doi:10.1164/ajrccm/140.2.531

Heintel, D., Kienle, D., Shehata, M., Krober, A., Kroemer, E., Schwarzinger, I., . . . Jager, U. (2005). High expression of lipoprotein lipase in poor risk B-cell chronic lymphocytic leukemia. *Leukemia, 19*(7), 1216-1223. doi:10.1038/sj.leu.2403748

Hempel, N., Carrico, P. M., & Melendez, J. A. (2011). Manganese superoxide dismutase (Sod2) and redox-control of signaling events that drive metastasis. *Anticancer Agents Med Chem, 11*(2), 191-201. doi:10.2174/187152011795255911

Hempel, N., Ye, H., Abessi, B., Mian, B., & Melendez, J. A. (2009). Altered redox status accompanies progression to metastatic human bladder cancer. *Free Radic Biol Med, 46*(1), 42-50. doi:10.1016/j.freeradbiomed.2008.09.020

Herishanu, Y., Pérez-Galán, P., Liu, D., Biancotto, A., Pittaluga, S., Vire, B., . . . Wiestner, A. (2011). The lymph node microenvironment promotes B-cell receptor signaling, NF-kappaB activation, and tumor proliferation in chronic lymphocytic leukemia. *Blood, 117*(2), 563-574. doi:10.1182/blood-2010-05-284984

Hernandez, J. M., Floyd, D. H., Weilbaecher, K. N., Green, P. L., & Boris-Lawrie, K. (2008). Multiple facets of junD gene expression are atypical among AP-1 family members. *Oncogene, 27*(35), 4757-4767. doi:10.1038/onc.2008.120

Herreros, B., Rodríguez-Pinilla, S. M., Pajares, R., Martínez-Gónzalez, M. A., Ramos, R., Munoz, I., . . . Piris, M. A. (2010). Proliferation centers in chronic lymphocytic leukemia: the niche where NF-kappaB activation takes place. *Leukemia, 24*(4), 872-876. doi:10.1038/leu.2009.285

Hirsch, D., Stahl, A., & Lodish, H. F. (1998). A family of fatty acid transporters conserved from mycobacterium to man. *Proc Natl Acad Sci U S A, 95*(15), 8625-8629. doi:10.1073/pnas.95.15.8625

Hirst, J., King, M. S., & Pryde, K. R. (2008). The production of reactive oxygen species by complex I. *Biochem Soc Trans, 36*(Pt 5), 976-980. doi:10.1042/bst0360976

Hodge, D. R., Peng, B., Pompeia, C., Thomas, S., Cho, E., Clausen, P. A., . . . Farrar, W. L. (2005). Epigenetic silencing of manganese superoxide dismutase (SOD-2) in KAS 6/1 human multiple myeloma cells increases cell proliferation. *Cancer Biol Ther, 4*(5), 585-592.

Hoellenriegel, J., Meadows, S. A., Sivina, M., Wierda, W. G., Kantarjian, H., Keating, M. J., . . . Burger. (2011). The phosphoinositide 3'-kinase delta inhibitor, CAL-101, inhibits B-cell receptor signaling and chemokine networks in chronic lymphocytic leukemia. *Blood, 118*(13), 3603-3612. doi:10.1182/blood-2011-05-352492

Holloway, G. P., Lally, J., Nickerson, J. G., Alkhateeb, H., Snook, L. A., Heigenhauser, G. J., . . . Bonen, A. (2007). Fatty acid binding protein facilitates sarcolemmal fatty acid transport but not mitochondrial oxidation in rat and human skeletal muscle. *J Physiol, 582*(Pt 1), 393-405. doi:10.1113/jphysiol.2007.135301

Honeychurch, J., Alduaij, W., Azizyan, M., Cheadle, E. J., Pelicano, H., Ivanov, A., . . . Illidge, T. M. (2012). Antibody-induced nonapoptotic cell death in human lymphoma and leukemia cells is mediated through a novel reactive oxygen species-dependent pathway. *Blood, 119*(15), 3523-3533. doi:10.1182/blood-2011-12-395541

Honigberg, L. A., Smith, A. M., Sirisawad, M., Verner, E., Loury, D., Chang, B., . . . Buggy, J. J. (2010). The Bruton tyrosine kinase inhibitor PCI-32765 blocks B-cell activation and is efficacious in models of autoimmune disease and B-cell malignancy. *Proc Natl Acad Sci U S A, 107*(29), 13075-13080. doi:10.1073/pnas.1004594107

Howard, M., Grimaldi, J. C., Bazan, J. F., Lund, F. E., Santos-Argumedo, L., Parkhouse, R. M., . . . Lee, H. C. (1993). Formation and hydrolysis of cyclic ADP-ribose catalyzed by lymphocyte antigen CD38. *Science, 262*(5136), 1056-1059. doi:10.1126/science.8235624

Huang, Y., He, T., & Domann, F. E. (1999). Decreased expression of manganese superoxide dismutase in transformed cells is associated with increased cytosine methylation of the SOD2 gene. *DNA Cell Biol, 18*(8), 643-652. doi:10.1089/104454999315051

Huang, Y., Peng, J., Oberley, L. W., & Domann, F. E. (1997). Transcriptional inhibition of manganese superoxide dismutase (SOD2) gene expression by DNA methylation of the 5' CpG island. *Free Radic Biol Med, 23*(2), 314-320.

Hug, H., Strand, S., Grambihler, A., Galle, J., Hack, V., Stremmel, W., . . . Galle, P. R. (1997). Reactive oxygen intermediates are involved in the induction of CD95 ligand mRNA expression by cytostatic drugs in hepatoma cells. *J Biol Chem, 272*(45), 28191-28193. doi:10.1074/jbc.272.45.28191

Huhn, D., von Schilling, C., Wilhelm, M., Ho, A. D., Hallek, M., Kuse, R., . . . Emmerich, B. (2001). Rituximab therapy of patients with B-cell chronic lymphocytic leukemia. *Blood, 98*(5), 1326-1331. doi:10.1182/blood.v98.5.1326

Hulkkonen, J., Vilpo, J., Vilpo, L., Koski, T., & Hurme, M. (2000). Interleukin-1 beta, interleukin-1 receptor antagonist and interleukin-6 plasma levels and cytokine gene polymorphisms in chronic lymphocytic leukemia: correlation with prognostic parameters. *Haematologica, 85*(6), 600-606.

Hunte, C., Zickermann, V., & Brandt, U. (2010). Functional modules and structural basis of conformational coupling in mitochondrial complex I. *Science, 329*(5990), 448-451. doi:10.1126/science.1191046

Hurt, E. M., Thomas, S. B., Peng, B., & Farrar, W. L. (2007a). Integrated molecular profiling of SOD2 expression in multiple myeloma. *Blood, 109*(9), 3953-3962. doi:10.1182/blood-2006-07-035162

Hurt, E. M., Thomas, S. B., Peng, B., & Farrar, W. L. (2007b). Molecular consequences of SOD2 expression in epigenetically silenced pancreatic carcinoma cell lines. *Br J Cancer, 97*(8), 1116-1123. doi:10.1038/sj.bjc.6604000

Inoue, S., Snowden, R. T., Dyer, M. J., & Cohen, G. M. (2004). CDDO induces apoptosis via the intrinsic pathway in lymphoid cells. *Leukemia, 18*(5), 948-952. doi:10.1038/sj.leu.2403328

Institute, N. C. (2013). Obinutuzumab. Retrieved from https://www.cancer.gov/about-cancer/treatment/drugs/obinutuzumab

Iverson, T. M. (2013). Catalytic mechanisms of complex II enzymes: a structural perspective. *Biochim Biophys Acta, 1827*(5), 648-657. doi:10.1016/j.bbabio.2012.09.008

Jain, N., Keating, M., Thompson, P., Ferrajoli, A., Burger, Borthakur, G., . . . Wierda, W. (2019). Ibrutinib and Venetoclax for First-Line Treatment of CLL. *N Engl J Med, 380*(22), 2095-2103. doi:10.1056/NEJMoa1900574

Jak, M., van Bochove, G. G., van Lier, R. A., Eldering, E., & van Oers, M. H. (2011). CD40 stimulation sensitizes CLL cells to rituximab-induced cell death. *Leukemia, 25*(6), 968-978. doi:10.1038/leu.2011.39

Jensen, M. A., Fukushima, M., & Davis, R. W. (2010). DMSO and betaine greatly improve amplification of GC-rich constructs in de novo synthesis. *PLoS One, 5*(6), e11024. doi:10.1371/journal.pone.0011024

Ji, G., Lv, K., Chen, H., Wang, T., Wang, Y., Zhao, D., . . . Li, Y. (2013). MiR-146a regulates SOD2 expression in H2O2 stimulated PC12 cells. *PLoS One, 8*(7), e69351. doi:10.1371/journal.pone.0069351

Jitschin, R., Hofmann, A. D., Bruns, H., Giessl, A., Bricks, J., Berger, J., . . . Mougiakakos, D. (2014). Mitochondrial metabolism contributes to oxidative stress and reveals therapeutic targets in chronic lymphocytic leukemia. *Blood, 123*(17), 2663-2672. doi:10.1182/blood-2013-10-532200

Joshi, A. D., Dickinson, J. D., Hegde, G. V., Sanger, W. G., Armitage, J. O., Bierman, P. J., . . . Joshi, S. S. (2007). Bulky lymphadenopathy with poor clinical outcome is associated with ATM downregulation in B-cell chronic lymphocytic leukemia patients irrespective of 11q23 deletion. *Cancer Genet Cytogenet, 172*(2), 120-126. doi:10.1016/j.cancergencyto.2006.07.010

Kadenbach, B., & Huttemann, M. (2015). The subunit composition and function of mammalian cytochrome c oxidase. *Mitochondrion, 24*, 64-76. doi:10.1016/j.mito.2015.07.002

Karam, Novak, L., Cyriac, J., Ali, A., Nazeer, T., & Nugent, F. (2006). Role of fluorine-18 fluoro-deoxyglucose positron emission tomography scan in the evaluation and follow-up of patients with low-grade lymphomas. *Cancer, 107*(1), 175-183. doi:10.1002/cncr.21967

Karam, R., Carvalho, J., Bruno, I., Graziadio, C., Senz, J., Huntsman, D., . . . Oliveira, C. (2008). The NMD mRNA surveillance pathway downregulates aberrant E-cadherin transcripts in gastric cancer cells and in CDH1 mutation carriers. *Oncogene, 27*(30), 4255-4260. doi:10.1038/onc.2008.62

Kassan, A., Herms, A., Fernández-Vidal, A., Bosch, M., Schieber, N. L., Reddy, B. J., . . . Pol, A. (2013). Acyl-CoA synthetase 3 promotes lipid droplet biogenesis in ER microdomains. *J Cell Biol, 203*(6), 985-1001. doi:10.1083/jcb.201305142

Ke, H., Bao, T., & Chen, W. (2019). Polysaccharide from Rubus chingii Hu affords protection against palmitic acid-induced lipotoxicity in human hepatocytes. *Int J Biol Macromol, 133*, 1063-1071. doi:10.1016/j.ijbiomac.2019.04.176

Kersten, S. (2014). Integrated physiology and systems biology of PPARalpha. *Mol Metab, 3*(4), 354-371. doi:10.1016/j.molmet.2014.02.002

Keum, Y. S., & Choi, B. Y. (2014). Molecular and chemical regulation of the Keap1-Nrf2 signaling pathway. *Molecules, 19*(7), 10074-10089. doi:10.3390/molecules190710074

Khan, M., Siddiqi, R., & Thompson, P. A. (2018). Approach to Richter transformation of chronic lymphocytic leukemia in the era of novel therapies. *Ann Hematol, 97*(1), 1-15. doi:10.1007/s00277-017-3149-9

Kienle, D., Benner, A., Kröber, A., Winkler, D., Mertens, D., Bühler, A., . . . Stilgenbauer, S. (2006). Distinct gene expression patterns in chronic lymphocytic leukemia defined by usage of specific VH genes. *Blood, 107*(5), 2090-2093. doi:10.1182/blood-2005-04-1483

Kim, Y. S., Gupta Vallur, P., Phaeton, R., Mythreye, K., & Hempel, N. (2017). Insights into the Dichotomous Regulation of SOD2 in Cancer. *Antioxidants (Basel), 6*(4). doi:10.3390/antiox6040086

Kimura, H., Sawada, T., Oshima, S., Kozawa, K., Ishioka, T., & Kato, M. (2005). Toxicity and roles of reactive oxygen species. *Curr Drug Targets Inflamm Allergy, 4*(4), 489-495.

Klein, & Dalla-Favera. (2010). New insights into the pathogenesis of chronic lymphocytic leukemia. *Semin Cancer Biol, 20*(6), 377-383. doi:10.1016/j.semcancer.2010.10.012

Klein, Lammens, A., Schafer, W., Georges, G., Schwaiger, M., Mossner, E., . . . Niederfellner, G. (2013). Epitope interactions of monoclonal antibodies targeting CD20 and their relationship to functional properties. *MAbs, 5*(1), 22-33. doi:10.4161/mabs.22771

Ko, H. L., Wang, Y. S., Fong, W. L., Chi, M. S., Chi, K. H., & Kao, S. J. (2014). Apolipoprotein C1 (APOC1) as a novel diagnostic and prognostic biomarker for lung cancer: A marker phase I trial. *Thorac Cancer, 5*(6), 500-508. doi:10.1111/1759-7714.12117

Kolahi, K., Louey, S., Varlamov, O., & Thornburg, K. (2016). Real-Time Tracking of BODIPY-C12 Long-Chain Fatty Acid in Human Term Placenta Reveals Unique Lipid Dynamics in Cytotrophoblast Cells. *PLoS One, 11*(4), e0153522. doi:10.1371/journal.pone.0153522

Kontos, C. K., Papageorgiou, S. G., Diamantopoulos, M. A., Scorilas, A., Bazani, E., Vasilatou, D., . . . Pappa, V. (2017). mRNA overexpression of the hypoxia inducible factor 1 alpha subunit gene (HIF1A): An independent predictor of poor overall survival in chronic lymphocytic leukemia. *Leuk Res, 53*, 65-73. doi:10.1016/j.leukres.2016.11.014

Koopman, G., Keehnen, R. M., Lindhout, E., Newman, W., Shimizu, Y., van Seventer, G. A., . . . Pals, S. T. (1994). Adhesion through the LFA-1 (CD11a/CD18)-ICAM-1 (CD54) and the VLA-4 (CD49d)-VCAM-1 (CD106) pathways prevents apoptosis of germinal center B cells. *J Immunol, 152*(8), 3760-3767.

Kopan, R., & Ilagan, M. X. (2009). The canonical Notch signaling pathway: unfolding the activation mechanism. *Cell, 137*(2), 216-233. doi:10.1016/j.cell.2009.03.045

Kowalski, P. S., Rudra, A., Miao, L., & Anderson, D. G. (2019). Delivering the Messenger: Advances in Technologies for Therapeutic mRNA Delivery. *Mol Ther, 27*(4), 710-728. doi:10.1016/j.ymthe.2019.02.012

Kowaltowski, A. J., de Souza-Pinto, N. C., Castilho, R. F., & Vercesi, A. E. (2009). Mitochondria and reactive oxygen species. *Free Radic Biol Med, 47*(4), 333-343. doi:10.1016/j.freeradbiomed.2009.05.004

Kuhajda, F. P., Jenner, K., Wood, F. D., Hennigar, R. A., Jacobs, L. B., Dick, J. D., & Pasternack, G. R. (1994). Fatty acid synthesis: a potential selective target for antineoplastic therapy. *Proc Natl Acad Sci U S A, 91*(14), 6379-6383. doi:10.1073/pnas.91.14.6379

Lannutti, B. J., Meadows, S. A., Herman, S. E., Kashishian, A., Steiner, B., Johnson, A. J., . . . Giese, N. A. (2011). CAL-101, a p110delta selective phosphatidylinositol-3-kinase inhibitor for the treatment of B-cell malignancies, inhibits PI3K signaling and cellular viability. *Blood, 117*(2), 591-594. doi:10.1182/blood-2010-03-275305

LeBien, T. W., & Tedder, T. F. (2008). B lymphocytes: how they develop and function. *Blood, 112*(5), 1570-1580. doi:10.1182/blood-2008-02-078071

Lee, Bae, Jeong, Kim, & Kim. (2004). Hypoxia-inducible factor (HIF-1)alpha: its protein stability and biological functions. *Exp Mol Med, 36*(1), 1-12. doi:10.1038/emm.2004.1

Lee, R. L., Westendorf, J., & Gold, M. R. (2007). Differential role of reactive oxygen species in the activation of mitogen-activated protein kinases and Akt by key receptors on B-lymphocytes: CD40, the B cell antigen receptor, and CXCR4. *J Cell Commun Signal, 1*(1), 33-43. doi:10.1007/s12079-007-0006-y

Lee, S., Kwon, H., Jeong, K., & Pak, Y. (2011). Regulation of cancer cell proliferation by caveolin-2 down-regulation and re-expression. *Int J Oncol, 38*(5), 1395-1402. doi:10.3892/ijo.2011.958

Li, N., Ragheb, K., Lawler, G., Sturgis, J., Rajwa, B., Melendez, J. A., & Robinson, J. P. (2003). Mitochondrial complex I inhibitor rotenone induces apoptosis through enhancing mitochondrial reactive oxygen species production. *J Biol Chem, 278*(10), 8516-8525. doi:10.1074/jbc.M210432200

Lin, H. P., Singla, B., Ghoshal, P., Faulkner, J. L., Cherian-Shaw, M., O'Connor, P. M., . . . Csányi, G. (2018). Identification of novel macropinocytosis inhibitors using a rational screen of Food and Drug Administration-approved drugs. *Br J Pharmacol, 175*(18), 3640-3655. doi:10.1111/bph.14429

Linley, A., Valle-Argos, B., Steele, A. J., Stevenson, F. K., Forconi, F., & Packham, G. (2015). Higher levels of reactive oxygen species are associated with anergy in chronic lymphocytic leukemia. *Haematologica, 100*(7), e265-268. doi:10.3324/haematol.2014.120824

Liu, Xiong, Li, Lv, Liu, Yi, . . . Qiu. (2016). Prognostic Significance of Serum LDH in B Cell Chronic Lymphoproliferative Disorders: A Single-Institution Study of 829 Cases in China. *Blood, 128*(22), 5336.

Liu, R., Wang, X., Curtiss, C., Landas, S., Rong, R., Sheikh, M. S., & Huang, Y. (2018). Monoglyceride lipase gene knockout in mice leads to increased incidence of lung adenocarcinoma. *Cell Death Dis, 9*(2), 36. doi:10.1038/s41419-017-0188-z

Liu, Y., Corcoran, M., Rasool, O., Ivanova, G., Ibbotson, R., Grander, D., . . . Oscier, D. (1997). Cloning of two candidate tumor suppressor genes within a 10kb region on chromosome 13q14, frequently deleted in chronic lymphocytic leukaemia. *Oncogene, 15*, 10.

Livak, K. J., & Schmittgen, T. D. (2001). Analysis of relative gene expression data using real-time quantitative PCR and the 2(-Delta Delta C(T)) Method. *Methods, 25*(4), 402-408. doi:10.1006/meth.2001.1262

Lu, J., Böttcher, M., Walther, T., Mougiakakos, D., Zenz, T., & Huber, W. (2019). Energy metabolism is co-determined by genetic variants in chronic lymphocytic leukemia and influences drug sensitivity. *Haematologica, 104*(9), 1830-1840. doi:10.3324/haematol.2018.203067

Lutzny, G., Kocher, T., Schmidt-Supprian, M., Rudelius, M., Klein-Hitpass, L., Finch, A. J., . . . Ringshausen, I. (2013). Protein kinase c-β-dependent activation of NF-κB in stromal cells is indispensable for the survival of chronic lymphocytic leukemia B cells in vivo. *Cancer Cell, 23*(1), 77-92. doi:10.1016/j.ccr.2012.12.003

Lydyard, P., Jamin, C., & Youinou, P. (1998). *CD5*. Oxford: Elsevier.

Maehara, K., Uekawa, N., & Isobe, K. (2002). Effects of histone acetylation on transcriptional regulation of manganese superoxide dismutase gene. *Biochem Biophys Res Commun, 295*(1), 187-192. doi:10.1016/s0006-291x(02)00646-0

Malavasi, F., Funaro, A., Roggero, S., Horenstein, A., Calosso, L., & Mehta, K. (1994). Human CD38: a glycoprotein in search of a function. *Immunol Today, 15*(3), 95-97. doi:10.1016/0167-5699(94)90148-1

Manna, A., De Sarkar, S., De, S., Bauri, A. K., Chattopadhyay, S., & Chatterjee, M. (2015). The variable chemotherapeutic response of Malabaricone-A in leukemic and solid tumor cell lines depends on the degree of redox imbalance. *Phytomedicine, 22*(7-8), 713-723. doi:10.1016/j.phymed.2015.05.007

Marshall, M. J. E., Stopforth, R. J., & Cragg, M. S. (2017). Therapeutic Antibodies: What Have We Learnt from Targeting CD20 and Where Are We Going? *Front Immunol, 8*, 1245. doi:10.3389/fimmu.2017.01245

Mátrai, Z., Andrikovics, H., Szilvási, A., Bors, A., Kozma, A., Ádám, E., . . . Masszi, T. (2017). Lipoprotein Lipase as a Prognostic Marker in Chronic Lymphocytic Leukemia. *Pathol Oncol Res, 23*(1), 165-171. doi:10.1007/s12253-016-0132-z

Mauri, C., & Bosma, A. (2012). Immune regulatory function of B cells. *Annu Rev Immunol, 30*, 221-241. doi:10.1146/annurev-immunol-020711-074934

McCall, M. N., McMurray, H. R., Land, H., & Almudevar, A. (2014). On non-detects in qPCR data. *Bioinformatics, 30*(16), 2310-2316. doi:10.1093/bioinformatics/btu239

Melo, J. V., Catovsky, D., & Galton, D. A. (1986). The relationship between chronic lymphocytic leukaemia and prolymphocytic leukaemia. I. Clinical and laboratory features of 300 patients and characterization of an intermediate group. *Br J Haematol, 63*(2), 377-387.

Memmert, S., Damanaki, A., Weykopf, B., Rath-Deschner, B., Nokhbehsaim, M., Götz, W., . . . Jäger, A. (2019). Autophagy in periodontal ligament fibroblasts under biomechanical loading. *Cell Tissue Res, 378*(3), 499-511. doi:10.1007/s00441-019-03063-1

Mertens, D., & Stilgenbauer, S. (2014). Prognostic and predictive factors in patients with chronic lymphocytic leukaemia: relevant in the era of novel treatment approaches? *J Clin oncol, 32*, 4.

Meshulam, T., Simard, J. R., Wharton, J., Hamilton, J. A., & Pilch, P. F. (2006). Role of caveolin-1 and cholesterol in transmembrane fatty acid movement. *Biochemistry, 45*(9), 2882-2893. doi:10.1021/bi051999b

Michallet, A. S., Cazin, B., Bouvet, E., Oberic, L., Schlaifer, D., Mosser, L., . . . Ysebaert, L. (2013). First immunochemotherapy outcomes in elderly patients with CLL: a retrospective analysis. *J Geriatr Oncol, 4*(2), 141-147. doi:10.1016/j.jgo.2013.01.002

Mole, D. R., Blancher, C., Copley, R. R., Pollard, P. J., Gleadle, J. M., Ragoussis, J., & Ratcliffe, P. J. (2009). Genome-wide association of hypoxia-inducible factor (HIF)-1alpha and HIF-2alpha DNA binding with expression profiling of hypoxia-inducible transcripts. *J Biol Chem, 284*(25), 16767-16775. doi:10.1074/jbc.M901790200

Moloney, J. N., & Cotter, T. G. (2018). ROS signalling in the biology of cancer. *Semin Cell Dev Biol, 80*, 50-64. doi:10.1016/j.semcdb.2017.05.023

Morgan, M. J., & Liu, Z. G. (2011). Crosstalk of reactive oxygen species and NF-kappaB signaling. *Cell Res, 21*(1), 103-115. doi:10.1038/cr.2010.178

Mossner, E., Brunker, P., Moser, S., Puntener, U., Schmidt, C., Herter, S., . . . Umana, P. (2010). Increasing the efficacy of CD20 antibody therapy through the engineering of a new type II anti-CD20 antibody with enhanced direct and immune effector cell-mediated B-cell cytotoxicity. *Blood, 115*(22), 4393-4402. doi:10.1182/blood-2009-06-225979

Murakami, M. (2011). Lipid mediators in life science. *Exp Anim, 60*(1), 7-20. doi:10.1538/expanim.60.7

Murphy, M. P. (2009). How mitochondria produce reactive oxygen species. *Biochem J, 417*(1), 1-13. doi:10.1042/bj20081386

Musso, M., Bocciardi, R., Parodi, S., Ravazzolo, R., & Ceccherini, I. (2006). Betaine, dimethyl sulfoxide, and 7-deaza-dGTP, a powerful mixture for amplification of GC-rich DNA sequences. *J Mol Diagn, 8*(5), 544-550. doi:10.2353/jmoldx.2006.060058

Nadeu, F., Delgado, J., Royo, C., Baumann, T., Stankovic, T., Pinyol, M., . . . Campo, E. (2016). Clinical impact of clonal and subclonal TP53, SF3B1, BIRC3, NOTCH1, and ATM mutations in chronic lymphocytic leukemia. *Blood, 127*(17), 2122-2130. doi:10.1182/blood-2015-07-659144

Nakano, A., Harada, T., Morikawa, S., & Kato, Y. (1990). Expression of leukocyte common antigen (CD45) on various human leukemia/lymphoma cell lines. *Acta Pathol Jpn, 40*(2), 107-115. doi:10.1111/j.1440-1827.1990.tb01549.x

National Cancer Institute, N. (2014). FDA Approval for Ofatumumab.

Nelson, D., & Cox, M. (2016). *Lehninger principles of biochemistry* (7th Edition ed.). USA: Macmillan Science & Education.

Nickerson, J. G., Alkhateeb, H., Benton, C. R., Lally, J., Nickerson, J., Han, X. X., . . . Bonen, A. (2009). Greater transport efficiencies of the membrane fatty acid transporters FAT/CD36 and FATP4 compared with FABPpm and FATP1 and differential effects on fatty acid esterification and oxidation in rat skeletal muscle. *J Biol Chem, 284*(24), 16522-16530. doi:10.1074/jbc.M109.004788

Niederfellner, G., Lammens, A., Mundigl, O., Georges, G. J., Schaefer, W., Schwaiger, M., . . . Klein, C. (2011). Epitope characterization and crystal structure of GA101 provide insights into the molecular basis for type I/II distinction of CD20 antibodies. *Blood, 118*(2), 358-367. doi:10.1182/blood-2010-09-305847

Nieman, K. M., Kenny, H. A., Penicka, C. V., Ladanyi, A., Buell-Gutbrod, R., Zillhardt, M. R., . . . Lengyel, E. (2011). Adipocytes promote ovarian cancer metastasis and provide energy for rapid tumor growth. *Nat Med, 17*(11), 1498-1503. doi:10.1038/nm.2492

Niesman, I. R., Zemke, N., Fridolfsson, H. N., Haushalter, K. J., Levy, K., Grove, A., . . . Patel, H. H. (2013). Caveolin isoform switching as a molecular, structural, and metabolic regulator of microglia. *Mol Cell Neurosci, 56*, 283-297. doi:10.1016/j.mcn.2013.07.002

Nuckel, H., Huttmann, A., Klein-Hitpass, L., Schroers, R., Fuhrer, A., Sellmann, L., . . . Durig, J. (2006). Lipoprotein lipase expression is a novel prognostic factor in B-cell chronic lymphocytic leukemia. *Leuk Lymphoma, 47*(6), 1053-1061. doi:10.1080/10428190500464161

O'Brien, Furman, R. R., Coutre, S., Flinn, I. W., Burger, Blum, K., . . . Byrd, J. C. (2018). Single-agent ibrutinib in treatment-naïve and relapsed/refractory chronic lymphocytic leukemia: a 5-year experience. *Blood, 131*(17), 1910-1919. doi:10.1182/blood-2017-10-810044

O'Brien, S. M., Kantarjian, H., Thomas, D. A., Giles, F. J., Freireich, E. J., Cortes, J., . . . Keating, M. J. (2001). Rituximab dose-escalation trial in chronic lymphocytic leukemia. *J Clin Oncol, 19*(8), 2165-2170. doi:10.1200/jco.2001.19.8.2165

Ohta, T., Iijima, K., Miyamoto, M., Nakahara, I., Tanaka, H., Ohtsuji, M., . . . Hirohashi, S. (2008). Loss of Keap1 function activates Nrf2 and provides advantages for lung cancer cell growth. *Cancer Res, 68*(5), 1303-1309. doi:10.1158/0008-5472.Can-07-5003

Oliveira, G. B., Pereira, F. G., Metze, K., & Lorand-Metze, I. (2001). Spontaneous apoptosis in chronic lymphocytic leukemia and its relationship to clinical and cell kinetic parameters. *Cytometry, 46*(6), 329-335. doi:10.1002/cyto.10031

Ookhtens, M., Kannan, R., Lyon, I., & Baker, N. (1984). Liver and adipose tissue contributions to newly formed fatty acids in an ascites tumor. *Am J Physiol, 247*(1 Pt 2), R146-153. doi:10.1152/ajpregu.1984.247.1.R146

Oppezzo, P., Vasconcelos, Y., Settegrana, C., Jeannel, D., Vuillier, F., Legarff-Tavernier, M., . . . Davi, F. (2005). The LPL/ADAM29 expression ratio is a novel prognosis indicator in chronic lymphocytic leukemia. *Blood, 106*(2), 650-657. doi:10.1182/blood-2004-08-3344

Orpana, A. K., Ho, T. H., & Stenman, J. (2012). Multiple heat pulses during PCR extension enabling amplification of GC-rich sequences and reducing amplification bias. *Anal Chem, 84*(4), 2081-2087. doi:10.1021/ac300040j

Orrenius, S., Gogvadze, V., & Zhivotovsky, B. (2007). Mitochondrial oxidative stress: implications for cell death. *Annu Rev Pharmacol Toxicol, 47*, 143-183. doi:10.1146/annurev.pharmtox.47.120505.105122

Ouillette, P., Collins, R., Shakhan, S., Li, J., Li, C., Shedden, K., & Malek, S. N. (2011). The prognostic significance of various 13q14 deletions in chronic lymphocytic leukemia. *Clin Cancer Res, 17*(21), 6778-6790. doi:10.1158/1078-0432.ccr-11-0785

Pallasch, C. P., Schwamb, J., Konigs, S., Schulz, A., Debey, S., Kofler, D., . . . Wendtner, C. M. (2008). Targeting lipid metabolism by the lipoprotein lipase inhibitor orlistat results in apoptosis of B-cell chronic lymphocytic leukemia cells. *Leukemia, 22*(3), 585-592. doi:10.1038/sj.leu.2405058

Palumbo, G. A., Parrinello, N., Fargione, G., Cardillo, K., Chiarenza, A., Berretta, S., . . . Di Raimondo, F. (2009). CD200 expression may help in differential diagnosis between mantle cell lymphoma and B-cell chronic lymphocytic leukemia. *Leuk Res, 33*(9), 1212-1216. doi:10.1016/j.leukres.2009.01.017

Papa, S., Martino, P. L., Capitanio, G., Gaballo, A., De Rasmo, D., Signorile, A., & Petruzzella, V. (2012). The oxidative phosphorylation system in mammalian mitochondria. *Adv Exp Med Biol, 942*, 3-37. doi:10.1007/978-94-007-2869-1_1

Pawluczkowycz, A., Beurskens, F., Beum, P., Lindorfer, M., Winkel, J. v. d., Parren, P., & Taylor, R. (2009). Binding of Submaximal C1q promotes complement-dependent cytotoxicity (CDC) of B cells opsonized with anti-CD20 mAbs Ofatumumab (OFA) or Rituximab (RTX): considerably higher levels of CDC are induced by OFA than by RTX. *The Journal of Immunology, 183*(1), 10.

Pedersen, I. M., Kitada, S., Schimmer, A., Kim, Y., Zapata, J. M., Charboneau, L., . . . Reed, J. C. (2002). The triterpenoid CDDO induces apoptosis in refractory CLL B cells. *Blood, 100*(8), 2965-2972. doi:10.1182/blood-2002-04-1174

Pepino, M. Y., Kuda, O., Samovski, D., & Abumrad, N. A. (2014). Structure-function of CD36 and importance of fatty acid signal transduction in fat metabolism. *Annu Rev Nutr, 34*, 281-303. doi:10.1146/annurev-nutr-071812-161220

Perrin-Vidoz, L., Sinilnikova, O. M., Stoppa-Lyonnet, D., Lenoir, G. M., & Mazoyer, S. (2002). The nonsense-mediated mRNA decay pathway triggers degradation of most BRCA1 mRNAs bearing premature termination codons. *Hum Mol Genet, 11*(23), 2805-2814. doi:10.1093/hmg/11.23.2805

Pilch, P. F., & Liu, L. (2011). Fat caves: caveolae, lipid trafficking and lipid metabolism in adipocytes. *Trends Endocrinol Metab, 22*(8), 318-324. doi:10.1016/j.tem.2011.04.001

Pinyol, M., Bea, S., Plà, L., Ribrag, V., Bosq, J., Rosenwald, A., . . . Jares, P. (2007). Inactivation of RB1 in mantle-cell lymphoma detected by nonsense-mediated mRNA decay pathway inhibition and microarray analysis. *Blood, 109*(12), 5422-5429. doi:10.1182/blood-2006-11-057208

Pizzimenti, S., Briatore, F., Laurora, S., Toaldo, C., Maggio, M., De Grandi, M., . . . Barrera, G. (2006). 4-Hydroxynonenal inhibits telomerase activity and hTERT expression in human leukemic cell lines. *Free Radic Biol Med, 40*(9), 1578-1591. doi:10.1016/j.freeradbiomed.2005.12.024

Pollyea, D. A., Stevens, B. M., Jones, C. L., Winters, A., Pei, S., Minhajuddin, M., . . . Jordan, C. T. (2018). Venetoclax with azacitidine disrupts energy metabolism and targets leukemia stem cells in patients with acute myeloid leukemia. *Nat Med, 24*(12), 1859-1866. doi:10.1038/s41591-018-0233-1

Polyak, M. J., Li, H., Shariat, N., & Deans, J. P. (2008). CD20 homo-oligomers physically associate with the B cell antigen receptor. Dissociation upon receptor engagement and recruitment of phosphoproteins and calmodulin-binding proteins. *J Biol Chem, 283*(27), 18545-18552. doi:10.1074/jbc.M800784200

Ponader, S., Chen, S. S., Buggy, J. J., Balakrishnan, K., Gandhi, V., Wierda, W. G., . . . Burger. (2012). The Bruton tyrosine kinase inhibitor PCI-32765 thwarts chronic lymphocytic leukemia cell survival and tissue homing in vitro and in vivo. *Blood, 119*(5), 1182-1189. doi:10.1182/blood-2011-10-386417

Prieto, D., & Oppezzo, P. (2017). Lipoprotein Lipase Expression in Chronic Lymphocytic Leukemia: New Insights into Leukemic Progression. *Molecules, 22*(12). doi:10.3390/molecules22122083

Qiao, L., Zou, C., Shao, P., Schaack, J., Johnson, P. F., & Shao, J. (2008). Transcriptional regulation of fatty acid translocase/CD36 expression by CCAAT/enhancer-binding protein alpha. *J Biol Chem, 283*(14), 8788-8795. doi:10.1074/jbc.M800055200

Quinlan, C. L., Orr, A. L., Perevoshchikova, I. V., Treberg, J. R., Ackrell, B. A., & Brand, M. D. (2012). Mitochondrial complex II can generate reactive oxygen species at high rates in both the forward and reverse reactions. *J Biol Chem, 287*(32), 27255-27264. doi:10.1074/jbc.M112.374629

Rai, K. R., & Jain, P. (2011). Advances in the clinical staging of chronic lymphocytic leukemia. *Clin Chem, 57*(12), 1771-1772. doi:10.1373/clinchem.2010.159004

Rai, K. R., & Jain, P. (2016). Chronic lymphocytic leukemia (CLL)-Then and now. *Am J Hematol, 91*(3), 330-340. doi:10.1002/ajh.24282

Rai, K. R., Sawitsky, A., Cronkite, E. P., Chanana, A. D., Levy, R. N., & Pasternack, B. S. (1975). Clinical staging of chronic lymphocytic leukemia. *Blood, 46*(2), 219-234.

Ramwadhdoebe, T. H., van Baarsen, L. G. M., Boumans, M. J. H., Bruijnen, S. T. G., Safy, M., Berger, F. H., . . . Tak, P. P. (2019). Effect of rituximab treatment on T and B cell subsets in lymph node biopsies of patients with rheumatoid arthritis. *Rheumatology (Oxford), 58*(6), 1075-1085. doi:10.1093/rheumatology/key428

Razani, B., Wang, X. B., Engelman, J. A., Battista, M., Lagaud, G., Zhang, X. L., . . . Lisanti, M. P. (2002). Caveolin-2-deficient mice show evidence of severe pulmonary dysfunction without disruption of caveolae. *Mol Cell Biol, 22*(7), 2329-2344. doi:10.1128/mcb.22.7.2329-2344.2002

Reff, M. E., Carner, K., Chambers, K. S., Chinn, P. C., Leonard, J. E., Raab, R., . . . Anderson, D. R. (1994). Depletion of B cells in vivo by a chimeric mouse human monoclonal antibody to CD20. *Blood, 83*(2), 435-445.

Ricci, F., Tedeschi, A., Morra, E., & Montillo, M. (2009). Fludarabine in the treatment of chronic lymphocytic leukemia: a review. *Ther Clin Risk Manag, 5*(1), 187-207.

Riches, J. C., Ramsay, A. G., & Gribben, J. G. (2010). T-cell function in chronic lymphocytic leukaemia. *Semin Cancer Biol, 20*(6), 431-438. doi:10.1016/j.semcancer.2010.09.006

Robak, T., Dmoszynska, A., Solal-Céligny, P., Warzocha, K., Loscertales, J., Catalano, J., . . . Moiseev, S. I. (2010). Rituximab plus fludarabine and cyclophosphamide prolongs progression-free survival

compared with fludarabine and cyclophosphamide alone in previously treated chronic lymphocytic leukemia. *J Clin Oncol, 28*(10), 1756-1765. doi:10.1200/jco.2009.26.4556

Robenek, H., Hofnagel, O., Buers, I., Robenek, M. J., Troyer, D., & Severs, N. J. (2006). Adipophilin-enriched domains in the ER membrane are sites of lipid droplet biogenesis. *J Cell Sci, 119*(Pt 20), 4215-4224. doi:10.1242/jcs.03191

Roberts, A. W., Davids, M. S., Pagel, J. M., Kahl, B. S., Puvvada, S. D., Gerecitano, J. F., . . . Seymour, J. F. (2016). Targeting BCL2 with Venetoclax in Relapsed Chronic Lymphocytic Leukemia. *N Engl J Med, 374*(4), 311-322. doi:10.1056/NEJMoa1513257

Rodal, S. K., Skretting, G., Garred, O., Vilhardt, F., van Deurs, B., & Sandvig, K. (1999). Extraction of cholesterol with methyl-beta-cyclodextrin perturbs formation of clathrin-coated endocytic vesicles. *Mol Biol Cell, 10*(4), 961-974. doi:10.1091/mbc.10.4.961

Rodriguez-Vicente, A. E., Diaz, M. G., & Hernandez-Rivas, J. M. (2013). Chronic lymphocytic leukemia: a clinical and molecular heterogenous disease. *Cancer Genet, 206*(3), 49-62. doi:10.1016/j.cancergen.2013.01.003

Ros, S., Santos, C. R., Moco, S., Baenke, F., Kelly, G., Howell, M., . . . Schulze, A. (2012). Functional metabolic screen identifies 6-phosphofructo-2-kinase/fructose-2,6-biphosphatase 4 as an important regulator of prostate cancer cell survival. *Cancer Discov, 2*(4), 328-343. doi:10.1158/2159-8290.cd-11-0234

Rosati, E., Sabatini, R., Rampino, G., Tabilio, A., Di Ianni, M., Fettucciari, K., . . . Marconi, P. (2009). Constitutively activated Notch signaling is involved in survival and apoptosis resistance of B-CLL cells. *Blood, 113*(4), 856-865. doi:10.1182/blood-2008-02-139725

Rosenwald, A., Alizadeh, A. A., Widhopf, G., Simon, R., Davis, R. E., Yu, X., . . . Staudt, L. M. (2001). Relation of gene expression phenotype to immunoglobulin mutation genotype in B cell chronic lymphocytic leukemia. *J Exp Med, 194*(11), 1639-1647.

Rossi, D., Fangazio, M., Rasi, S., Vaisitti, T., Monti, S., Cresta, S., . . . Gaidano, G. (2012). Disruption of BIRC3 associates with fludarabine chemorefractoriness in TP53 wild-type chronic lymphocytic leukemia. *Blood, 119*(12), 2854-2862. doi:10.1182/blood-2011-12-395673

Rossi, D., Rasi, S., Fabbri, G., Spina, V., Fangazio, M., Forconi, F., . . . Gaidano, G. (2012). Mutations of NOTCH1 are an independent predictor of survival in chronic lymphocytic leukemia. *Blood, 119*(2), 521-529. doi:10.1182/blood-2011-09-379966

Rozovski, U., Grgurevic, S., Bueso-Ramos, C., Harris, D. M., Li, P., Liu, Z., . . . Estrov, Z. (2015). Aberrant LPL Expression, Driven by STAT3, Mediates Free Fatty Acid Metabolism in CLL Cells. *Mol Cancer Res, 13*(5), 944-953. doi:10.1158/1541-7786.mcr-14-0412

Ruan, H., & Dong, L. Q. (2016). Adiponectin signaling and function in insulin target tissues. *J Mol Cell Biol, 8*(2), 101-109. doi:10.1093/jmcb/mjw014

Rushmore, T. H., Morton, M. R., & Pickett, C. B. (1991). The antioxidant responsive element. Activation by oxidative stress and identification of the DNA consensus sequence required for functional activity. *J Biol Chem, 266*(18), 11632-11639.

Rushworth, S. A., Zaitseva, L., Murray, M. Y., Shah, N. M., Bowles, K. M., & MacEwan, D. J. (2012). The high Nrf2 expression in human acute myeloid leukemia is driven by NF-κB and underlies its chemo-resistance. *Blood, 120*(26), 5188-5198. doi:10.1182/blood-2012-04-422121

Sagatys, E. M., & Zhang, L. (2012). Clinical and laboratory prognostic indicators in chronic lymphocytic leukemia. *Cancer Control, 19*(1), 18-25. doi:10.1177/107327481201900103

Saitoh, M., Nishitoh, H., Fujii, M., Takeda, K., Tobiume, K., Sawada, Y., . . . Ichijo, H. (1998). Mammalian thioredoxin is a direct inhibitor of apoptosis signal-regulating kinase (ASK) 1. *Embo j, 17*(9), 2596-2606. doi:10.1093/emboj/17.9.2596

Sandvig, K., & van Deurs, B. (1994). Endocytosis without clathrin. *Trends Cell Biol, 4*(8), 275-277. doi:10.1016/0962-8924(94)90211-9

Sanz, L., Garcia-Marco, J. A., Casanova, B., de La Fuente, M. T., García-Gila, M., Garcia-Pardo, A., & Silva, A. (2004). Bcl-2 family gene modulation during spontaneous apoptosis of B-chronic lymphocytic

leukemia cells. *Biochem Biophys Res Commun, 315*(3), 562-567. doi:10.1016/j.bbrc.2004.01.095

Sarras, H., Wu, M., Celebre, A., Merico, D., Karamchandani, J., & Das, S. (2016). A novel amplification-based approach to enable gene expression profiling from small clinical tumor specimens. *J Neurooncol, 126*(1), 69-75. doi:10.1007/s11060-015-1953-4

Sauer, H., Wartenberg, M., & Hescheler, J. (2001). Reactive oxygen species as intracellular messengers during cell growth and differentiation. *Cell Physiol Biochem, 11*(4), 173-186. doi:10.1159/000047804

Sawaoka, H., Kawano, S., Tsuji, S., Tsujii, M., Gunawan, E. S., Takei, Y., . . . Hori, M. (1998). Cyclooxygenase-2 inhibitors suppress the growth of gastric cancer xenografts via induction of apoptosis in nude mice. *Am J Physiol, 274*(6), G1061-1067. doi:10.1152/ajpgi.1998.274.6.G1061

Scarfò, L., Ferreri, A. J., & Ghia, P. (2016). Chronic lymphocytic leukaemia. *Crit Rev Oncol Hematol, 104*, 169-182. doi:10.1016/j.critrevonc.2016.06.003

Schaffer, J. E., & Lodish, H. F. (1994). Expression cloning and characterization of a novel adipocyte long chain fatty acid transport protein. *Cell, 79*(3), 427-436.

Scherer, P. E., Lewis, R. Y., Volonte, D., Engelman, J. A., Galbiati, F., Couet, J., . . . Lisanti, M. P. (1997). Cell-type and tissue-specific expression of caveolin-2. Caveolins 1 and 2 co-localize and form a stable hetero-oligomeric complex in vivo. *J Biol Chem, 272*(46), 29337-29346. doi:10.1074/jbc.272.46.29337

Scherer, P. E., Okamoto, T., Chun, M., Nishimoto, I., Lodish, H. F., & Lisanti, M. P. (1996). Identification, sequence, and expression of caveolin-2 defines a caveolin gene family. *Proc Natl Acad Sci U S A, 93*(1), 131-135. doi:10.1073/pnas.93.1.131

Schreck, R., Rieber, P., & Baeuerle, P. A. (1991). Reactive oxygen intermediates as apparently widely used messengers in the activation of the NF-kappa B transcription factor and HIV-1. *Embo j, 10*(8), 2247-2258.

Schroeder, H., Imboden, J., & Torres, R. (2019). *4 - Antigen Receptor Genes, Gene Products, and Coreceptors* (Fifth Edition ed.). London: Content Repository.

Schulz, H. (2008). *Oxidation of fatty acids in eukaryotes. In: Biochemistry of Lipids, Lipoproteins and Membranes (5th Edition)* (D. V. a. J. Vance Ed.). Amsterdam: Elsevier.

Schulze, P. C., Drosatos, K., & Goldberg, I. J. (2016). Lipid Use and Misuse by the Heart. *Circ Res, 118*(11), 1736-1751. doi:10.1161/circresaha.116.306842

Schwenk, R. W., Holloway, G. P., Luiken, J. J., Bonen, A., & Glatz, J. F. (2010). Fatty acid transport across the cell membrane: regulation by fatty acid transporters. *Prostaglandins Leukot Essent Fatty Acids, 82*(4-6), 149-154. doi:10.1016/j.plefa.2010.02.029

Schwenk, R. W., Luiken, J. J., Bonen, A., & Glatz, J. F. (2008). Regulation of sarcolemmal glucose and fatty acid transporters in cardiac disease. *Cardiovasc Res, 79*(2), 249-258. doi:10.1093/cvr/cvn116

Secchiero, P., Barbarotto, E., Gonelli, A., Tiribelli, M., Zerbinati, C., Celeghini, C., . . . Zauli, G. (2005). Potential pathogenetic implications of cyclooxygenase-2 overexpression in B chronic lymphoid leukemia cells. *Am J Pathol, 167*(6), 1599-1607. doi:10.1016/s0002-9440(10)61244-8

Sellner, L., Dietrich, S., Dreger, P., Glimm, H., & Zenz, T. (2012). Can prognostic factors be used to direct therapy in chronic lymphocytic leukemia? *Curr Hematol Malig Rep, 7*(1), 3-12. doi:10.1007/s11899-011-0110-1

Sena, L. A., & Chandel, N. S. (2012). Physiological roles of mitochondrial reactive oxygen species. *Mol Cell, 48*(2), 158-167. doi:10.1016/j.molcel.2012.09.025

Shahjahani, M., Mohammadiasl, J., Noroozi, F., Seghatoleslami, M., Shahrabi, S., Saba, F., & Saki, N. (2015). Molecular basis of chronic lymphocytic leukemia diagnosis and prognosis. *Cell Oncol (Dordr), 38*(2), 93-109. doi:10.1007/s13402-014-0215-3

Shan, D., Ledbetter, J. A., & Press, O. W. (2000). Signaling events involved in anti-CD20-induced apoptosis of malignant human B cells. *Cancer Immunol Immunother, 48*(12), 673-683.

Shanafelt, T. D., Geyer, S. M., Bone, N. D., Tschumper, R. C., Witzig, T. E., Nowakowski, G. S., . . . Kay, N. E. (2008). CD49d expression is an independent predictor of overall survival in patients with chronic lymphocytic leukaemia: a prognostic parameter with therapeutic potential. *Br J Haematol, 140*(5), 537-546. doi:10.1111/j.1365-2141.2007.06965.x

Shaulian, E. (2010). AP-1--The Jun proteins: Oncogenes or tumor suppressors in disguise? *Cell Signal, 22*(6), 894-899. doi:10.1016/j.cellsig.2009.12.008

Shibata, T., Ohta, T., Tong, K. I., Kokubu, A., Odogawa, R., Tsuta, K., . . . Hirohashi, S. (2008). Cancer related mutations in NRF2 impair its recognition by Keap1-Cul3 E3 ligase and promote malignancy. *Proc Natl Acad Sci U S A, 105*(36), 13568-13573. doi:10.1073/pnas.0806268105

Simonsson, B., Wibell, L., & Nilsson, K. (1980). Beta 2-microglobulin in chronic lymphocytic leukaemia. *Scand J Haematol, 24*(2), 174-180. doi:10.1111/j.1600-0609.1980.tb02364.x

Solis, L. M., Behrens, C., Dong, W., Suraokar, M., Ozburn, N. C., Moran, C. A., . . . Wistuba, II. (2010). Nrf2 and Keap1 abnormalities in non-small cell lung carcinoma and association with clinicopathologic features. *Clin Cancer Res, 16*(14), 3743-3753. doi:10.1158/1078-0432.Ccr-09-3352

Spaner, D. E., Lee, E., Shi, Y., Wen, F., Li, Y., Tung, S., . . . Gorzcynski, R. (2013). PPAR-alpha is a therapeutic target for chronic lymphocytic leukemia. *Leukemia, 27*(5), 1090-1099. doi:10.1038/leu.2012.329

Sportoletti, P., Baldoni, S., Cavalli, L., Del Papa, B., Bonifacio, E., Ciurnelli, R., . . . Falzetti, F. (2010). NOTCH1 PEST domain mutation is an adverse prognostic factor in B-CLL. *Br J Haematol, 151*(4), 404-406. doi:10.1111/j.1365-2141.2010.08368.x

Srivastava, S., Tsongalis, G. J., & Kaur, P. (2013). Recent advances in microRNA-mediated gene regulation in chronic lymphocytic leukemia. *Clin Biochem, 46*(10-11), 901-908. doi:10.1016/j.clinbiochem.2013.03.007

St Clair, D. K., & Holland, J. C. (1991). Complementary DNA encoding human colon cancer manganese superoxide dismutase and the expression of its gene in human cells. *Cancer Res, 51*(3), 939-943.

Stamatopoulos, B., Meuleman, N., De Bruyn, C., Pieters, K., Anthoine, G., Mineur, P., . . . Lagneaux, L. (2010). A molecular score by quantitative PCR as a new prognostic tool at diagnosis for chronic lymphocytic leukemia patients. *PLoS One, 5*(9). doi:10.1371/journal.pone.0012780

Stashenko, P., Nadler, L. M., Hardy, R., & Schlossman, S. F. (1980). Characterization of a human B lymphocyte-specific antigen. *J Immunol, 125*(4), 1678-1685.

Stevenson, F. K., Krysov, S., Davies, A. J., Steele, A. J., & Packham, G. (2011). B-cell receptor signaling in chronic lymphocytic leukemia. *Blood, 118*(16), 4313-4320. doi:10.1182/blood-2011-06-338855

Stilgenbauer, S., Eichhorst, B., Schetelig, J., Coutre, S., Seymour, J. F., Munir, T., . . . Wierda, W. G. (2016). Venetoclax in relapsed or refractory chronic lymphocytic leukaemia with 17p deletion: a multicentre, open-label, phase 2 study. *Lancet Oncol, 17*(6), 768-778. doi:10.1016/s1470-2045(16)30019-5

Stilgenbauer, S., Schnaiter, A., Paschka, P., Zenz, T., Rossi, M., Döhner, K., . . . Döhner, H. (2014). Gene mutations and treatment outcome in chronic lymphocytic leukemia: results from the CLL8 trial. *Blood, 123*(21), 3247-3254. doi:10.1182/blood-2014-01-546150

Sulda, M. (2009). *Investigation of biological targets for prognostication and therapy in B-cell chronic lymphocytic leukaemia.* (Doctorate), Flinders University of South Australia, Adelaide, Australia.

Sullivan, K. D., Gallant-Behm, C. L., Henry, R. E., Fraikin, J. L., & Espinosa, J. M. (2012). The p53 circuit board. *Biochim Biophys Acta, 1825*(2), 229-244. doi:10.1016/j.bbcan.2012.01.004

Sun, F., Huo, X., Zhai, Y., Wang, A., Xu, J., Su, D., . . . Rao, Z. (2005). Crystal structure of mitochondrial respiratory membrane protein complex II. *Cell, 121*(7), 1043-1057. doi:10.1016/j.cell.2005.05.025

Sun, G. G., Wang, Y. D., Chen, L. Q., Wang, S. J., Liu, G. L., Yu, X. R., . . . Liu, Q. (2011). Novel cancer suppressor gene for esophageal cancer: manganese superoxide dismutase. *Dis Esophagus, 24*(5), 346-353. doi:10.1111/j.1442-2050.2010.01149.x

Suzuki, Y. J., Forman, H. J., & Sevanian, A. (1997). Oxidants as stimulators of signal transduction. *Free Radic Biol Med, 22*(1-2), 269-285. doi:10.1016/s0891-5849(96)00275-4

Suzuma, K., Takahara, N., Suzuma, I., Isshiki, K., Ueki, K., Leitges, M., . . . King, G. L. (2002). Characterization of protein kinase C beta isoform's action on retinoblastoma protein phosphorylation, vascular endothelial growth factor-induced endothelial cell proliferation, and retinal neovascularization. *Proc Natl Acad Sci U S A, 99*(2), 721-726. doi:10.1073/pnas.022644499

Svensson, R. U., Parker, S. J., Eichner, L. J., Kolar, M. J., Wallace, M., Brun, S. N., . . . Shaw, R. J. (2016). Inhibition of acetyl-CoA carboxylase suppresses fatty acid synthesis and tumor growth of non-small-cell lung cancer in preclinical models. *Nat Med, 22*(10), 1108-1119. doi:10.1038/nm.4181

Sztalryd, C., & Brasaemle, D. L. (2017). The perilipin family of lipid droplet proteins: Gatekeepers of intracellular lipolysis. *Biochim Biophys Acta Mol Cell Biol Lipids, 1862*(10 Pt B), 1221-1232. doi:10.1016/j.bbalip.2017.07.009

Talley, A. K., Dewhurst, S., Perry, S. W., Dollard, S. C., Gummuluru, S., Fine, S. M., . . . Gelbard, H. A. (1995). Tumor necrosis factor alpha-induced apoptosis in human neuronal cells: protection by the antioxidant N-acetylcysteine and the genes bcl-2 and crmA. *Mol Cell Biol, 15*(5), 2359-2366. doi:10.1128/mcb.15.5.2359

Tam, O'Brien, S., Wierda, W., Kantarjian, H., Wen, S., Do, K. A., . . . Keating, M. J. (2008). Long-term results of the fludarabine, cyclophosphamide, and rituximab regimen as initial therapy of chronic lymphocytic leukemia. *Blood, 112*(4), 975-980. doi:10.1182/blood-2008-02-140582

Tam, Trotman, J., Opat, S., Burger, Cull, G., Gottlieb, D., . . . Roberts, A. W. (2019). Phase 1 study of the selective BTK inhibitor zanubrutinib in B-cell malignancies and safety and efficacy evaluation in CLL. *Blood, 134*(11), 851-859. doi:10.1182/blood.2019001160

Tam, C., O'Brien, S., Wierda, W., Kantarjian, H., Wen, S., Do, K., . . . Keating, M. (2008). Long-term results of the fludarabine, cyclophosphamide, and rituximab regimen as initial therapy of chronic lymphocytic leukaemia. *Blood, 112*(4), 5.

Tamura, K., Makino, A., Hullin-Matsuda, F., Kobayashi, T., Furihata, M., Chung, S., . . . Nakagawa, H. (2009). Novel lipogenic enzyme ELOVL7 is involved in prostate cancer growth through saturated long-chain fatty acid metabolism. *Cancer Res, 69*(20), 8133-8140. doi:10.1158/0008-5472.Can-09-0775

Tanaka, T., Nakata, T., Oka, T., Ogawa, T., Okamoto, F., Kusaka, Y., . . . Itakura, K. (2001). Defect in human myocardial long-chain fatty acid uptake is caused by FAT/CD36 mutations. *J Lipid Res, 42*(5), 751-759.

Thurgood, L. A., Dwyer, E. S., Lower, K. M., Chataway, T. K., & Kuss, B. J. (2019). Altered expression of metabolic pathways in CLL detected by unlabelled quantitative mass spectrometry analysis. *Br J Haematol, 185*(1), 65-78. doi:10.1111/bjh.15751

Tili, E., Michaille, J. J., Luo, Z., Volinia, S., Rassenti, L. Z., Kipps, T. J., & Croce, C. M. (2012). The down-regulation of miR-125b in chronic lymphocytic leukemias leads to metabolic adaptation of cells to a transformed state. *Blood, 120*(13), 2631-2638. doi:10.1182/blood-2012-03-415737

To, L. B., Levesque, J. P., & Herbert, K. E. (2011). How I treat patients who mobilize hematopoietic stem cells poorly. *Blood, 118*(17), 4530-4540. doi:10.1182/blood-2011-06-318220

Tontonoz, P., Hu, E., & Spiegelman, B. M. (1994). Stimulation of adipogenesis in fibroblasts by PPAR gamma 2, a lipid-activated transcription factor. *Cell, 79*(7), 1147-1156. doi:10.1016/0092-8674(94)90006-x

Trachootham, D., Alexandre, J., & Huang, P. (2009). Targeting cancer cells by ROS-mediated mechanisms: a radical therapeutic approach? *Nat Rev Drug Discov, 8*(7), 579-591. doi:10.1038/nrd2803

Trachootham, D., Zhang, H., Zhang, W., Feng, L., Du, M., Zhou, Y., . . . Huang, P. (2008). Effective elimination of fludarabine-resistant CLL cells by PEITC through a redox-mediated mechanism. *Blood, 112*(5), 1912-1922. doi:10.1182/blood-2008-04-149815

Trumpower, B. L. (2002). A concerted, alternating sites mechanism of ubiquinol oxidation by the dimeric cytochrome bc(1) complex. *Biochim Biophys Acta, 1555*(1-3), 166-173. doi:10.1016/s0005-2728(02)00273-6

Tsai, H. T., Cross, A. J., Graubard, B. I., Oken, M., Schatzkin, A., & Caporaso, N. E. (2010). Dietary factors and risk of chronic lymphocytic leukemia and small lymphocytic lymphoma: a pooled analysis of two prospective studies. *Cancer Epidemiol Biomarkers Prev, 19*(10), 2680-2684. doi:10.1158/1055-9965.Epi-10-0585

Tsuji, Y., Nakagawa, T., Hatanaka, M., Takeuchi, T., Matsumoto, E., Takenaka, H., & Shimizu, A. (2006). Quantification of caveolin isoforms using quantitative real-time RT-PCR, and analysis of promoter CpG methylation of caveolin-1alpha in human T cell leukemia cell lines. *Int J Mol Med, 18*(3), 489-495.

Tsujii, M., & DuBois, R. N. (1995). Alterations in cellular adhesion and apoptosis in epithelial cells overexpressing prostaglandin endoperoxide synthase 2. *Cell, 83*(3), 493-501. doi:10.1016/0092-8674(95)90127-2

Tucci, J., Alhushki, W., Chen, T., Sheng, X., Kim, Y. M., & Mittelman, S. D. (2018). Switch to low-fat diet improves outcome of acute lymphoblastic leukemia in obese mice. *Cancer Metab, 6*, 15. doi:10.1186/s40170-018-0189-0

Turrens, J. F., Alexandre, A., & Lehninger, A. L. (1985). Ubisemiquinone is the electron donor for superoxide formation by complex III of heart mitochondria. *Arch Biochem Biophys, 237*(2), 408-414. doi:10.1016/0003-9861(85)90293-0

Um, H. D., Orenstein, J. M., & Wahl, S. M. (1996). Fas mediates apoptosis in human monocytes by a reactive oxygen intermediate dependent pathway. *J Immunol, 156*(9), 3469-3477.

Vaisitti, T., Aydin, S., Rossi, D., Cottino, F., Bergui, L., D'Arena, G., . . . Deaglio, S. (2010). CD38 increases CXCL12-mediated signals and homing of chronic lymphocytic leukemia cells. *Leukemia, 24*(5), 958-969. doi:10.1038/leu.2010.36

Valceckiene, V., Kontenyte, R., Jakubauskas, A., & Griskevicius, L. (2010). Selection of reference genes for quantitative polymerase chain reaction studies in purified B cells from B cell chronic lymphocytic leukaemia patients. *Br J Haematol, 151*(3), 232-238. doi:10.1111/j.1365-2141.2010.08363.x

Valko, M., Leibfritz, D., Moncol, J., Cronin, M. T., Mazur, M., & Telser, J. (2007). Free radicals and antioxidants in normal physiological functions and human disease. *Int J Biochem Cell Biol, 39*(1), 44-84. doi:10.1016/j.biocel.2006.07.001

Valko, M., Rhodes, C. J., Moncol, J., Izakovic, M., & Mazur, M. (2006). Free radicals, metals and antioxidants in oxidative stress-induced cancer. *Chem Biol Interact, 160*(1), 1-40. doi:10.1016/j.cbi.2005.12.009

van Deurs, B., Petersen, O. W., Olsnes, S., & Sandvig, K. (1989). The ways of endocytosis. *Int Rev Cytol, 117*, 131-177. doi:10.1016/s0074-7696(08)61336-4

Van Driel, B. E., Lyon, H., Hoogenraad, D. C., Anten, S., Hansen, U., & Van Noorden, C. J. (1997). Expression of CuZn- and Mn-superoxide dismutase in human colorectal neoplasms. *Free Radic Biol Med, 23*(3), 435-444. doi:10.1016/s0891-5849(97)00102-0

Vargova, K., Curik, N., Burda, P., Basova, P., Kulvait, V., Pospisil, V., . . . Stopka, T. (2011). MYB transcriptionally regulates the miR-155 host gene in chronic lymphocytic leukemia. *Blood, 117*(14), 3816-3825. doi:10.1182/blood-2010-05-285064

Veal, G. J., Cole, M., Chinnaswamy, G., Sludden, J., Jamieson, D., Errington, J., . . . Boddy, A. V. (2016). Cyclophosphamide pharmacokinetics and pharmacogenetics in children with B-cell non-Hodgkin's lymphoma. *Eur J Cancer, 55*, 56-64. doi:10.1016/j.ejca.2015.12.007

Vilpo, J., Vilpo, L., Hurme, M., & Vuorinen, P. (1999). Induction of beta-2-microglobulin release in vitro by chronic lymphocytic leukaemia cells: relation to total protein synthesis. *Leuk Res, 23*(10), 913-920. doi:10.1016/s0145-2126(99)00109-5

Viswanathan, V. K., Krcmarik, K., & Cianciotto, N. P. (1999). Template secondary structure promotes polymerase jumping during PCR amplification. *Biotechniques, 27*(3), 508-511. doi:10.2144/99273st04

Vitols, S., Angelin, B., & Juliusson, G. (1997). Simvastatin impairs mitogen-induced proliferation of malignant B-lymphocytes from humans--in vitro and in vivo studies. *Lipids, 32*(3), 255-262. doi:10.1007/s11745-997-0032-1

Vousden, K. H., & Lane, D. P. (2007). p53 in health and disease. *Nat Rev Mol Cell Biol, 8*(4), 275-283. doi:10.1038/nrm2147

Wang, J. X., Gao, J., Ding, S. L., Wang, K., Jiao, J. Q., Wang, Y., . . . Li, P. F. (2015). Oxidative Modification of miR-184 Enables It to Target Bcl-xL and Bcl-w. *Mol Cell, 59*(1), 50-61. doi:10.1016/j.molcel.2015.05.003

Wang, L., Lawrence, M. S., Wan, Y., Stojanov, P., Sougnez, C., Stevenson, K., . . . Wu, C. J. (2011). SF3B1 and other novel cancer genes in chronic lymphocytic leukemia. *N Engl J Med, 365*(26), 2497-2506. doi:10.1056/NEJMoa1109016

Wang, X., Wang, Z., Liu, J. Z., Hu, J. X., Chen, H. L., Li, W. L., & Hai, C. X. (2011). Double antioxidant activities of rosiglitazone against high glucose-induced oxidative stress in hepatocyte. *Toxicol In Vitro, 25*(4), 839-847. doi:10.1016/j.tiv.2011.02.004

Warburg, O. (1956a). On respiratory impairment in cancer cells. *Science, 124*, 269-270.

Warburg, O. (1956b). On the origin of cancer cells. *Science, 123*, 309-314.

Warburg, O., Posener, K., & Negelein, E. (1930). Ueber den Stoffwechsel der Tumoren. *Biochemische Zeitschrift, 152*, 319-344.

Ware, M. D., DeSilva, D., Sinilnikova, O. M., Stoppa-Lyonnet, D., Tavtigian, S. V., & Mazoyer, S. (2006). Does nonsense-mediated mRNA decay explain the ovarian cancer cluster region of the BRCA2 gene? *Oncogene, 25*(2), 323-328. doi:10.1038/sj.onc.1209033

Watanabe, T., Hotta, T., Ichikawa, A., Kinoshita, T., Nagai, H., Uchida, T., . . . Saito, H. (1994). The MDM2 oncogene overexpression in chronic lymphocytic leukemia and low-grade lymphoma of B-cell origin. *Blood, 84*(9), 3158-3165.

Watson, L., Wyld, P., & Catovsky, D. (2008). Disease burden of chronic lymphocytic leukaemia within the European Union. *Eur J Haematol, 81*(4), 253-258. doi:10.1111/j.1600-0609.2008.01114.x

Watt, M. J., Clark, A. K., Selth, L. A., Haynes, V. R., Lister, N., Rebello, R., . . . Taylor, R. A. (2019). Suppressing fatty acid uptake has therapeutic effects in preclinical models of prostate cancer. *Sci Transl Med, 11*(478). doi:10.1126/scitranslmed.aau5758

Watters, D. J. (2003). Oxidative stress in ataxia telangiectasia. *Redox Rep, 8*(1), 23-29. doi:10.1179/135100003125001206

Weinberg, J., & Friedman, D. (2013). Inhibition of B-cell Receptor Signaling as a Therapeutic Strategy for Treatment of CLL. *The Hematologist, 10*(3).

Weiss, L., Hoffmann, G. E., Schreiber, R., Andres, H., Fuchs, E., Korber, E., & Kolb, H. J. (1986). Fatty-acid biosynthesis in man, a pathway of minor importance. Purification, optimal assay conditions, and organ distribution of fatty-acid synthase. *Biol Chem Hoppe Seyler, 367*(9), 905-912. doi:10.1515/bchm3.1986.367.2.905

Werlenius, O., Aurelius, J., Hallner, A., Akhiani, A. A., Simpanen, M., Martner, A., . . . Thoren, F. B. (2016). Reactive oxygen species induced by therapeutic CD20 antibodies inhibit natural killer cell-mediated antibody-dependent cellular cytotoxicity against primary CLL cells. *Oncotarget, 7*(22), 32046-32053. doi:10.18632/oncotarget.8769

Werner, M., Hobeika, E., & Jumaa, H. (2010). Role of PI3K in the generation and survival of B cells. *Immunol Rev, 237*(1), 55-71. doi:10.1111/j.1600-065X.2010.00934.x

Wheeler, M. L., & Defranco, A. L. (2012). Prolonged production of reactive oxygen species in response to B cell receptor stimulation promotes B cell activation and proliferation. *J Immunol, 189*(9), 4405-4416. doi:10.4049/jimmunol.1201433

Wierda, W., O'Brien, S., Wen, S., Faderl, S., Garcia-Manero, G., Thomas, D., . . . Keating, M. (2005). Chemoimmunotherapy with fludarabine, cyclophosphamide, and rituximab for relapsed and

refractory chronic lymphocytic leukemia. *J Clin Oncol, 23*(18), 4070-4078. doi:10.1200/jco.2005.12.516

Wiestner, A. (2012). Emerging role of kinase-targeted strategies in chronic lymphocytic leukemia. *Hematology Am Soc Hematol Educ Program, 2012*, 88-96. doi:10.1182/asheducation-2012.1.88

Wikstrom, M. K. (1977). Proton pump coupled to cytochrome c oxidase in mitochondria. *Nature, 266*(5599), 271-273. doi:10.1038/266271a0

Williamson, K. E., Kelly, J. D., Hamilton, P. W., McManus, D., & Johnston, S. R. (1998). Bcl-2/Bax ratios in chronic lymphocytic leukaemia and their correlation with in vitro apoptosis and clinical resistance. *Br J Cancer, 78*(4), 553-554. doi:10.1038/bjc.1998.533

Wolf, S., Mertens, D., Schaffner, C., Korz, C., Dohner, H., Stilgenbauer, S., & Lichter, P. (2001). B-cell neoplasia associated gene with multiple splicing (BCMS): the candidate B-CLL gene on 13q14 comprises more than 560 kb covering all critical regions. *Hum Mol Genet, 10*(12), 1275-1285. doi:10.1093/hmg/10.12.1275

Wood, Z. A., Schroder, E., Robin Harris, J., & Poole, L. B. (2003). Structure, mechanism and regulation of peroxiredoxins. *Trends Biochem Sci, 28*(1), 32-40. doi:10.1016/s0968-0004(02)00003-8

Woyach, J. A., Furman, R. R., Liu, T. M., Ozer, H. G., Zapatka, M., Ruppert, A. S., . . . Byrd, J. C. (2014). Resistance mechanisms for the Bruton's tyrosine kinase inhibitor ibrutinib. *N Engl J Med, 370*(24), 2286-2294. doi:10.1056/NEJMoa1400029

Wu, R. P., Hayashi, T., Cottam, H. B., Jin, G., Yao, S., Wu, C. C., . . . Carson, D. A. (2010). Nrf2 responses and the therapeutic selectivity of electrophilic compounds in chronic lymphocytic leukemia. *Proc Natl Acad Sci U S A, 107*(16), 7479-7484. doi:10.1073/pnas.1002890107

Xu, Y., Krishnan, A., Wan, X. S., Majima, H., Yeh, C. C., Ludewig, G., . . . St Clair, D. K. (1999). Mutations in the promoter reveal a cause for the reduced expression of the human manganese superoxide dismutase gene in cancer cells. *Oncogene, 18*(1), 93-102. doi:10.1038/sj.onc.1202265

Xu, Y., Porntadavity, S., & St Clair, D. K. (2002). Transcriptional regulation of the human manganese superoxide dismutase gene: the role of specificity protein 1 (Sp1) and activating protein-2 (AP-2). *Biochem J, 362*(Pt 2), 401-412. doi:10.1042/0264-6021:3620401

Yang, S., Hwang, S., Kim, M., Seo, S. B., Lee, J. H., & Jeong, S. M. (2018). Mitochondrial glutamine metabolism via GOT2 supports pancreatic cancer growth through senescence inhibition. *Cell Death Dis, 9*(2), 55. doi:10.1038/s41419-017-0089-1

Yu, W., Denu, R. A., Krautkramer, K. A., Grindle, K. M., Yang, D. T., Asimakopoulos, F., . . . Denu, J. M. (2016). Loss of SIRT3 Provides Growth Advantage for B Cell Malignancies. *J Biol Chem, 291*(7), 3268-3279. doi:10.1074/jbc.M115.702076

Zechner, R., Zimmermann, R., Eichmann, T. O., Kohlwein, S. D., Haemmerle, G., Lass, A., & Madeo, F. (2012). FAT SIGNALS--lipases and lipolysis in lipid metabolism and signaling. *Cell Metab, 15*(3), 279-291. doi:10.1016/j.cmet.2011.12.018

Zenz, T., Benner, A., Dohner, H., & Stilgenbauer, S. (2008). Chronic lymphocytic leukemia and treatment resistance in cancer: the role of the p53 pathway. *Cell Cycle, 7*(24), 3810-3814. doi:10.4161/cc.7.24.7245

Zhang, Wang, Vikash, Ye, Wu, Liu, & Dong. (2016). ROS and ROS-Mediated Cellular Signaling. *Oxid Med Cell Longev, 2016*, 4350965. doi:10.1155/2016/4350965

Zhang, I., Cui, Y., Amiri, A., Ding, Y., Campbell, R. E., & Maysinger, D. (2016). Pharmacological inhibition of lipid droplet formation enhances the effectiveness of curcumin in glioblastoma. *Eur J Pharm Biopharm, 100*, 66-76. doi:10.1016/j.ejpb.2015.12.008

Zirlik, K., & Veelken, H. (2018). Idelalisib. *Recent Results Cancer Res, 212*, 243-264. doi:10.1007/978-3-319-91439-8_12

Appendix A: SOD2 investigation

Table A1: Primer information for *SOD2* promoter sequencing (from Xu *et al.* (1999)).

Amplicon	Primer sequence (5'→3')	Amplicon size (bp)	Location to TSS
PCR-1	F: GCA GAT CAC TTC AGT CTA GGA GT R: GGC TAG TTA GGA AGC TGG TAC	1509	-3322 – -1813
PCR-2	F: TCC AGT TCT CAT AGC TAG TGC C R: ATA TGA TGG AAG GTA GCA GGT GC	799	-1892 – -1093
PCR-3	F: TTA CCG GAA GCC TAG TCA TCC TT R: TGC CTG TCT GCC GTA CTT GAG	940	-1182 – -242
PCR-4	F: GCC TTC GGG CCG TAC CAA CTC CAA R: CTA GTG CTG GTG CTA CCG CTG ATG C	391	-321 – +70

Table A2: Primer information for *SOD2* promoter sequencing using bisulphite-treated genomic DNA (from Hodge *et al.* (2005)).

Gene symbol	Primer sequence (5'→3')	Amplicon size (bp)
***SOD2* (round 1)**	F: GTA TTT TTA GGG G[C/T]G GAT [C/T]GG AGG TAG GGT TT	494
	R: CCA AAC CC[A/G] ATA C[A/G]A CCA CTA TC[A/G] CCA TTA C	
***SOD2* (round 2)**	F: GGG T[C/T]G TAT TAA TTT TA[C/T] GGG GGT AGG GGT	407
	R: AAC CCC TTA CCC CTT AAA AC[A/G] TAA CC[A/G] AAT CCC	

Table A3: Primer information for *SOD2* real-time qPCR.

Gene symbol	Primer sequence (5'→3')	Amplicon size (bp)	Source of sequence
SOD2	F: TTT CAA TAA GGA ACG GGG ACA C R: GTG CTC CCA CAC ATC AAT CC	109	PrimerBank

Table A4: Primer information for transcription factor real-time qPCR.

Gene symbol	Primer sequence (5'→3')	Amplicon size (bp)	Source of sequence
SP1	F: ACG CTT CAC ACG TTC GGA TGA G R: TGA CAG GTG GTC ACT CCT CAT G	107	Self-designed
TFAP2A	F: GAC TCG GAG ACC TCT CGA TCC R: GAC GGC ATT GCT GTT GGA C	143	PrimerBank
TFAP2B	F: GTT GAA GAT GCC AAT AAC AGC GG R: GGA CGG AGC AAA ACA CCT CGC	157	Self-designed
TFAP2C	F: CTG TTG CTG CAC GAT CAG ACA R: CTC AGT GGG GTT CAT TAC GGC	114	PrimerBank
TFAP2D	F: GCC TCA ATG CTT CAC TCT TGG G R: GCT TTC CGT CTT CCT GCT GGT A	121	Self-designed
TFAP2E	F: GCT CAG CTC AAC GTC CAA GTA R: TCT CTA ACC GTT CCC GCA AAC	152	Self-designed

Appendix B: Lipid investigation

Table B1: RNA quality and quantity information.
*, also used in the SOD2 investigation.

Sample	RNA quality score	RNA concentration (ng/µL)
NOR1 (healthy control)*	7.1	10.3
NOR2 (healthy control)*	8.0	6.67
NOR3 (healthy control)*	7.0	8.57
CLL1/FMC279*	8.4	12.9
CLL2/FMC124*	8.1	10.5
CLL3/FMC292*	8.7	10.9
CLL4/FMC10*	8.2	7.78
CLL5/FMC297*	5.9	14.07
CLL6/FMC234*	7.2	13.8
NOR4 (healthy control)	8.2	10.4
NOR5 (healthy control)	9.4	57.9
FMC207	7.9	48.3
FMC206	8.1	75
FMC272	8.0	105
FMC194	7.6	315
FMC121	7.7	119.3
FMC278	6.0	97
FMC11	8.5	92
FMC281	9.1	74.2
FMC174	8.1	65.2
FMC293	8.4	15.7

Table B2: Genes screened using PrimePCR™ real-time qPCR.

Gene symbol	Accession number	Gene name	Localisation
ABCA1	NC_000009.11	ATP-binding cassette, sub-family A (ABC1), member 1	9q31.1
ACAA1	NC_000003.11	Acetyl-CoA acyltransferase 1	3p22.2
ACACB	NC_000012.11	Acetyl-CoA carboxylase beta	12q24.11
ACAD8	NC_000011.9	Acyl-CoA dehydrogenase family, member 8	11q25
ACAT1	NC_000011.9	Acetyl-CoA acetyltransferase 1	11q22.3
ACLY	NC_000017.10	ATP citrate lyase	17q21.2
ACOX1	NC_000017.10	Acyl-CoA oxidase 1, palmitoyl	17q25.1
ACSL5	NC_000010.10	Acyl-CoA synthetase long-chain family member 5	10q25.2
ADIPOQ	NC_000003.11	Adiponectin, C1Q and collagen domain containing	3q27.3
ADIPOR1	NC_000001.10	Adiponectin receptor 1	1q32.1
ALOX5	NC_000010.10	Arachidonate 5-lipoxygenase	10q11.21
ANGPTL4	NC_000019.9	Angiopoietin-like 4	19p13.2
APOA1	NC_000011.9	Apolipoprotein A-I	11q23.3
APOA4	NC_000011.9	Apolipoprotein A-IV	11q23.3
APOB	NC_000002.11	Apolipoprotein B (including Ag(x) antigen)	2p24.1
APOC1	NC_000019.9	Apolipoprotein C-I	19q13.32
APOC2	NC_000019.9	Apolipoprotein C-II	19q13.32
APOC3	NC_000011.9	Apolipoprotein C-III	11q23.3
APOE	NC_000019.9	Apolipoprotein E	19q13.32
B2M	NC_000015.9	Beta-2-microglobulin	15q21.1
C3	NC_000019.9	Complement component 3	19p13.3
CD36	NC_000007.13	CD36 molecule (thrombospondin receptor)	7q21.11
CEL	NC_000009.11	Carboxyl ester lipase (bile salt-stimulated lipase)	9q34.13
CETP	NC_000016.9	Cholesteryl ester transfer protein, plasma	16q13
CPT1A	NC_000011.9	Carnitine palmitoyltransferase 1A (liver)	11q13.3
CROT	NC_000007.13	Carnitine O-octanoyltransferase	7q21.12
DECR1	NC_000008.10	2,4-dienoyl CoA reductase 1, mitochondrial	8q21.3
FAAH	NC_000001.10	Fatty acid amide hydrolase	1p33
FABP1	NC_000002.11	Fatty acid binding protein 1, liver	2p11.2
FABP2	NC_000004.11	Fatty acid binding protein 2, intestinal	4q26
FADS1	NC_000011.9	Fatty acid desaturase 1	11q12.2
FADS2	NC_000011.9	Fatty acid desaturase 2	11q12.2
FASN	NC_000017.10	Fatty acid synthase	17q25.3
GAPDH	NC_000012.11	Glyceraldehyde-3-phosphate dehydrogenase	12p13.31
GCK	NC_000007.13	Glucokinase (hexokinase 4)	7p13
GGT1	NC_000022.10	Gamma-glutamyltransferase 1	22q11.23
GOT1	NC_000010.10	Glutamic-oxaloacetic transaminase 1, soluble (aspartate aminotransferase 1)	10q24.2
GUSB	NC_000007.13	Glucuronidase, beta	7q11.21
HADH	NC_000004.11	Hydroxyacyl-CoA dehydrogenase	4q25
HMGCR	NC_000005.9	3-hydroxy-3-methylglutaryl-CoA reductase	5q13.3
HMOX1	NC_000022.10	Heme oxygenase (decycling) 1	22q12.3
HPRT1	NC_000023.10	Hypoxanthine phosphoribosyltransferase 1	X26.2-q26.3
HPSE	NC_000004.11	Heparanase	4q21.23
IL6R	NC_000001.10	Interleukin 6 receptor	1q21.3
LCAT	NC_000016.9	Lecithin-cholesterol acyltransferase	16q22.1
LDLR	NC_000019.9	Low density lipoprotein receptor	19p13.2
LEP	NC_000007.13	Leptin	7q32.1
LIPC	NC_000015.9	Lipase, hepatic	15q21.3
LIPE	NC_000019.9	Lipase, hormone-sensitive	19q13.2
LIPG	NC_000018.9	Lipase, endothelial	18q21.1
LMF1	NC_000016.9	Lipase maturation factor 1	16p13.3

Gene symbol	Accession number	Gene name	Localisation
LPIN1	NC_000002.11	Lipin 1	2p25.1
LPL	NC_000008.10	Lipoprotein lipase	8p21.3
MAPK1	NC_000022.10	Mitogen-activated protein kinase 1	22q11.22
MAPK14	NC_000006.11	Mitogen-activated protein kinase 14	6p21.31
MAPK3	NC_000016.9	Mitogen-activated protein kinase 3	16p11.2
MGLL	NC_000003.11	Monoglyceride lipase	3q21.3
MTHFR	NC_000001.10	Methylenetetrahydrofolate reductase (NAD(P)H)	1p36.22
NPC1	NC_000018.10	NPC intracellular cholesterol transporter 1	18q11.2
NR1H3	NC_000011.9	Nuclear receptor subfamily 1, group H, member 3	11p11.2
NR1H4	NC_000012.11	Nuclear receptor subfamily 1, group H, member 4	12q23.1
PCSK9	NC_000001.10	Proprotein convertase subtilisin/kexin type 9	1p32.2
PDGFRB	NC_000005.9	Platelet-derived growth factor receptor, beta polypeptide	5q32
PIK3CA	NC_000003.11	Phosphoinositide-3-kinase, catalytic, alpha polypeptide	3q26.32
PIK3CG	NC_000007.13	Phosphoinositide-3-kinase, catalytic, gamma polypeptide	7q22.3
PIK3R1	NC_000005.9	Phosphoinositide-3-kinase, regulatory subunit 1 (alpha)	5q13.1
PLA2G2A	NC_000001.10	Phospholipase A2, group IIA (platelets, synovial fluid)	1p36.13
PLA2G4A	NC_000001.10	Phospholipase A2, group IVA (cytosolic, calcium-dependent)	1q31.1
PLA2G7	NC_000006.11	Phospholipase A2, group VII (platelet-activating factor acetylhydrolase, plasma)	6p12.3
PLIN1	NC_000015.9	Perilipin 1	15q26.1
PLIN2	NC_000009.11	Perilipin 2	9p22.1
PNPLA3	NC_000022.10	Patatin-like phospholipase domain containing 3	22q13.31
PON1	NC_000007.13	Paraoxonase 1	7q21.3
PPARA	NC_000022.10	Peroxisome proliferator-activated receptor alpha	22q13.31
PPARD	NC_000006.11	Peroxisome proliferator-activated receptor delta	6p21.31
PPARG	NC_000003.11	Peroxisome proliferator-activated receptor gamma	3p25.2
PPARGC1A	NC_000004.11	Peroxisome proliferator-activated receptor gamma, coactivator 1 alpha	4p15.2
PRKAA2	NC_000001.10	Protein kinase, AMP-activated, alpha 2 catalytic subunit	1p32.2
PRKAB1	NC_000012.11	Protein kinase, AMP-activated, beta 1 non-catalytic subunit	12q24.23
PRKCB	NC_000016.9	Protein kinase C, beta	16p12.2-p12.1
PTEN	NC_000010.10	Phosphatase and tensin homolog	10q23.31
SCD	NC_000010.10	Stearoyl-CoA desaturase (delta-9-desaturase)	10q24.31
SCD5	NC_000004.11	Stearoyl-CoA desaturase 5	4q21.22
SDC1	NC_000002.11	Syndecan 1	2p24.1
SIRT1	NC_000010.10	Sirtuin 1	10q21.3
SLC27A1	NC_000019.9	Solute carrier family 27 (fatty acid transporter), member 1	19p13.11
SORL1	NC_000011.9	Sortilin-related receptor, L(DLR class) A repeats containing	11q24.1
SREBF1	NC_000017.10	Sterol regulatory element binding transcription factor 1	17p11.2
TNFRSF1A	NC_000012.11	Tumor necrosis factor receptor superfamily, member 1A	12p13.31
VDR	NC_000012.11	Vitamin D (1,25- dihydroxyvitamin D3) receptor	12q13.11

Table B3: Primer information for in-laboratory real-time qPCR.

Gene symbol	Primer sequence (5'→3')	Amplicon size (bp)	Source of sequence
ACSL5	F: CTC AAC CCG TCT TAC CTC TTC T R: GCA GCA ACT TGT TAG GTC ATT G	107	PrimerBank
ADIPOQ	F: GAC CAG GAA ACC ACG ACT CA R: GGT TTC ACC GAT GTC TCC CT	201 (exonic)	Self-designed
ALOX5	F: ACA AGC CCT TCT ACA ACG ACT R: AGC TGG ATC TCG CCC AGT T	85	PrimerBank
APOC1	F: TTC TGT CGA TCG TCT TGG AA R: TCA GCT TAT CCA AGG CAC TG	75	(Ko et al., 2014)
APOC3	F: CAA GAC CGC CAA GGA TGC A R: CTC GCA GGA TGG ATA GGC AG	223	Self-designed
APOE	F: GTT GCT GGT CAC ATT CCT GG R: GCA GGT AAT CCC AAA AGC GAC	146	PrimerBank
CD36	F: CCC AAA TGA AGA AGA ACA TAG R: CAC AAT ATA GTT CCT CTT CAG	147	In-house-designed
FABP1	F: TTA TGT CGC CGT TGA GTT CG R: ATC GTG CAG AAT GGG AAG CA	205	Self-designed
FADS2	F: AGC CCT CCT TTT CCT CAA CTT R: GAG GTG GTG CTC AAT CTG GA	208	Self-designed
HMOX1	F: AAG ACT GCG TTC CTG CTC AAC R: AAA GCC CTA CAG CAA CTG TCG	247	PrimerBank
LIPC	F: ATC AAG TGC CCT TGG ACA AAG R: TGA CAG CCC TGA TTG GTT TCT	132	PrimerBank
LIPG	F: GGG AGC CCC GTA CCT TTT G R: CCT CAC AGA TGG TTT GAC CTC A	93	PrimerBank
LPL	F: TCA TTC CCG GAG TAG CAG AGT R: GGC CAC AAG TTT TGG CAC C	125	PrimerBank
MGLL	F: AAT GCA GAC GGA CAG TAC CTC R: GAG CCA GCT CTT CAT AGC GG	118	PrimerBank
PDGFRB	F: AGA CAC GGG AGA ATA CTT TTG C R: AGT TCC TCG GCA TCA TTA GGG	126	PrimerBank
PLA2G2A	F: GAA AGG AAG CCG CAC TCA GTT R: CAG ACG TTT GTA GCA ACA GTC A	122	PrimerBank
PLA2G7	F: GGA AAG CCA GTG AAG AAT GCA R: GAG GGG CTG AGG AAT TCT GG	219	Self-designed
PLIN1	F: GGC TTC CTT AGT GCT GGT GT R: CCT CAC CTT GCT GGA TGG AG	124	Self-designed
PLIN2	F: TTG CAG TTG CCA ATA CCT ATG C R: CCA GTC ACA GTA GTC GTC ACA	148	PrimerBank
PON1	F: GAT ACT GCC TAA TGG ACT GGC R: GTG ATC CCC AAT TCC AAC ACT	141	PrimerBank
PPARG	F: TAC TGT CGG TTT CAG AAA TGC C R: GTC AGC GGA CTC TGG ATT CAG	141	PrimerBank
PPARGC1A	F: TCT GAG TCT GTA TGG AGT GAC AT R: CCA AGT CGT TCA CAT CTA GTT CA	112	PrimerBank
SREBF1	F: GCC CCT GTA ACG ACC ACT G R: CAG CGA GTC TGC CTT GAT G	84	PrimerBank

Table B4: Cost analysis of PrimePCR™ and in-laboratory real-time qPCR methods for use in this study.

Product (in-laboratory)	Assumptions/Notes	Cost	Quantity	Total
Custom DNA Oligos	20 bp at 25c per base	$5.00	89	**$445.00**
Universal Human Reference RNA	10 µg First set of primers were efficient and specific	$68.00	1	**$68.00**
SuperScript™ II Reverse Transcriptase	10,000 U at 500 U/µL First strand buffer and 0.1 M DTT supplied with product	$587.00	2	**$1,174.00**
Random Hexamer Primer	120 µL	$96.00	1	**$96.00**
RNaseOUT™ Recombinant Ribonuclease Inhibitor	5,000 U	$257.00	2	**$514.00**
dNTP Mix	10 mM each, 100 µL	$171.00	2	**$342.00**
SYBR Green PCR Master Mix	5 mL	$578.00	4	**$2,312.00**
MicroAmp™ Optical 384-Well Reaction Plate with Barcode	50 plates	$603.00	1	**$603.00**
MicroAmp™ Optical Adhesive Film	25 covers	$141.00	1	**$141.00**
Labour	Technical Assistant 20 hours of computer-based work + 40 hours of laboratory-based work	$40.00/hour	60	**$2,400.00**
TOTAL for in-laboratory method				**$8,095.00**
Product (PrimePCR™)	**Assumptions/Notes**	**Cost**	**Quantity**	**Total**
PrimePCR™ Lipid metabolism OPTIMISED H384 384-well SYBR plate	Primers pre-lipophilised to wells of plates	$565.00	6	**$3,390.00**
iScript™ Reverse Transcription Supermix	25 x 20 µL reactions 100 µL RNA control included with product	$245.00	1	**$245.00**
SsoAdvanced™ Universal SYBR® Green Supermix	1,000 x 20 µL reactions 10 x 1 mL	$925.00	1	**$925.00**
SsoAdvanced™ Universal SYBR® Green Supermix	200 x 20 µL reactions 2 x 1 mL	$220.00	1	**$220.00**
Labour	Technical Assistant 10 hours of computer-based work + 40 hours of laboratory-based work	$40.00/hour	50	**$2,000.00**
TOTAL for PrimePCR™ method				**$6,780.00**

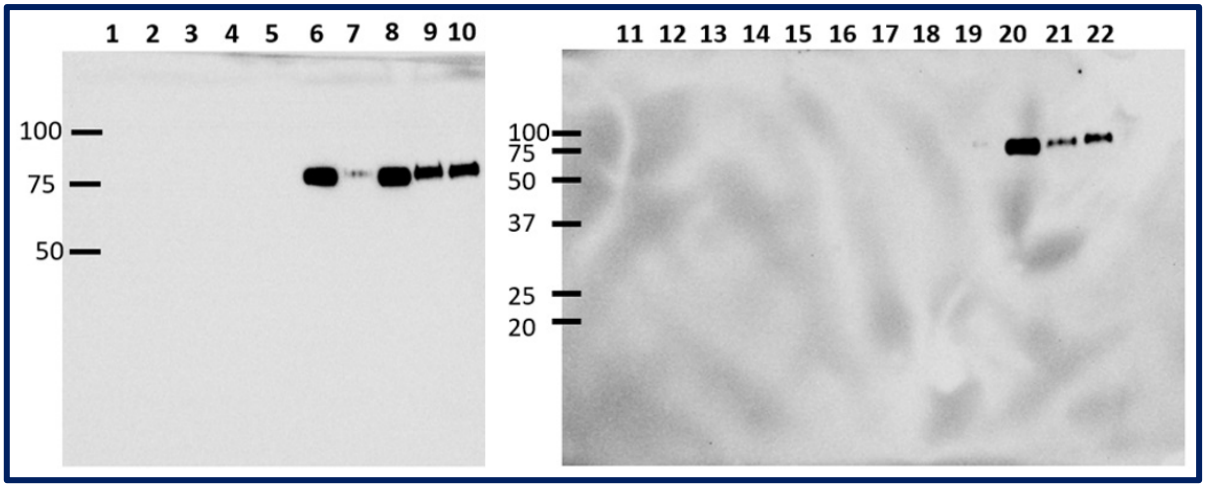

Figure B1: Raw western blot images.
Lanes 2-5 and 12-18, CLL B-lymphocyte samples; lanes 6-10 and 19-21, healthy controls. Samples 2, 3, and 18 were excluded from analysis due to sample degradation. Data generated by Dr. Lauren Thurgood.

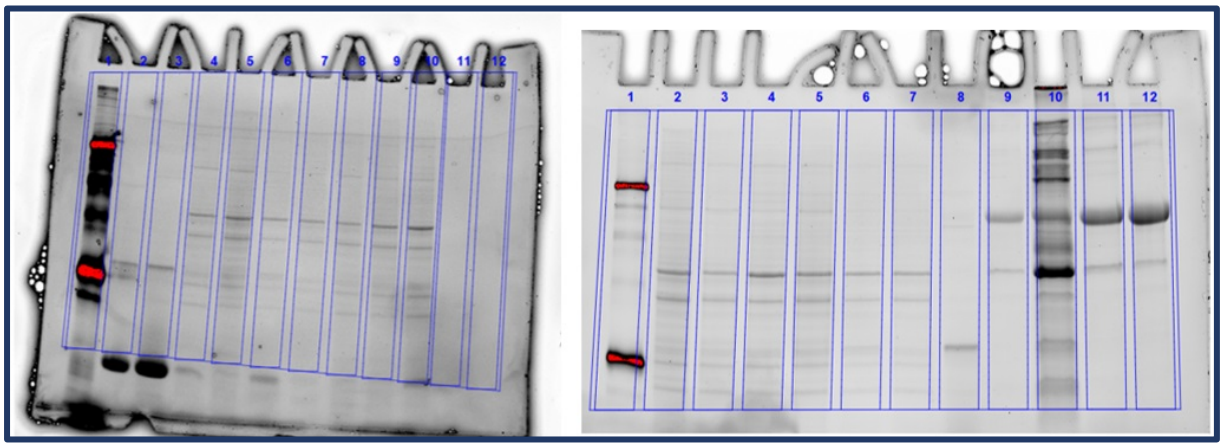

Figure B2: Raw SDS-PAGE gel images used for normalisation of protein loading.
Lanes 2-5 (left) and 2-8 (right), CLL B-lymphocyte samples; lanes 6-10 (left) and 9-12 (right), healthy controls. Samples 2 (left), 3 (left), and 8 (right) were excluded from analysis due to sample degradation. Data generated by Dr. Lauren Thurgood.

Table B5: Genes screened in the fatty acid import investigation.

Gene symbol	Accession number	Gene name	Localisation
ACSL1	NC_000004.12	Long-chain fatty acid-CoA ligase 1	4q35.1
ACSL3	NC_000002.12	Long-chain fatty acid-CoA ligase 1	2q36.1
CAV1	NC_000007.14	Caveolin 1	7q31.2
CAV2	NC_000007.14	Caveolin 2	7q31.2
FABP3	NC_000001.11	Fatty acid binding protein 3	1p35.2
FATP1	NC_000019.10	Fatty acid transport protein 1	19p13.11
FATP2	NC_000015.10	Fatty acid transport protein 2	15q21.2
FATP3	NC_000001.11	Fatty acid transport protein 3	1q21.3
FATP4	NC_000009.12	Fatty acid transport protein 4	9q34.11
FATP5	NC_000019.10	Fatty acid transport protein 5	19q13.43
FATP6	NC_000005.10	Fatty acid transport protein 6	5q23.3
GOT2	NC_000016.10	Plasma membrane-associated fatty acid binding protein	16q21
SLC22A9	NC_000011.10	Solute carrier family 22 member 9	11q12.3

Table B6: Primer information for fatty acid import real-time qPCR gene panel.

Gene symbol	Primer sequence (5'→3')	Amplicon size (bp)	Source of sequence
ACSL1	F: CTTATGGGCTTCGGAGCTTTT R: CAAGTAGTGCGGATCTTCGTG	142	PrimerBank
ACSL3	F: GCCGAGTGGATGATAGCTGC R: ATGGCTGGACCTCCTAGAGTG	86	PrimerBank
CAV1	F: CTG GGG GCA AAT ACG TAG A R: CTT GAC CAC GTC ATC GTT G	191	(Tsuji et al., 2006)
CAV2	F: GCC CTC TTT GAA ATC AGC R: CAA GTA TTC AAT CCT GGC TC	241	(Tsuji et al., 2006)
FABP3	F: TGG AGT TCG ATG AGA CAA CAG C R: CTC TTG CCC GTC CCA TTT CTG	101	PrimerBank
FATP1	F: GGG GCA GTG TCT CAT CTA TGG R: CCG ATG TAC TGA ACC ACC GT	111 (exonic)	PrimerBank
FATP2	F: GGC GCT CCT TAT GGG TAA CG R: CTT GGC AGT ATC TCT TCG ACA G	192	PrimerBank
FATP3	F: GGC TGG TCA GTT CTG GGA AG R: GTT GAC AAG GTA TCG GCA CAG	85 (exonic)	PrimerBank
FATP4	F: GGA CCC AGG TGG GAT TCT C R: CGC GCC TGA TGG TCT TGA T	90 (exonic)	PrimerBank
FATP5	F: GCT TCG GTC CTA TTC GGA TCT R: CAG CGC CCC ACA TAG TTG A	79 (exonic)	PrimerBank
FATP6	F: CTT CTG TCA TGG CTA ACA GTT CT R: AGG TTT CCG AGG TTG TCT TTT G	210 (exonic)	PrimerBank
GOT2	F: GTT TGC CTC TGC CAA TCA TAT G R: GAG GGT TGG AAT ACA TGG GAC	195	(Yang et al., 2018)
SLC22A9	F: AGG TTC GTG CTC AGA TGG TG R: CCA TGG CCT GGA ATC TGT GT	176	(Fujiwara, Takenaka, Hashimoto, Narawa, & Itoh, 2014)